

UNIVERSIDAD DE CONCEPCIÓN
DIRECCIÓN DE POSTGRADO
CONCEPCIÓN-CHILE



MÉTODOS DE ELEMENTOS FINITOS PARA
PROBLEMAS EN BIOELECTROMAGNETISMO

*Tesis para optar al grado de
Doctor en Ciencias Aplicadas con mención en Ingeniería Matemática*

JESSIKA PAMELA CAMAÑO VALENZUELA

JUNIO 2013

FACULTAD DE CIENCIAS FÍSICAS Y MATEMÁTICAS
DEPARTAMENTO DE INGENIERÍA MATEMÁTICA

**MÉTODOS DE ELEMENTOS FINITOS PARA PROBLEMAS EN
BIOELECTROMAGNETISMO**

Jessika Pamela Camaño Valenzuela

Directores de Tesis: Rodolfo Rodríguez, Universidad de Concepción, Chile.
Alberto Valli, Università degli Studi di Trento, Italia.
Ana Alonso Rodríguez, Università degli Studi di Trento, Italia.

Director de Programa: Prof. Raimund Bürger, Universidad de Concepción, Chile

COMISIÓN EVALUADORA

Prof. Salim Meddahi, Universidad de Oviedo, España.
Prof. Peter Monk, University of Delaware, E.E.U.U.
Prof. Ilaria Perugia, Università degli Studi di Pavia, Italia.

COMISIÓN EXAMINADORA

Firma: _____
Prof. Gabriel N. Gatica.
Universidad de Concepción, Chile.

Firma: _____
Prof. Carlos Jerez-Hanckes.
Pontificia Universidad Católica de Chile, Chile.

Firma: _____
Prof. Rodolfo Rodríguez.
Universidad de Concepción, Chile.

Firma: _____
Prof. Alberto Valli.
Università degli Studi di Trento, Italia.

Fecha Examen de Grado: _____

Calificación: _____

AGRADECIMIENTOS

Quisiera comenzar agradeciendo a mi director de tesis, Rodolfo Rodríguez, a quien admiro y aprecio mucho. Le agradezco infinitamente su paciencia, su buena disposición, su apoyo y el tiempo que invirtió en mi formación. Cada vez que lo necesité, siempre estuvo allí para brindarme su ayuda. Gran parte de lo que he logrado durante la etapa de tesis ha sido, sin duda, gracias al respaldo de Rodolfo. La verdad fue un gusto trabajar bajo su dirección.

Vorrei anche ringraziare Ana Alonso Rodríguez e Alberto Valli per la dedizione e l'appoggio dimostrati. Li ringrazio per l'ospitalità e l'interesse che hanno sempre mostrato per me durante il periodo di sviluppo della tesi. Mi sento fortunata ad aver lavorato con persone di tale livello accademico ed umano. Li ringrazio anche per avermi dato l'opportunità di lavorare ed imparare da loro, per la buona volontà e l'energia investita in ognuno dei lavori intrapresi insieme. Vorrei evidenziare il grande appoggio manifestato in particolare nella parte finale del mio percorso: senza il loro aiuto sarebbe stato molto più difficile finire entro i termini previsti. Infine un grazie per le volte che mi hanno accolto a Trento, permettendomi di vivere un'ottima esperienza.

Agradezco a mi esposo, Ricardo, por el apoyo y la comprensión que me brindó todos estos años de doctorado. Le agradezco por acompañarme en los momentos difíciles, también por compartir mis alegrías, por su lealtad, por su complicidad y por ser mi compañero y mi amigo. Ricardo es una persona de la cual día a día voy aprendiendo y agradezco a la vida por haberlo puesto en mi camino.

También agradezco de todo corazón a mi familia, principalmente a mis padres quienes siempre me brindaron su apoyo y a quienes les debo lo que soy. Gracias por el apoyo con el que siempre he contado, tanto en lo académico como en mi formación como persona, gracias por los valores que he recibido de ustedes, por vibrar con mis logros y por acompañarme en mis penas, gracias por guiarme para que fuera una persona de bien. También por ayudarme y aconsejarme cada vez que lo he necesitado. Gracias por ser unos excelentes padres.

A todos y cada uno de los profesores del Programa que me brindaron su tiempo y conocimiento. En particular, agradezco al profesor Gabriel Gatica quien aparte de ser un excelente profesional, de lo cual no cabe ninguna duda, es una gran persona, siempre preocupado no sólo del alumno, sino de la persona que hay detrás. Gracias por la preocupación mostrada, por los consejos y por el cariño que siempre sentí de su parte, el cual es mutuo. También agradezco el apoyo que recibí cuando decidí ingresar a este doctorado.

A mis compañeros del doctorado a quienes les tengo un cariño muy grande, en especial a

Pablo Venegas y a quien fue estudiante de este doctorado, Bibiana López Rodríguez. Gracias por los lindos momentos que tuvimos la oportunidad de compartir. La verdad a ambos los siento mucho más que compañeros, son mis amigos.

A Lorena, Angelina y Eduardo con los cuales tuve la oportunidad de compartir momentos muy agradables y me quedan lindos recuerdos de aquello.

Agradezco también a mis amigos, amigos de mi niñez que siempre me han apoyado y querido. También a los amigos que he conocido en la universidad, en particular le agradezco a René Mateluna y a Viviana Solano quienes llegaron a ser personas relevantes en mi vida y ocupan un lugar en mi corazón.

A mis amigos Trentinos los cuales fueron una gran compañía las veces que estuve en Italia.

A los profesores Freddy Paiva y Carlos Mora por apoyarme en esta aventura de ingresar al doctorado.

Al proyecto MECESUP UCO0713, al CI²MA, a CONICYT, a dirección de postgrado de la Universidad de Concepción y a Becas Chile.

Agradezco a la vida porque me ha entregado mucho más de lo que imaginaba.

RESUMEN

El objetivo principal de esta tesis es proponer, analizar y testear modelos matemáticos y computacionales eficientes a través de los cuales poder localizar actividad cerebral a partir de mediciones de los campos eléctricos y magnéticos en la superficie de la cabeza. Estas mediciones se pueden obtener a través de un electroencefalograma y un magnetoencefalograma. En términos matemáticos, esta tesis se centra en resolver un problema inverso.

En primer lugar se estudia el problema inverso usando como modelo las ecuaciones de corrientes inducidas. Igual que para el sistema completo de ecuaciones de Maxwell, se demuestra que una fuente de corriente volumétrica no puede ser identificada por el conocimiento de las componentes tangenciales de los campos electromagnéticos sobre la frontera, y se caracteriza el espacio de las fuentes no radiantes. Por otro lado, se prueba que el problema inverso tiene una única solución si la fuente está soportada en la frontera de un subdominio o si es la suma de un número finito de dipolos. También este trabajo se enfoca en la aplicabilidad de estos resultados para la localización de la actividad cerebral a partir de las mediciones que se obtienen mediante la electroencefalografía y la magnetoencefalografía.

Posteriormente, se analiza el problema electrostático con fuente de corriente dipolar. Este es un problema singular, ya que tal modelo considera derivadas de primer orden de una distribución delta de Dirac. Su solución pertenece a L^p , con $1 \leq p < 3/2$ en el caso tridimensional y con $1 \leq p < 2$ en el caso bidimensional. Se consideran la aproximación numérica del problema directo a través de elementos finitos lineales a trozos y continuos. Se prueba una estima a priori del error en norma L^p . Además, se propone un estimador de error a posteriori de tipo residual. Se demuestra que tal estimador es confiable y eficiente. Por último, se utiliza este estimador para guiar un procedimiento adaptativo, el cual experimentalmente muestra un orden óptimo de convergencia.

Luego, se comparan distintos métodos de aproximación de la solución del problema directo considerando un dominio con varias regiones con diferentes conductividades. Para el problema directo, se analiza el caso en el que el dipolo se encuentra en una interfaz. En este caso específico, se usa una aproximación de la distribución delta de Dirac ya que los otros métodos considerados anteriormente no están definidos. Por otro lado, para el problema inverso, se analizan los resultados obtenidos utilizando los distintos métodos ya usados en el problema directo y se añaden a estos, un último método que consiste en usar un procedimiento adaptativo guiado por el estimador de error a posteriori encontrado en el Capítulo 4. Se consideran dos situaciones: una fuente dipolar situada en una región con conductividad regular y lejana a la interfaz y por otra parte, el caso en el que la tal fuente es cercana a una interfaz. Se estudia también el caso de una

fuelle distribuida y se compara las matrices de influencia cuando el soporte de dicha fuente se encuentra dentro de una región homogénea y es lejana a la interfaz y en el caso en que el soporte es cercano a la interfaz.

Por último, se considera el problema de corrientes inducidas dependiente del tiempo. Se formula el problema en términos de dos variables, una definida sólo en el dominio conductor y la otra, en la frontera del dominio. Se combinan el método de elementos finitos (FEM) y los elementos de frontera (BEM) para obtener una formulación variacional acoplada FEM-BEM. Se establece la existencia y unicidad de la solución en el caso continuo y en el caso totalmente discreto. Finalmente, se investiga el orden de convergencia del esquema totalmente discreto.

ABSTRACT

The main goal of this thesis is to propose, test and analyze mathematical and computational efficient models for the localization of brain activity from measurements of the electric and magnetic fields on the surface of the head. These measurements can be obtained using electroencephalography or magnetoencephalography. In mathematical terms, this thesis focus in the study of an inverse problem.

First, we consider the inverse source problem for the eddy current approximation of Maxwell equations. We show that as for the full system of Maxwell equations, a volume current source cannot be uniquely identified by the knowledge of the tangential components of the electromagnetic fields on the boundary, and we characterize the space of non-radiating sources. On the other hand, we prove that the inverse source problem has a unique solution if the source is supported on the boundary of a subdomain or if it is the sum of a finite number of dipoles. We address the applicability of this result for the localization of brain activity from electroencephalography and magnetoencephalography measurements.

Afterwards, we analyze the electrostatics problem with a current dipole source. This is a singular problem, since the current dipole model involves first-order derivatives of a Dirac delta measure. Its solution lies in L^p for $1 \leq p < 3/2$ in three dimensional domains and $1 \leq p < 2$ in the two dimensional case. We consider the numerical approximation of the forward problem by means of standard piecewise linear continuous finite elements. We prove a priori error estimates in L^p norm. Then, we propose a residual-type a posteriori error estimator. We prove that it is reliable and efficient; namely, it yields global upper and local lower bounds for the corresponding norms of the error. Finally, we use this estimator to guide an adaptive procedure, which is experimentally shown to lead to an optimal order of convergence.

Subsequently, we compare different approximation methods for the solution of the direct problem in the case of a domain with several regions with different conductivities. For the direct problem, we analyze the case in which the dipole is located at an interface between two regions with different conductivities. In this specific case we use an approximation of the delta function since other methods are not defined in this situation. On the other hand, for the inverse problem, we analyze the results obtained using the previous methods and one last method that incorporates an adaptive procedure guided by the a posteriori error estimator found in Chapter 4. Two situations are considered: a source located within a homogeneous region and the case where the source is close to an interface. We study also the case of a distributed source and we compare the lead field matrices when the support of such source is located within a homogeneous

region and when its support is close to an interface.

Finally, the three-dimensional eddy current time-dependent problem is considered. We formulate it in terms of two variables, one lying only on the conducting domain and the other on its boundary. We combine finite elements (FEM) and boundary elements (BEM) to obtain a FEM-BEM coupled variational formulation. We establish the existence and uniqueness of the solution in the continuous and the fully discrete case. Finally, we investigate the convergence order of the fully discrete scheme.

Contents

1	Introducción	1
1.1	Modelización del problema	3
1.2	Organización de la tesis	7
2	Introduction	11
2.1	Modelization the problem	13
2.2	Organization of the thesis	17
3	Inverse source problems for eddy current equations	21
3.1	Introduction	21
3.2	Non-uniqueness of volume currents	25
3.3	Uniqueness of surface currents	28
3.4	Uniqueness for dipole sources	29
3.4.1	Explicit determination of the dipole source	33
3.5	Application to EEG/MEG	35
4	A posteriori error estimates for the problem of electrostatics with a dipole source	37
4.1	Introduction	37
4.2	Model problem	38
4.2.1	Continuous problem	39
4.2.2	Discrete problem	40
4.3	Preliminary results	43
4.4	An a posteriori error estimator	48
4.4.1	Reliability	49
4.4.2	Efficiency	50
4.5	Three-dimensional case	57
4.6	Numerical experiments	59

4.6.1	Test 1. Isotropic constant conductivity	59
4.6.2	Test 2. Anisotropic non-constant conductivity	63
4.6.3	Test 3. Anisotropic constant conductivity	64
5	Numerical behavior of different approximation methods for the direct and inverse problems of electrostatics with a dipole source	67
5.1	Introduction	67
5.1.1	Continuous problem	68
5.1.2	Discrete problem	72
5.2	General considerations for \boldsymbol{x}_0 on the interface between two regions with different conductivities	75
5.2.1	Test 1.	75
5.2.2	Test 2.	82
5.3	Inverse problem	83
5.3.1	Test 3.	85
5.3.2	Test 4.	88
5.4	Lead field matrix	89
5.4.1	Test 5.	94
5.4.2	Test 6.	97
5.4.3	Test 7.	98
5.5	Conclusions	99
6	Analysis of a FEM-BEM model posed on the conducting domain for the time-dependent eddy current problem	101
6.1	Introduction	101
6.2	Preliminaries	102
6.2.1	Basic spaces for time dependent problems	103
6.3	The model problem	103
6.4	A FEM-BEM coupling variational formulation	107
6.4.1	Existence and Uniqueness.	111
6.5	Fully-discrete scheme	112
6.5.1	Matrix form	118
6.6	Error estimates	120
7	Conclusiones y trabajo futuro	127
7.1	Conclusiones	127

7.2 Trabajo futuro 129

Bibliography **131**

Chapter 1

Introducción

El lograr reconstruir las fuentes de corrientes del cerebro humano es materia de interés en la investigación cognitiva y en la rutina clínica. Tal reconstrucción es posible a través de medidas del potencial eléctrico y del flujo magnético generados. El potencial eléctrico se mide mediante electrodos fijados en el cuero cabelludo (EEG) y el flujo magnético, mediante magnetómetros particularmente sensibles, situados a poca distancia de la superficie de la cabeza (MEG).

La actividad electromagnética del cerebro se debe al movimiento de iones en las regiones activadas. Este movimiento genera las llamadas *corrientes impresas* (o corrientes primarias) que a su vez generan las corrientes óhmicas en el medio que las rodea llamadas *corrientes de retorno*. Las mediciones que se obtienen mediante EEG y MEG corresponden a ambas corrientes, pero la fuente de interés son las corrientes impresas, dado que ellas representan el área de actividad neuronal asociada a un estímulo sensorial.

El primer EEG en una persona fue efectuado por H. Berger en 1924. El midió diferencias de potencial eléctrico entre pares de electrodos ubicados en el cuero cabelludo. Hoy en día estos electrodos pueden ser pegados directamente a la piel o insertados en una gorra elástica, y es usual que hayan hasta 256 electrodos.

El primer MEG fue realizado a finales de 1960 por D. Cohen. La señal magnética en relación con la actividad cerebral es extremadamente débil, aproximadamente 100 veces menor que el campo geomagnético de la tierra. Su medición sólo llega a ser posible con el magnetómetro SQUID (Superconducting QUantum Interface Devices) introducido por Zimmerman [70]. Esta instrumentación mide algunas componentes de la inducción magnética en diferentes ubicaciones, hoy en día hasta 100, cercanas pero externas a la cabeza.

La localización de la fuente es un problema inverso: conociendo el valor del campo magnético o del campo eléctrico sobre la superficie de la cabeza (o, posiblemente, externo a la cabeza, pero cercano a su superficie), el objetivo es determinar la posición y algunas características físicas de

la densidad de corriente que ha generado esos valores.

Dado que la distribución dentro de un conductor no se puede recuperar únicamente a partir del conocimiento del campo electromagnético fuera del conductor, el problema matemático no tiene una única solución si no se asumen algunas condiciones adicionales sobre la fuente (ver Sarvas [61]). Han sido utilizados principalmente dos aproximaciones distintas para reconstruir la fuente de actividad cerebral: el *modelo dipolar* y de *corriente distribuida* con espacios de parámetros discretos. En el modelo dipolar la densidad de corriente primaria es representada como

$$\mathbf{J}_p = \mathbf{p}\delta_{\mathbf{x}_0},$$

donde \mathbf{x}_0 corresponde a la *localización* del dipolo y $\mathbf{p} \neq \mathbf{0}$, recibe el nombre de *polarización*. Este enfoque es coherente con la realidad dado que las corrientes impresas son unidireccionales y se deben a la activación de un gran número de células piramidales concentradas en una región pequeña. En general, se asume que la densidad de corriente primaria se puede descomponer como una suma de un número fijo (y no muy alto) de dipolos. Encontrar la posición de estos dipolos, se transforma en una búsqueda no lineal por mínimos cuadrados.

Por otra parte, en el caso de la fuente distribuida con espacio de parámetros discretos, se discretiza la región del cerebro donde se sabe que se genera la corriente impresa. Después se resuelve un problema de tipo lineal donde sólo los momentos dipolares tienen que ser reconstruidos, no la localización ni la orientación.

Dado que el espectro de frecuencias para señales electrofisiológicas en EEG y MEG está bajo los 1000 Hz, frecuentemente entre 0.1 y 100 Hz, la mayoría de los trabajos teóricos sobre aplicaciones biomédicas, tales como [29, 34, 36, 44, 67] usan la *aproximación estática de las ecuaciones de Maxwell* en la cual la variación temporal tanto del campo eléctrico como magnético se omiten. El modelo estático no es la única simplificación posible de las ecuaciones de Maxwell. Otros modelos que se pueden tener en cuenta son el *modelo electro-cuasiestático*, en el cual la variación temporal de la inducción magnética no es considerada, y el *modelo magneto-cuasiestático o ecuaciones de corrientes inducidas*, las cuales se derivan de las ecuaciones de Maxwell donde lo que se desprecia es la derivada temporal del campo eléctrico. También es posible estudiar el problema usando el *sistema completo de Maxwell*. Algunas referencias respecto a este punto de vista son [7, 3, 40].

El objetivo de esta tesis es analizar y proponer nuevos modelos en el estudio matemático, teórico y numérico de la electroencefalografía y la magnetoencefalografía. Se ha comenzado estudiando el modelo de corrientes inducidas y la posibilidad de usarlo en este contexto. En relación a estas ecuaciones, dentro de esta tesis se ha analizado un nuevo método numérico. También se ha estudiado el modelo electrostático usado generalmente en estas aplicaciones. En

concreto, para el modelo estático se ha desarrollado un análisis a priori y a posteriori del error en la aproximación mediante elementos finitos. El estimador encontrado se ha utilizado para idear una estrategia computacional mediante la cual es posible resolver el problema inverso en modo eficiente. Se han investigado también nuevos modelos para la aproximación de la corriente primaria, robustos desde el punto de vista computacional.

A continuación se introducen en forma detallada cada uno de los conjuntos de ecuaciones previamente mencionados.

1.1 Modelización del problema

Las ecuaciones de Maxwell son un conjunto de cuatro ecuaciones que describen por completo los fenómenos electromagnéticos. James Clerk Maxwell contribuyó reuniendo en estas ecuaciones largos años de resultados experimentales, debidos a Coulomb, Gauss, Ampère, Faraday y otros.

El sistema completo de ecuaciones de Maxwell corresponde a

$$\left\{ \begin{array}{ll} \frac{\partial \mathcal{D}}{\partial t} + \mathcal{J} = \text{curl } \mathcal{H} & \text{(ley de Maxwell - Ampère)} \\ \frac{\partial \mathcal{B}}{\partial t} + \text{curl } \mathcal{E} = \mathbf{0} & \text{(ley de Faraday)} \\ \text{div } \mathcal{D} = \rho & \text{(ley Eléctrica de Gauss)} \\ \text{div } \mathcal{B} = 0 & \text{(ley Magnética de Gauss)} \end{array} \right. \quad (1.1)$$

donde \mathcal{E} es el campo eléctrico, \mathcal{D} es el desplazamiento eléctrico, \mathcal{H} es el campo magnético, \mathcal{B} es la inducción magnética, \mathcal{J} es la densidad de corriente y ρ es la densidad de carga libre. Todos los campos que aparecen en estas ecuaciones son funciones vectoriales que dependen de la variable espacial $\mathbf{x} \in \mathbb{R}^3$ y del tiempo t .

Los distintos campos \mathcal{E} , \mathcal{D} , \mathcal{B} y \mathcal{H} están relacionados por medio de las leyes constitutivas, las cuales dependen de los materiales que forman el dominio de estudio. Usualmente se asume una dependencia lineal de la forma $\mathcal{D} = \boldsymbol{\varepsilon} \mathcal{E}$, $\mathcal{B} = \boldsymbol{\mu} \mathcal{H}$, donde $\boldsymbol{\varepsilon}$ y $\boldsymbol{\mu}$ reciben el nombre de *permitividad eléctrica* y *permeabilidad magnética*, respectivamente. En los problemas más interesantes de la física e ingeniería, la región de interés está compuesta de un medio no homogéneo y no isotrópico: esto es, $\boldsymbol{\varepsilon}$ y $\boldsymbol{\mu}$ no son constantes, pero son matrices simétricas y uniformemente definidas positivas con coeficientes que son funciones acotadas dependientes de la posición. En general, también puede considerarse una dependencia no lineal entre \mathcal{D} y \mathcal{E} , \mathcal{B} y \mathcal{H} (por ejemplo, para problemas de histéresis). Sin embargo en esta tesis, se considerará sólo una dependencia de tipo lineal.

El sistema se completa con la *ley de Ohm* que relaciona la densidad de corriente en el

conductor con el campo eléctrico de la siguiente manera:

$$\mathcal{J} = \boldsymbol{\sigma}\mathcal{E},$$

donde $\boldsymbol{\sigma}$ recibe el nombre de *conductividad eléctrica*, la cual, en regiones conductoras se supone que es una matriz simétrica y definida positiva (con coeficientes que son funciones acotadas dependientes de la posición), mientras que es nula en regiones no conductoras o dieléctricos.

Cuando el problema está dado por una densidad de corriente aplicada \mathcal{J}_e , uno necesita considerar la *ley de Ohm generalizada* $\mathcal{J} = \boldsymbol{\sigma}\mathcal{E} + \mathcal{J}_e$. Como consecuencia de la ecuación de Maxwell-Ampère y la ecuación eléctrica de Gauss, es necesario asumir que $\text{div } \mathcal{J}_e = 0$ en cualquier región no conductora y libre de cargas.

Esta tesis, con excepción del Capítulo 6, se centra en problemas en donde las cantidades físicas varían periódicamente en el tiempo, lo cual generalmente sucede cuando la densidad de corriente aplicada \mathcal{J}_e es una corriente alterna, a saber,

$$\mathcal{J}_e(\mathbf{x}, t) = \mathbf{J}_*(\mathbf{x}) \cos(\omega t + \phi),$$

donde \mathbf{J}_* es una función vectorial en \mathbb{R}^3 , $\omega \neq 0$ es la frecuencia angular y ϕ es el ángulo de fase. Esto es equivalente a la representación

$$\mathcal{J}_e(\mathbf{x}, t) = \text{Re}[\mathbf{J}_*(\mathbf{x})e^{i(\omega t + \phi)}] = \text{Re}[\mathbf{J}_e(\mathbf{x})e^{i\omega t}]$$

donde se ha introducido la función de variable compleja $\mathbf{J}_e(\mathbf{x}) = \mathbf{J}_*(\mathbf{x})e^{i\omega\phi}$. De acuerdo a esto, se busca una solución periódica en el tiempo dada por

$$\mathcal{E}(\mathbf{x}, t) = \text{Re}[\mathbf{E}(\mathbf{x})e^{i\omega t}],$$

$$\mathcal{H}(\mathbf{x}, t) = \text{Re}[\mathbf{H}(\mathbf{x})e^{i\omega t}],$$

donde \mathbf{E} y \mathbf{H} son funciones vectoriales cuyas entradas corresponden a valores complejos (a menudo llamadas “fasores”). Las ecuaciones de Maxwell armónicas en el tiempo que corresponden a las siguientes:

$$\begin{cases} \text{curl } \mathbf{H} - (i\omega\boldsymbol{\varepsilon} + \boldsymbol{\sigma})\mathbf{E} = \mathbf{J}_e & \text{en } \Omega, \\ \text{curl } \mathbf{E} + i\omega\boldsymbol{\mu}\mathbf{H} = \mathbf{0} & \text{en } \Omega, \end{cases} \quad (1.2)$$

donde Ω corresponde al dominio físico. Tales ecuaciones se derivan directamente del sistema completo bajo las suposiciones que se hicieron previamente.

Notar que la ecuación magnética de Gauss $\text{div } (\boldsymbol{\mu}\mathbf{H}) = 0$ es una consecuencia de la ecuación de Faraday.

Como se ha observado en experimentos y también establece la ley de Faraday, una variación temporal del campo magnético genera un campo eléctrico. Por tanto, en cada conductor surge

una densidad de corriente $\mathbf{J}_{eddy} = \boldsymbol{\sigma}\mathbf{E}$; este término expresa la presencia en un medio conductor de las corrientes inducidas.

Cuando el término de desplazamiento de corriente $\frac{\partial \mathcal{D}}{\partial t}$ (o en forma equivalente, $i\omega\boldsymbol{\varepsilon}\mathbf{E}$) es despreciado, el sistema de ecuaciones que se obtiene recibe el nombre de aproximación por corrientes inducidas de las ecuaciones de Maxwell (o aproximación magneto-cuasiestática). En el caso armónico en el tiempo, el sistema de ecuaciones corresponde a

$$\begin{cases} \operatorname{curl} \mathbf{H} - \boldsymbol{\sigma}\mathbf{E} = \mathbf{J}_e & \text{en } \Omega, \\ \operatorname{curl} \mathbf{E} + i\omega\boldsymbol{\mu}\mathbf{H} = \mathbf{0} & \text{en } \Omega, \\ \operatorname{div}(\boldsymbol{\varepsilon}\mathbf{E}) = 0 & \text{en } \Omega_I, \end{cases} \quad (1.3)$$

donde Ω_I corresponde al dieléctrico. Como en el caso del sistema completo de Maxwell, se debe asumir que

$$\operatorname{div} \mathbf{J}_e = 0 \quad \text{en } \Omega_I. \quad (1.4)$$

También se desprende de este conjunto de ecuaciones la restricción $\operatorname{div}(\boldsymbol{\mu}\mathbf{H}) = 0$, la cual se sigue de la ley de Faraday. Finalmente, notamos que en la aproximación por corrientes inducidas $\operatorname{div}(\boldsymbol{\varepsilon}\mathbf{E}) = 0$ en Ω_I , lo que asegura que la carga eléctrica se anula en el dieléctrico, lo cual no es una consecuencia de la ecuación de Ampère ni de (1.4).

Cuando se consideran problemas dependientes del tiempo y la variación temporal de los campos es lenta, uno puede simplificar el modelo de ecuaciones de Maxwell, despreciando las derivadas temporales $\frac{\partial \mathcal{D}}{\partial t}$ y $\frac{\partial \mathcal{B}}{\partial t}$ (o en el caso de las ecuaciones armónicas en el tiempo, esto equivale a considerar $\omega = 0$). Tal modelo recibe el nombre de modelo electro-magnetostático. En el caso armónico en el tiempo, las ecuaciones corresponden a

$$\begin{cases} \operatorname{curl} \mathbf{H} - \boldsymbol{\sigma}\mathbf{E} = \mathbf{J}_e & \text{en } \Omega, \\ \operatorname{curl} \mathbf{E} = \mathbf{0} & \text{en } \Omega, \\ \operatorname{div}(\boldsymbol{\mu}\mathbf{H}) = 0 & \text{en } \Omega, \\ \operatorname{div}(\boldsymbol{\varepsilon}\mathbf{E}) = 0 & \text{en } \Omega_I. \end{cases} \quad (1.5)$$

De la segunda ecuación de (1.5), se deriva que el campo eléctrico es un gradiente de un potencial escalar $\mathbf{E} = -\nabla V$ y por tanto, de la primera ecuación en (1.5) se obtiene

$$\operatorname{div}(\boldsymbol{\sigma}\nabla V) = \operatorname{div} \mathbf{J}_e.$$

Así, se obtiene el siguiente sistema de ecuaciones:

$$\left\{ \begin{array}{ll} \operatorname{div}(\boldsymbol{\sigma}\nabla V) = \operatorname{div} \mathbf{J}_e & \text{en } \Omega_C, \\ \operatorname{curl} \mathbf{H} - \boldsymbol{\sigma}\nabla V = \mathbf{J}_e & \text{en } \Omega, \\ \operatorname{div}(\boldsymbol{\mu}\mathbf{H}) = 0 & \text{en } \Omega, \\ \operatorname{div}(\boldsymbol{\varepsilon}\nabla V) = 0 & \text{en } \Omega_I. \end{array} \right. \quad (1.6)$$

donde Ω_C corresponde al conductor. Ahora se presentan las geometrías, propiedades de las cantidades físicas y ecuaciones junto con condiciones de frontera, que se utilizaron en cada capítulo de esta tesis.

En el Capítulo 3 se considera un conductor $\Omega_C \subset \mathbb{R}^3$, el cual representa una parte del cuerpo humano. Se asume que Ω_C es un dominio acotado con una frontera Lipschitz y conexa Γ . En el conductor, la conductividad es una matriz simétrica y uniformemente definida positiva con coeficientes en L^∞ . También se considera un dominio computacional $\Omega \subset \mathbb{R}^3$, que contiene completamente a Ω_C . El dominio Ω es un dominio acotado y simplemente conexo y con frontera Lipschitz $\partial\Omega$. El dieléctrico se define como $\Omega_I := \Omega \setminus \overline{\Omega}_C$. Éste es un conjunto conexo y corresponde al aire que rodea la cabeza. La permeabilidad magnética y la permitividad eléctrica son matrices simétricas y uniformemente definidas positivas con coeficientes en L^∞ . Por otra parte, en la frontera exterior $\partial\Omega$ se impone la condición de frontera magnética $\mathbf{H} \times \mathbf{n} = \mathbf{0}$. Además, agregamos la condición necesaria para la unicidad $\operatorname{div}(\boldsymbol{\varepsilon}\mathbf{E}) = 0$ en Ω_I . Cuando se impone una condición de frontera magnética sobre la frontera, se debe imponer otra condición de frontera necesaria: $\boldsymbol{\varepsilon}\mathbf{E} \cdot \mathbf{n} = 0$ sobre $\partial\Omega$. Así, el sistema de ecuaciones se convierte en

$$\left\{ \begin{array}{ll} \operatorname{curl} \mathbf{H} - \boldsymbol{\sigma}\mathbf{E} = \mathbf{J}_e & \text{en } \Omega, \\ \operatorname{curl} \mathbf{E} + i\omega\boldsymbol{\mu}\mathbf{H} = \mathbf{0} & \text{en } \Omega, \\ \operatorname{div}(\boldsymbol{\varepsilon}\mathbf{E}) = 0, & \text{en } \Omega_I \\ \boldsymbol{\varepsilon}\mathbf{E} \cdot \mathbf{n} = 0 & \text{sobre } \partial\Omega, \\ \mathbf{H} \times \mathbf{n} = \mathbf{0} & \text{sobre } \partial\Omega, \end{array} \right. \quad (1.7)$$

donde la fuente \mathbf{J}_e es una fuente distribuida ($\mathbf{J}_e \in (L^2(\Omega_C))^2$) o una corriente superficial ($\mathbf{J}_e \in H^{-1/2}(\operatorname{div}_\tau; \partial B)$ con $B \subset \mathbb{R}^3$ abierto y conexo, con frontera Lipschitz ∂B y satisface $\overline{B} \subset \Omega_C$) o una corriente dipolar ($\mathbf{J}_e = \sum_{k=1}^M \mathbf{p}_k \delta_{\mathbf{x}_k}$, con \mathbf{x}_k punto interior de Ω_C , $k = 1, \dots, M$). Serán necesarias condiciones adicionales sobre la conductividad $\boldsymbol{\sigma}$, condiciones sobre las cuales se dará más detalle en este capítulo.

En Capítulos 4 y 5, se considera el modelo electrostático, en el cual sólo es de interés encontrar el campo eléctrico y deriva del modelo electro-magnetostático. Como conductor, se considera un

abierto acotado $\Omega_C \subset \mathbb{R}^d$, donde d puede tomar los valores 2 o 3 en Capítulo 4 y toma el valor 2 en Capítulo 5. Se considera como condición de frontera $(\boldsymbol{\sigma}\nabla V) \cdot \mathbf{n} = 0$ sobre $\partial\Omega_C$, la cual viene del hecho que $\operatorname{div}(\mathbf{J}_e - \boldsymbol{\sigma}\nabla V) = \operatorname{div}(\operatorname{curl} \mathbf{H}) = 0$ en Ω , de aquí $(\mathbf{J}_e - \boldsymbol{\sigma}\nabla V) \cdot \mathbf{n}$ no tiene saltos sobre $\partial\Omega_C$. Además \mathbf{J}_e se localiza en el interior de la cabeza y la conductividad se anula fuera de ella. Por tanto, el conjunto de ecuaciones que modelan tal problema es el siguiente:

$$\begin{cases} \operatorname{div}(\boldsymbol{\sigma}\nabla V) = \operatorname{div}(\mathbf{p}\delta_{\mathbf{x}_0}) & \text{en } \Omega_C, \\ (\boldsymbol{\sigma}\nabla V) \cdot \mathbf{n} = 0 & \text{sobre } \partial\Omega_C. \end{cases} \quad (1.8)$$

La conductividad $\boldsymbol{\sigma}$ corresponde a una matriz simétrica y uniformemente definida positiva, con coeficientes en $L^\infty(\Omega_C)$. Para probar existencia y unicidad de solución de tal problema, es necesario asumir una mayor regularidad de $\boldsymbol{\sigma}$ en un entorno del soporte de la delta; en concreto los coeficientes de la matriz $\boldsymbol{\sigma}$ deben pertenecer a $W^{1,\infty}(B_{r_0}(\mathbf{x}_0))$, donde $B_{r_0}(\mathbf{x}_0) := \{\mathbf{x} \in \mathbb{R}^d : |\mathbf{x} - \mathbf{x}_0| < r_0\}$ para un r_0 adecuado.

Finalmente, en el Capítulo 6, se considera como dominio conductor $\Omega_C \subset \mathbb{R}^3$ el cual es un poliedro conexo, acotado, con frontera Γ conexa y Lipschitz continua. El dieléctrico, corresponde a $\Omega_I := \mathbb{R}^3 \setminus \overline{\Omega_C}$ el cual también es conexo. Se consideran las ecuaciones de corrientes inducidas dependientes del tiempo que corresponden a

$$\begin{cases} \partial_t(\boldsymbol{\mu}\mathbf{H}) + \operatorname{curl} \mathbf{E} = \mathbf{0} & \text{in } \mathbb{R}^3 \times (0, T), \\ \operatorname{curl} \mathbf{H} - \boldsymbol{\sigma}\mathbf{E} = \mathbf{J}_e & \text{in } \mathbb{R}^3 \times [0, T], \\ \operatorname{div}(\boldsymbol{\varepsilon}\mathbf{E}) = 0 & \text{in } \Omega_I \times [0, T], \\ \mathbf{H}(\mathbf{x}, t), \mathbf{E}(\mathbf{x}, t) = \mathcal{O}(|\mathbf{x}|^{-1}) & \text{as } |\mathbf{x}| \rightarrow \infty, \\ \mathbf{H}(\mathbf{x}, 0) = \mathbf{H}_0(\mathbf{x}) & \mathbf{x} \in \mathbb{R}^3, \end{cases} \quad (1.9)$$

donde $T > 0$, la densidad de corriente $\mathbf{J}_e \in L^2(0, T; (L^2(\Omega_C))^3)$ y además tiene soporte compacto en el conductor. La cuarta condición de (1.9) se satisface uniformemente en $[0, T]$. El dato inicial $\mathbf{H}_0 \in (L^2(\Omega_C))^3$ y satisface $\operatorname{div}(\boldsymbol{\mu}\mathbf{H}_0) = 0$ en \mathbb{R}^3 . Los coeficientes $\boldsymbol{\sigma}$, $\boldsymbol{\mu}$ y $\boldsymbol{\varepsilon}$ son matrices simétricas con componentes acotadas. La conductividad es nula en el dieléctrico. La permeabilidad magnética $\boldsymbol{\mu}$ es definida positiva en todo \mathbb{R}^3 y satisface $\boldsymbol{\mu} = \mu_0 I$ en Ω_I , donde I se entiende como la matriz identidad. La permitividad eléctrica $\boldsymbol{\varepsilon}$ es necesaria sólo en el dieléctrico en esta formulación y se asume satisfacer $\boldsymbol{\varepsilon} = \varepsilon_0 I$ en Ω_I ; μ_0 y ε_0 son los coeficientes correspondientes en el vacío.

1.2 Organización de la tesis

Este trabajo se organiza de la siguiente manera. En el **Capítulo 3**, se estudia la unicidad de la solución del problema inverso para el problema de corrientes inducidas, siguiendo el enfoque

propuesto por Albanese y Monk [3] para el sistema de ecuaciones de Maxwell. Como fuente de corriente, se han considerado tres situaciones distintas: una fuente de corriente distribuida, una corriente superficial y finalmente, una corriente dipolar. En relación a la primera, se demuestra que cuando la fuente está en L^2 el problema inverso no tiene una única solución y se caracteriza el espacio de fuentes no radiantes. Con respecto a la segunda, se demuestra que conociendo la componente tangencial del campo eléctrico sobre la frontera del dominio, existe una única corriente superficial que la genera. En el caso de la fuente dipolar, primero se demuestra existencia y unicidad del problema directo y posteriormente, se analiza el problema inverso. Como en el caso de la corriente superficial se demuestra que la componente tangencial del campo eléctrico en el borde del conductor determina de manera única el número de dipolos, localización y polarización. Además, se presenta una fórmula mediante el cual es posible encontrar la fuente dipolar, sabiendo a priori la componente tangencial del campo eléctrico sobre la frontera del dominio. Finalmente, se estudia como encontrar la componente tangencial del campo eléctrico a partir de los datos medidos a través de EEG y MEG. Este capítulo está constituido por el siguiente artículo:

A. ALONSO RODRÍGUEZ, J. CAMAÑO AND A. VALLI, *Inverse source problems for eddy current equations*. Inverse Problems, vol. 28, 1, (2012).

En el **Capítulo 4** usando la formulación estudiada por Valli [65], se desarrolla un análisis a priori y a posteriori para una formulación variacional del problema electrostático, el cual es un problema con singularidad dado que la fuente de corriente contiene derivadas de primer orden de la distribución delta de Dirac. En [65] se demostró que la solución de este problema pertenece a L^p para $1 \leq p < 3/2$ en dominios tridimensionales y siguiendo la misma técnica de demostración, se prueba que la solución en el caso bidimensional también pertenece a L^p , con $1 \leq p < 2$. En este capítulo, se da una estima de error a priori en norma L^p , válida para mallas cuasiuniformes, y se propone un estimador de error a posteriori, el cual se demuestra que resulta confiable y eficiente bajo las hipótesis de convexidad del dominio y mayor regularidad de la conductividad. Todo este análisis se presenta inicialmente en un dominio bidimensional y posteriormente en un dominio tridimensional, pero este último caso bajo suposiciones más restrictivas (geometría cúbica y conductividad constante). Finalmente, el estimador se usa para guiar un procedimiento adaptativo, el cual muestra experimentalmente un orden óptimo de convergencia. Este capítulo está constituido por el siguiente artículo:

A. ALONSO RODRÍGUEZ, J. CAMAÑO, R. RODRÍGUEZ AND A. VALLI, *A posteriori error estimates for the problem of electrostatics with a dipole source*. (enviado).

En el **Capítulo 5** se compara la solución aproximada del problema directo usando el método de substracción y el método directo en el caso concreto de un dominio con varias regiones con distintas conductividades. Para el problema directo, se analiza el caso en el cual el dipolo se localiza cerca o exactamente en una interfaz entre dos regiones con conductividades diferentes. Se estudia también un tercer método que aproxima a la distribución delta de Dirac usando la función característica. Numéricamente se observa que en esta situación el tercer modelo es el único que da buenos resultados. Para el problema inverso se analizan los resultados obtenidos usando los tres métodos ya mencionados y se agrega a estos tres, un último método que corresponde a trabajar el método directo en conjunto con un procedimiento adaptativo guiado por el estimador encontrado en el Capítulo 4. Se consideran dos situaciones: una fuente localizada en el interior de una región y el caso en que la fuente es cercana a una interfaz. Se estudia también el caso de una fuente distribuida y se comparan las matrices de influencia en distintas situaciones. Este capítulo está constituido por el siguiente artículo:

A. ALONSO RODRÍGUEZ, J. CAMAÑO, R. RODRÍGUEZ AND A. VALLI, *Numerical behavior of different approximation methods for the direct and inverse problems of electrostatics with a dipole source.* (en preparación).

Finalmente, en paralelo al trabajo que se presenta en el Capítulo 3, en el **Capítulo 6** se estudia un nuevo método numérico para las ecuaciones de corrientes inducidas dependientes del tiempo en un dominio conductor acotado contenido en \mathbb{R}^3 . El problema se reformula expresando los campos magnético y eléctrico en términos de nuevas variables que resultan ser más convenientes: la primitiva temporal del campo eléctrico la cual desempeña el papel de un potencial vectorial para el campo magnético en el conductor y la traza del potencial escalar magnético en el aislante. Luego, se deriva una formulación FEM-BEM y se demuestra existencia y unicidad de solución para el problema. Se discretiza el problema usando como espacios de discretización el de elementos finitos de Nédélec para la variable definida en el conductor y funciones lineales a trozos y continuas para una variable adicional en la frontera del dominio, la cual surge a partir de las ecuaciones integrales. Para la discretización temporal se usa un método backward Euler. Finalmente, se prueba que el esquema discreto converge con un orden óptimo a la solución. Este capítulo está constituido por el siguiente artículo:

J. CAMAÑO AND R. RODRÍGUEZ, *Analysis of a FEM-BEM model posed on the conducting domain for the time-dependent eddy current problem.* Journal of Computational and Applied Mathematics, vol. 236, issue 13, pp. 3084-3100, (2012).

Es importante resaltar que con respecto al problema inverso, en el primer capítulo son necesarias tanto las mediciones que se obtienen con EEG como con MEG, no así en el tercer y cuarto

capítulo, donde lo que se estudia es el modelo electrostático y por esta misma razón, los únicos datos necesarios son los que se obtienen mediante EEG.

Chapter 2

Introduction

The reconstruction of electromagnetic sources in the human brain is of great interest in cognitive research and in clinical routine. Such reconstruction is possible through measurements of the scalp electric potential and the external magnetic flux. The electric potential is measured by electrodes attached to the scalp (EEG) and magnetic flux through particularly sensitive magnetometers, located within short distance from the surface of the head (MEG).

Electromagnetic activity of the brain is due to the motion of ions in activated regions. This movement generates the so called *impressed currents* (or primary currents) that in turn create ohmic currents in the surrounding environment called *return currents*. The measurements obtained by EEG and MEG correspond to both currents, but the source of interest are the impressed currents, since they represent the area of neural activity associated with sensory stimuli.

The first EEG was performed by H. Berger in 1924. He measured the electric potential differences between pairs of electrodes placed on the scalp. Today these electrodes can be attached directly to the skin or inserted into an elastic cap. Up to 256 electrodes can be used.

The first MEG was realized in late 1960 by D. Cohen. The magnetic signal due to brain activity is extremely weak, approximately 100 times less than the geomagnetic field of the earth. Its measurement becomes possible only with the SQUID magnetometer (Superconducting QUantum Interface Devices) introduced by Zimmerman [70]. This instrumentation measures some components of the magnetic induction in different locations; today these can reach the quantity of 100, near but outside the head.

The location of the source is an inverse problem: knowing the value of the magnetic field or the electric field on the surface of the head (or possibly outside the head, but close to the surface), the goal is to determine the position and some physical characteristics of the current density that generated these values.

Since the distribution inside a conductor can not be recovered only from knowledge of the electromagnetic field outside the conductor, the mathematical problem does not have a unique solution unless some additional conditions are assumed on the source (see Sarvas [61]). There have been used mainly two different approaches to reconstruct the source of the brain activity: the *dipole model* and the *model of a distributed source* (with a discrete spaces). The primary current density in the dipolar model is modeled as

$$\mathbf{J}_p = \mathbf{p}\delta_{\mathbf{x}_0},$$

where \mathbf{x}_0 corresponds to the *location* of the dipole and $\mathbf{p} \neq \mathbf{0}$ is called *polarization*. This is a good approximation of unidirectional impressed currents, due to activation of a large number of pyramidal cells concentrated in a small region. It can also be assumed that the primary current density is decomposed as the sum of a fixed number (not too high) of dipoles. Finding the position of these dipoles becomes a nonlinear least squares search.

On the other hand, in the case of a distributed source with a discrete parameter space, the region of the brain where it is known that the impressed current is generated is triangulated and dipolar sources are placed at fixed points of each element. Then, a linear inverse problem is solved where only the dipole moments have to be rebuilt, not the locations.

Since the frequency spectrum for electrophysiological signals in EEG and MEG is below 1000 Hz, often between 0.1 and 100 Hz, most theoretical works on biomedical applications, such as [29, 34, 36, 44, 67], use the *static approximation of the Maxwell equations* in which the time variation of both electric and magnetic fields are disregarded. The static model is not the only possible simplification of the Maxwell equations. Other models that can be taken into account are the *electro-quasistatic model*, in which the time variation of the magnetic induction is not considered and the *magneto-quasistatic model* or *eddy current equations*, which are derived from the Maxwell equations neglecting is the time derivative of the electric field. It is also possible to study the problem using the *full system of Maxwell*. Some references on this last approach are [7, 3, 40].

The aim of this thesis is to analyze and to propose new models in the mathematical theoretical and numerical study of electroencephalography and magnetoencephalography. We start studying the eddy currents model and the possibility of using it in this context. We analyze a new numerical method for this model. We have also studied the electrostatic model, which is more often used in these applications. Specifically, for the static model a priori and a posteriori analysis of the error in the finite element approximation have been developed. The estimate found has been used to devise a computational strategy by which it is possible to solve the inverse problem in an efficient way. We have also investigated new models for the approximation of the primary current, that are robust from the computational point of view.

In the next section each of the aforementioned sets of equations are introduced in detail.

2.1 Modelization the problem

Maxwell equations are a set of four equations completely describing electromagnetic phenomena. James Clerk Maxwell gathered in these equations, after long years of experimental results, due to Coulomb, Gauss, Ampère, Faraday and others.

The full system of Maxwell equations reads

$$\left\{ \begin{array}{ll} \frac{\partial \mathcal{D}}{\partial t} + \mathcal{J} = \text{curl } \mathcal{H} & \text{(Maxwell - Ampère equation)} \\ \frac{\partial \mathcal{B}}{\partial t} + \text{curl } \mathcal{E} = \mathbf{0} & \text{(Faraday equation)} \\ \text{div } \mathcal{D} = \rho & \text{(Gauss electrical equation)} \\ \text{div } \mathcal{B} = 0 & \text{(Gauss magnetic equation)} \end{array} \right. \quad (2.1)$$

where \mathcal{E} is the electric field, \mathcal{D} is the electric displacement, \mathcal{H} is the magnetic field, \mathcal{B} is the magnetic induction, \mathcal{J} is the current density and ρ is the free charge density. All the fields that appear in these equations are vector functions that depend on the spatial variable $\mathbf{x} \in \mathbb{R}^3$ and the time t .

The fields \mathcal{E} , \mathcal{D} , \mathcal{B} and \mathcal{H} are related by constitutive laws, which depend on the materials that constitute the considered physical domain. Usually a linear dependence of the form $\mathcal{D} = \boldsymbol{\varepsilon} \mathcal{E}$, $\mathcal{B} = \boldsymbol{\mu} \mathcal{H}$ is assumed, where $\boldsymbol{\varepsilon}$ and $\boldsymbol{\mu}$ are called *electric permittivity* and *magnetic permeability*, respectively. In physiological applications the media are non-homogeneous and anisotropic: that is, $\boldsymbol{\varepsilon}$ and $\boldsymbol{\mu}$ are not constant, but are symmetric and uniformly positive definite matrices with coefficients that are bounded functions of the position.

The system is completed by *Ohm law* relating the current density in the conductor with the electric field as follows:

$$\mathcal{J} = \boldsymbol{\sigma} \mathcal{E},$$

where $\boldsymbol{\sigma}$ is called *electric conductivity*, is a symmetric and positive definite matrix in conductive regions (with coefficients that are bounded functions of the position), while it is null in nonconductive regions or dielectrics.

When the problem is driven by an applied current density \mathcal{J}_e , the *generalized Ohm law* $\mathcal{J} = \boldsymbol{\sigma} \mathcal{E} + \mathcal{J}_e$ is considered. As a consequence of the Maxwell-Ampère equation and the Gauss electrical equation, it is necessary to assume that $\text{div } \mathcal{J}_e = 0$ in any free of charge non-conductive region.

This thesis, with the exception of Chapter 6, is centered on problems where the physical quantities vary periodically in time, which usually happens when the current density \mathcal{J}_e is an alternating current, namely

$$\mathcal{J}_e(\mathbf{x}, t) = \mathbf{J}_*(\mathbf{x}) \cos(\omega t + \phi),$$

where \mathbf{J}_* is a vector function in \mathbb{R}^3 , $\omega \neq 0$ is the angular frequency and ϕ is the phase angle. This is equivalent to the representation

$$\mathcal{J}_e(\mathbf{x}, t) = \operatorname{Re}[\mathbf{J}_*(\mathbf{x})e^{i(\omega t + \phi)}] = \operatorname{Re}[\mathbf{J}_e(\mathbf{x})e^{i\omega t}]$$

where the complex variable function $\mathbf{J}_e(\mathbf{x}) = \mathbf{J}_*(\mathbf{x})e^{i\omega\phi}$ has been introduced. Accordingly, we look for a periodic in time solution given by

$$\begin{aligned} \mathcal{E}(\mathbf{x}, t) &= \operatorname{Re}[\mathbf{E}(\mathbf{x})e^{i\omega t}], \\ \mathcal{H}(\mathbf{x}, t) &= \operatorname{Re}[\mathbf{H}(\mathbf{x})e^{i\omega t}], \end{aligned}$$

where \mathbf{E} and \mathbf{H} are vector functions whose entries correspond to complex values (often called “phasors”). The time-harmonic Maxwell equations read:

$$\begin{cases} \operatorname{curl} \mathbf{H} - (i\omega\boldsymbol{\varepsilon} + \boldsymbol{\sigma})\mathbf{E} = \mathbf{J}_e & \text{in } \Omega, \\ \operatorname{curl} \mathbf{E} + i\omega\boldsymbol{\mu}\mathbf{H} = \mathbf{0} & \text{in } \Omega, \end{cases} \quad (2.2)$$

where Ω corresponds to the physical domain. They are derived directly from the complete system under the assumptions above.

Note that the Gauss magnetic equation $\operatorname{div}(\boldsymbol{\mu}\mathbf{H}) = 0$ is a consequence of the Faraday equation.

A time-variation of the magnetic field generates an electric field. Therefore, in each conductor a current density $\mathbf{J}_{eddy} = \boldsymbol{\sigma}\mathbf{E}$ arises; this term expresses the presence in conducting media of the so-called eddy current.

When the displacement current term $\frac{\partial \mathcal{D}}{\partial t}$ (or equivalently, $i\omega\boldsymbol{\varepsilon}\mathbf{E}$) is neglected, the system of equations obtained is called eddy current approximation of the Maxwell equations (or magneto-quasistatic approximation). In the time-harmonic case, the system of equations is

$$\begin{cases} \operatorname{curl} \mathbf{H} - \boldsymbol{\sigma}\mathbf{E} = \mathbf{J}_e & \text{in } \Omega, \\ \operatorname{curl} \mathbf{E} + i\omega\boldsymbol{\mu}\mathbf{H} = \mathbf{0} & \text{in } \Omega, \\ \operatorname{div}(\boldsymbol{\varepsilon}\mathbf{E}) = 0 & \text{in } \Omega_I, \end{cases} \quad (2.3)$$

where Ω_I corresponds to the dielectric. As for the full-Maxwell system, it must be assumed that

$$\operatorname{div} \mathbf{J}_e = 0 \quad \text{in } \Omega_I. \quad (2.4)$$

From Faraday law it follows that $\operatorname{div}(\boldsymbol{\mu}\mathbf{H}) = 0$. Equation $\operatorname{div}(\boldsymbol{\varepsilon}\mathbf{E}) = 0$ in Ω_I ensures that the electric charge vanishes in the dielectric, which is not a consequence of the Ampère equation or (2.4).

When time-dependent problems are considered and time-variation of the fields is slow, one can simplify the model of the Maxwell equations, neglecting both time derivatives $\frac{\partial \mathcal{D}}{\partial t}$ and $\frac{\partial \mathcal{B}}{\partial t}$ (or in the time-harmonic case, this is equivalent to consider $\omega = 0$). Such a model is called electro-magnetostatic model. In the time-harmonic case, the equations are

$$\begin{cases} \operatorname{curl} \mathbf{H} - \boldsymbol{\sigma}\mathbf{E} = \mathbf{J}_e & \text{in } \Omega, \\ \operatorname{curl} \mathbf{E} = \mathbf{0} & \text{in } \Omega, \\ \operatorname{div}(\boldsymbol{\mu}\mathbf{H}) = 0 & \text{in } \Omega, \\ \operatorname{div}(\boldsymbol{\varepsilon}\mathbf{E}) = 0 & \text{in } \Omega_I. \end{cases} \quad (2.5)$$

From the second equation in (2.5), for a simply-connected domain Ω it follows that the electric field is a gradient of a scalar potential $\mathbf{E} = -\nabla V$ and therefore from the first equation in (2.5) we obtain

$$\operatorname{div}(\boldsymbol{\sigma}\nabla V) = \operatorname{div} \mathbf{J}_e.$$

Thus, we have the following system of equations:

$$\begin{cases} \operatorname{div}(\boldsymbol{\sigma}\nabla V) = \operatorname{div} \mathbf{J}_e & \text{in } \Omega_C, \\ \operatorname{curl} \mathbf{H} - \boldsymbol{\sigma}\nabla V = \mathbf{J}_e & \text{in } \Omega, \\ \operatorname{div}(\boldsymbol{\mu}\mathbf{H}) = 0 & \text{in } \Omega, \\ \operatorname{div}(\boldsymbol{\varepsilon}\nabla V) = 0 & \text{in } \Omega_I, \end{cases} \quad (2.6)$$

where Ω_C corresponds to the conductor. In the chapters of this thesis we consider different electromagnetic models.

In Chapter 3 we focus on the time-harmonic eddy-current model. We consider a conductor $\Omega_C \subset \mathbb{R}^3$, which represents a part of the human body. We assume that Ω_C is a bounded domain with a Lipschitz and connected boundary Γ . In the conductor, the conductivity is a symmetric and uniformly positive definite matrix with coefficients in L^∞ . Also we consider a computational domain $\Omega \subset \mathbb{R}^3$, which completely contains Ω_C . The domain Ω is a bounded and simply-connected domain with Lipschitz boundary $\partial\Omega$. The dielectric is defined as $\Omega_I := \Omega \setminus \overline{\Omega}_C$. It is assumed to be connected and corresponds to the air surrounding the head. The magnetic permeability and the electric permittivity are symmetric and uniformly positive definite matrices with coefficients in L^∞ . Moreover, at the external border $\partial\Omega$ we impose a magnetic boundary condition $\mathbf{H} \times \mathbf{n} = \mathbf{0}$. Also, we add the condition $\operatorname{div}(\boldsymbol{\varepsilon}\mathbf{E}) = 0$ in Ω_I that is necessary for

uniqueness. When we impose a magnetic boundary condition on the boundary, we must impose the other necessary boundary condition $\boldsymbol{\varepsilon}\mathbf{E}\cdot\mathbf{n} = 0$ on $\partial\Omega$. Thus, the system of equations becomes

$$\left\{ \begin{array}{ll} \operatorname{curl} \mathbf{H} - \boldsymbol{\sigma}\mathbf{E} = \mathbf{J}_e & \text{in } \Omega, \\ \operatorname{curl} \mathbf{E} + i\omega\boldsymbol{\mu}\mathbf{H} = \mathbf{0} & \text{in } \Omega, \\ \operatorname{div}(\boldsymbol{\varepsilon}\mathbf{E}) = 0, & \text{in } \Omega_I, \\ \boldsymbol{\varepsilon}\mathbf{E}\cdot\mathbf{n} = 0 & \text{on } \partial\Omega, \\ \mathbf{H}\times\mathbf{n} = \mathbf{0} & \text{on } \partial\Omega, \end{array} \right. \quad (2.7)$$

where the source \mathbf{J}_e is a distributed source ($\mathbf{J}_e \in (L^2(\Omega_C))^2$) or a surface current ($\mathbf{J}_e \in H^{-1/2}(\operatorname{div}_\tau; \partial B)$ with $B \subset \mathbb{R}^3$ open and connected, with Lipschitz boundary ∂B and satisfying $\overline{B} \subset \Omega_C$) or a current dipole ($\mathbf{J}_e = \sum_{k=1}^M \mathbf{p}_k \delta_{\mathbf{x}_k}$, with \mathbf{x}_k an internal point of Ω_C , $k = 1, \dots, M$). Additional necessary conditions on the conductivity $\boldsymbol{\sigma}$, have to be added, and about them we give more details in this chapter.

In Chapters 4 and 5 we consider the electrostatic model, a reduced form of the electro-magnetostatic model. We work in an open bounded conductor domain $\Omega_C \subset \mathbb{R}^d$, where d can take the values 2 or 3 in Chapter 4 and take the value 2 in Chapter 5. The boundary condition is $(\boldsymbol{\sigma}\nabla V)\cdot\mathbf{n} = 0$ on $\partial\Omega_C$. This comes from the fact that $\operatorname{div}(\mathbf{J}_e - \boldsymbol{\sigma}\nabla V) = \operatorname{div}(\operatorname{curl} \mathbf{H}) = 0$ in Ω , hence $(\mathbf{J}_e - \boldsymbol{\sigma}\nabla V)\cdot\mathbf{n}$ does not jump on $\partial\Omega_C$; moreover, \mathbf{J}_e is located inside the head and conductivity vanishes outside it. Therefore, the boundary value problem that we study is:

$$\left\{ \begin{array}{ll} \operatorname{div}(\boldsymbol{\sigma}\nabla V) = \operatorname{div}(\mathbf{p}\delta_{\mathbf{x}_0}) & \text{in } \Omega_C, \\ (\boldsymbol{\sigma}\nabla V)\cdot\mathbf{n} = 0 & \text{sobre } \partial\Omega_C. \end{array} \right. \quad (2.8)$$

The conductivity $\boldsymbol{\sigma}$ corresponds to a symmetric and uniformly positive definite matrix, with coefficients in $L^\infty(\Omega_C)$. To prove existence and uniqueness of solution of this problem, it is necessary to assume higher regularity of $\boldsymbol{\sigma}$ in a vicinity of the support of the delta distribution, in particular the coefficients of $\boldsymbol{\sigma}$ must belong to $W^{1,\infty}(B_{r_0}(\mathbf{x}_0))$, where $B_{r_0}(\mathbf{x}_0) := \{\mathbf{x} \in \mathbb{R}^d : |\mathbf{x} - \mathbf{x}_0| < r_0\}$ for a suitable r_0 .

Finally, in Chapter 6 we focus on the time-dependent eddy current model in the whole space. The conductor $\Omega_C \subset \mathbb{R}^3$ is a bounded connected polyhedron with boundary Γ connected and Lipschitz continuous. The dielectric, $\Omega_I := \mathbb{R}^3 \setminus \overline{\Omega}_C$ is assumed to be connected. The boundary value problem reads:

$$\left\{ \begin{array}{ll} \partial_t(\boldsymbol{\mu}\mathbf{H}) + \operatorname{curl} \mathbf{E} = \mathbf{0} & \text{in } \mathbb{R}^3 \times (0, T), \\ \operatorname{curl} \mathbf{H} - \boldsymbol{\sigma}\mathbf{E} = \mathbf{J}_e & \text{in } \mathbb{R}^3 \times [0, T], \\ \operatorname{div}(\boldsymbol{\varepsilon}\mathbf{E}) = 0 & \text{in } \Omega_I \times [0, T], \\ \mathbf{H}(\mathbf{x}, t), \mathbf{E}(\mathbf{x}, t) = \mathcal{O}(|\mathbf{x}|^{-1}) & \text{as } |\mathbf{x}| \rightarrow \infty, \\ \mathbf{H}(\mathbf{x}, 0) = \mathbf{H}_0(\mathbf{x}) & \mathbf{x} \in \mathbb{R}^3, \end{array} \right. \quad (2.9)$$

where $T > 0$, the current density $\mathbf{J}_e \in L^2(0, T; (L^2(\Omega_C))^3)$ and has compact support in the conductor. The fourth condition of (2.9) is satisfied uniformly in $[0, T]$. The initial datum satisfies $\mathbf{H}_0 \in (L^2(\Omega_C))^3$ and $\operatorname{div}(\boldsymbol{\mu}\mathbf{H}_0) = 0$ in \mathbb{R}^3 . The coefficients $\boldsymbol{\sigma}$, $\boldsymbol{\mu}$ and $\boldsymbol{\varepsilon}$ are symmetric matrices with bounded elements. The conductivity vanishes in the dielectric. The magnetic permeability $\boldsymbol{\mu}$ is positive definite at all \mathbb{R}^3 and satisfies $\boldsymbol{\mu} = \mu_0 I$ in Ω_I , where I is the identity matrix. In this formulation the electric permittivity $\boldsymbol{\varepsilon}$ appears only in the dielectric in this formulation and therefore we assume that $\boldsymbol{\varepsilon} = \varepsilon_0 I$ in Ω_I ; μ_0 and ε_0 are the corresponding coefficients in the vacuum.

2.2 Organization of the thesis

This thesis is organized as follows. In **Chapter 3**, we study the uniqueness of the solution of the inverse problem for the eddy current problem, following the approach proposed by Albanese and Monk [3] for the complete system of Maxwell equations. We consider three different kinds of current sources: a distributed source, a surface current source and a dipole source. Concerning to the first one, we show that the inverse problem has not a unique solution when the source is in L^2 and we characterize the space of non-radiating sources. On the other hand, we prove that the inverse problem has a unique solution if we assume that the source is supported on a surface internal to Ω . In the case of the dipole source, we first prove existence and uniqueness of the direct problem and then we analyze the inverse problem. As in the case of the surface current we show that the tangential component of the electric field at the boundary of the conductor uniquely determines the number of dipoles, location and polarization. In addition, we present a formula by which it is possible to determine the source dipole, knowing a priori the tangential component of the electric field on the boundary of the domain. Finally, we study how to find the tangential component of the electric field from the measured data through EEG and MEG. This chapter has been published in:

A. ALONSO RODRÍGUEZ, J. CAMAÑO AND A. VALLI, *Inverse source problems for eddy current equations*. Inverse Problems, vol. 28, 1, (2012).

In **Chapter 4** we use the formulation studied by Valli [65], and we develop an a priori and a posteriori analysis for a variational formulation of the electrostatic problem. This is a singular problem since the current source contains first-order derivatives of the Dirac delta distribution. In [65] it is proved that the solution belongs to L^p for $1 \leq p < 3/2$ in three-dimensional domains and following the same demonstration technique, we prove that the solution in the bidimensional case belongs to L^p , with $1 \leq p < 2$. In this chapter, we give an a priori error estimate in L^p -norm, which is valid for quasiuniform meshes, and we propose an a posteriori error estimator. We show that it is reliable and efficient under the hypothesis of convexity of domain and higher regularity of the conductivity. All this analysis is presented initially in a two-dimensional domain and then in a three-dimensional domain, but in the last case under more restrictive assumptions (cubic geometry and constant conductivity). Finally, the estimator is used to guide an adaptive procedure, which shows experimentally optimal convergence rate. This chapter corresponds to the following article:

A. ALONSO RODRÍGUEZ, J. CAMAÑO, R. RODRÍGUEZ AND A. VALLI, *A posteriori error estimates for the problem of electrostatics with a dipole source*. (submitted).

In **Chapter 5** we compare the approximate solution of the direct problem using different methods, including the subtraction method and the direct method, in the case of a domain with several regions with different conductivities. We analyze the cases in which the dipole is close to or exactly located at an interface between two regions with different conductivities. Numerically we see that, when the source is on the interface, the only method that gives good results is a third one, in which the delta distribution is approximated by a characteristic function. For the inverse problem we analyze the results obtained using the three methods mentioned above and a last one that corresponds to the direct method with an adaptive procedure guided by the estimates found in Chapter 4. Two situations are considered: the case of a source located well inside a homogeneous region and the case of a source close to an interface between two homogeneous regions. We study also the case of a distributed source (the sum of several dipoles) and we compare the lead field matrices in different situations. This chapter corresponds to the following article:

A. ALONSO RODRÍGUEZ, J. CAMAÑO, R. RODRÍGUEZ AND A. VALLI, *Numerical behavior of different approximation methods for the direct and inverse problems of electrostatics with a dipole source*. (in preparation).

Finally, in parallel to the work presented in Chapter 3, in **Chapter 6** we study a new numerical method for the time-dependent eddy currents equations in a conductor bounded

domain contained in \mathbb{R}^3 . The problem is reformulated by expressing the electric and magnetic fields in terms of new variables that turn out to be more convenient: the temporal primitive electric field which plays the role of a vector potential for the magnetic field in the conductor, and the magnetic scalar potential trace on the interface. Then, we derive a FEM-BEM formulation and prove existence and uniqueness of the solution to the problem. It is discretized using Nédélec finite elements for the variable defined in the conductor and piecewise linear and continuous finite elements for an additional variable on the boundary of the domain. For the temporal discretization we use the backward Euler method. Finally, we prove that the discrete scheme converges with optimal order to the solution. This chapter has been published in:

J. CAMAÑO AND R. RODRÍGUEZ, *Analysis of a FEM-BEM model posed on the conducting domain for the time-dependent eddy current problem*. Journal of Computational and Applied Mathematics, vol. 236, issue 13, pp. 3084-3100, (2012).

Chapter 3

Inverse source problems for eddy current equations

3.1 Introduction

Electroencephalography (EEG) and magnetoencephalography (MEG) are two non-invasive techniques used to localize electric activity in the brain from measurements of external electromagnetic signals. EEG measures the scalp electric potential, while MEG measures the external magnetic flux. From the mathematical point of view the goal is to solve an inverse problem for determining the source current distribution in a heterogeneous media from boundary measurements of the fields.

The frequency spectrum for electrophysiological signals in EEG and MEG is typically below 1000 Hz, most frequently between 0.1 and 100 Hz. For this reason most theoretical works on biomedical applications focus on the static approximation of the Maxwell equations, in which the time variation of both electric and magnetic fields is disregarded.

Recently He and Romanov [40], Ammari *et al.* [7] and Albanese and Monk [3] investigated the localization of brain activity through the inverse source problem for the full Maxwell system of equations. In this chapter we analyze the inverse source problem for an alternative model: the eddy current (or low frequency approximation) of Maxwell equations. In the eddy current model the time variation of the electric field is disregarded, while time variation of the magnetic field is kept.

Let us consider electromagnetic phenomena at frequency $\omega \neq 0$. The time-harmonic full Maxwell system of equations read

$$\begin{aligned} \operatorname{curl} \mathbf{H} - i\omega\epsilon\mathbf{E} &= \sigma\mathbf{E} + \mathbf{J}_e && \text{(Maxwell–Ampère equation)} \\ \operatorname{curl} \mathbf{E} + i\omega\mu\mathbf{H} &= \mathbf{0} && \text{(Faraday equation)}. \end{aligned} \tag{3.1}$$

Here \mathbf{E} , \mathbf{H} denote the electric and magnetic fields, respectively; \mathbf{J}_e is the applied current density; ϵ is the electric permittivity, μ the magnetic permeability and σ the electric conductivity.

The eddy current model is formally obtained by neglecting the displacement current term:

$$\begin{aligned} \operatorname{curl} \mathbf{H} &= \sigma \mathbf{E} + \mathbf{J}_e \\ \operatorname{curl} \mathbf{E} + i\omega \mu \mathbf{H} &= \mathbf{0}. \end{aligned} \quad (3.2)$$

Let us consider a conductor $\Omega_C \subset \mathbb{R}^3$, say, the human head. We assume that Ω_C is a bounded domain with a Lipschitz and connected boundary Γ . In Ω_C the conductivity σ is a symmetric and uniformly positive definite matrix with entries in $L^\infty(\Omega_C)$. We consider also a computational domain $\Omega \subset \mathbb{R}^3$, say, the room where the problem is studied. We assume that Ω is a bounded simply-connected domain, completely containing Ω_C and with Lipschitz boundary $\partial\Omega$. Moreover we assume that $\Omega_I := \Omega \setminus \overline{\Omega}_C$ is connected. Ω_I is an insulator, the air surrounding the head, hence σ is vanishing in Ω_I . We also assume that the electric permeability μ and the electric permittivity ϵ are symmetric and uniformly positive definite matrices with entries in $L^\infty(\Omega)$.

On the boundary $\partial\Omega$, we can impose either the magnetic boundary condition $\mathbf{H} \times \mathbf{n} = \mathbf{0}$ or the electric boundary condition $\mathbf{E} \times \mathbf{n} = \mathbf{0}$ (Here \mathbf{n} denotes the unit outward normal vector on $\partial\Omega$).

Since σ is equal zero in insulators, equations (3.2) do not completely determine the electric field in Ω_I . In that region, one has to add $\operatorname{div}(\epsilon \mathbf{E}) = 0$ because there are no charges in an insulator. This is a “gauge” condition necessary for having uniqueness. When imposing the magnetic boundary condition, the additional “gauge” condition $\epsilon \mathbf{E} \cdot \mathbf{n} = 0$ on $\partial\Omega$ is also necessary.

From Faraday law, $\mu^{-1} \operatorname{curl} \mathbf{E} = -i\omega \mathbf{H}$ and inserting this result in Ampère law one has $\operatorname{curl}(\mu^{-1} \operatorname{curl} \mathbf{E}) = -i\omega(\sigma \mathbf{E} + \mathbf{J}_e)$. So the \mathbf{E} -based formulation of the eddy current model reads

$$\begin{cases} \operatorname{curl}(\mu^{-1} \operatorname{curl} \mathbf{E}) + i\omega \sigma \mathbf{E} = -i\omega \mathbf{J}_e & \text{in } \Omega \\ \operatorname{div}(\epsilon \mathbf{E}) = 0 & \text{in } \Omega_I \\ (\mu^{-1} \operatorname{curl} \mathbf{E}) \times \mathbf{n} = \mathbf{0} & \text{on } \partial\Omega \\ \epsilon \mathbf{E} \cdot \mathbf{n} = 0 & \text{on } \partial\Omega \end{cases} \quad (3.3)$$

for the magnetic boundary condition, and

$$\begin{cases} \operatorname{curl}(\mu^{-1} \operatorname{curl} \mathbf{E}) + i\omega \sigma \mathbf{E} = -i\omega \mathbf{J}_e & \text{in } \Omega \\ \operatorname{div}(\epsilon \mathbf{E}) = 0 & \text{in } \Omega_I \\ \mathbf{E} \times \mathbf{n} = \mathbf{0} & \text{on } \partial\Omega \end{cases} \quad (3.4)$$

for the electric boundary condition. In this chapter, we will focus on problem (3.3); the same results can be proved for problem (3.4).

In the static approximation also the time variation of the magnetic field is disregarded; thus, one has:

$$\begin{aligned}\operatorname{curl} \mathbf{H} &= \sigma \mathbf{E} + \mathbf{J}_e \\ \operatorname{curl} \mathbf{E} &= \mathbf{0}\end{aligned}\tag{3.5}$$

(where \mathbf{J}_e can still depend on time, which has to be regarded as a parameter). From the second equation in (3.5), the electric field is the gradient of a scalar potential $\mathbf{E} = -\operatorname{grad} V$ and then from the first equation in (3.5), we obtain $\operatorname{div}(\sigma \operatorname{grad} V) = \operatorname{div} \mathbf{J}_e$ in Ω_C . On the other hand, $\sigma \mathbf{E} + \mathbf{J}_e$ is divergence free in Ω ; hence, we have $(\sigma \operatorname{grad} V - \mathbf{J}_{e|\Omega_C}) \cdot \mathbf{n}_\Gamma = -\mathbf{J}_{e|\Omega_I} \cdot \mathbf{n}_\Gamma$ on Γ , with \mathbf{n}_Γ being the unit normal vector on Γ pointing outwards Ω_C . Since we are interested in electric sources located in the conductor, namely $\operatorname{supp} \mathbf{J}_e \subset \Omega_C$, the boundary condition for the static approximation is the homogeneous Neumann boundary condition $\sigma \operatorname{grad} V \cdot \mathbf{n}_\Gamma = 0$ on Γ . The static problem thus reads

$$\begin{cases} \operatorname{div}(\sigma \operatorname{grad} V) = \operatorname{div} \mathbf{J}_e & \text{in } \Omega_C \\ \sigma \operatorname{grad} V \cdot \mathbf{n}_\Gamma = 0 & \text{on } \Gamma, \end{cases}\tag{3.6}$$

and the related magnetic field is computed in terms of the primary current \mathbf{J}_e and the return current $\sigma \mathbf{E} = -\sigma \operatorname{grad} V$ using the Biot–Savart law in \mathbb{R}^3 :

$$\mathbf{H}(\mathbf{x}) = \frac{1}{4\pi} \int_{\Omega_C} [\mathbf{J}_e(\mathbf{y}) - \sigma \operatorname{grad} V(\mathbf{y})] \times \frac{\mathbf{x} - \mathbf{y}}{|\mathbf{x} - \mathbf{y}|^3} d\mathbf{y}.\tag{3.7}$$

The inverse source problem consists in the determination of the current source \mathbf{J}_e from boundary measurements of the electromagnetic fields. Helmholtz had already observed that this problem does not have a unique solution. For instance, if the source is a radial dipole, the magnetic field given by (3.7) vanishes outside a spherical conductor Ω_C (see, e.g., Sarvas [61]), hence, when using the static model, knowledge of the magnetic field on Γ does not contribute to the localization of radial dipoles.

The characterization of the source currents that can be reconstructed from suitable measurements on the boundary is not an easy task and depends on the model considered. For the static model in Kress *et al.* [44], the authors prove that the Biot–Savart operator has a non-trivial null space. Fokas *et al.* [36] characterized which part of a volume current source in a spherical conductor can be reconstructed from knowledge of the magnetic field on the boundary. In the same framework, Dassios and Hadjiloizi [29] determined which part of the source can be reconstructed from the electric potential. Instead, concerning dipole sources, He and Romanov [40] showed that the measurement of the electric potential on the boundary of the conductor is enough to identify their location and polarization, and proposed an identification procedure. In the case of a layered spherical model, Dassios and Fokas [27] derived an algorithm for the identification of a source consisting of a finite number of dipoles from measurements of the electric potential or the magnetic potential. For a general layered domain, El Badia and Nara [34]

proposed an algebraic algorithm for the identification of the number, locations and moments of the dipoles from knowledge of the tangential components of the electric and magnetic fields.

Considering the full Maxwell system, the existence of non-radiating sources was proved in Bleistein and Cohen [18]. On the other hand, He and Romanov [40] showed that the location and the polarization of a current dipole in a conducting object can be uniquely determined by measuring at a fixed frequency the magnetic field and its normal derivative on the whole surface. The same result was obtained by Ammari *et al.* [7] from knowledge of the tangential component of either the electric or the magnetic field on Γ . Albanese and Monk [3] have characterized which part of a volume source confined in Ω_C can be uniquely identified from measurements of the tangential component of the electric field on Γ . Moreover, they also proved the uniqueness of the inverse source problem if the source is supported on the surface of a priori known subdomain contained in Ω_C or if it is the sum of a finite number of dipole sources. In the last case, the tangential component of the electric field uniquely determines the number, position and polarization of the dipoles.

The reconstruction of a current source from boundary measurements of the electromagnetic fields is interesting also for other types of applications. For instance, the imaging of small electromagnetic inclusions can be reduced to inverse source problems for the full Maxwell system where the current is a sum of a finite number of dipoles. Localization techniques for these problems have been developed by Ammari *et al.* [12], [11], [10].

The aim of this chapter is to study the uniqueness of the solution of the inverse source problem for the eddy current approximation of Maxwell equations, mainly following the approach proposed by Albanese and Monk [3] for the full Maxwell system of equations. The outline of the chapter is as follows. Section 3.2 is devoted to volume source currents. We prove that when looking for $\mathbf{J}_e \in (L^2(\Omega_C))^3$, the inverse problem does not have a unique solution and we characterize the space of non-radiating sources. In Section 3.3, we obtain the uniqueness result for a source current supported on the boundary of a subdomain of Ω_C ; it is worth noting that the support of the surface source is not assumed to be known, but it is uniquely determined from the boundary data. In Section 3.4, we consider the case of dipole sources. First, we study the well-posedness of the direct problem, that is, the existence and uniqueness of the solution for the eddy current model assuming that the source is a finite sum of dipoles. Then we prove uniqueness of the inverse source problem, determining the number, location and polarization of the dipole source. We also present an algebraic algorithm for the determination of a dipole source assuming that the tangential component of the electric field on Γ is known. In the last section, we study how to recover the tangential component of the electric field on Γ , the data that we use in the inverse problem, from the data that are measured in MEG and EEG.

To conclude this section, let us introduce some notation that will be used in the following. The space $H(\text{curl}; \Omega)$ indicates the set of real or complex vector valued functions $\mathbf{v} \in (L^2(\Omega))^3$ such that $\text{curl } \mathbf{v} \in (L^2(\Omega))^3$. We also use the spaces $H^{-1/2}(\text{curl}_\tau; \Gamma) := \{(\mathbf{n}_\Gamma \times \mathbf{v} \times \mathbf{n}_\Gamma)|_\Gamma \mid \mathbf{v} \in H(\text{curl}; \Omega_C)\}$ and $H^{-1/2}(\text{div}_\tau; \Gamma) := \{(\mathbf{v} \times \mathbf{n}_\Gamma)|_\Gamma \mid \mathbf{v} \in H(\text{curl}; \Omega_C)\}$. These two spaces are in duality and the following formula of integration by parts holds true:

$$\int_{\Omega_C} (\mathbf{w} \cdot \text{curl } \bar{\mathbf{v}} - \text{curl } \mathbf{w} \cdot \bar{\mathbf{v}}) = \int_{\Gamma} (\mathbf{w} \times \mathbf{n}_\Gamma) \cdot \bar{\mathbf{v}} \quad \forall \mathbf{w}, \mathbf{v} \in H(\text{curl}; \Omega_C).$$

The last integral is indeed the duality pairing between $\mathbf{w} \times \mathbf{n}_\Gamma \in H^{-1/2}(\text{div}_\tau; \Gamma)$ and $\mathbf{n}_\Gamma \times \mathbf{v} \times \mathbf{n}_\Gamma \in H^{-1/2}(\text{curl}_\tau; \Gamma)$.

3.2 Non-uniqueness of volume currents

In this section, we investigate the uniqueness of the inverse source problem assuming that the unknown source \mathbf{J}_e is a function in $(L^2(\Omega_C))^3$. First we will prove that without additional information, the source cannot be reconstructed from the knowledge of the tangential component of the electric field on Γ . We then characterize the space of non-radiating sources (those sources in $(L^2(\Omega_C))^3$ that generate an electric field normal to the surface Γ) and prove that sources $\mathbf{J}_e \in (L^2(\Omega_C))^3$ that are orthogonal to the space of non-radiating sources are uniquely determined by the tangential component on Γ of the electric field. The result is analogous to the one obtained by Albanese and Monk [3] for the full Maxwell system.

If $\mathbf{J}_e \in (L^2(\Omega_C))^3$, it is known that problems (3.3) has a unique solution \mathbf{E} and the magnetic field can be computed from Faraday law: $\mathbf{H} = -(i\omega\mu)^{-1} \text{curl } \mathbf{E}$ in Ω .

Multiplying the first equation in (3.3) by a regular enough test function \mathbf{z} , integration by parts in Ω_C easily yields

$$-i\omega \int_{\Omega_C} \mathbf{J}_e \cdot \bar{\mathbf{z}} = \int_{\Omega_C} \mathbf{E} \cdot [\text{curl}(\mu^{-1} \text{curl } \bar{\mathbf{z}}) + i\omega\sigma\bar{\mathbf{z}}] - \int_{\Gamma} [\mathbf{E} \times \mathbf{n}_\Gamma \cdot (\mu^{-1} \text{curl } \bar{\mathbf{z}}) - i\omega\mathbf{H} \times \mathbf{n}_\Gamma \cdot \bar{\mathbf{z}}].$$

Therefore, if $\mathbf{z} \in H(\text{curl}; \Omega_C)$ is such that

$$\text{curl}(\mu^{-1} \text{curl } \mathbf{z}) - i\omega\sigma\mathbf{z} = \mathbf{0} \text{ in } \Omega_C,$$

the current density \mathbf{J}_e satisfies the representation formula

$$\int_{\Omega_C} \mathbf{J}_e \cdot \bar{\mathbf{z}} = (i\omega)^{-1} \int_{\Gamma} \mathbf{E} \times \mathbf{n}_\Gamma \cdot (\mu^{-1} \text{curl } \bar{\mathbf{z}}) - \int_{\Gamma} \mathbf{H} \times \mathbf{n}_\Gamma \cdot \bar{\mathbf{z}}. \quad (3.8)$$

The right hand term in (3.8) has been called *reciprocity* functional, taking the name from the Lorentz reciprocity principle in electromagnetism, or else the Maxwell–Betti reciprocity principle in elastostatics (see, e.g., Andrieux and Ben Abda [14], El Badia and Ha-Duong [33]). It is often

used in the analysis of inverse source problems (see, e.g., Novikov [55], Isakov [41], Ammari and Kang [9]).

Let us define

$$\mathcal{W} = \{ \mathbf{z} \in H(\text{curl}; \Omega_C) \mid \text{curl}(\mu^{-1} \text{curl} \mathbf{z}) - i\omega\sigma\mathbf{z} = \mathbf{0} \text{ in } \Omega_C \}.$$

It is clear that \mathcal{W} is not a trivial subspace of $(L^2(\Omega_C))^3$, since both μ and σ are bounded and uniformly positive definite in Ω ; for each $\xi \in H_{\text{div},\tau}^{-1/2}(\Gamma)$, there exists a unique $\mathbf{u}(\xi) \in H(\text{curl}; \Omega_C)$ such that $\mathbf{u}(\xi) \in \mathcal{W}$ and $\mathbf{u}(\xi) \times \mathbf{n}_\Gamma = \xi$ on Γ .

Denoting by W the closure of \mathcal{W} in $(L^2(\Omega_C))^3$ we have the orthogonal splitting

$$(L^2(\Omega_C))^3 = W \oplus W^\perp.$$

Lemma 3.2.1 *Consider $\boldsymbol{\eta} \in (C_0^\infty(\Omega_C))^3$ and set $\boldsymbol{\phi} = \text{curl}(\mu^{-1} \text{curl} \boldsymbol{\eta}) + i\omega\sigma\boldsymbol{\eta}$. Then $\boldsymbol{\phi} \in W^\perp$ (and W^\perp is not a trivial subspace).*

Proof. Take $\mathbf{z} \in \mathcal{W}$. Then

$$\begin{aligned} \int_{\Omega_C} \boldsymbol{\phi} \cdot \bar{\mathbf{z}} &= \int_{\Omega_C} [\text{curl}(\mu^{-1} \text{curl} \boldsymbol{\eta}) + i\omega\sigma\boldsymbol{\eta}] \cdot \bar{\mathbf{z}} \\ &= \int_{\Omega_C} \boldsymbol{\eta} \cdot [\text{curl}(\mu^{-1} \text{curl} \bar{\mathbf{z}}) + i\omega\sigma\bar{\mathbf{z}}] = 0, \end{aligned}$$

and a density argument shows that $\boldsymbol{\phi} \in W^\perp$.

Note that, if $\boldsymbol{\eta}$ is a non-vanishing real vector field, one obtains $\text{Im} \boldsymbol{\phi} \neq \mathbf{0}$, hence W^\perp is not a trivial subspace. \square

Let us split the current density \mathbf{J}_e as

$$\mathbf{J}_e = \mathbf{J}_e^\sharp + \mathbf{J}_e^\perp, \quad \mathbf{J}_e^\sharp \in W, \quad \mathbf{J}_e^\perp \in W^\perp.$$

Theorem 3.2.1 (i) *Let us assume that $\mathbf{J}_e = \mathbf{J}_e^\sharp \in W$ and that \mathbf{E}^\sharp is the corresponding solution of the eddy current problem. Then knowledge of $\mathbf{E}^\sharp \times \mathbf{n}_\Gamma$ on Γ uniquely determines \mathbf{J}_e^\sharp .*

(ii) *Let us assume that $\mathbf{J}_e = \mathbf{J}_e^\perp \in W^\perp$ and that \mathbf{E}^\perp is the corresponding solution of the eddy current problem. Then $\mathbf{E}^\perp \times \mathbf{n}_\Gamma = \mathbf{0}$ and $\mathbf{H}^\perp \times \mathbf{n}_\Gamma = \mathbf{0}$ on Γ , namely, \mathbf{J}_e^\perp is a non-radiating source.*

Proof. (i) The electric field in the insulator satisfies

$$\begin{aligned} \text{curl}(\mu^{-1} \text{curl} \mathbf{E}^\sharp) &= \mathbf{0} && \text{in } \Omega_I \\ \text{div}(\epsilon \mathbf{E}^\sharp) &= 0 && \text{in } \Omega_I \\ (\mu^{-1} \text{curl} \mathbf{E}^\sharp) \times \mathbf{n} &= \mathbf{0} && \text{on } \partial\Omega \\ \epsilon \mathbf{E}^\sharp \cdot \mathbf{n} &= 0 && \text{on } \partial\Omega. \end{aligned}$$

If $\mathbf{E}^\sharp \times \mathbf{n}_\Gamma = \mathbf{0}$ on Γ , multiplying the first equation by \mathbf{E}^\sharp and integrating by parts, one easily finds $\operatorname{curl} \mathbf{E}^\sharp = \mathbf{0}$, then $\mathbf{E}^\sharp = \mathbf{0}$ in Ω_I . Consequently, $\mathbf{H}^\sharp = -(i\omega\mu)^{-1} \operatorname{curl} \mathbf{E}^\sharp = \mathbf{0}$ in Ω_I and in particular $\mathbf{H}^\sharp \times \mathbf{n}_\Gamma = \mathbf{0}$ on Γ . Therefore, from (3.8), we know that $\int_{\Omega_C} \mathbf{J}_e^\sharp \cdot \bar{\mathbf{z}} = 0$ for each $\mathbf{z} \in \mathcal{W}$, hence, by a density argument, for each $\mathbf{z} \in W$. Taking $\mathbf{z} = \mathbf{J}_e^\sharp \in W$, the thesis follows.

(ii) Since $\mathbf{J}_e^\perp \in W^\perp$, from (3.8), we have that for all $\mathbf{z} \in W$

$$\int_{\Gamma} \mathbf{E}^\perp \times \mathbf{n}_\Gamma \cdot (\mu^{-1} \operatorname{curl} \bar{\mathbf{z}}) - i\omega \int_{\Gamma} \mathbf{H}^\perp \times \mathbf{n}_\Gamma \cdot \bar{\mathbf{z}} = 0. \quad (3.9)$$

For each $\boldsymbol{\eta} \in H_{\operatorname{div},\tau}^{-1/2}(\Gamma)$, we denote by $\mathbf{Z} \in H(\operatorname{curl}; \Omega)$ the solution to

$$\begin{cases} \operatorname{curl}(\mu^{-1} \operatorname{curl} \mathbf{Z}) - i\omega\sigma \mathbf{Z} = \mathbf{0} & \text{in } \Omega_C \cup \Omega_I \\ \operatorname{div}(\epsilon \mathbf{Z}) = 0 & \text{in } \Omega_I \\ (\mu^{-1} \operatorname{curl} \mathbf{Z}) \times \mathbf{n} = \mathbf{0} & \text{on } \partial\Omega \\ \epsilon \mathbf{Z} \cdot \mathbf{n} = 0 & \text{on } \partial\Omega \\ (\mu^{-1} \operatorname{curl} \mathbf{Z})|_{\Omega_C} \times \mathbf{n}_\Gamma = (\mu^{-1} \operatorname{curl} \mathbf{Z})|_{\Omega_I} \times \mathbf{n}_\Gamma + \boldsymbol{\eta} & \text{on } \Gamma, \end{cases} \quad (3.10)$$

which in weak form reads

$$\text{find } \mathbf{Z} \in V : \int_{\Omega} (\mu^{-1} \operatorname{curl} \mathbf{Z} \cdot \operatorname{curl} \bar{\mathbf{v}} - i\omega\sigma \mathbf{Z} \cdot \bar{\mathbf{v}}) = \int_{\Gamma} \boldsymbol{\eta} \cdot \bar{\mathbf{v}} \quad \forall \mathbf{v} \in V,$$

where $V := \{\mathbf{v} \in H(\operatorname{curl}; \Omega) : \operatorname{div}(\epsilon \mathbf{v}) = 0 \text{ in } \Omega_I \text{ and } \epsilon \mathbf{v} \cdot \mathbf{n} = 0 \text{ on } \partial\Omega\}$. It is well known that the sesquilinear form on the left-hand side is coercive in V (see Alonso Rodríguez and Valli [5], theorem 2.3); therefore, the problem is uniquely solvable.

As a test function in (3.9) we can thus select $\mathbf{Z}|_{\Omega_C} \in W$, obtaining

$$\begin{aligned} \int_{\Gamma} \mathbf{E}^\perp \times \mathbf{n}_\Gamma \cdot \mu^{-1} \operatorname{curl} \bar{\mathbf{Z}}|_{\Omega_C} &= - \int_{\Gamma} \mathbf{E}^\perp \cdot \bar{\boldsymbol{\eta}} - \int_{\Gamma} \mathbf{E}^\perp \cdot (\mu^{-1} \operatorname{curl} \bar{\mathbf{Z}}|_{\Omega_I} \times \mathbf{n}_\Gamma) \\ &= - \int_{\Gamma} \mathbf{E}^\perp \cdot \bar{\boldsymbol{\eta}} + \int_{\Omega_I} \mu^{-1} \operatorname{curl} \mathbf{E}^\perp \cdot \operatorname{curl} \bar{\mathbf{Z}}|_{\Omega_I} \\ -i\omega \int_{\Gamma} \mathbf{H}^\perp \times \mathbf{n}_\Gamma \cdot \bar{\mathbf{Z}}|_{\Omega_C} &= - \int_{\Gamma} \mu^{-1} \operatorname{curl} \mathbf{E}^\perp \cdot \bar{\mathbf{Z}}|_{\Omega_I} \times \mathbf{n}_\Gamma \\ &= - \int_{\Omega_I} \mu^{-1} \operatorname{curl} \mathbf{E}^\perp \cdot \operatorname{curl} \bar{\mathbf{Z}}|_{\Omega_I}. \end{aligned}$$

In conclusion, we have found

$$\int_{\Gamma} \mathbf{E}^\perp \cdot \bar{\boldsymbol{\eta}} = 0$$

for each $\boldsymbol{\eta} \in H_{\operatorname{div},\tau}^{-1/2}(\Gamma)$, hence $\mathbf{n}_\Gamma \times \mathbf{E}^\perp \times \mathbf{n}_\Gamma = \mathbf{0}$ on Γ .

Proceeding as in the proof of (i), we show that $\mathbf{E}^\perp \times \mathbf{n}_\Gamma = \mathbf{0}$ on Γ , implies $\mathbf{H}^\perp \times \mathbf{n}_\Gamma = \mathbf{0}$ on Γ , and the proof is complete. \square

3.3 Uniqueness of surface currents

In this section, we prove that if the source current is known to be supported on the surface of a subdomain contained in Ω_C , then both the surface and the value of the surface current are uniquely determined by the tangential component of the electric field on Γ . A similar result, but assuming that the surface is a priori known, has been previously obtained for the full Maxwell systems (see Albanese and Monk [3]).

First, we start by considering a surface current $\mathbf{J}_* \in H^{-1/2}(\text{div}_\tau; \partial B)$, where B is an open connected set with Lipschitz and connected boundary ∂B and satisfying $\overline{B} \subset \Omega_C$.

The direct problem reads

$$\left\{ \begin{array}{ll} \text{curl } \mathbf{E}_* + i\omega\mu\mathbf{H}_* = \mathbf{0} & \text{in } \Omega \\ \text{curl } \mathbf{H}_* = \sigma\mathbf{E}_* & \text{in } B \cup (\Omega \setminus \overline{B}) \\ \text{div}(\epsilon\mathbf{E}_*) = 0 & \text{in } \Omega_I \\ \mathbf{H}_* \times \mathbf{n} = \mathbf{0} & \text{on } \partial\Omega \\ \epsilon\mathbf{E}_* \cdot \mathbf{n} = 0 & \text{on } \partial\Omega \\ \mathbf{H}_{*|B} \times \mathbf{n}_B - \mathbf{H}_{*|\Omega \setminus \overline{B}} \times \mathbf{n}_B = \mathbf{J}_* & \text{on } \partial B, \end{array} \right. \quad (3.11)$$

where \mathbf{n}_B is the unit normal vector on ∂B , pointing outward B . It is easy to see that its weak formulation in terms of the electric field is

$$\text{find } \mathbf{E}_* \in V : \int_{\Omega} (\mu^{-1} \text{curl } \mathbf{E}_* \cdot \text{curl } \overline{\mathbf{v}} + i\omega\sigma\mathbf{E}_* \cdot \overline{\mathbf{v}}) = -i\omega \int_{\partial B} \mathbf{J}_* \cdot \overline{\mathbf{v}} \quad \forall \mathbf{v} \in V,$$

with V being the space introduced for the weak formulation of (3.10). Since the sesquilinear form at the left hand side is coercive, for each given $\mathbf{J}_* \in H^{-1/2}(\text{div}_\tau; \partial B)$ the direct problem has a unique solution.

Our first result in this section is the following.

Theorem 3.3.1 *Assume that the coefficients μ and σ are Lipschitz continuous and piecewise C^1 scalar functions in $\overline{\Omega}_C$, and that the discontinuity surfaces of their gradients are Lipschitz surfaces. Let $(\mathbf{E}_*, \mathbf{H}_*)$ be the solution of the eddy current problem driven by the surface current $\mathbf{J}_* \in H^{-1/2}(\text{div}_\tau; \partial B)$. The knowledge of $\mathbf{E}_* \times \mathbf{n}_\Gamma$ on Γ uniquely determines \mathbf{J}_* .*

Proof. It is enough to show that if $\mathbf{E}_* \times \mathbf{n}_\Gamma = \mathbf{0}$ on Γ , then $\mathbf{J}_* = \mathbf{0}$ on ∂B . As in the preceding case, by solving the problem in Ω_I , we easily show that $\mathbf{E}_* \times \mathbf{n}_\Gamma = \mathbf{0}$ on Γ also gives $\mathbf{E}_* = \mathbf{0}$ in Ω_I , $\mathbf{H}_* = \mathbf{0}$ in Ω_I and in particular $\mathbf{H}_* \times \mathbf{n}_\Gamma = \mathbf{0}$ on Γ . By virtue of the assumptions on the coefficients μ and σ , we can apply the unique continuation principle in $\Omega_C \setminus \overline{B}$ (see Ōkaji [56]) and deduce that $\mathbf{E}_* = \mathbf{0}$ and $\mathbf{H}_* = \mathbf{0}$ in $\Omega \setminus \overline{B}$.

Multiplying the second equation in (3.11) by a function $\mathbf{z} \in H(\text{curl}; B)$ with $\text{curl}(\mu^{-1} \text{curl } \mathbf{z}) \in (L^2(B))^3$ and integrating by parts, we have

$$\int_B \sigma \mathbf{E}_* \cdot \bar{\mathbf{z}} = \int_B \text{curl } \mathbf{H}_* \cdot \bar{\mathbf{z}} = - \int_{\partial B} \mathbf{H}_{*|B} \times \mathbf{n}_B \cdot \bar{\mathbf{z}} + \int_B \mathbf{H}_* \cdot \text{curl } \bar{\mathbf{z}}.$$

Since $\mathbf{H}_* = -(i\omega\mu)^{-1} \text{curl } \mathbf{E}$, taking into account that $\mathbf{E}_* \times \mathbf{n}_B = \mathbf{0}$ on ∂B , another integration by parts gives

$$\int_B \sigma \mathbf{E}_* \cdot \bar{\mathbf{z}} = - \int_{\partial B} \mathbf{H}_{*|B} \times \mathbf{n}_B \cdot \bar{\mathbf{z}} - (i\omega)^{-1} \int_B \mathbf{E}_* \cdot \text{curl}(\mu^{-1} \text{curl } \bar{\mathbf{z}}).$$

Hence for each $\mathbf{z} \in H(\text{curl}; B)$ such that $\text{curl}(\mu^{-1} \text{curl } \mathbf{z}) - i\omega\sigma\mathbf{z} = \mathbf{0}$ in B , one finds $\int_{\partial B} \mathbf{H}_{*|B} \times \mathbf{n}_B \cdot \bar{\mathbf{z}} = 0$. Therefore,

$$\int_{\partial B} \mathbf{J}_* \cdot \bar{\mathbf{z}} = \int_{\partial B} \left[\mathbf{H}_{*|B} \times \mathbf{n}_B - \mathbf{H}_{*|\Omega \setminus \bar{B}} \times \mathbf{n}_B \right] \cdot \bar{\mathbf{z}} = 0$$

for each $\mathbf{z} \in H(\text{curl}; B)$ such that $\text{curl}(\mu^{-1} \text{curl } \mathbf{z}) - i\omega\sigma\mathbf{z} = \mathbf{0}$ in B .

Given $\boldsymbol{\rho} \in H^{-1/2}(\text{curl}_\tau; \Gamma)$, we can choose $\mathbf{z} \in H(\text{curl}; B)$, the solution to

$$\begin{cases} \text{curl}(\mu^{-1} \text{curl } \mathbf{z}) - i\omega\sigma\mathbf{z} = \mathbf{0} & \text{in } B \\ \mathbf{z} \times \mathbf{n}_B = \boldsymbol{\rho} \times \mathbf{n}_B & \text{on } \partial B. \end{cases}$$

Hence $\int_{\partial B} \mathbf{J}_* \cdot \bar{\boldsymbol{\rho}} = 0$ for each $\boldsymbol{\rho} \in H^{-1/2}(\text{curl}_\tau; \Gamma)$, and this space is the dual space of $H^{-1/2}(\text{div}_\tau; \Gamma)$. This ends the proof. \square

Remark 3.3.1 *Proceeding as in Section 3.2, we can obtain a representation formula similar to (3.8), namely*

$$\int_{\partial B} \mathbf{J}_* \cdot \bar{\mathbf{z}} = (i\omega)^{-1} \int_\Gamma \mathbf{E}_* \times \mathbf{n}_\Gamma \cdot (\mu^{-1} \text{curl } \bar{\mathbf{z}}) - \int_\Gamma \mathbf{H}_* \times \mathbf{n}_\Gamma \cdot \bar{\mathbf{z}} \quad (3.12)$$

for each $\mathbf{z} \in H(\text{curl}; \Omega_C)$ satisfying

$$\text{curl}(\mu^{-1} \text{curl } \mathbf{z}) - i\omega\sigma\mathbf{z} = \mathbf{0} \quad \text{in } \Omega_C.$$

3.4 Uniqueness for dipole sources

Let us consider now the eddy current problem with a dipole source

$$\begin{cases} \text{curl}(\mu^{-1} \text{curl } \mathbf{E}) + i\omega\sigma\mathbf{E} = -i\omega\mathbf{p}_0\delta_{\mathbf{x}_0} & \text{in } \Omega \\ \text{div}(\epsilon\mathbf{E}) = 0 & \text{in } \Omega_I \\ (\mu^{-1} \text{curl } \mathbf{E}) \times \mathbf{n} = \mathbf{0} & \text{on } \partial\Omega \\ \epsilon\mathbf{E} \cdot \mathbf{n} = 0 & \text{on } \partial\Omega, \end{cases} \quad (3.13)$$

where $\mathbf{p}_0 \neq \mathbf{0}$, $\mathbf{x}_0 \in \Omega_C$ and $\delta_{\mathbf{x}_0}$ denotes the Dirac delta distribution centered at \mathbf{x}_0 .

First, we study the well posedness of this problem. We will assume that the magnetic permeability μ and the conductivity σ satisfy the *homogeneity condition*: there exist $r_0 > 0$, $\mu_0 > 0$ and $\sigma_0 > 0$ such that

$$\mu(\mathbf{x}) = \mu_0 I \text{ and } \sigma(\mathbf{x}) = \sigma_0 I \text{ for each } \mathbf{x} \in B_{r_0}(\mathbf{x}_0), \quad (3.14)$$

where I is the identity matrix and $B_{r_0}(\mathbf{x}_0) := \{\mathbf{x} \in \Omega : |\mathbf{x} - \mathbf{x}_0| < r_0\}$.

We set $\kappa^2 = -i\omega\mu_0\sigma_0$ and $\mathbf{q}_0 = -i\omega\mu_0\mathbf{p}_0$. The following result is quite classical (and also appears in the theory of linear elasticity, see, e.g., [45]). It can be found in Ammari *et al.* [7], and we report the proof for the sake of completeness.

Theorem 3.4.1 *The fundamental solution \mathbf{K} of the operator $\text{curl curl} - \kappa^2 I$, that is, the solution to*

$$\text{curl curl } \mathbf{K} - \kappa^2 \mathbf{K} = \mathbf{q}_0 \delta_0,$$

is given by

$$\mathbf{K}(\mathbf{x}) = \mathbf{q}_0 \frac{e^{i\kappa|\mathbf{x}|}}{4\pi|\mathbf{x}|} + \frac{1}{\kappa^2} (\mathbf{q}_0 \cdot \text{grad}) \text{grad} \frac{e^{i\kappa|\mathbf{x}|}}{4\pi|\mathbf{x}|}. \quad (3.15)$$

Proof. We start from the fundamental solution Φ of the Helmholtz operator

$$-\Delta\Phi - \kappa^2\Phi = \delta_0,$$

which, as it is well known, is given by

$$\Phi(\mathbf{x}) = \frac{e^{i\kappa|\mathbf{x}|}}{4\pi|\mathbf{x}|}.$$

From this, we obtain at once

$$-\Delta(\mathbf{q}_0\Phi) - \kappa^2(\mathbf{q}_0\Phi) = \mathbf{q}_0\delta_0.$$

Then we look for \mathbf{K} in the form

$$\mathbf{K} = \mathbf{q}_0\Phi + \mathbf{q},$$

and we have

$$\begin{aligned} \text{curl curl } \mathbf{K} - \kappa^2 \mathbf{K} &= -\Delta(\mathbf{q}_0\Phi) + \text{grad div}(\mathbf{q}_0\Phi) - \kappa^2(\mathbf{q}_0\Phi) + \text{curl curl } \mathbf{q} - \kappa^2 \mathbf{q} \\ &= \mathbf{q}_0\delta_0 + \text{grad div}(\mathbf{q}_0\Phi) + \text{curl curl } \mathbf{q} - \kappa^2 \mathbf{q}. \end{aligned}$$

Hence, \mathbf{q} has to satisfy

$$\text{curl curl } \mathbf{q} - \kappa^2 \mathbf{q} = -\text{grad div}(\mathbf{q}_0\Phi),$$

and we easily find

$$\mathbf{q} = \frac{1}{\kappa^2} \text{grad div}(\mathbf{q}_0 \Phi).$$

In conclusion, we have obtained

$$\begin{aligned} \mathbf{K}(\mathbf{x}) &= \mathbf{q}_0 \Phi(\mathbf{x}) + \frac{1}{\kappa^2} \text{grad div}(\mathbf{q}_0 \Phi(\mathbf{x})) \\ &= \mathbf{q}_0 \frac{e^{i\kappa|\mathbf{x}|}}{4\pi|\mathbf{x}|} + \frac{1}{\kappa^2} (\mathbf{q}_0 \cdot \text{grad}) \text{grad} \frac{e^{i\kappa|\mathbf{x}|}}{4\pi|\mathbf{x}|}, \end{aligned}$$

namely, the representation formula (3.15). \square

Note that the fundamental solution \mathbf{K} is much more singular than the fundamental solution of the Laplace or the Helmholtz operator; while the first term belongs to L_{loc}^2 , the second one has a singularity like $|\mathbf{x}|^{-3}$. It can also be remarked that setting $\hat{\mathbf{K}}(\mathbf{x}) := \mathbf{K}(\mathbf{x} - \mathbf{x}_0)$, we have $\hat{\mathbf{K}} \in H^{-2}(\Omega)$, the dual space of $H_0^2(\Omega)$; however, $\hat{\mathbf{K}}$ is a regular function far from $\mathbf{x} = \mathbf{x}_0$; in particular, it is regular in $\overline{\Omega}_I$.

Theorem 3.4.2 *Assuming that condition (3.14) is satisfied, there exists a solution $\mathbf{E} \in H^{-2}(\Omega)$ to (3.13), satisfying $(\mathbf{E} - \hat{\mathbf{K}}) \in H(\text{curl}; \Omega)$. It is unique among all the solutions \mathbf{E}^* such that $(\mathbf{E}^* - \hat{\mathbf{K}}) \in H(\text{curl}; \Omega)$.*

Proof. We split the solution to (3.13) in the following way: $\mathbf{E}(\mathbf{x}) = \hat{\mathbf{K}}(\mathbf{x}) + \mathbf{Q}(\mathbf{x})$. It is easily seen that we have to look for the solution $\mathbf{Q} \in H(\text{curl}; \Omega)$ to

$$\begin{cases} \text{curl}(\mu^{-1} \text{curl} \mathbf{Q}) + i\omega\sigma\mathbf{Q} = \mathbf{J} & \text{in } \Omega \\ \text{div}(\epsilon\mathbf{Q}) = -\text{div}(\epsilon\hat{\mathbf{K}}) & \text{in } \Omega_I \\ (\mu^{-1} \text{curl} \mathbf{Q}) \times \mathbf{n} = -(\mu^{-1} \text{curl} \hat{\mathbf{K}}) \times \mathbf{n} & \text{on } \partial\Omega \\ \epsilon\mathbf{Q} \cdot \mathbf{n} = -\epsilon\hat{\mathbf{K}} \cdot \mathbf{n} & \text{on } \partial\Omega, \end{cases} \quad (3.16)$$

where

$$\mathbf{J}(\mathbf{x}) := \begin{cases} \mathbf{0} & \text{if } \mathbf{x} \in B_{r_0}(\mathbf{x}_0) \\ -\text{curl}(\mu^{-1} \text{curl} \hat{\mathbf{K}})(\mathbf{x}) - i\omega\sigma\hat{\mathbf{K}}(\mathbf{x}) & \text{if } \mathbf{x} \in \Omega \setminus \overline{B_{r_0}(\mathbf{x}_0)}. \end{cases}$$

We introduce now the solution $\eta_I \in H^1(\Omega_I)$ of the mixed problem

$$\begin{cases} \text{div}(\epsilon \text{grad} \eta_I) = -\text{div}(\epsilon\hat{\mathbf{K}}) & \text{in } \Omega_I \\ \epsilon \text{grad} \eta_I \cdot \mathbf{n} = -\epsilon\hat{\mathbf{K}} \cdot \mathbf{n} & \text{on } \partial\Omega \\ \eta_I = 0 & \text{on } \Gamma, \end{cases}$$

which exists and is unique since $\hat{\mathbf{K}}|_{\Omega_I} \in (L^2(\Omega_I))^3$; we also define

$$\eta(\mathbf{x}) := \begin{cases} 0 & \text{if } \mathbf{x} \in \Omega_C \\ \eta_I(\mathbf{x}) & \text{if } \mathbf{x} \in \Omega_I, \end{cases}$$

and we see at once that $\eta \in H^1(\Omega)$.

We are now in a position to finish the construction of the solution to (3.13). The solution \mathbf{Q} to (3.16) will be found in the form $\mathbf{Q} = \mathbf{Q}^* + \text{grad } \eta$, where $\mathbf{Q}^* \in H(\text{curl}; \Omega)$ is the solution to

$$\begin{cases} \text{curl}(\mu^{-1} \text{curl } \mathbf{Q}^*) + i\omega\sigma\mathbf{Q}^* = \mathbf{J} & \text{in } \Omega \\ \text{div}(\epsilon\mathbf{Q}^*) = 0 & \text{in } \Omega_I \\ (\mu^{-1} \text{curl } \mathbf{Q}^*) \times \mathbf{n} = -(\mu^{-1} \text{curl } \hat{\mathbf{K}}) \times \mathbf{n} & \text{on } \partial\Omega \\ \epsilon\mathbf{Q}^* \cdot \mathbf{n} = 0 & \text{on } \partial\Omega. \end{cases}$$

The existence and uniqueness of such a solution follows from the fact that the compatibility conditions

$$\begin{aligned} \text{div } \mathbf{J}|_{\Omega_I} &= -\text{div} [\text{curl}(\mu^{-1} \text{curl } \hat{\mathbf{K}}|_{\Omega_I})] = 0 \text{ in } \Omega_I \\ \mathbf{J} \cdot \mathbf{n} &= -\text{curl}(\mu^{-1} \text{curl } \hat{\mathbf{K}}) \cdot \mathbf{n} = -\text{div}_\tau(\mu^{-1} \text{curl } \hat{\mathbf{K}} \times \mathbf{n}) \text{ on } \partial\Omega \end{aligned}$$

are satisfied (see Alonso Rodríguez and Valli [5], chapter 3).

We have thus found a solution $\mathbf{E} = \hat{\mathbf{K}} + \text{grad } \eta + \mathbf{Q}^*$ of (3.13). Concerning uniqueness, suppose that we have another solution \mathbf{E}^* such that $(\mathbf{E}^* - \hat{\mathbf{K}}) \in H(\text{curl}; \Omega)$. We can write it as $\mathbf{E}^* = \hat{\mathbf{K}} + (\mathbf{E}^* - \hat{\mathbf{K}})$, and it is readily verified that $\mathbf{E}^* - \hat{\mathbf{K}}$ is a solution to (3.16), a problem for which uniqueness holds in $H(\text{curl}; \Omega)$. Therefore $\mathbf{E}^* - \hat{\mathbf{K}} = \mathbf{Q} = \mathbf{E} - \hat{\mathbf{K}}$, and uniqueness is proved. \square

Concerning the uniqueness of the inverse problem, suppose that the source is a finite sum of dipoles, in different positions and with non-vanishing polarizations, namely,

$$\mathbf{J}_\dagger = \sum_{k=1}^M \mathbf{p}_k \delta_{\mathbf{x}_k}, \quad (3.17)$$

where $\mathbf{x}_k \in \Omega_C$, $\mathbf{x}_k \neq \mathbf{x}_j$ for $k \neq j$, $\mathbf{p}_k \neq \mathbf{0}$.

Theorem 3.4.3 *Assume that μ and σ are Lipschitz continuous and piecewise C^1 scalar functions in $\overline{\Omega_C}$ and that the discontinuity surfaces of their gradients are Lipschitz surfaces. Assume also that there exists the solution \mathbf{E}_\dagger of the eddy current problem (3.3) driven by the surface current \mathbf{J}_\dagger introduced in (3.17), with the same properties reported in Theorem 3.4.2. Knowledge of $\mathbf{E}_\dagger \times \mathbf{n}_\Gamma$ on Γ uniquely determines \mathbf{J}_\dagger , namely the number, the position and the polarization of the dipoles.*

Proof. We start proving that the number and the position of the dipoles are uniquely determined.

By contradiction, let us denote by Q_1 and Q_2 two different sets of points where the dipoles are located, and by $\mathbf{E}_{\dagger,1}$, $\mathbf{H}_{\dagger,1}$ and $\mathbf{E}_{\dagger,2}$, $\mathbf{H}_{\dagger,2}$ the corresponding solutions, with the same value

$\mathbf{E}_\dagger \times \mathbf{n}_\Gamma$ on Γ . As in the preceding cases, by solving the problem in Ω_I with datum $\mathbf{E}_\dagger \times \mathbf{n}_\Gamma$ on Γ , we obtain that $\mathbf{E}_{\dagger,1} = \mathbf{E}_{\dagger,2}$ and $\mathbf{H}_{\dagger,1} = \mathbf{H}_{\dagger,2}$ in Ω_I .

From the unique continuation principle, it follows that $\mathbf{E}_{\dagger,1} = \mathbf{E}_{\dagger,2}$ in $\Omega \setminus (Q_1 \cup Q_2)$. Let \mathbf{x}_* be a point belonging, say, to Q_1 but not to Q_2 . We have that $\mathbf{E}_{\dagger,2}$ is bounded in a neighborhood of \mathbf{x}_* , while $\mathbf{E}_{\dagger,1}$ is unbounded there, a contradiction since $\mathbf{E}_{\dagger,1}$ and $\mathbf{E}_{\dagger,2}$ coincide around \mathbf{x}_* . Therefore $Q_1 = Q_2$.

Let us now prove that the polarizations are uniquely determined. It is not restrictive to assume that $M = 1$ and that $\mathbf{x}_1 = \mathbf{0}$. We can write $\mathbf{E}_{\dagger,1} = \mathbf{K}_1 + \hat{\mathbf{E}}_{\dagger,1}$ and $\mathbf{E}_{\dagger,2} = \mathbf{K}_2 + \hat{\mathbf{E}}_{\dagger,2}$, where \mathbf{K}_1 and \mathbf{K}_2 are defined as in (3.15), with two different polarizations $\mathbf{q}_{0,1}$ and $\mathbf{q}_{0,2}$; in particular, we know that $\hat{\mathbf{E}}_{\dagger,1}$ and $\hat{\mathbf{E}}_{\dagger,2}$ belong to $H(\text{curl}; \Omega)$. Proceeding as before, the unique continuation principle yields $\mathbf{E}_{\dagger,1} = \mathbf{E}_{\dagger,2}$ in $\Omega \setminus B_r(\mathbf{0})$ for each $r > 0$; therefore, $\mathbf{K}_1 - \mathbf{K}_2 = \hat{\mathbf{E}}_{\dagger,2} - \hat{\mathbf{E}}_{\dagger,1}$ in $\Omega \setminus B_r(\mathbf{0})$. Since $(\hat{\mathbf{E}}_{\dagger,2} - \hat{\mathbf{E}}_{\dagger,1}) \in (L^2(\Omega))^3$, it follows that $\mathbf{K}_1 - \mathbf{K}_2 \in (L^2(\Omega))^3$, and this is not possible, due to the singularity of the fundamental solution, unless $\mathbf{K}_1 = \mathbf{K}_2$, namely $\mathbf{q}_{0,1} = \mathbf{q}_{0,2}$. \square

Remark 3.4.1 *In Theorem 3.4.2, we have proved the existence and uniqueness of the solution \mathbf{E}_\dagger under the homogeneity assumption (3.14). We do not have similar result under the assumption of Theorem 3.4.3.*

3.4.1 Explicit determination of the dipole source

For the sake of simplicity, consider a source given by only one dipole: $\mathbf{J}_e = p^* \delta_{\mathbf{x}^*}$. Proceeding as in the proof of (3.8), one obtains the representation formula

$$p^* \cdot \bar{\mathbf{z}}(\mathbf{x}^*) = (i\omega)^{-1} \int_{\Gamma} \mathbf{E}^* \times \mathbf{n}_\Gamma \cdot (\mu^{-1} \text{curl } \bar{\mathbf{z}}) - \int_{\Gamma} \mathbf{H}^* \times \mathbf{n}_\Gamma \cdot \bar{\mathbf{z}}, \quad (3.18)$$

for each $\mathbf{z} \in H(\text{curl}; \Omega_C)$, continuous around \mathbf{x}^* and satisfying

$$\text{curl}(\mu^{-1} \text{curl } \mathbf{z}) - i\omega\sigma\mathbf{z} = \mathbf{0} \quad \text{in } \Omega_C. \quad (3.19)$$

To determine the source, we have to find the polarization p^* and the position \mathbf{x}^* : therefore, the components of these two vectors, on the whole six unknowns. The natural idea is to choose in a suitable way six functions \mathbf{z} in (3.18), and solve the corresponding nonlinear system.

Let us assume that μ and σ are constants. The usual choice is to take $\mathbf{z}(\mathbf{x}) = \mathbf{b}e^{i\kappa\mathbf{d}\cdot\mathbf{x}}$, with $\kappa \in \mathbb{C}$, $\mathbf{b} \in \mathbb{R}^3$, $\mathbf{d} \in \mathbb{R}^3$. In order that \mathbf{z} is a solution to (3.19) we need

$$\kappa^2 = i\omega\mu\sigma, \quad \mathbf{b} \cdot \mathbf{d} = 0.$$

Hence, $\kappa = \sqrt{\frac{\omega\mu\sigma}{2}}(1+i)$ if $\omega > 0$ and $\kappa = \sqrt{\frac{|\omega\mu\sigma|}{2}}(1-i)$ if $\omega < 0$. It is not restrictive to assume $|\mathbf{d}| = |\mathbf{b}| = 1$.

The values of \mathbf{p}^* and \mathbf{x}^* are uniquely determined by solving the nonlinear system (3.18) obtained by suitable selections of \mathbf{b} and \mathbf{d} . For instance, taking $\mathbf{b} = \mathbf{e}_1$, $\mathbf{d} = \mathbf{e}_2$, or $\mathbf{b} = \mathbf{e}_2$, $\mathbf{d} = \mathbf{e}_3$, or $\mathbf{b} = \mathbf{e}_3$, $\mathbf{d} = \mathbf{e}_2$, where \mathbf{e}_i represents the standard euclidean basis, one has

$$-i\omega p_1^* e^{-i\bar{\kappa}x_2^*} = A_{1,2}, \quad -i\omega p_2^* e^{-i\bar{\kappa}x_3^*} = A_{2,3}, \quad -i\omega p_3^* e^{-i\bar{\kappa}x_2^*} = A_{3,2}. \quad (3.20)$$

Here, $A_{i,j}$ denotes the right hand side in equation (3.18), hence a computable complex number, corresponding to the choice $\mathbf{z}(\mathbf{x}) = \mathbf{b}e^{i\bar{\kappa}\mathbf{d}\cdot\mathbf{x}}$, with $\mathbf{b} = \mathbf{e}_i$, $\mathbf{d} = \mathbf{e}_j$. Since $\mathbf{p}^* \neq \mathbf{0}$, at least one of its components is different from 0; hence at least one of the values $A_{1,2}$, $A_{2,3}$ or $A_{3,2}$ is different from 0. Let us assume for instance that $p_1^* \neq 0$, $A_{1,2} \neq 0$. Taking $\mathbf{b} = \mathbf{e}_1$, $\mathbf{d} = \mathbf{e}_3$ and $\mathbf{b} = \mathbf{e}_1$, $\mathbf{d} = \frac{1}{\sqrt{2}}(\mathbf{e}_2 + \mathbf{e}_3)$ one has

$$-i\omega p_1^* e^{-i\bar{\kappa}x_3^*} = A_{1,3}, \quad -i\omega p_1^* e^{-i\bar{\kappa}\frac{1}{\sqrt{2}}(x_2^*+x_3^*)} = A_{1,23},$$

where $A_{1,23}$ is obtained as before from the latter choice of \mathbf{b} and \mathbf{d} . Hence

$$e^{-i\bar{\kappa}(x_3^*-x_2^*)} = \frac{A_{1,3}}{A_{1,2}}, \quad e^{-i\bar{\kappa}\left[\frac{1}{\sqrt{2}}(x_2^*+x_3^*)-x_2^*\right]} = \frac{A_{1,23}}{A_{1,2}},$$

For the sake of simplicity let us assume $\omega > 0$, so that $-i\bar{\kappa} = -\sqrt{\frac{\omega\mu\sigma}{2}}(1+i)$ and

$$\begin{aligned} |e^{-i\bar{\kappa}(x_3^*-x_2^*)}| &= e^{-\sqrt{\frac{\omega\mu\sigma}{2}}(x_3^*-x_2^*)} = \left| \frac{A_{1,3}}{A_{1,2}} \right| \\ |e^{-i\bar{\kappa}\left[\frac{1}{\sqrt{2}}(x_2^*+x_3^*)-x_2^*\right]}| &= e^{-\sqrt{\frac{\omega\mu\sigma}{2}}\left[\frac{1}{\sqrt{2}}(x_2^*+x_3^*)-x_2^*\right]} = \left| \frac{A_{1,23}}{A_{1,2}} \right|. \end{aligned}$$

Therefore one has the following linear system for x_2^* and x_3^*

$$\begin{aligned} x_3^* - x_2^* &= -\sqrt{\frac{2}{\omega\mu\sigma}} \log \left| \frac{A_{1,3}}{A_{1,2}} \right|, \\ \frac{1}{\sqrt{2}}(x_2^* + x_3^*) - x_2^* &= -\sqrt{\frac{2}{\omega\mu\sigma}} \log \left| \frac{A_{1,23}}{A_{1,2}} \right|, \end{aligned}$$

obtaining

$$\begin{aligned} x_2^* &= \frac{\sqrt{2}+1}{\sqrt{\omega\mu\sigma}} \left[\log \left| \frac{A_{1,3}}{A_{1,2}} \right| - \sqrt{2} \left| \frac{A_{1,23}}{A_{1,2}} \right| \right] \\ x_3^* &= \frac{1}{\sqrt{\omega\mu\sigma}} \left[\log \left| \frac{A_{1,3}}{A_{1,2}} \right| - (2 + \sqrt{2}) \left| \frac{A_{1,23}}{A_{1,2}} \right| \right]. \end{aligned}$$

Replacing in (3.20) we can compute the three components of \mathbf{p}^* .

It remains to compute x_1^* . If \mathbf{p}^* has two components different from zero, say, $p_1^* \neq 0$ and $p_2^* \neq 0$, taking $\mathbf{b} = \mathbf{e}_2$ and $\mathbf{d} = \mathbf{e}_1$ we have the equation

$$-i\omega p_2^* e^{-i\bar{\kappa}x_1^*} = A_{2,1},$$

from which we determine x_1^* . Otherwise, taking $\mathbf{b} = \frac{1}{\sqrt{2}}(\mathbf{e}_1 + \mathbf{e}_2)$ and $\mathbf{d} = \frac{1}{\sqrt{2}}(\mathbf{e}_1 - \mathbf{e}_2)$ we obtain

$$-i\omega \frac{1}{\sqrt{2}} p_1^* e^{-i\bar{\kappa}\frac{1}{\sqrt{2}}(x_1^*-x_2^*)} = A_{12,12},$$

with the usual notation for $A_{12,12}$.

3.5 Application to EEG/MEG

MEG measures the magnetic induction along a certain direction depending on the magnetometer. Typically, it measures the normal component of the magnetic induction, namely $\mu\mathbf{H} \cdot \mathbf{n}_\Gamma$. On the other hand, EEG measures the electric potential on the surface of the head. We have obtained some explicit relations between the source and the tangential component of the electric field and the magnetic field on Γ (equations (3.8), (3.12) and (3.18)). We will show that, when using the eddy current model, both $(\mathbf{E} \times \mathbf{n}_\Gamma)|_\Gamma$ and $(\mathbf{H} \times \mathbf{n}_\Gamma)|_\Gamma$ can be computed from the normal component of the magnetic induction $(\mu\mathbf{H} \cdot \mathbf{n}_\Gamma)|_\Gamma$ and the electric potential $V|_\Gamma$.

We have already seen that knowledge of $(\mathbf{E} \times \mathbf{n}_\Gamma)|_\Gamma$ furnishes \mathbf{H}_I in Ω_I , hence in particular $(\mathbf{H} \times \mathbf{n}_\Gamma)|_\Gamma$ (see for instance the arguments in the proof of Theorem 3.2.1, (i)). Thus it is enough to show that $(\mathbf{E} \times \mathbf{n}_\Gamma)|_\Gamma$ can be determined from $(\mu\mathbf{H} \cdot \mathbf{n}_\Gamma)|_\Gamma$ and $V|_\Gamma$.

Now we need some preliminaries concerning tangential differential operators. The standard definition of the tangential gradient and the tangential curl on the flat surface $\{x_3 = 0\}$ with unit normal vector $\mathbf{n} = (0, 0, 1)$ is

$$\text{grad}_\tau \phi = (\partial_1 \phi, \partial_2 \phi, 0) \quad \text{Curl}_\tau \phi = \text{grad}_\tau \phi \times \mathbf{n} = (\partial_2 \phi, -\partial_1 \phi, 0).$$

Using local coordinates, it is possible to define the operators grad_τ and Curl_τ for function belonging to $H^1(\Gamma)$. By a duality argument, the adjoin operators div_τ and curl_τ are also introduced, as well as the Laplace–Beltrami operator $\Delta_\tau := \text{div}_\tau \text{grad}_\tau = -\text{curl}_\tau \text{Curl}_\tau$.

On Γ one has the following Hodge decomposition of the electric field (see Buffa *et al.* [22]):

$$\mathbf{n}_\Gamma \times \mathbf{E} \times \mathbf{n}_\Gamma = \text{grad}_\tau v + \text{Curl}_\tau q, \quad (3.21)$$

with $q \in H^1(\Gamma)/\mathbb{C}$ such that

$$\begin{aligned} \Delta_\tau q &= -\text{curl}_\tau \text{Curl}_\tau q = -\text{curl}_\tau (\mathbf{n}_\Gamma \times \mathbf{E} \times \mathbf{n}_\Gamma) \\ &= -\text{div}_\tau (\mathbf{E} \times \mathbf{n}_\Gamma) = -\text{curl} \mathbf{E} \cdot \mathbf{n}_\Gamma = i\omega\mu\mathbf{H} \cdot \mathbf{n}_\Gamma, \end{aligned}$$

and $v \in H^{1/2}(\Gamma)$, $v = V|_\Gamma$ with $V \in H^1(\Omega_C)$ and $\text{grad}_\tau v = \mathbf{n}_\Gamma \times \text{grad} V \times \mathbf{n}_\Gamma$. Hence, $\mathbf{n}_\Gamma \times \mathbf{E} \times \mathbf{n}_\Gamma$ can be obtained from knowledge of $\mu\mathbf{H} \cdot \mathbf{n}_\Gamma$ and V on Γ .

Remark 3.5.1 *Though it could sound strange, it is not completely clear what we say when we speak about the measure of the scalar electric potential (see, e.g., [53], [19], and references therein). In fact, with the exception of the static case, the electric field is not irrotational; therefore it has not a scalar potential.*

As it is well known, the electric field \mathbf{E} can be split into the sum of a gradient and a solenoidal field, but this can be done in several different way (see, e.g., Alonso Rodríguez and Valli [5],

Sect. A.3). Hence, here we are saying that, if the measure obtained by a voltmeter is the scalar v appearing in (3.21) (up to an additive constant) and the measure obtained by a magnetometer is $\mu \mathbf{H} \cdot \mathbf{n}_\Gamma$, then we can reconstruct the value of $\mathbf{n}_\Gamma \times \mathbf{E} \times \mathbf{n}_\Gamma$ on Γ .

In real-life applications, the measurements are only made on a subset of the boundary $\Gamma_m \subset \Gamma$. Also in this case it is possible to obtain a representation formula for the source in terms of the tangential components of the electric and the magnetic fields on Γ_m . Following Albanese and Monk [3], it is easy to show formally that for any $\mathbf{z} \in H(\text{curl}; \Omega \setminus \Gamma_m)$ such that $\text{curl}(\mu^{-1} \text{curl } \mathbf{z}) - i\omega \sigma \mathbf{z} = \mathbf{0}$ in $\Omega \setminus \Gamma_m$ and $(\mu^{-1} \text{curl } \mathbf{z}) \times \mathbf{n} = \mathbf{0}$ on $\partial\Omega$, we have

$$\langle \mathbf{J}_e, \mathbf{z} \rangle = (i\omega)^{-1} \int_{\Gamma_m} \mathbf{E} \times \mathbf{n}_\Gamma \cdot [[\mu^{-1} \text{curl } \bar{\mathbf{z}}]]_T - \int_{\Gamma_m} \mathbf{H} \times \mathbf{n}_\Gamma \cdot [[\bar{\mathbf{z}}]]_T, \quad (3.22)$$

where $[[\mathbf{v}]]_T$ denotes the jump of the tangential trace of $\mathbf{v} \in H(\text{curl}; \Omega \setminus \Gamma_m)$ across Γ_m and $\langle \mathbf{J}_e, \mathbf{z} \rangle = \int_{\Omega_C} \mathbf{J}_e \cdot \bar{\mathbf{z}}$ for volume currents $\mathbf{J}_e \in (L^2(\Omega_C))^3$, $\langle \mathbf{J}_e, \mathbf{z} \rangle = \int_{\partial B} \mathbf{J}_e \cdot \bar{\mathbf{z}}$ for surface currents $\mathbf{J}_e \in H^{-1/2}(\text{div}_\tau; \partial B)$ and $\langle \mathbf{J}_e, \mathbf{z} \rangle = \mathbf{p}^* \cdot \bar{\mathbf{z}}(\mathbf{x}^*)$ for a dipole source $\mathbf{J}_e = \mathbf{p}^* \delta_{\mathbf{x}^*}$.

Also, in this case the tangential component of the electric field on Γ_m can be obtained from the electric potential and the normal component of the magnetic induction, provided that the measured electric potential V is such that

$$\text{grad } V \cdot \mathbf{t} = \mathbf{E} \cdot \mathbf{t} \quad \text{on } \partial\Gamma_m,$$

where \mathbf{t} is the unit tangent vector on $\partial\Gamma_m$. In this way $q \in H^1(\Gamma_m)/\mathbb{C}$ is the solution of

$$\begin{cases} \Delta_\tau q = i\omega \mu \mathbf{H} \cdot \mathbf{n}_\Gamma & \text{in } \Gamma_m \\ \text{Curl}_\tau q \cdot \mathbf{t} = 0 & \text{on } \partial\Gamma_m. \end{cases}$$

However, if we know $\mathbf{E} \times \mathbf{n}_\Gamma$ only on Γ_m and not in the whole boundary Γ , it is not possible to obtain $(\mathbf{H} \times \mathbf{n}_\Gamma)_{|\Gamma_m}$. So in order to use the representation formula (3.22) in an inversion scheme, it would be necessary to measure also the tangential component of the magnetic field on Γ_m .

Chapter 4

A posteriori error estimates for the problem of electrostatics with a dipole source

4.1 Introduction

Electroencephalography (EEG) is a widely used technique for reconstruction of brain activity. The task is to estimate the cerebral current sources underlying a measured distribution of the scalp electric potential. The inverse problem requires a model for the forward problem, i.e., the computation of the scalp potential given a neural current source. Since the frequency spectrum for electrophysiological signal is frequently between 0.1 and 100 Hz, most works on biomedical applications focus on the static approximation of Maxwell equations. Concerning the source, the activity measured in EEG is the result of movement of ions that, creating an electrical potential difference, generates the so-called primary current. Since the source is localized, it is generally modeled as a current dipole centered at a point \mathbf{x}_0 with moment \mathbf{p} .

For computing the solution of the forward problem, the finite element method has become popular because it allows a realistic representation of the geometry and conductivity of the different tissues. In particular it allows to deal with anisotropic conductivities. In this case the forward problem is non-standard and it is usually solved by the subtraction approach (see [16], [67], [46]). Recently the well-posedness of the problem was studied in [65] using the duality method. There it is proved that, in the three dimensional (3D) case, the solution belongs to L^p for $1 \leq p < 3/2$. The same arguments allow proving that in the two dimensional case (2D) the solution belongs to L^p for $1 \leq p < 2$. Finite elements have been used in practice for both approaches: the subtraction method and the direct one. For the former, a sound mathematical

and numerical analysis can be found in [67] under the assumption that there is a neighborhood of the source position \boldsymbol{x}_0 with constant conductivity. On the other hand, the direct approach is widely used in source reconstruction (see e.g. [68], [21], [66], [62]) and can be used even for a variable conductivity (smooth in a neighborhood of \boldsymbol{x}_0). However it has not been rigorously analyzed yet. The aim of this chapter is to take advantage of the method in [65] to provide such analysis.

In spite of the fact that the solution is only in L^p , it can be approximated by standard finite elements. Specifically we use piecewise linear continuous elements on polyhedral or polygonal domains. Even though the original problem is three dimensional we present the results in more detail in the 2D framework. Under the assumption that the computational domain Ω is bounded, convex and polygonal, we develop a priori and a posteriori error analyses in L^p norm for this problem. In particular, we prove an a priori error estimate under the assumption that the meshes are quasiuniform. Since the solution is highly singular at \boldsymbol{x}_0 , quasiuniformity is an excessively restrictive assumption in practice. This is the reason why we also derive an a posteriori error analysis which does not need the quasiuniformity assumption. We introduce a posteriori error indicators and prove their reliability and efficiency. Subsequently, we briefly discuss the 3D case and present similar results under more stringent assumptions on the geometry of the domain and the electric conductivity. We use these error indicators to guide an adaptive scheme, which experimentally exhibits optimal order of convergence.

The chapter is organized as follows. In Section 4.2 we state the model problem, a finite element discretization (in 2D and 3D), and give an a priori estimate of the error in L^p norm for the 2D case. In Section 4.3, we introduce some generalized bubble functions and prove some technical lemmas, which will be used in the sequel. The main result is presented in Section 4.4, where we perform the a posteriori error analysis for the 2D case. In Section 4.5, we briefly analyze the a priori and a posteriori estimates in 3D. Finally, in Section 4.6, we report some numerical results illustrating the performance of the adaptive scheme.

4.2 Model problem

In this section we introduce the model problem, propose a variational formulation and recall the existence and uniqueness of solution. Then, we consider a finite element discretization and give an a priori error estimate.

4.2.1 Continuous problem

We start introducing the Maxwell equations:

$$\begin{cases} \operatorname{curl} \mathbf{H} - \epsilon \frac{\partial \mathbf{E}}{\partial t} = \boldsymbol{\sigma} \mathbf{E} + \mathbf{J}_p, \\ \operatorname{curl} \mathbf{E} + \mu \frac{\partial \mathbf{H}}{\partial t} = \mathbf{0}, \end{cases}$$

where \mathbf{E} and \mathbf{H} are the electric and magnetic fields, respectively, \mathbf{J}_p is the source current density, ϵ the electric permittivity, μ the magnetic permeability and $\boldsymbol{\sigma}$ the electric conductivity.

By disregarding the time variation one obtains the static model:

$$\begin{cases} \operatorname{curl} \mathbf{H} = \boldsymbol{\sigma} \mathbf{E} + \mathbf{J}_p, \\ \operatorname{curl} \mathbf{E} = \mathbf{0}. \end{cases}$$

If we consider a simply connected domain $D \subset \mathbb{R}^3$, then there exists a scalar potential u such that $\mathbf{E} = -\nabla u$ in D . As a consequence, calculating the divergence of the first equation, we obtain

$$\operatorname{div}(\boldsymbol{\sigma} \nabla u) = \operatorname{div} \mathbf{J}_p \quad \text{in } D.$$

If Ω is a conductive domain completely included in D and $D \setminus \overline{\Omega}$ is not conductive, then, due to the properties of the div operator, the equation above is equivalent to $\operatorname{div}(\boldsymbol{\sigma} \nabla u - \mathbf{J}_p)|_{\Omega} = 0$ in Ω , $\operatorname{div}(\boldsymbol{\sigma} \nabla u - \mathbf{J}_p)|_{D \setminus \overline{\Omega}} = 0$ and $(\boldsymbol{\sigma} \nabla u - \mathbf{J}_p)|_{\Omega} \cdot \mathbf{n} = (\boldsymbol{\sigma} \nabla u - \mathbf{J}_p)|_{D \setminus \overline{\Omega}} \cdot \mathbf{n}$ on the interface $\partial\Omega$, being \mathbf{n} the outer unit normal vector to $\partial\Omega$. Since $\boldsymbol{\sigma}$ vanishes outside $\overline{\Omega}$ and \mathbf{J}_p is assumed to be supported in Ω , the electrostatics problem reads

$$\begin{cases} \operatorname{div}(\boldsymbol{\sigma} \nabla u) = \operatorname{div} \mathbf{J}_p & \text{in } \Omega, \\ (\boldsymbol{\sigma} \nabla u) \cdot \mathbf{n} = 0 & \text{on } \partial\Omega. \end{cases}$$

This is the model more frequently used for the electrical brain activity (see e.g. [61], [39], [51]).

Let us assume that a small activated region is centered at a point \mathbf{x}_0 and that the observation point is far from it. In this case the primary current \mathbf{J}_p is typically modeled as a dipole. So, in the following, we consider the electrostatic problem with a dipole as source term and homogeneous Neumann boundary condition:

$$\begin{cases} \operatorname{div}(\boldsymbol{\sigma} \nabla u) = \operatorname{div}(\mathbf{p} \delta_{\mathbf{x}_0}) & \text{in } \Omega, \\ (\boldsymbol{\sigma} \nabla u) \cdot \mathbf{n} = 0 & \text{on } \partial\Omega. \end{cases} \quad (4.1)$$

Here \mathbf{x}_0 is an inner point of Ω , and $\mathbf{p} \neq \mathbf{0}$ is the polarization vector. The conductivity $\boldsymbol{\sigma}$ is a matrix with entries in $L^\infty(\Omega)$ and uniformly positive definite, namely, there exists a positive constant σ_0 such that

$$\sum_{i,j=1}^3 \xi_i \sigma_{i,j}(\mathbf{x}) \xi_j \geq \sigma_0 \sum_{i=1}^3 \xi_i^2 \quad \forall \boldsymbol{\xi} \in \mathbb{R}^3, \quad \text{a.e. } \mathbf{x} \in \Omega. \quad (4.2)$$

Moreover we assume that there exists $r_0 > 0$ such that $\sigma_{i,j} \in W^{1,\infty}(B_{r_0}(\mathbf{x}_0))$ for $i, j = 1, 2, 3$, where $B_{r_0}(\mathbf{x}_0) := \{\mathbf{x} \in \mathbb{R}^3 : |\mathbf{x} - \mathbf{x}_0| < r_0\}$. This is a technical assumption used in [65] for the proof of the well-posedness of the problem by means of a duality argument.

Let us consider the following weak formulation of (4.1) given in [65]: find $u \in L^p(\Omega)$ such that

$$\begin{cases} \int_{\Omega} u \operatorname{div}(\boldsymbol{\sigma} \nabla \varphi) = -\mathbf{p} \cdot \nabla \varphi(\mathbf{x}_0) & \forall \varphi \in X_q, \\ \int_{\Omega} u = 0, \end{cases} \quad (4.3)$$

where

$$X_q := \{\varphi \in W^{1,q}(\Omega) : \varphi \in C^1(B_{r^*}(\mathbf{x}_0)), \operatorname{div}(\boldsymbol{\sigma} \nabla \varphi) \in L^q(\Omega), (\boldsymbol{\sigma} \nabla \varphi) \cdot \mathbf{n} = 0 \text{ on } \partial\Omega\},$$

being r^* a fixed number such that $0 < r^* < r_0$. Moreover, here and thereafter $\frac{1}{p} + \frac{1}{q} = 1$.

The second condition of (4.3) filters out additive constants and therefore is suitable for assuring uniqueness of the solution u .

The following theorem, which is proved in [65, Remark 3.3], ensures the existence and uniqueness of solution to (4.3):

Theorem 4.2.1 *For all p with $1 \leq p < 3/2$, there exists a unique solution $u \in L^p(\Omega)$ to (4.3), which is the same for all p in this range.*

Remark 4.2.1 *The same arguments used for the previous theorem allow us to prove the well-posedness of the problem in the 2D case; in such a case, we have existence and uniqueness of a solution $u \in L^p(\Omega)$ for each p with $1 \leq p < 2$.*

4.2.2 Discrete problem

We assume that Ω is either a Lipschitz polyhedron (3D) or a Lipschitz polygon (2D).

We consider a regular family of tetrahedral (or triangular) meshes \mathcal{T}_h of Ω (see, for instance, [23]). As usual, h denotes the mesh size: $h := \max_{T \in \mathcal{T}_h} h_T$, h_T being the diameter of T . We consider the space of Lagrange finite elements of degree one:

$$H_h := \{v_h \in C(\Omega) : v_h|_T \in \mathcal{P}_1 \forall T \in \mathcal{T}_h\}.$$

(\mathcal{P}_k denotes the set of polynomials with degree not larger than $k \in \mathbb{N}$.) Notice that $H_h \subset L^p(\Omega)$ for all $p \geq 1$.

Let $T_0 \in \mathcal{T}_h$ be such that $\mathbf{x}_0 \in T_0$. Usually \mathbf{x}_0 will be an inner point of an element of \mathcal{T}_h , however if \mathbf{x}_0 belongs to more than one $T \in \mathcal{T}_h$, any element T_0 containing \mathbf{x}_0 can be chosen.

The finite element approximation of (4.3) reads: find $u_h \in H_h$ such that

$$\begin{cases} \int_{\Omega} \boldsymbol{\sigma} \nabla u_h \cdot \nabla v_h = \mathbf{p} \cdot \nabla (v_h|_{T_0})(\mathbf{x}_0) & \forall v_h \in H_h, \\ \int_{\Omega} u_h = 0. \end{cases} \quad (4.4)$$

Although some average of the gradients of different elements containing \mathbf{x}_0 could also be used, our analysis shows that the simplest minded approach of choosing a particular arbitrary element works fine.

To find an a priori error estimate in $L^p(\Omega)$, with $1 \leq p < 2$ in the 2D case and $1 \leq p < 3/2$ in the 3D case, we will use a duality argument. With this end, we consider the following auxiliary problem: given $\psi \in L^q(\Omega)$, find $\varphi \in H^1(\Omega)$ such that

$$\begin{cases} \operatorname{div}(\boldsymbol{\sigma} \nabla \varphi) = \psi - \frac{1}{|\Omega|} \int_{\Omega} \psi & \text{in } \Omega, \\ (\boldsymbol{\sigma} \nabla \varphi) \cdot \mathbf{n} = 0 & \text{on } \partial\Omega, \\ \int_{\Omega} \varphi = 0. \end{cases} \quad (4.5)$$

This problem is well-posed if $q > 1$ (2D case) or $q > 6/5$ (3D case). Since q will be the dual exponent of p , we will consider this problem for $q > 2$ (2D case) or $q > 3$ (3D case).

We will need the solution of this problem to be in $W^{2,q}(\Omega)$. This is true under suitable assumptions. First of all, we require that $\boldsymbol{\sigma} \in [C^1(\overline{\Omega})]^{2 \times 2}$ (note that this not a realistic assumption when modeling the brain conductivity, which presents discontinuities across the different tissues). Moreover, we assume that Ω is convex. Then the arguments used to prove [31, Corollary 3.12] allow us to show that $\varphi \in W^{2,q}(\Omega)$ for each q such that $2 < q < q_0$, for a suitable q_0 (for the Laplace operator in the 2D case, it is known that $q_0 = \frac{2}{2-\pi/\theta}$, θ being the largest inner angle of Ω). Moreover

$$\|\varphi\|_{2,q,\Omega} \leq C \|\psi\|_{0,q,\Omega}. \quad (4.6)$$

We do not know if, for a general convex polyhedron, one has $q_0 > 3$. Therefore, despite the original problem is set in the 3D case, from now on we will present our results in the 2D framework. In Section 4.5, we will extend them to the 3D case, although under additional stringent assumptions. So, in the following we will consider a convex Lipschitz polygon $\Omega \subset \mathbb{R}^2$.

In what follows we will denote $v^I \in H_h$ the Lagrange interpolant of v . Notice that, in particular, φ^I is well defined because $\varphi \in W^{2,q}(\Omega)$. Let us recall the following 2D interpolation error estimates. For their proof see, e.g., [20, Theorem 4.4.4 and Corollary 4.4.7].

Proposition 4.2.1 *Suppose $1 < q \leq \infty$ and $m > \frac{2}{q}$. Then, for $0 \leq i \leq m$ and $v \in W^{m,q}(T)$, $T \in \mathcal{T}_h$, we have*

$$|v - v^I|_{i,q,T} \leq Ch_T^{m-i} |v|_{m,q,T}, \quad (4.7)$$

$$|v - v^I|_{i,\infty,T} \leq Ch_T^{m-i-2/q} |v|_{m,q,T}. \quad (4.8)$$

Here and thereafter C , as well as C' , denote strictly positive constants, not necessarily the same at each occurrence, but always independent of the mesh size.

Moreover we have the following error estimate for the elliptic projection:

Lemma 4.2.1 *Let Ω be a convex Lipschitz polygon. Let $\{\mathcal{T}_h\}$ be a quasiuniform family of subdivisions of Ω (namely, there exists a positive constant τ , independent of h , such that $\tau h \leq h_T \leq h$ for all $T \in \mathcal{T}_h$ and for all \mathcal{T}_h). Assume that $\sigma \in [C^1(\bar{\Omega})]^{2 \times 2}$. Consider a function $\xi \in W^{2,q}(\Omega)$ for $q > 2$ and let $\xi^P \in H_h$ be the unique solution of*

$$\begin{cases} \int_{\Omega} \sigma \nabla v_h \cdot \nabla \xi^P = \int_{\Omega} \sigma \nabla v_h \cdot \nabla \xi & \forall v_h \in H_h, \\ \int_{\Omega} \xi^P = 0. \end{cases} \quad (4.9)$$

Then there exists $h_0 > 0$ such that

$$|\xi - \xi^P|_{1,\infty,T} \leq Ch^{1-2/q} \|\xi\|_{2,q,\Omega} \quad \forall T \in \mathcal{T}_h \quad (4.10)$$

for $0 < h < h_0$.

Proof. This is a standard estimate for the elliptic projection; we include a brief proof for completeness. We consider an arbitrary $T \in \mathcal{T}_h$. Using (4.8) and an inverse estimate (see [20, Lemma 4.5.3]) we have

$$\begin{aligned} |\xi - \xi^P|_{1,\infty,T} &\leq |\xi - \xi^I|_{1,\infty,T} + |(\xi - \xi^P)^I|_{1,\infty,T} \\ &\leq C \left(h_T^{1-2/q} |\xi|_{2,q,T} + h_T^{-2/q} \|(\xi - \xi^P)^I\|_{1,q,T} \right). \end{aligned}$$

On the other hand,

$$\|(\xi - \xi^P)^I\|_{1,q,\Omega} \leq \|\xi - \xi^I\|_{1,q,\Omega} + \|\xi - \xi^P\|_{1,q,\Omega} \leq Ch \|\xi\|_{2,q,\Omega}$$

(see, for instance, [20, Theorem 4.4.4 and equation (8.5.4)]), and the desired result follows by using the quasiuniformity of the meshes. \square

Now we are in a position to prove an a priori error estimate for the proposed finite element scheme.

Theorem 4.2.2 *Let \mathcal{T}_h be a quasiuniform family of subdivisions of the convex Lipschitz polygon Ω and assume that $\sigma_{i,j} \in C^1(\bar{\Omega})$ for each $i, j = 1, 2$. Let u and u_h be the respective solutions to problems (4.3) and (4.4). Then there exists $h_0 > 0$ such that*

$$\|u - u_h\|_{0,p,\Omega} \leq Ch^{2/p-1}$$

for all $0 < h < h_0$ and for all p such that $\frac{q_0}{q_0-1} < p < 2$, where q_0 is the maximal regularity exponent in (4.6).

Proof. Given $\psi \in L^q(\Omega)$ with $\frac{1}{p} + \frac{1}{q} = 1$, we know that the solution φ of (4.5) satisfies $\varphi \in W^{2,q}(\Omega)$ for $2 < q < q_0$. By using (4.3) and integration by parts, we obtain

$$\begin{aligned}
\int_{\Omega} (u - u_h)\psi &= \int_{\Omega} (u - u_h) \left(\operatorname{div}(\boldsymbol{\sigma}\nabla\varphi) + \frac{1}{|\Omega|} \int_{\Omega} \psi \right) \\
&= \int_{\Omega} u \operatorname{div}(\boldsymbol{\sigma}\nabla\varphi) - \int_{\Omega} u_h \operatorname{div}(\boldsymbol{\sigma}\nabla\varphi) \\
&= -\boldsymbol{p} \cdot \nabla\varphi(\boldsymbol{x}_0) + \int_{\Omega} \boldsymbol{\sigma}\nabla u_h \cdot \nabla\varphi \\
&= -\boldsymbol{p} \cdot \nabla\varphi(\boldsymbol{x}_0) + \int_{\Omega} \boldsymbol{\sigma}\nabla u_h \cdot \nabla\varphi^P \\
&= -\boldsymbol{p} \cdot \nabla\varphi(\boldsymbol{x}_0) + \boldsymbol{p} \cdot \nabla(\varphi^P|_{T_0})(\boldsymbol{x}_0),
\end{aligned} \tag{4.11}$$

where φ^P is the unique solution to problem (4.9) (with φ at the right hand side instead of ξ). From Lemma 4.2.1 we have

$$|\nabla\varphi(\boldsymbol{x}_0) - \nabla\varphi^P(\boldsymbol{x}_0)| \leq Ch^{1-2/q}\|\varphi\|_{2,q,\Omega} \leq Ch^{1-2/q}\|\psi\|_{0,q,\Omega},$$

where the last inequality follows from (4.6). Therefore we have

$$\|u - u_h\|_{0,p,\Omega} = \sup_{\psi \in L^q(\Omega)} \frac{\int_{\Omega} (u - u_h)\psi}{\|\psi\|_{0,q,\Omega}} \leq Ch^{1-2/q} = Ch^{2/p-1}.$$

□

The quasiuniformity assumption on the meshes seems unfitting for this problem, because the strong singularity of the solution at \boldsymbol{x}_0 suggests using meshes highly refined in the vicinity of this point. In what follows we will introduce a posteriori estimators of the L^p norm of the error which will be proved to be efficient and reliable without the need of the quasiuniformity assumption. Later on these estimates will be used to devise an adaptive scheme which will lead to an optimal order of convergence in terms of the number of degrees of freedom.

4.3 Preliminary results

For the a posteriori analysis, we will have to deal with three kinds of bubble functions, one associated with triangles, another associated with edges and the last one associated with the point \boldsymbol{x}_0 . In this section we introduce these bubble functions and prove some properties that will be used in the sequel. From now on \boldsymbol{n} will denote a generic unit vector normal to a curve which will be clear from the context.

Let b_T be the bubble function with support in T defined in Ω by

$$b_T(\mathbf{x}) := \begin{cases} (\lambda_1^T \lambda_2^T \lambda_3^T)^2 \frac{|\mathbf{x} - \mathbf{x}_0|^2}{h_T^2} & \text{if } \mathbf{x}_0 \in T \\ (\lambda_1^T \lambda_2^T \lambda_3^T)^2 & \text{otherwise.} \end{cases} \quad (4.12)$$

where λ_i^T is the barycentric coordinate of \mathbf{x} associated with the triangle T and its vertex P_i , $i = 1, 2, 3$. The function b_T have the following properties:

Lemma 4.3.1 *Given $T \in \mathcal{T}_h$, let b_T be defined as above. Then*

$$0 \leq b_T \leq 1, \quad (4.13)$$

$$b_T = 0 \quad \text{on} \quad \partial T, \quad (4.14)$$

$$\nabla b_T = 0 \quad \text{on} \quad \partial T, \quad (4.15)$$

$$\int_T b_T \geq C|T|, \quad (4.16)$$

$$\|b_T\|_{2,q,T} \leq C|T|^{-1/p}. \quad (4.17)$$

Proof. Equations (4.13), (4.14), and (4.15) are immediate consequences of the definition of b_T . Estimate (4.16) follows from straightforward computations and (4.17) from standard scaling arguments (see [24, Theorem 15.1]):

$$\|b_T\|_{2,q,T} \leq Ch_T^{-4/p} \|b_T\|_{0,p,T} \leq Ch_T^{-2/p} \leq C|T|^{-1/p}.$$

□

Let $\mathcal{E}_{h,i}$ be the set of all the inner edges and $\mathcal{E}_{h,e}$ the set of boundary edges of the triangulation \mathcal{T}_h . Given $\ell \in \mathcal{E}_h := \mathcal{E}_{h,i} \cup \mathcal{E}_{h,e}$ we will define a bubble function with support $\omega_\ell := \{T \in \mathcal{T}_h : \ell \subset \partial T\}$ (see Figure 4.1).

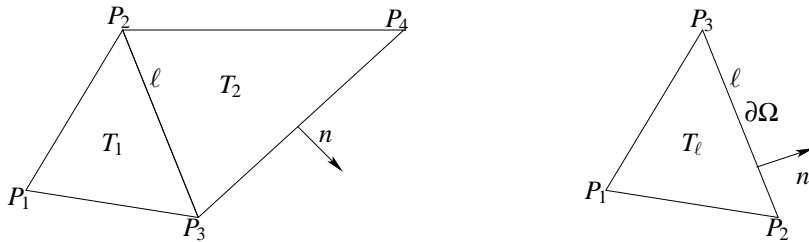


Figure 4.1: The support ω_ℓ of b_ℓ with $\ell \in \mathcal{E}_{h,i}$ and $\ell \in \mathcal{E}_{h,e}$.

In the case $\ell \in \mathcal{E}_{h,i}$ we define b_ℓ for $\mathbf{x} \in \omega_\ell$ by

$$b_\ell(\mathbf{x}) := \begin{cases} \left(\lambda_2^{T_1} \lambda_3^{T_1} \lambda_2^{T_2} \lambda_3^{T_2} \right)^2 \frac{|\mathbf{x} - \mathbf{x}_0|^2}{|\ell|^2} & \text{if } \mathbf{x}_0 \in \omega_\ell \\ \left(\lambda_2^{T_1} \lambda_3^{T_1} \lambda_2^{T_2} \lambda_3^{T_2} \right)^2 & \text{if } \mathbf{x}_0 \notin \omega_\ell, \end{cases} \quad (4.18)$$

where $|\ell|$ denotes the length of ℓ . Since $\lambda_i^{T_j}$ is a linear function in the whole plane, b_ℓ is a polynomial in ω_ℓ .

It remains to define bubble functions b_ℓ for $\ell \in \mathcal{E}_{h,e}$, which, in particular, must satisfy

$$(\boldsymbol{\sigma} \nabla b_\ell) \cdot \mathbf{n} = \nabla b_\ell \cdot (\boldsymbol{\sigma} \mathbf{n}) = 0 \quad \text{on } \ell \quad \text{for all } \ell \in \mathcal{E}_{h,e}.$$

Let T_ℓ be the triangle in \mathcal{T}_h that contains ℓ . For simplicity we assume that $\mathbf{x}_0 \notin T_\ell$. Let (x_i, y_i) be the coordinates of the vertices P_i , $i = 1, 2, 3$, of the triangle T_ℓ , as shown in Figure 4.2. Let $F_\ell : \mathbb{R}^2 \rightarrow \mathbb{R}^2$ be defined by

$$F_\ell \begin{pmatrix} \hat{x} \\ \hat{y} \end{pmatrix} = \begin{pmatrix} x_2 \\ y_2 \end{pmatrix} + Q \begin{pmatrix} \hat{x} \\ \hat{y} \end{pmatrix}$$

where $Q = \begin{pmatrix} x_3 - x_2 & -(y_3 - y_2) \\ y_3 - y_2 & x_3 - x_2 \end{pmatrix}$. Notice that $Q = |\ell| \begin{pmatrix} \mathbf{t} & -\mathbf{n} \end{pmatrix}$ (see Figure 4.2) and that $Q^t Q = |\ell|^2 I$. Hence, denoting $\widehat{T}_\ell := F_\ell^{-1}(T_\ell)$, the triangles \widehat{T}_ℓ and T_ℓ are similar (in particular, both have the same aspect ratio). Let us set $\widehat{\boldsymbol{\sigma}} := Q^t (\boldsymbol{\sigma} \circ F_\ell) Q$; this matrix is symmetric and positive definite for all $(\hat{x}, \hat{y}) \in \widehat{T}_\ell$. It is easy to show that there exists $\delta > 0$ such that $[1/2 - \delta, 1/2 + \delta] \times (0, 2\delta]$ is contained in the interior of \widehat{T}_ℓ (see Figure 4.3). Since δ only depends on the aspect ratio of the triangle \widehat{T}_ℓ , hence of that of T_ℓ , it can be bounded from above and from below by two positive constants, uniformly with respect to h . Now let $g_1 \in \mathcal{D}((1/2 - \delta, 1/2 + \delta))$ be such that $g_1 \geq 0$ and $\int_{\mathbb{R}} g_1 = 1$, and let $g_2 \in C^\infty(\mathbb{R})$ be such that $0 \leq g_2 \leq 1$, $g_2|_{(-\infty, \delta)} = 1$, $g_2|_{(2\delta, +\infty)} = 0$ and $|g_2'| \leq C\delta^{-1}$. We first define

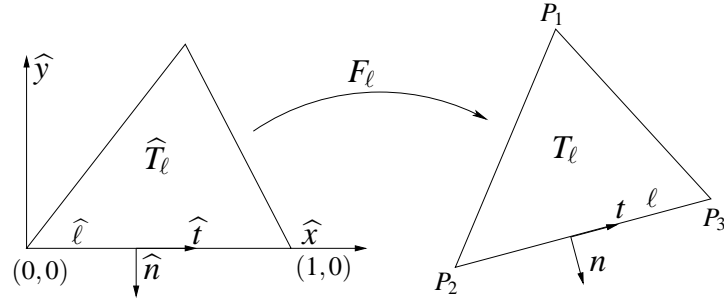
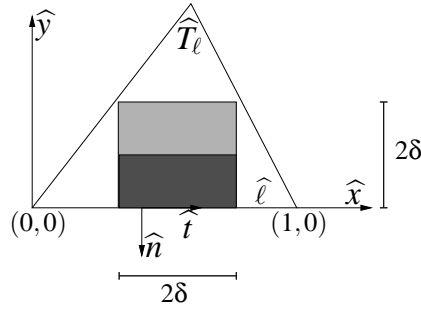
$$\widehat{b}(\hat{x}, \hat{y}) := g_1(\hat{x}) - g_1(\hat{x}) \frac{\widehat{\sigma}_{12}(\hat{x}, 0)}{\widehat{\sigma}_{22}(\hat{x}, 0)} g_2(\hat{y}) \hat{y},$$

then

$$b_\ell := \widehat{b} \circ F_\ell^{-1}|_{T_\ell}. \quad (4.19)$$

Notice that $\widehat{\sigma}_{22}(\hat{x}, 0)$ cannot vanish because $\widehat{\boldsymbol{\sigma}}$ is positive definite. Since $\frac{\partial \widehat{b}}{\partial \hat{x}}(\hat{x}, 0) = g_1'(\hat{x})$ and $\frac{\partial \widehat{b}}{\partial \hat{y}}(\hat{x}, 0) = -g_1(\hat{x}) \frac{\widehat{\sigma}_{12}(\hat{x}, 0)}{\widehat{\sigma}_{22}(\hat{x}, 0)}$, straightforward computations allow us to show that $(\boldsymbol{\sigma} \mathbf{n})^t \nabla b_\ell = |\ell|^{-2} (\widehat{\boldsymbol{\sigma}} \widehat{\mathbf{n}})^t \widehat{\nabla} \widehat{b} = 0$.

Now it is easy to prove the following result for b_ℓ :

Figure 4.2: The definition of F_ℓ .Figure 4.3: The support of b_ℓ .

Lemma 4.3.2 *Given $\ell \in \mathcal{E}_h$, let b_ℓ and ω_ℓ be defined as above. Then*

$$b_\ell|_{\ell^*} = 0 \quad \forall \ell^* \in \mathcal{E}_h, \ell^* \neq \ell, \quad (4.20)$$

$$(\boldsymbol{\sigma} \nabla b_\ell) \cdot \mathbf{n} = 0 \quad \text{on } \partial \omega_\ell, \quad (4.21)$$

$$C|\ell| \leq \int_\ell b_\ell \leq C'|\ell|, \quad (4.22)$$

$$|b_\ell|_{m,q,\omega_\ell} \leq C|\ell|^{2-m-2/p}, \quad m = 0, 1, 2. \quad (4.23)$$

Proof. For the case $\ell \in \mathcal{E}_{h,i}$, the proof runs essentially identical to that of [15, Lemma 3.1]. For $\ell \in \mathcal{E}_{h,e}$ the first three properties have already been checked. The last one follows from standard scaling arguments. \square

The third kind of bubble function concerns the point \mathbf{x}_0 and the triangle T_0 that we have chosen such that $\mathbf{x}_0 \in T_0$. We will denote by h_0 the diameter of T_0 . Let us set

$$\omega_{T_0} := \{T' \in \mathcal{T}_h : T' \cap T_0 \neq \emptyset\} \quad (4.24)$$

and $d := \text{dist}(\mathbf{x}_0, \partial \omega_{T_0})$ (since \mathbf{x}_0 is an inner point of Ω then $d > 0$). Notice that, because of the regularity of the mesh, there exist two positive constants such that $Ch_0 \leq d \leq C'h_0$. Let $\chi(\mathbf{x})$

be the convolution of the characteristic function of the set $\{\mathbf{x} \in \Omega : |\mathbf{x} - \mathbf{x}_0| < d/2\}$ with an appropriate mollifier, so that $\chi(\mathbf{x}) = 1$ if $|\mathbf{x} - \mathbf{x}_0| \leq d/4$, $\chi(\mathbf{x}) = 0$ if $|\mathbf{x} - \mathbf{x}_0| \geq 3d/4$ and $|\nabla\chi(x)| \leq Cd^{-1}$.

We define the bubble function

$$b_0(\mathbf{x}) := \mathbf{p} \cdot (\mathbf{x} - \mathbf{x}_0) \chi(\mathbf{x}). \quad (4.25)$$

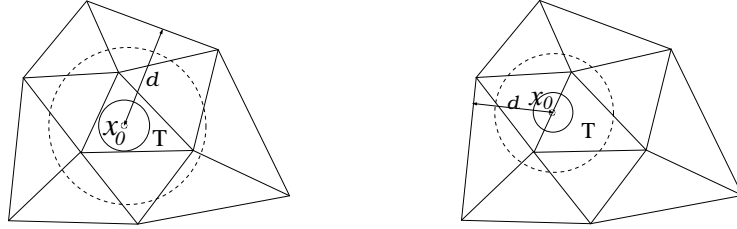


Figure 4.4: Two examples of ω_{T_0} .

The support of b_0 is contained in ω_{T_0} . Moreover the following results hold true:

Lemma 4.3.3 *Let b_0 be defined as above. Then*

$$\nabla b_0(\mathbf{x}_0) = \mathbf{p}, \quad (4.26)$$

$$\nabla b_0 = 0 \quad \text{on } \partial\omega_{T_0}, \quad (4.27)$$

$$b_0(\mathbf{x}) = \mathbf{p} \cdot (\mathbf{x} - \mathbf{x}_0) \quad \forall \mathbf{x} \in \Omega : |\mathbf{x} - \mathbf{x}_0| \leq \frac{d}{4}, \quad (4.28)$$

$$b_0(\mathbf{x}) = 0 \quad \forall \mathbf{x} \in \Omega : |\mathbf{x} - \mathbf{x}_0| \geq \frac{3d}{4}, \quad (4.29)$$

$$|b_0|_{m,\infty,\omega_{T_0}} \leq Cd^{1-m}, \quad m = 0, 1, 2. \quad (4.30)$$

Proof. It follows from straightforward calculations. In particular, (4.30) follows by combining that $|\chi|_{m,\infty,\omega_{T_0}} \leq Cd^{-m}$ (see [15, equation (3.8)]) with the fact that $\mathbf{p} \cdot (\mathbf{x} - \mathbf{x}_0)$ is linear and continuous. \square

Corollary 4.3.1 *Let b_0 and ω_{T_0} be defined as above. Then,*

$$|b_0|_{m,q,\omega_{T_0}} \leq Ch_0^{3-m-2/p}, \quad m = 0, 1, 2,$$

and, for all edge ℓ ,

$$\|b_0\|_{0,q,\ell} \leq C|\ell|^{2-1/p}.$$

Proof. Using (4.30) and the fact that $h_0 \leq Cd \leq Ch_0$, we have

$$|b_0|_{m,q,\omega_{T_0}} \leq |b_0|_{m,\infty,\omega_{T_0}} |\omega_{T_0}|^{1/q} \leq Cd^{1-m} h_0^{2/q} \leq Ch_0^{3-m-2/p}.$$

Moreover, using that

$$\|v\|_{0,q,\partial T} \leq C \|v\|_{0,q,T}^{1-1/q} \|v\|_{1,q,T}^{1/q} \quad \forall v \in W^{1,q}(T)$$

(see [20, Theorem 1.6.6]), we have

$$\|b_0\|_{0,q,\ell} \leq C \|b_0\|_{0,q,\omega_{T_0}}^{1-1/q} \|b_0\|_{1,q,\omega_{T_0}}^{1/q} \leq C |\ell|^{(3-2/p)(1-1/q)} |\ell|^{(2-2/p)(1/q)} = C |\ell|^{2-1/p}.$$

□

To end this section, we recall an error estimate for the Lagrange interpolant $v^I \in H_h$ of a function $v \in C(\bar{\Omega})$.

Lemma 4.3.4 *Given $\ell \in \mathcal{E}_h$, let ω_ℓ be defined as above. There holds*

$$\|v - v^I\|_{0,q,\ell} \leq C |\ell|^{1+1/p} |v|_{2,q,\omega_\ell} \quad \forall v \in W^{2,q}(\omega_\ell), \quad 1 < q < \infty.$$

Proof. See, for instance, [15, Lemma 3.4]. □

4.4 An a posteriori error estimator

According to Remark 4.2.1 the solution of problem (4.3) belongs to $L^p(\Omega)$ with $1 \leq p < 2$. In this section we will define an a posteriori error estimator in the $L^p(\Omega)$ -norm for the finite element approximation error $u - u_h$. We will prove the reliability and efficiency of the estimator for a particular range of p . Let us emphasize that this proof holds for a regular family of meshes and does not need the quasiuniformity assumption, so that the error estimator can be used to drive an adaptive scheme.

For all $T \in \mathcal{T}_h$ we define

$$\begin{aligned} \varepsilon_{T,p} := & \left(h_T^{2p} \|\operatorname{div}(\boldsymbol{\sigma} \nabla u_h)\|_{0,p,T}^p + \frac{1}{2} \sum_{\ell \in \mathcal{E}(T) \cap \mathcal{E}_{h,i}} |\ell|^{p+1} \|\llbracket \boldsymbol{\sigma} \nabla u_h \cdot \mathbf{n} \rrbracket\|_{0,p,\ell}^p \right. \\ & \left. + \sum_{\ell \in \mathcal{E}(T) \cap \mathcal{E}_{h,e}} |\ell|^{p+1} \|\boldsymbol{\sigma} \nabla u_h \cdot \mathbf{n}\|_{0,p,\ell}^p \right)^{1/p}, \end{aligned}$$

where $\mathcal{E}(T)$ is the set of the edges of T and $\llbracket g \rrbracket$ denotes the jump of g across an edge. We define the local a posteriori error indicator $\eta_{T,p}$ for all $T \in \mathcal{T}_h$ as follows:

$$\eta_{T,p} := \begin{cases} \left(h_0^{2-p} + \varepsilon_{T_0,p}^p \right)^{1/p} & \text{if } T = T_0, \\ \varepsilon_{T,p} & \text{otherwise.} \end{cases}$$

Next, we define the global error estimator from these indicators as follows:

$$\eta_p := \left(\sum_{T \in \mathcal{T}_h} \eta_{T,p}^p \right)^{1/p}.$$

4.4.1 Reliability

To show that this estimator is reliable, we prove the following theorem which is based on a duality argument as that used for Theorem 4.2.2.

Theorem 4.4.1 *Let Ω be a convex Lipschitz polygon and let $\sigma_{i,j} \in C^1(\bar{\Omega})$ for each $i, j = 1, 2$. Let η_p be defined as above with $p \in (\frac{q_0}{q_0-1}, 2)$, where $q_0 > 2$ is the maximal regularity exponent in (4.6). Then, the following estimate holds true:*

$$\|u - u_h\|_{0,p,\Omega} \leq C\eta_p.$$

Proof. Given $\psi \in L^q(\Omega)$, let $\varphi \in W^{2,q}(\Omega)$ be the solution of (4.5). Proceeding as in (5.13), using (4.4) tested with $v_h = \varphi^I$ (the Lagrange interpolant of φ), and integrating by parts, we obtain

$$\begin{aligned} \int_{\Omega} (u - u_h)\psi &= -\mathbf{p} \cdot \nabla \varphi(\mathbf{x}_0) + \int_{\Omega} \boldsymbol{\sigma} \nabla u_h \cdot \nabla \varphi \\ &= \mathbf{p} \cdot (\nabla \varphi^I(\mathbf{x}_0) - \nabla \varphi(\mathbf{x}_0)) + \int_{\Omega} \boldsymbol{\sigma} \nabla u_h \cdot \nabla (\varphi - \varphi^I) \\ &= \mathbf{p} \cdot (\nabla \varphi^I(\mathbf{x}_0) - \nabla \varphi(\mathbf{x}_0)) - \sum_{T \in \mathcal{T}_h} \int_T \operatorname{div}(\boldsymbol{\sigma} \nabla u_h)(\varphi - \varphi^I) \\ &\quad + \sum_{\ell \in \mathcal{E}_{h,i}} \int_{\ell} [\![\boldsymbol{\sigma} \nabla u_h \cdot \mathbf{n}]\!] (\varphi - \varphi^I) + \sum_{\ell \in \mathcal{E}_{h,e}} \int_{\ell} \boldsymbol{\sigma} \nabla u_h \cdot \mathbf{n} (\varphi - \varphi^I). \end{aligned} \tag{4.31}$$

Using Hölder inequality, Proposition 4.2.1, and Lemma 4.3.4 we estimate each term on the right hand side as follows:

$$|\mathbf{p} \cdot \nabla (\varphi - \varphi^I)(\mathbf{x}_0)| \leq |\mathbf{p}| |\varphi - \varphi^I|_{1,\infty,T_0} \leq Ch_0^{1-2/q} |\varphi|_{2,q,T_0},$$

$$\begin{aligned} \sum_{T \in \mathcal{T}_h} \int_T \operatorname{div}(\boldsymbol{\sigma} \nabla u_h)(\varphi - \varphi^I) &\leq \sum_{T \in \mathcal{T}_h} \|\operatorname{div}(\boldsymbol{\sigma} \nabla u_h)\|_{0,p,T} \|\varphi - \varphi^I\|_{0,q,T} \\ &\leq C \sum_{T \in \mathcal{T}_h} h_T^2 \|\operatorname{div}(\boldsymbol{\sigma} \nabla u_h)\|_{0,p,T} |\varphi|_{2,q,T} \\ &\leq C \left(\sum_{T \in \mathcal{T}_h} h_T^{2p} \|\operatorname{div}(\boldsymbol{\sigma} \nabla u_h)\|_{0,p,T}^p \right)^{1/p} |\varphi|_{2,q,\Omega}, \end{aligned}$$

$$\begin{aligned}
\sum_{\ell \in \mathcal{E}_{h,i}} \int_{\ell} \llbracket \boldsymbol{\sigma} \nabla u_h \cdot \mathbf{n} \rrbracket (\varphi - \varphi^I) &\leq \sum_{\ell \in \mathcal{E}_{h,i}} \|\llbracket \boldsymbol{\sigma} \nabla u_h \cdot \mathbf{n} \rrbracket\|_{0,p,\ell} \|\varphi - \varphi^I\|_{0,q,\ell} \\
&\leq C \sum_{\ell \in \mathcal{E}_{h,i}} |\ell|^{1+1/p} \|\llbracket \boldsymbol{\sigma} \nabla u_h \cdot \mathbf{n} \rrbracket\|_{0,p,\ell} |\varphi|_{2,q,\omega_\ell} \\
&\leq C \left(\sum_{\ell \in \mathcal{E}_{h,i}} |\ell|^{p+1} \|\llbracket \boldsymbol{\sigma} \nabla u_h \cdot \mathbf{n} \rrbracket\|_{0,p,\ell}^p \right)^{1/p} |\varphi|_{2,q,\Omega}, \\
\sum_{\ell \in \mathcal{E}_{h,e}} \int_{\ell} \boldsymbol{\sigma} \nabla u_h \cdot \mathbf{n} (\varphi - \varphi^I) &\leq \sum_{\ell \in \mathcal{E}_{h,e}} \|\boldsymbol{\sigma} \nabla u_h \cdot \mathbf{n}\|_{0,p,\ell} \|\varphi - \varphi^I\|_{0,q,\ell} \\
&\leq C \sum_{\ell \in \mathcal{E}_{h,e}} |\ell|^{1+1/p} \|\boldsymbol{\sigma} \nabla u_h \cdot \mathbf{n}\|_{0,p,\ell} |\varphi|_{2,q,\omega_\ell} \\
&\leq C \left(\sum_{\ell \in \mathcal{E}_{h,e}} |\ell|^{p+1} \|\boldsymbol{\sigma} \nabla u_h \cdot \mathbf{n}\|_{0,p,\ell}^p \right)^{1/p} |\varphi|_{2,q,\Omega}.
\end{aligned}$$

Substituting all these estimates in (4.31) and using (4.6), we obtain

$$\begin{aligned}
\int_{\Omega} (u - u_h) \psi &\leq C \left(h_0^{2-p} + \sum_{T \in \mathcal{T}_h} h_T^{2p} \|\operatorname{div}(\boldsymbol{\sigma} \nabla u_h)\|_{0,p,T}^p \right. \\
&\quad \left. + \sum_{\ell \in \mathcal{E}_{h,i}} |\ell|^{p+1} \|\llbracket \boldsymbol{\sigma} \nabla u_h \cdot \mathbf{n} \rrbracket\|_{0,p,\ell}^p + \sum_{\ell \in \mathcal{E}_{h,e}} |\ell|^{p+1} \|\boldsymbol{\sigma} \nabla u_h \cdot \mathbf{n}\|_{0,p,\ell}^p \right)^{1/p} \|\psi\|_{0,q,\Omega}.
\end{aligned}$$

Therefore,

$$\begin{aligned}
\|u - u_h\|_{0,p,\Omega} &= \sup_{\psi \in L^q(\Omega)} \frac{\int_{\Omega} (u - u_h) \psi}{\|\psi\|_{0,q,\Omega}} \\
&\leq C \left(h_0^{2-p} + \sum_{T \in \mathcal{T}_h} h_T^{2p} \|\operatorname{div}(\boldsymbol{\sigma} \nabla u_h)\|_{0,p,T}^p + \sum_{\ell \in \mathcal{E}_{h,i}} |\ell|^{p+1} \|\llbracket \boldsymbol{\sigma} \nabla u_h \cdot \mathbf{n} \rrbracket\|_{0,p,\ell}^p \right. \\
&\quad \left. + \sum_{\ell \in \mathcal{E}_{h,e}} |\ell|^{p+1} \|\boldsymbol{\sigma} \nabla u_h \cdot \mathbf{n}\|_{0,p,\ell}^p \right)^{1/p}
\end{aligned}$$

and from this we conclude the theorem. \square

4.4.2 Efficiency

In this subsection we always assume that $\sigma_{i,j} \in C^1(\bar{\Omega})$ for each $i, j = 1, 2$.

To prove the efficiency estimate, we will use some techniques that appears in [54]. For that, we introduce the matrix $\boldsymbol{\sigma}^I$, whose entries are the Lagrange interpolants of $\sigma_{i,j}$:

$$\boldsymbol{\sigma}^I := (\sigma_{i,j}^I)_{1 \leq i, j \leq 2}.$$

The following four lemmas provide upper bounds for each term defining $\eta_{T,p}^p$. Here and thereafter $\mathbf{div}(\cdot)$ must be understood in the following row-wise sense: $(\mathbf{div}(\boldsymbol{\sigma}))_j = \sum_i \frac{\partial \sigma_{i,j}}{\partial x_i}$.

Lemma 4.4.1 *The following estimate holds true:*

$$h_T^{2p} \|\mathbf{div}(\boldsymbol{\sigma} \nabla u_h)\|_{0,p,T}^p \leq C \left(\|\boldsymbol{\sigma}\|_{1,\infty,T}^p \|u - u_h\|_{0,p,T}^p + h_T^{2p} \|[\mathbf{div}(\boldsymbol{\sigma} - \boldsymbol{\sigma}^I)] \cdot \nabla u_h\|_{0,p,T}^p \right)$$

for all $T \in \mathcal{T}_h$.

Proof. Let us consider an arbitrary $T \in \mathcal{T}_h$, the bubble function b_T defined in (4.12) and the function ψ_T defined in Ω as

$$\psi_T := \mathbf{div}(\boldsymbol{\sigma}^I \nabla u_h) b_T \quad \text{in } T.$$

Like b_T , this function is supported in T .

The fact that $\mathbf{div}(\boldsymbol{\sigma}^I \nabla u_h)|_T \in \mathcal{P}_0$, (4.16), (4.14), (4.15), and integration by parts yield

$$\begin{aligned} \|\mathbf{div}(\boldsymbol{\sigma}^I \nabla u_h)\|_{0,p,T}^2 &= |T|^{2/p-1} \|\mathbf{div}(\boldsymbol{\sigma}^I \nabla u_h)\|_{0,2,T}^2 \\ &\leq C |T|^{2/p-1} \|b_T^{1/2} \mathbf{div}(\boldsymbol{\sigma}^I \nabla u_h)\|_{0,2,T}^2 \\ &= C |T|^{2/p-1} \left(\int_T \mathbf{div}(\boldsymbol{\sigma} \nabla u_h) \psi_T + \int_T \mathbf{div}((\boldsymbol{\sigma}^I - \boldsymbol{\sigma}) \nabla u_h) \psi_T \right) \\ &= C |T|^{2/p-1} \left(\int_T u_h \mathbf{div}(\boldsymbol{\sigma} \nabla \psi_T) + \int_T [\mathbf{div}(\boldsymbol{\sigma}^I - \boldsymbol{\sigma})] \cdot \nabla u_h \psi_T \right). \end{aligned}$$

Next we notice that, since u is solution of (4.3) and $\nabla b_T(\mathbf{x}_0) = 0$, one has

$$\int_T u \mathbf{div}(\boldsymbol{\sigma} \nabla \psi_T) = -\mathbf{p} \cdot \nabla \psi_T(\mathbf{x}_0) = 0.$$

Therefore, we can write

$$\begin{aligned} \|\mathbf{div}(\boldsymbol{\sigma}^I \nabla u_h)\|_{0,p,T}^2 &\leq C |T|^{2/p-1} \left(\int_T (u_h - u) \mathbf{div}(\boldsymbol{\sigma} \nabla \psi_T) + \int_T [\mathbf{div}(\boldsymbol{\sigma}^I - \boldsymbol{\sigma})] \cdot \nabla u_h \psi_T \right). \end{aligned}$$

For the first term we have

$$\left| \int_T (u_h - u) \mathbf{div}(\boldsymbol{\sigma} \nabla \psi_T) \right| \leq 2 \|u - u_h\|_{0,p,T} \|\boldsymbol{\sigma}\|_{1,\infty,T} \|\psi_T\|_{2,q,T}$$

and, using (4.17),

$$\begin{aligned} \|\psi_T\|_{2,q,T} &= \|\mathbf{div}(\boldsymbol{\sigma}^I \nabla u_h)\| \|b_T\|_{2,q,T} \\ &\leq C \|\mathbf{div}(\boldsymbol{\sigma}^I \nabla u_h)\| |T|^{-1/p} \leq C \|\mathbf{div}(\boldsymbol{\sigma}^I \nabla u_h)\|_{0,p,T} |T|^{-2/p}. \end{aligned}$$

For the second one,

$$\left| \int_T [\mathbf{div}(\boldsymbol{\sigma}^I - \boldsymbol{\sigma})] \cdot \nabla u_h \psi_T \right| \leq \| [\mathbf{div}(\boldsymbol{\sigma}^I - \boldsymbol{\sigma})] \cdot \nabla u_h \|_{0,p,T} \|\psi_T\|_{0,q,T}$$

and, now using (4.13),

$$\|\psi_T\|_{0,q,T} \leq C |\mathbf{div}(\boldsymbol{\sigma}^I \nabla u_h)| |T|^{1/q} \leq C \|\mathbf{div}(\boldsymbol{\sigma}^I \nabla u_h)\|_{0,p,T} |T|^{1/q-1/p}.$$

Hence

$$\|\mathbf{div}(\boldsymbol{\sigma}^I \nabla u_h)\|_{0,p,T} \leq C (h_T^{-2} \|\boldsymbol{\sigma}\|_{1,\infty,T} \|u - u_h\|_{0,p,T} + \| [\mathbf{div}(\boldsymbol{\sigma}^I - \boldsymbol{\sigma})] \cdot \nabla u_h \|_{0,p,T})$$

from which we easily obtain the desired result. \square

Lemma 4.4.2 *The following estimate holds true*

$$\begin{aligned} & |\ell|^{p+1} \| \llbracket \boldsymbol{\sigma} \nabla u_h \cdot \mathbf{n} \rrbracket \|_{0,p,\ell}^p \\ & \leq C \left(\|\boldsymbol{\sigma}\|_{1,\infty,\omega_\ell}^p \|u - u_h\|_{0,p,\omega_\ell}^p + \sum_{T' \subset \omega_\ell} h_{T'}^{2p} \| [\mathbf{div}(\boldsymbol{\sigma}^I - \boldsymbol{\sigma})] \cdot \nabla u_h \|_{0,p,T'}^p \right), \end{aligned}$$

for all $\ell \in \mathcal{E}_{h,i}$.

Proof.

We consider an arbitrary $\ell \in \mathcal{E}_{h,i}$, the bubble function b_ℓ defined in (4.18) and

$$\psi_\ell := \llbracket \nabla u_h \cdot \mathbf{n} \rrbracket b_\ell \quad \text{in } \Omega.$$

Like b_ℓ , this function is supported in ω_ℓ .

We know that the entries of $\boldsymbol{\sigma}$ belong to $L^\infty(\Omega)$ and, therefore, we have

$$\| \llbracket \boldsymbol{\sigma} \nabla u_h \cdot \mathbf{n} \rrbracket \|_{0,p,\ell} \leq C \| \llbracket \nabla u_h \cdot \mathbf{n} \rrbracket \|_{0,p,\ell} = C \| \llbracket \nabla u_h \rrbracket \|_{0,p,\ell}, \quad (4.32)$$

because the jump of the tangential component of ∇u_h is zero.

On the other hand, from (4.22) and the uniform positivity of $\boldsymbol{\sigma}$ we obtain

$$\begin{aligned} \| \llbracket \nabla u_h \rrbracket \|_{0,p,\ell}^2 &= |\ell|^{2/p-1} \| \llbracket \nabla u_h \rrbracket \|_{0,2,\ell}^2 \\ &\leq C |\ell|^{2/p-1} \| b_\ell^{1/2} \llbracket \nabla u_h \rrbracket \|_{0,2,\ell}^2 \\ &\leq C |\ell|^{2/p-1} \int_\ell b_\ell \llbracket \nabla u_h \rrbracket_\ell^\dagger \boldsymbol{\sigma} \llbracket \nabla u_h \rrbracket_\ell \\ &= C |\ell|^{2/p-1} \int_\ell \llbracket \boldsymbol{\sigma} \nabla u_h \cdot \mathbf{n} \rrbracket \psi_\ell. \end{aligned} \quad (4.33)$$

Taking ψ_ℓ as a test function in (4.3), using that $\nabla b_\ell(\mathbf{x}_0) = \mathbf{0}$, integrating by parts, and recalling (4.20) and (4.21), we have

$$\begin{aligned} \int_{\omega_\ell} (u - u_h) \operatorname{div}(\boldsymbol{\sigma} \nabla \psi_\ell) &= - \sum_{T' \subset \omega_\ell} \int_{T'} u_h \operatorname{div}(\boldsymbol{\sigma} \nabla \psi_\ell) \\ &= - \sum_{T' \subset \omega_\ell} \int_{T'} \operatorname{div}(\boldsymbol{\sigma} \nabla u_h) \psi_\ell + \int_\ell \llbracket \boldsymbol{\sigma} \nabla u_h \cdot \mathbf{n} \rrbracket \psi_\ell. \end{aligned}$$

Hence

$$\begin{aligned} \int_\ell \llbracket \boldsymbol{\sigma} \nabla u_h \cdot \mathbf{n} \rrbracket \psi_\ell &= \sum_{T' \subset \omega_\ell} \int_{T'} \operatorname{div}(\boldsymbol{\sigma} \nabla u_h) \psi_\ell + \int_{\omega_\ell} (u - u_h) \operatorname{div}(\boldsymbol{\sigma} \nabla \psi_\ell) \\ &\leq C \left(\|\operatorname{div}(\boldsymbol{\sigma} \nabla \psi_\ell)\|_{0,q,\omega_\ell} \|u - u_h\|_{0,p,\omega_\ell} \right. \\ &\quad \left. + \sum_{T' \subset \omega_\ell} \|\operatorname{div}(\boldsymbol{\sigma} \nabla u_h)\|_{0,p,T'} \|\psi_\ell\|_{0,q,T'} \right) \tag{4.34} \\ &\leq C \left(\|\boldsymbol{\sigma}\|_{1,\infty,\omega_\ell} \|u - u_h\|_{0,p,\omega_\ell} \|\psi_\ell\|_{2,q,\omega_\ell} \right. \\ &\quad \left. + \sum_{T' \subset \omega_\ell} \|\operatorname{div}(\boldsymbol{\sigma} \nabla u_h)\|_{0,p,T'} \|\psi_\ell\|_{0,q,T'} \right) \end{aligned}$$

From standard scaling arguments and (4.23), we have

$$\|\psi_\ell\|_{0,q,\omega_\ell} \leq \llbracket \nabla u_h \rrbracket_\ell \|b_\ell\|_{0,q,\omega_\ell} \leq C \llbracket \nabla u_h \rrbracket_\ell \|b_\ell\|_{0,p,\ell} |\ell|^{2-3/p} \tag{4.35}$$

and

$$\|\psi_\ell\|_{2,q,\omega_\ell} \leq C |\ell|^{-2} \|\psi_\ell\|_{0,q,\omega_\ell} \leq C \llbracket \nabla u_h \rrbracket_\ell \|b_\ell\|_{0,p,\ell} |\ell|^{-3/p}. \tag{4.36}$$

Hence, from (4.33) and (4.34), we write

$$\begin{aligned} \llbracket \nabla u_h \rrbracket_\ell \|b_\ell\|_{0,p,\ell} &\leq C |\ell|^{2/p-1} \left(|\ell|^{-3/p} \|\boldsymbol{\sigma}\|_{1,\infty,\omega_\ell} \|u - u_h\|_{0,p,\omega_\ell} \right. \\ &\quad \left. + \sum_{T' \subset \omega_\ell} |\ell|^{2-3/p} \|\operatorname{div}(\boldsymbol{\sigma} \nabla u_h)\|_{0,p,T'} \right) \end{aligned}$$

and, from (4.32),

$$\begin{aligned} |\ell|^{p+1} \llbracket \boldsymbol{\sigma} \nabla u_h \cdot \mathbf{n} \rrbracket_{0,p,\ell}^p &\leq C \left(\|\boldsymbol{\sigma}\|_{1,\infty,\omega_\ell}^p \|u - u_h\|_{0,p,\omega_\ell}^p \right. \\ &\quad \left. + \sum_{T' \subset \omega_\ell} h_{T'}^{2p} \|\operatorname{div}(\boldsymbol{\sigma} \nabla u_h)\|_{0,p,T'}^p \right). \end{aligned}$$

We conclude the proof by using Lemma 4.4.1 to bound the last term. \square

Lemma 4.4.3 *The following estimate holds true*

$$\begin{aligned} |\ell|^{p+1} \|\boldsymbol{\sigma} \nabla u_h \cdot \mathbf{n}\|_{0,p,\ell}^p &\leq C \left(\|\boldsymbol{\sigma}\|_{1,\infty,T_\ell}^p \|u - u_h\|_{0,p,T_\ell}^p + h_{T_\ell}^{2p} \|\operatorname{div}(\boldsymbol{\sigma}^I - \boldsymbol{\sigma})\| \cdot \nabla u_h\|_{0,p,T_\ell}^p \right. \\ &\quad \left. + |\ell|^{p+1} \|(\boldsymbol{\sigma} - \boldsymbol{\sigma}_\ell) \nabla u_h \cdot \mathbf{n}\|_{0,p,\ell}^p \right), \end{aligned}$$

for all $\ell \in \mathcal{E}_{h,e}$, where $\boldsymbol{\sigma}_\ell$ is any constant matrix.

Proof.

We consider an arbitrary $\ell \in \mathcal{E}_{h,e}$, the bubble function b_ℓ defined in (4.19) and

$$\psi_\ell := \boldsymbol{\sigma}_\ell \nabla u_h \cdot \mathbf{n} b_\ell \quad \text{in } \Omega.$$

Like b_ℓ , this function is supported in T_ℓ .

Since $\boldsymbol{\sigma}_\ell$ is constant and b_ℓ satisfies (4.22), it is easy to prove that

$$\begin{aligned} \|\boldsymbol{\sigma}_\ell \nabla u_h \cdot \mathbf{n}\|_{0,p,\ell}^2 &= |\ell|^{2/p-1} \|\boldsymbol{\sigma}_\ell \nabla u_h \cdot \mathbf{n}\|_{0,2,\ell}^2 \\ &\leq C |\ell|^{2/p-1} \|b_\ell^{1/2} \boldsymbol{\sigma}_\ell \nabla u_h \cdot \mathbf{n}\|_{0,2,\ell}^2 \\ &= |\ell|^{2/p-1} \left(\int_\ell (\boldsymbol{\sigma}_\ell - \boldsymbol{\sigma}) \nabla u_h \cdot \mathbf{n} \psi_\ell + \int_\ell \boldsymbol{\sigma} \nabla u_h \cdot \mathbf{n} \psi_\ell \right). \end{aligned} \quad (4.37)$$

On the other hand, using that $\|\psi_\ell\|_{0,q,\ell} \leq C |\ell|^{-1/q} \|\psi_\ell\|_{0,q,T_\ell}$ and the arguments used for proving the previous result, we obtain

$$\begin{aligned} \int_\ell (\boldsymbol{\sigma}_\ell - \boldsymbol{\sigma}) \nabla u_h \cdot \mathbf{n} \psi_\ell &\leq C \|(\boldsymbol{\sigma}_\ell - \boldsymbol{\sigma}) \nabla u_h \cdot \mathbf{n}\|_{0,p,\ell} |\ell|^{-1/q} \|\psi_\ell\|_{0,q,T_\ell} \\ &\leq C \|(\boldsymbol{\sigma}_\ell - \boldsymbol{\sigma}) \nabla u_h \cdot \mathbf{n}\|_{0,p,\ell} |\ell|^{1-2/p} \|\boldsymbol{\sigma}_\ell \nabla u_h \cdot \mathbf{n}\|_{0,p,\ell} \end{aligned}$$

and

$$\begin{aligned} \int_\ell \boldsymbol{\sigma} \nabla u_h \cdot \mathbf{n} \psi_\ell &= \int_{T_\ell} (u - u_h) \operatorname{div}(\boldsymbol{\sigma} \nabla \psi_\ell) + \int_{T_\ell} \operatorname{div}(\boldsymbol{\sigma} \nabla u_h) \psi_\ell \\ &\leq C (\|\boldsymbol{\sigma}\|_{1,\infty,T_\ell} \|u - u_h\|_{0,p,T_\ell} |\ell|^{-3/p} \\ &\quad + \|\operatorname{div}(\boldsymbol{\sigma} \nabla u_h)\|_{0,p,T_\ell} |\ell|^{2-3/p}) \|\boldsymbol{\sigma}_\ell \nabla u_h \cdot \mathbf{n}\|_{0,p,\ell}. \end{aligned}$$

Substituting these expressions in (4.37), we have

$$\begin{aligned} \|\boldsymbol{\sigma}_\ell \nabla u_h \cdot \mathbf{n}\|_{0,p,\ell} &\leq C |\ell|^{2/p-1} (|\ell|^{-3/p} \|\boldsymbol{\sigma}\|_{1,\infty,T_\ell} \|u - u_h\|_{0,p,T_\ell} \\ &\quad + |\ell|^{2-3/p} \|\operatorname{div}(\boldsymbol{\sigma} \nabla u_h)\|_{0,p,T_\ell} \\ &\quad + |\ell|^{1-2/p} \|(\boldsymbol{\sigma}_\ell - \boldsymbol{\sigma}) \nabla u_h \cdot \mathbf{n}\|_{0,p,\ell}) \end{aligned}$$

and, therefore,

$$\begin{aligned} |\ell|^{p+1} \|\boldsymbol{\sigma}_\ell \nabla u_h \cdot \mathbf{n}\|_{0,p,\ell}^p &\leq C \left(\|\boldsymbol{\sigma}\|_{1,\infty,T_\ell}^p \|u - u_h\|_{0,p,T_\ell}^p + h_{T_\ell}^{2p} \|\operatorname{div}(\boldsymbol{\sigma} \nabla u_h)\|_{0,p,T_\ell}^p \right. \\ &\quad \left. + |\ell|^{p+1} \|(\boldsymbol{\sigma}_\ell - \boldsymbol{\sigma}) \nabla u_h \cdot \mathbf{n}\|_{0,p,\ell}^p \right). \end{aligned}$$

Thus, using this result, Lemma 4.4.1, and the fact that

$$\|\boldsymbol{\sigma} \nabla u_h \cdot \mathbf{n}\|_{0,p,\ell} \leq \|(\boldsymbol{\sigma}_\ell - \boldsymbol{\sigma}) \nabla u_h \cdot \mathbf{n}\|_{0,p,\ell} + \|\boldsymbol{\sigma}_\ell \nabla u_h \cdot \mathbf{n}\|_{0,p,\ell},$$

we conclude the proof. \square

Lemma 4.4.4 *The following estimate holds true:*

$$h_0^{2-p} \leq C \left(\|\boldsymbol{\sigma}\|_{1,\infty,\omega_{T_0}}^p \|u - u_h\|_{0,p,\omega_{T_0}}^p + \sum_{T' \subset \omega_{T_0}} h_{T'}^{2p} \|[\mathbf{div}(\boldsymbol{\sigma} - \boldsymbol{\sigma}^I)] \cdot \nabla u_h\|_{0,p,T'}^p \right).$$

Proof. Let \mathcal{E}_h^0 be the set of edges ℓ of triangles $T \subset \omega_{T_0}$, such that $\ell \not\subset \partial\omega_{T_0}$. Testing equation (4.3) with the bubble function b_0 defined in (4.25), we obtain

$$\begin{aligned} |\mathbf{p}|^2 &= \mathbf{p} \cdot \nabla b_0(\mathbf{x}_0) = - \int_{\Omega} (u - u_h) \operatorname{div}(\boldsymbol{\sigma} \nabla b_0) - \int_{\Omega} u_h \operatorname{div}(\boldsymbol{\sigma} \nabla b_0) \\ &\leq \|u - u_h\|_{0,p,\omega_{T_0}} \|\operatorname{div}(\boldsymbol{\sigma} \nabla b_0)\|_{0,q,\omega_{T_0}} - \sum_{T' \subset \omega_{T_0}} \int_{T'} \operatorname{div}(\boldsymbol{\sigma} \nabla u_h) b_0 + \sum_{\ell \in \mathcal{E}_h^0} \int_{\ell} [\boldsymbol{\sigma} \nabla u_h]_{\ell} b_0 \\ &\leq C \left(\|u - u_h\|_{0,p,\omega_{T_0}} \|\boldsymbol{\sigma}\|_{1,\infty,\omega_{T_0}} \|b_0\|_{2,q,\omega_{T_0}} \right. \\ &\quad \left. + \|b_0\|_{0,q,\omega_{T_0}} \sum_{T' \subset \omega_{T_0}} \|\operatorname{div}(\boldsymbol{\sigma} \nabla u_h)\|_{0,p,T'} + \sum_{\ell \in \mathcal{E}_h^0} \|[\boldsymbol{\sigma} \nabla u_h \cdot \mathbf{n}]\|_{0,p,\ell} \|b_0\|_{0,q,\ell} \right), \end{aligned}$$

where we have used (4.26), integration by parts, and Hölder inequality.

We estimate $\|b_0\|_{2,q,\omega_{T_0}}$, $\|b_0\|_{0,q,\omega_{T_0}}$, and $\|b_0\|_{0,q,\ell}$ by Corollary 4.3.1. Thus, we have

$$\begin{aligned} |\mathbf{p}|^2 &\leq C h_0^{1-2/p} \left(\|\boldsymbol{\sigma}\|_{1,\infty,\omega_{T_0}} \|u - u_h\|_{0,p,\omega_{T_0}} + h_0^2 \sum_{T' \subset \omega_{T_0}} \|\operatorname{div}(\boldsymbol{\sigma} \nabla u_h)\|_{0,p,T'} \right. \\ &\quad \left. + \sum_{\ell \in \mathcal{E}_h^0} |\ell|^{1+1/p} \|[\boldsymbol{\sigma} \nabla u_h \cdot \mathbf{n}]\|_{0,p,\ell} \right). \end{aligned}$$

Since $h_0 \leq C h_{T'}$ for each $T' \subset \omega_{T_0}$, this estimate together with Lemmas 4.4.1 and 4.4.2 lead to the desired result. \square

Now we are in a position to conclude an efficiency estimate by collecting the previous four lemmas. Notice that these lemmas hold true for any $p \in (1, 2)$ (and not only for $p \in (\frac{q_0}{q_0-1}, 2)$ as Theorem 4.31).

Theorem 4.4.2 *Let $\sigma_{i,j} \in C^1(\bar{\Omega})$ for each $i, j = 1, 2$. Let u and u_h be the solutions of (4.3) and (4.4), respectively. Then, for all $p \in (1, 2)$ and for all $T \in \mathcal{T}_h$*

$$\begin{aligned} \eta_{T,p} &\leq C \left(\|\boldsymbol{\sigma}\|_{1,\infty,\omega_T}^p \|u - u_h\|_{0,p,\omega_T}^p + \sum_{T' \subset \omega_T} h_{T'}^{2p} \|[\mathbf{div}(\boldsymbol{\sigma}^I - \boldsymbol{\sigma})] \cdot \nabla u_h\|_{0,p,T'}^p \right. \\ &\quad \left. + \sum_{\ell \in \mathcal{E}(T) \cap \mathcal{E}_{h,e}} |\ell|^{p+1} \|(\boldsymbol{\sigma} - \boldsymbol{\sigma}_{\ell}) \nabla u_h \cdot \mathbf{n}\|_{0,p,\ell}^p \right)^{1/p}, \end{aligned}$$

where $\omega_T := \{T' \in \mathcal{T}_h : T \cap T' \neq \emptyset\}$, and for each $\ell \in \mathcal{E}(T) \cap \mathcal{E}_{h,e}$, $\boldsymbol{\sigma}_{\ell}$ is any constant matrix.

Notice that the last term in the estimate above vanishes for all triangles which do not intersect $\partial\Omega$.

The above inequalities are actual efficiency estimates if we show that the terms

$$\sum_{T' \subset \omega_T} h_{T'}^{2p} \|[\mathbf{div}(\boldsymbol{\sigma}^I - \boldsymbol{\sigma})] \cdot \nabla u_h\|_{0,p,T'}^p, \quad \sum_{\ell \in \mathcal{E}(T) \cap \mathcal{E}_{h,e}} |\ell|^{p+1} \|(\boldsymbol{\sigma} - \boldsymbol{\sigma}_\ell) \nabla u_h \cdot \mathbf{n}\|_{0,p,\ell}^p$$

are negligible. In what follows we will show that this holds true under some additional assumptions; we also note that our final result is true on the whole domain Ω (and not locally, as it would be preferable).

Regarding the term $\sum_{\ell \in \mathcal{E}(T) \cap \mathcal{E}_{h,e}} |\ell|^{p+1} \|(\boldsymbol{\sigma} - \boldsymbol{\sigma}_\ell) \nabla u_h \cdot \mathbf{n}\|_{0,p,\ell}^p$, since $\boldsymbol{\sigma}_\ell$ is any arbitrary constant matrix, it clearly vanishes when $\boldsymbol{\sigma}|_\ell$ is already constant: namely, when the tissue on the scalp is piecewise homogeneous, which is a realistic assumption in practice. On the other hand, an alternative proof for Lemma 4.4.3 also holds true when the conductivity on $\partial\Omega$ is of the form $\boldsymbol{\sigma} = \sigma I$, with σ a scalar function; namely, when the tissue of the scalp is isotropic. In fact, in that case we have the following result.

Lemma 4.4.5 *We have*

$$|\ell|^{p+1} \|\sigma \nabla u_h \cdot \mathbf{n}\|_{0,p,\ell}^p \leq C \left(\|\sigma\|_{1,\infty,T_\ell}^p \|u - u_h\|_{0,p,T_\ell}^p + h_{T_\ell}^{2p} \|[\mathbf{div}(\boldsymbol{\sigma}^I - \boldsymbol{\sigma})] \cdot \nabla u_h\|_{0,p,T_\ell}^p \right)$$

for all $\ell \in \mathcal{E}_{h,e}$, provided $\boldsymbol{\sigma}|_\ell = \sigma I$, with $\sigma : \ell \rightarrow \mathbb{R}$ a scalar function, belonging to $C^1(T_\ell)$.

Proof. We consider an arbitrary $\ell \in \mathcal{E}_{h,e}$, the bubble function b_ℓ defined in (4.19) and

$$\psi_\ell := \sigma_0 \nabla u_h \cdot \mathbf{n} b_\ell \quad \text{in } \Omega,$$

with σ_0 as in (4.2). Like b_ℓ , this function is supported in T_ℓ .

From (4.22) and (4.2), we have that $\int_\ell b_\ell \sigma \geq C \sigma_0 |\ell|$. Using this result, we obtain

$$\begin{aligned} \|\sigma \nabla u_h \cdot \mathbf{n}\|_{0,p,\ell}^2 &\leq \|\sigma\|_{0,\infty,\ell}^2 \|\nabla u_h \cdot \mathbf{n}\|_{0,p,\ell}^2 \\ &= \|\sigma\|_{0,\infty,\ell}^2 |\ell|^{2/p-1} |\ell| \|\nabla u_h \cdot \mathbf{n}\|^2 \\ &\leq C \frac{\|\sigma\|_{0,\infty,\ell}^2}{\sigma_0^2} |\ell|^{2/p-1} \int_\ell \sigma \nabla u_h \cdot \mathbf{n} \psi_\ell. \end{aligned}$$

The rest of the proof runs almost identically as that of Lemma 4.4.2, by using that

$$\|\psi_\ell\|_{0,q,T_\ell} \leq \|b_\ell\|_{0,q,T_\ell} |\ell|^{-1/p} \|\sigma \nabla u_h \cdot \mathbf{n}\|_{0,p,\ell} \leq C |\ell|^{2-3/p} \|\sigma \nabla u_h \cdot \mathbf{n}\|_{0,p,\ell}$$

and

$$\|\psi_\ell\|_{2,q,T_\ell} \leq C |\ell|^{-2} \|\psi_\ell\|_{0,q,T_\ell} \leq C |\ell|^{-3/p} \|\sigma \nabla u_h \cdot \mathbf{n}\|_{0,p,\ell}$$

instead of (4.35) and (4.36), respectively. \square

In order to prove that the term $\sum_{T' \subset \omega_T} h_{T'}^{2p} \|[\mathbf{div}(\boldsymbol{\sigma}^I - \boldsymbol{\sigma})] \cdot \nabla u_h\|_{0,p,T'}^p$ in Theorem 4.4.2 is globally negligible, we proceed as in [54] and make the following additional non-degeneracy assumption: there exists $C > 0$ such that

$$\|u - u_h\|_{0,p,\Omega} \geq Ch^2. \quad (4.38)$$

As explained in [54], this assumption looks quite reasonable.

In such a case we conclude with the following result.

Theorem 4.4.3 *Let us assume that for each $\ell \in \mathcal{E}_{h,e}$, either $\boldsymbol{\sigma}|_\ell$ is a constant matrix, or $\boldsymbol{\sigma}|_\ell = \sigma I$ with $\sigma : \ell \rightarrow \mathbb{R}$ a scalar function. Moreover, we assume that $\boldsymbol{\sigma} \in [C^1(\bar{\Omega})]^{2 \times 2}$ and $\boldsymbol{\sigma} \in [W^{2,\infty}(T)]^{2 \times 2}$ for all $T \in \mathcal{T}_h$. Let u and u_h be the solutions of (4.3) and (4.4), respectively. If (4.38) holds true, then*

$$\eta_p \leq C \|u - u_h\|_{0,p,\Omega}$$

for all $p \in (1, 2)$.

Proof. It is enough to estimate the last term in the inequality of Theorem 4.4.2:

$$\begin{aligned} & \sum_{T \in \mathcal{T}_h} \sum_{T' \subset \omega_T} h_{T'}^{2p} \|[\mathbf{div}(\boldsymbol{\sigma}^I - \boldsymbol{\sigma})] \cdot \nabla u_h\|_{0,p,T'}^p \\ & \leq \sum_{T \in \mathcal{T}_h} \sum_{T' \subset \omega_T} h_{T'}^{2p} \|\mathbf{div}(\boldsymbol{\sigma}^I - \boldsymbol{\sigma})\|_{0,\infty,T'}^p \|\nabla u_h\|_{0,p,T'}^p \\ & \leq C \sum_{T \in \mathcal{T}_h} \sum_{T' \subset \omega_T} h_{T'}^{2p} h_{T'}^p \|\boldsymbol{\sigma}\|_{2,\infty,T'}^p h_{T'}^{-p} \|u_h\|_{0,p,T'}^p \\ & \leq Ch^{2p} (\max_{T \in \mathcal{T}_h} \|\boldsymbol{\sigma}\|_{2,\infty,\omega_T}^p) \sum_{T \in \mathcal{T}_h} \|u_h\|_{0,p,\omega_T}^p \\ & \leq Ch^{2p} (\|u - u_h\|_{0,p,\Omega}^p + \|u\|_{0,p,\Omega}^p) \\ & \leq C \|u - u_h\|_{0,p,\Omega}^p + C \|u - u_h\|_{0,p,\Omega}^p \|u\|_{0,p,\Omega}^p, \end{aligned}$$

where we have used (4.38) for the last inequality. \square

4.5 Three-dimensional case

In what follows we briefly discuss the results that are preserved in 3D. First, let us recall that the existence and uniqueness of solution of the model problem (4.3) was proved in [65] in the 3D case for all $p \in [1, 3/2)$.

To obtain a priori and a posteriori error estimates for the numerical solution, we resort to the auxiliary problem (4.5). The critical point is the regularity of the solution of this problem.

We need that the solution belongs to $W^{2,q}(\Omega)$ for $q > 3$ (namely, q such that $\frac{1}{p} + \frac{1}{q} = 1$ with $1 \leq p < 3/2$). In [30, Theorem 2] it is proved that if Ω is a cube and the conductivity σ is a positive constant, (i.e. isotropic homogeneous material), then the solution of (4.5) belongs to $W^{2,q}(\Omega)$ for all $q > 1$. Therefore, within this section we assume that Ω is a cube in \mathbb{R}^3 and that $\boldsymbol{\sigma} = \sigma I$ with σ a positive constant. In such a case we have the following result, that is the analogue in the 3D case of Theorem 4.2.2.

Theorem 4.5.1 *Let $\{\mathcal{T}_h\}$ be a quasiuniform family of subdivisions of the cube Ω . Let u and u_h be the solutions to problems (4.3) and (4.4) respectively. Then the following estimate holds true*

$$\|u - u_h\|_{0,p,\Omega} \leq Ch^{3/p-2},$$

for all $p \in (1, 3/2)$.

Proof. The proof runs as that of Theorem 4.2.2. \square

The a posteriori error analysis also extends to the 3D framework. Let $\mathcal{F}_{h,i}$ be the set of all the inner faces and $\mathcal{F}_{h,e}$ that of external faces of the mesh \mathcal{T}_h . Let $\mathcal{F}_h := \mathcal{F}_{h,i} \cup \mathcal{F}_{h,e}$. For all $T \in \mathcal{T}_h$ we define

$$\begin{aligned} \widehat{\varepsilon}_{T,p} := & \left(\frac{1}{2} \sum_{F \in \mathcal{F}(T) \cap \mathcal{F}_{h,i}} |F|^{(p+3)/2} \|\nabla u_h \cdot \mathbf{n}_F\|^p \right. \\ & \left. + \sum_{F \in \mathcal{F}(T) \cap \mathcal{F}_{h,e}} |F|^{(p+3)/2} |\nabla u_h \cdot \mathbf{n}_F|^p \right)^{1/p}, \end{aligned}$$

where $\mathcal{F}(T)$ is the set of faces of T and $|F|$ is the area of F .

We define the local a posteriori error indicator $\widehat{\eta}_{T,p}$ for all $T \in \mathcal{T}_h$ by

$$\widehat{\eta}_{T,p} := \begin{cases} \left(h_0^{3-2p} + \widehat{\varepsilon}_{T_0,p}^p \right)^{1/p} & \text{if } T = T_0, \\ \widehat{\varepsilon}_{T,p} & \text{otherwise,} \end{cases}$$

where $h_0 := h_{T_0}$, and the global error estimator from these indicators as follows:

$$\widehat{\eta}_p := \left(\sum_{T \in \mathcal{T}_h} \widehat{\eta}_{T,p}^p \right)^{1/p}.$$

Note that, as we are assuming that $\boldsymbol{\sigma}$ is constant, the second and third terms that appear in Theorem 4.4.2 vanish in the estimate of $\widehat{\eta}_{T,p}$. The following results are obtained by adapting to the 3D framework the proofs of Theorem 4.4.1, and Lemmas 4.4.2 and 4.4.4. We have the following result regarding the reliability of the estimator:

Theorem 4.5.2 *Let u and u_h be the solutions of (4.3) and (4.4), respectively. Then, the following estimate holds true:*

$$\|u - u_h\|_{0,p,\Omega} \leq C\widehat{\eta}_p.$$

The efficiency follows from these two lemmas:

Lemma 4.5.1 *Let us set $\omega_F := \{T \in \mathcal{T}_h : F \subset \partial T\}$. The following estimates hold true:*

$$|F|^{(p+3)/2} \|\llbracket \nabla u_h \cdot \mathbf{n}_F \rrbracket\|^p \leq C \|u - u_h\|_{0,p,\omega_F}^p, \quad \text{for all } F \in \mathcal{F}_{h,i}$$

and

$$|F|^{(p+3)/2} |\nabla u_h \cdot \mathbf{n}_F|^p \leq C \|u - u_h\|_{0,p,\omega_F}^p, \quad \text{for all } F \in \mathcal{F}_{h,e}.$$

Lemma 4.5.2 *Let ω_{T_0} be defined as in (4.24). Then,*

$$h_0^{3-2p} \leq C \|u - u_h\|_{0,p,\omega_{T_0}}^p.$$

Notice that no negligible higher order term appears in this case in the efficiency estimate. Therefore, we have the following version of Theorem 4.4.3: under the more stringent assumptions we have required, the result now holds locally on each triangle T .

Theorem 4.5.3 *Let u and u_h be the solutions of (4.3) and (4.4), respectively. Then*

$$\hat{\eta}_{T,p} \leq C \|u - u_h\|_{0,p,\omega_T},$$

for all $T \in \mathcal{T}_h$ and $p \in (1, 3/2)$.

4.6 Numerical experiments

In this section we report some numerical experiments in 2D. The adaptive procedure consists in solving problem (4.4) on a sequence of meshes up to finally attain a solution with an estimated error within a prescribed tolerance. Each mesh is a local refinement of the previous one. We compute the local error indicators $\eta_{T,p}$ for all T in the ‘old’ mesh \mathcal{T}_h , and then we refine those elements T with $\eta_{T,p} \geq \theta \max\{\eta_{T,p} : T \in \mathcal{T}_h\}$, where $\theta \in (0, 1)$ is a prescribed parameter. In particular we take $\theta = 1/2$ in all our experiments.

The algorithm is implemented in a Matlab code using the mesh generator Triangle. This generator allows creating successively refined meshes based on a hybrid Delaunay refinement algorithm (see [64]).

4.6.1 Test 1. Isotropic constant conductivity

The first test consists of solving problem (4.4) in a regular polygon of 16 edges inscribed in a circumference centered at $(0, 0)$ with radius 1. The dipole is located at $\mathbf{x}_0 = (0.2605, -0.3054)$, the polarization is $\mathbf{p} = (-0.2425, 0.9701)$ and the conductivity is assumed to be the identity.

Since $\sigma = 1$, we can obtain an accurate solution by means of the subtraction technique. This technique uses a particular function u_0 satisfying $\operatorname{div}(\sigma \nabla u_0) = \operatorname{div}(\mathbf{p} \delta_{\mathbf{x}_0})$, which is analytically known. Subtracting u_0 to the solution of problem (4.4) leads to a non-homogeneous Neumann problem, whose solution is not singular at \mathbf{x}_0 . Therefore, this problem can be accurately solved by using standard finite elements (see [67] for more details). The solution computed by this subtraction technique in the finest mesh of the adaptive procedure will be taken as the reference solution, $u_{\text{ref}}(\mathbf{x})$.

Figure 4.5 shows some of the successively refined meshes created in the process driven by $\eta_{T,p}$ with $p = 1.25$. Parameters “iter” and “d.o.f.” refer to the iteration number and the total number of vertices of the corresponding mesh.

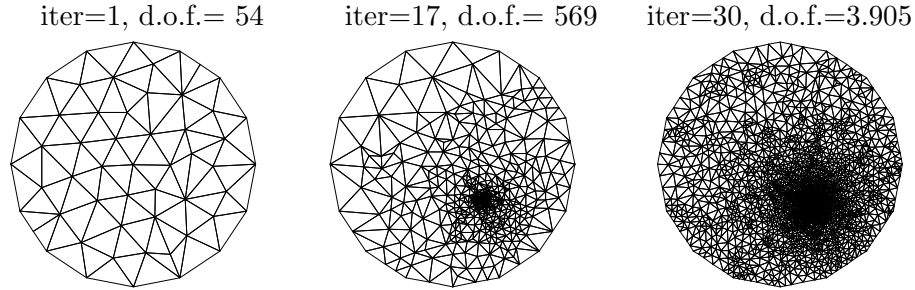


Figure 4.5: Test 1. Meshes obtained with $\eta_{T,p}$; $p = 1.25$.

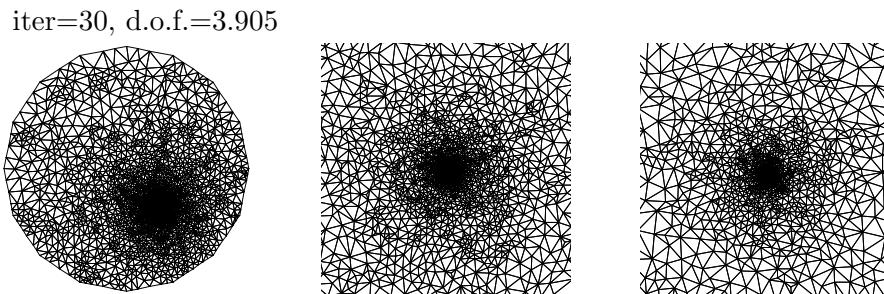


Figure 4.6: Test 1. Zooms of the mesh for iter=30.

Figure 4.6 shows two successive zooms around the singularity of the finer mesh in Figure 4.5. Each figure is a 200% zoom of the previous one. It can be appreciated that the mesh is extremely refined in the neighborhood of the singular point. Such a behavior can be expected from the singularity of the solution at \mathbf{x}_0 , which can be seen from Figure 4.7, which shows the computed solution on some of the coarser meshes. (Notice that the vertical scales are different on each subfigure.)

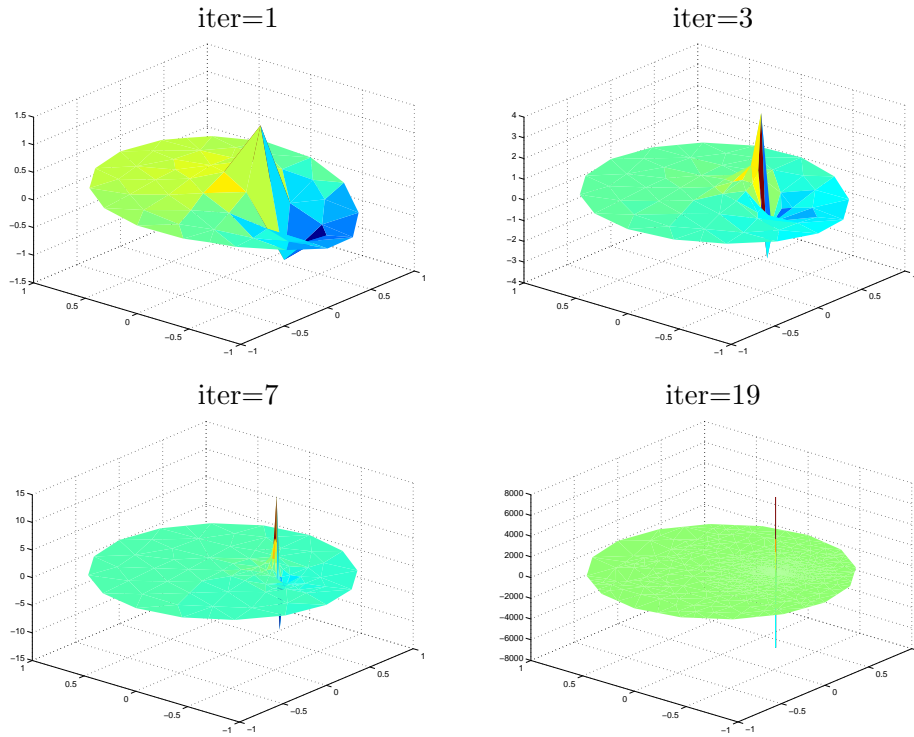


Figure 4.7: Test 1. Approximate solutions on some coarser meshes.

This extremely singular behavior is the reason why the adaptively created meshes are so localized. This can be appreciated in Figure 4.8, which contains two graphs. The one on the left shows the plot of the discrete solution corresponding to the different meshes on the segment $\mathbf{x} = \mathbf{x}_0 + t\mathbf{p}$, $t \in [-0.002, 0.002]$. The right subfigure is a zoom of previous the plot.

The behavior of the (absolute) error along the adaptive process can be seen from Figure 4.9. We report log-log plots of the estimated error and the “reference error” versus the number of degrees of freedom. The “reference error” is computed by comparing the solution of problem (4.4) with the reference solution. The figure also shows a line of slope -1 which corresponds to the optimal order of convergence for the finite elements used. It can be seen that the estimated and the reference errors both attain this optimal order.

In Table 4.1 we compare the reference (relative) error for the solution of problem (4.4) computed using adapted meshes and a quasiuniform mesh with approximately the same number of nodes (5780). It can be seen that, to obtain a solution with an error around 5 %, the number of d.o.f. in the uniform mesh is 40 times the number of d.o.f. in the adapted mesh. Moreover, with almost the same number of d.o.f., the adaptive algorithm yields a computed solution with an error 50 times smaller than the one obtained with a uniform mesh.

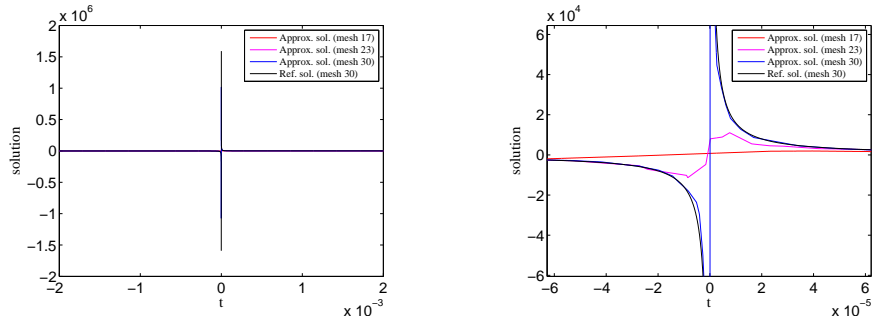


Figure 4.8: Test 1. Approximate solution and exact solution on the segment $\mathbf{x} = \mathbf{x}_0 + t\mathbf{p}$, $t \in [-0.002, 0.002]$.

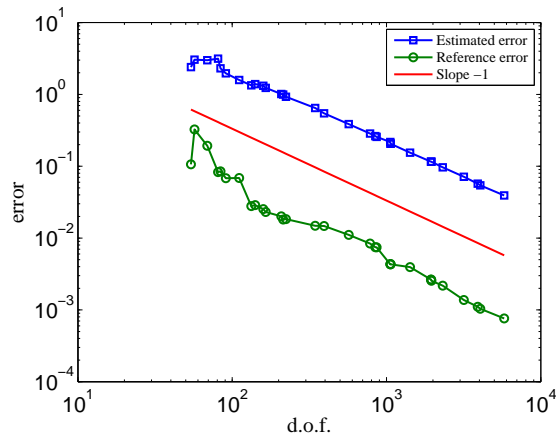


Figure 4.9: Test 1. Estimator η_p and reference (absolute) L^p error curves; $p = 1.25$.

We notice also that, though the error indicator is designed to estimate the L^p -norm in Ω , when using this adaptive procedure the error on the boundary decreases at the optimal rate, too. Thus, this error indicator can be used in the forward solver when facing the inverse problem of electroencephalography (namely, the problem aiming at determining the source localization from suitable boundary measurements). In Figure 4.10 we present a log-log plot of the averaged relative error $\sqrt{\sum_{n=1}^{12} |(u_h - u_{\text{ref}})(\mathbf{x}_n)|^2 / \sum_{n=1}^{12} |u_{\text{ref}}(\mathbf{x}_n)|^2}$ in twelve different points of $\partial\Omega$ (twelve consecutive vertexes of the polygon Ω), which can be thought as the localization of the electrodes. Although this error is more noisy, a fated optimal order (slope -1) can be appreciated.

	Degrees of freedom	L^p relative error
Adapted mesh 9	141	$0.4368 \cdot 10^{-1}$
Adapted mesh 32	5794	$0.1152 \cdot 10^{-2}$
Quasiuniform mesh	5780	$0.5508 \cdot 10^{-1}$

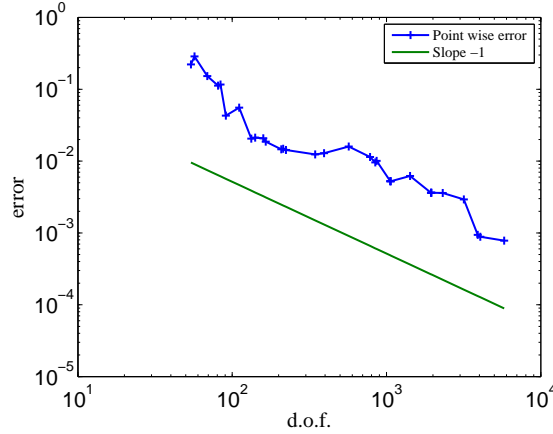
Table 4.1: Test 1. The L^p relative error for $p = 1.25$ in three different meshes

Figure 4.10: Test 1. Averaged relative error at boundary points.

4.6.2 Test 2. Anisotropic non-constant conductivity

In the second test, Ω is a square centered at $(0, 0)$ with side-length 2. The dipole is located at $\mathbf{x}_0 = (-0.25000, -0.08333)$, and the polarization is $\mathbf{p} = (0.9015, 0.4327)$. We consider a non-constant anisotropic conductivity

$$\boldsymbol{\sigma} = \begin{pmatrix} 4x^2 + 1 & 0 \\ 0 & 2y^2 + 1 \end{pmatrix}.$$

The results are very similar to those of the previous example. Figure 4.11 contains the meshes corresponding to three different iterations of the adaptive scheme and Figure 4.12 shows two successive zooms around the singularity.

We report in Figure 4.13 a log-log plot of the estimated error versus the number of degrees of freedom. The slope is close to -1 which confirms the success of the approach. In this case we have not a reference solution because the subtracting approach can not be used in this case, since the conductivity is not constant around the point where the source is located.

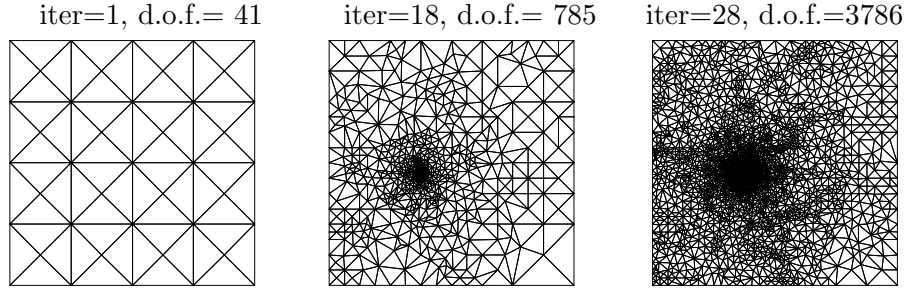
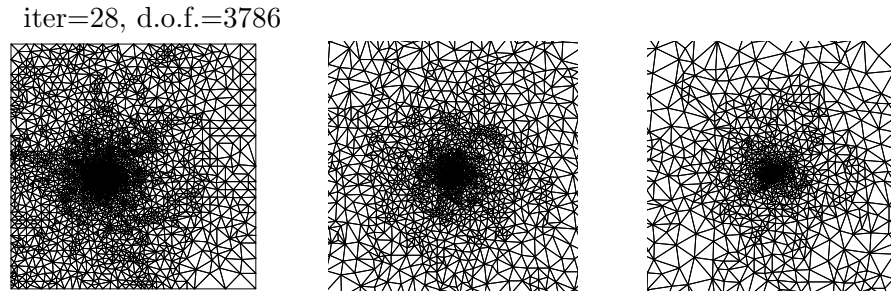
Figure 4.11: Test 2. Meshes obtained with $\eta_{T,p}$; $p = 1.25$.

Figure 4.12: Test 2. Zooms of the mesh for iter=28.

4.6.3 Test 3. Anisotropic constant conductivity

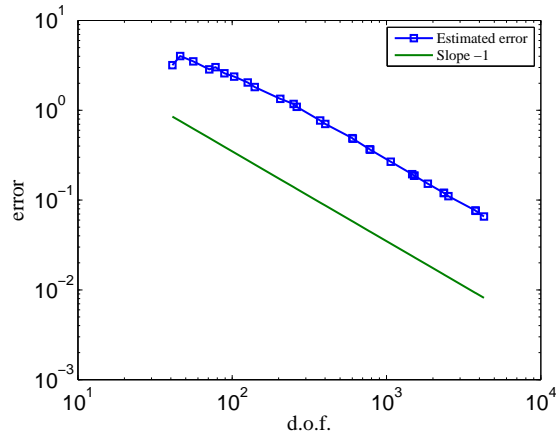
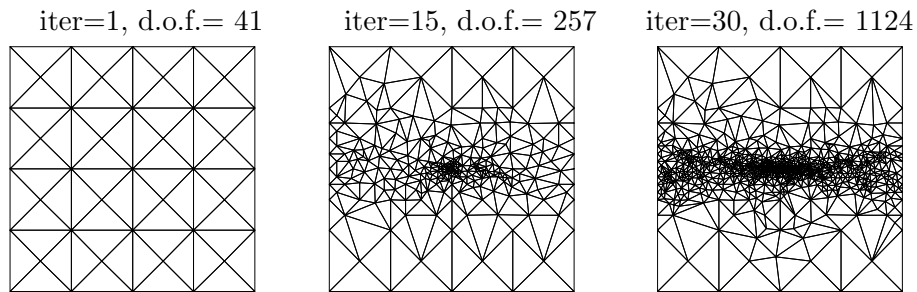
Finally, we consider a strongly anisotropic conductivity: $\boldsymbol{\sigma} = \begin{pmatrix} 10 & 0 \\ 0 & 0.1 \end{pmatrix}$. The domain Ω is a square centered at $(0,0)$, with side-length 2. The dipole is located at $\mathbf{x}_0 = (0,0)$ and the polarization is $\mathbf{p} = (1,1)$. Since the conductivity is constant, as in the first test we can compute the reference solution using the subtraction approach.

We show in Figure 4.14 the meshes corresponding to three different iterations of the adaptive scheme. Figure 4.15 shows two successive zooms around the singularity of the finest mesh considered (iter=45, d.o.f.=4168).

It can be clearly seen that in this case the meshes are not only refined around the singular point. The reason for this is that, because of the anisotropy of the conductivity, the solution has an inner layer at $x_2 = 0$. In fact, the fundamental solution (which is the only source of singularity) reads in this case

$$u_0(\mathbf{x}) = \frac{1}{2\pi} \frac{x_1 + 100x_2}{x_1^2 + 100x_2^2}.$$

Therefore, it is easy to check that the slope of the graph in the x_2 -direction is approximately $\frac{100}{x_1^2}$ at $x_2 = 0$. This can be seen from Figure 4.16, which shows the plot of the fundamental solution

Figure 4.13: Test 2. Estimator η_p curve; $p = 1.25$.Figure 4.14: Test 3. Meshes obtained with $\eta_{T,p}$; $p = 1.25$.

in a uniform mesh with 8321 vertices.

We notice from Figure 4.17 that the computed order of convergence is not optimal in this example. In fact, the fitted slope is close to -0.57 . Very likely, the reason for this suboptimal order is that our adaptive scheme only uses regular meshes, while appropriate anisotropic meshes seem to be necessary around the inner layer. Nevertheless, the use of our adaptive procedure turns out to be convenient, as can be seen by comparison with the results obtained with uniform refinement (see Table 4.2).

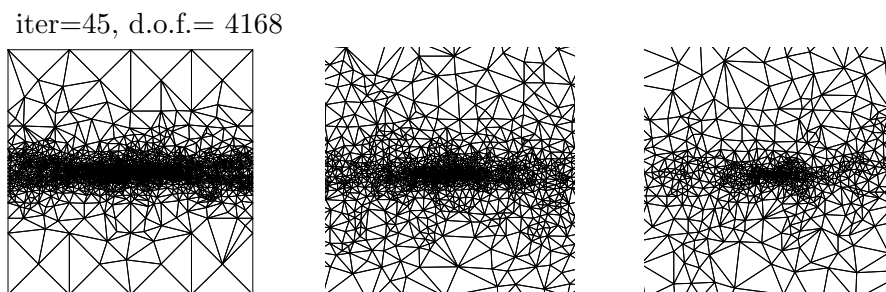


Figure 4.15: Test 3. Zooms of the mesh around the singular point for iter=45.

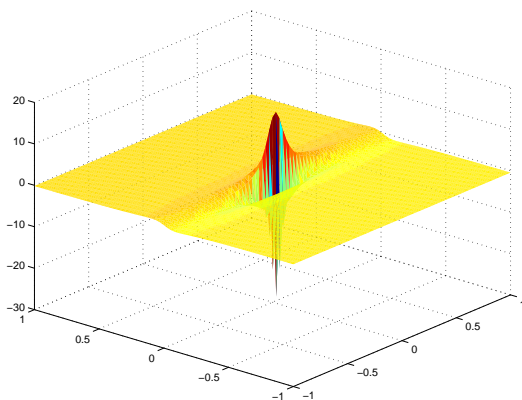
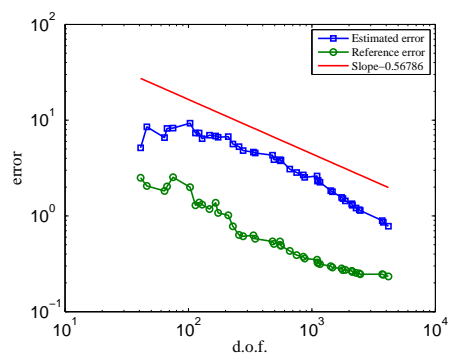


Figure 4.16: Test 3. Fundamental solution.

Figure 4.17: Test 3. L^p (absolute) error curves for $p = 1.25$: estimated and reference error on adapted meshes.

	Degrees of freedom	L^p relative error
Adapted mesh 15	257	$0.7217 \cdot 10^{-1}$
Adapted mesh 38	2118	$0.3007 \cdot 10^{-1}$
Quasiuniform mesh	2113	$0.7417 \cdot 10^{-1}$

Table 4.2: Test 3. The L^p relative error for $p = 1.25$ in three different meshes.

Chapter 5

Numerical behavior of different approximation methods for the direct and inverse problems of electrostatics with a dipole source

5.1 Introduction

It is common practice in cognitive research to reconstruct current sources in the human brain by means of their electric potentials, measured with electrodes which are fixed on the scalp (EEG).

Electromagnetic activity of the brain is due to the motion of ions in the active regions of the brain. This movement generates the so called *impressed current* (or primary currents) that in turn create ohmic currents in the surrounding environment calls *return currents*. We are interested in determining the impressed current.

The reconstruction of the position and of some physical characteristics of the current density that has given rise to the EEG measurements is called the inverse problem. For an accurate reconstruction of the primary current it is important to be able to realistically model tissue conductivity inhomogeneities.

In this chapter we present a series of numerical computations in order to compare different methods used for the approximation of the direct and inverse problem when the conductivity is not continuous across the interface of the different tissues (we recall that this is the case in the real physiological situation). We study in particular the case of a dipolar source located close to

the interface between two regions with different conductivities.

The obtained results have to be seen as a first step towards a better understanding of which is the most accurate procedure to use in this context.

We start introducing the equations.

5.1.1 Continuous problem

In almost all the studies concerning the neural generation of electromagnetic fields the static approximation of Maxwell equations is considered

$$\begin{cases} \operatorname{div} \mathbf{D} = \rho, \\ \operatorname{curl} \mathbf{E} = \mathbf{0}, \\ \operatorname{curl} \mathbf{H} = \mathbf{J}, \\ \operatorname{div} \mathbf{B} = 0, \end{cases} \quad (5.1)$$

where \mathbf{E} and \mathbf{D} are the electric field and electric displacement, respectively, ρ the electric field charge density and \mathbf{J} is the electric current density. By \mathbf{H} and \mathbf{B} we denote the magnetic field and the magnetic induction, respectively.

For biological tissues, the linear constitutive equations $\mathbf{D} = \boldsymbol{\varepsilon} \mathbf{E}$ and $\mathbf{B} = \boldsymbol{\mu} \mathbf{H}$ can be assumed (see Plonsey and Heppner [57]), where $\boldsymbol{\varepsilon}$ and $\boldsymbol{\mu}$ correspond to the electric permittivity and the magnetic permeability, respectively. It can be assumed that $\boldsymbol{\mu}$ is constant over the whole space and equal to the permeability of vacuum [61].

From second equation of (5.1), we conclude that there exists a scalar potential u such that $\mathbf{E} = -\nabla u$. From Ohm law the total current density \mathbf{J} is the sum of the impressed currents plus the return currents

$$\mathbf{J} = \mathbf{J}_p + \boldsymbol{\sigma} \mathbf{E} = \mathbf{J}_p - \boldsymbol{\sigma} \nabla u,$$

where $\boldsymbol{\sigma}$ is the conductivity, which is a uniformly positive definite matrix with entries in L^∞ .

From the third equation in (5.1) it follows that

$$0 = \operatorname{div} \mathbf{J} = \operatorname{div} (\mathbf{J}_p - \boldsymbol{\sigma} \nabla u).$$

Hence u is solution of the equation

$$\operatorname{div} (\boldsymbol{\sigma} \nabla u) = \operatorname{div} \mathbf{J}_p,$$

Let Ω be an open connected bounded set with Lipschitz continuous boundary $\partial\Omega$ included in \mathbb{R}^d , where $d = 2$ or $d = 3$ (Ω represents the human head). We assume that \mathbf{J}_p is supported

in Ω . Since $\mathbf{J} \cdot \mathbf{n}|_{\Omega} = \mathbf{J} \cdot \mathbf{n}|_{\mathbb{R}^d \setminus \bar{\Omega}} = 0$ and $\mathbf{J}_p \cdot \mathbf{n} = 0$ on the interface $\partial\Omega$, then $(\boldsymbol{\sigma} \nabla u) \cdot \mathbf{n} = 0$ on $\partial\Omega$. We define \mathbf{n} to be the outer unit normal vector on $\partial\Omega$. Then, we obtain this problem:

$$\begin{cases} \operatorname{div}(\boldsymbol{\sigma} \nabla u) = \operatorname{div}(\mathbf{J}_p) & \text{in } \Omega, \\ (\boldsymbol{\sigma} \nabla u) \cdot \mathbf{n} = 0 & \text{on } \partial\Omega. \end{cases} \quad (5.2)$$

Let us assume that a small activated region is centered at a point \mathbf{x}_0 and that the observation point is far from it. In this case the primary current \mathbf{J}_p is typically modeled as a dipole. So, in the following, we consider the electrostatic problem with a dipole as source term and homogeneous Neumann boundary condition:

$$\begin{cases} \operatorname{div}(\boldsymbol{\sigma} \nabla u) = \operatorname{div}(\mathbf{p} \delta_{\mathbf{x}_0}) & \text{in } \Omega, \\ (\boldsymbol{\sigma} \nabla u) \cdot \mathbf{n} = 0 & \text{on } \partial\Omega. \end{cases} \quad (5.3)$$

where \mathbf{x}_0 is an inner point of Ω , and $\mathbf{p} \neq 0$ is the polarization vector. In [65] the existence and uniqueness of solution $u \in L^p(\Omega)$, $1 \leq p < 3/2$ of this problem has been studied under of the assumption of more regularity of $\boldsymbol{\sigma}$ in a vicinity of \mathbf{x}_0 and $d = 3$. We give more details later on.

The singularity of the dipole source can also be treated using the so-called *subtraction approach*. We explain in more detail this technique below. We need to assume that there exists a nonempty open subdomain $\Omega_0 \subset \Omega$ around the source position \mathbf{x}_0 with constant conductivity $\boldsymbol{\sigma}_0$ (in general, a matrix). The conductivity $\boldsymbol{\sigma}$ is then split into two parts,

$$\boldsymbol{\sigma} = \boldsymbol{\sigma}_0 + \boldsymbol{\sigma}_s, \quad (5.4)$$

so that $\boldsymbol{\sigma}_0$ is constant over the whole domain Ω and $\boldsymbol{\sigma}_s$ is zero in the subdomain Ω_0 , i.e., $\boldsymbol{\sigma}_s(\mathbf{x}) = 0$ for all $\mathbf{x} \in \Omega_0$. The total potential u can be split into two parts,

$$u = u_0 + u_s, \quad (5.5)$$

where u_0 denotes the solution in a infinity homogeneous conductor. The potential u_0 satisfies

$$\operatorname{div}(\boldsymbol{\sigma}_0 \nabla u_0) = \operatorname{div}(\mathbf{p} \delta_{\mathbf{x}_0}) \quad \text{in } \mathbb{R}^d. \quad (5.6)$$

An analytic formula for u_0 in the case of a homogeneous and isotropic conductivity $\boldsymbol{\sigma}_0 = \sigma_0 I$, $\sigma_0 \in \mathbb{R}$ is

$$u_0(\mathbf{x}) = \begin{cases} \frac{\langle \mathbf{p}, (\mathbf{x} - \mathbf{x}_0) \rangle}{2\pi\sigma_0 |\mathbf{x} - \mathbf{x}_0|^2} & \text{if } d = 2, \\ \frac{\langle \mathbf{p}, (\mathbf{x} - \mathbf{x}_0) \rangle}{4\pi\sigma_0 |\mathbf{x} - \mathbf{x}_0|^3} & \text{if } d = 3. \end{cases}$$

When the conductivity $\boldsymbol{\sigma}_0$ is homogeneous and anisotropic (namely, $\boldsymbol{\sigma}_0$ is a constant matrix), we find

$$u_0(\mathbf{x}) = \begin{cases} \frac{\langle \mathbf{p}, (\boldsymbol{\sigma}_0)^{-1}(\mathbf{x} - \mathbf{x}_0) \rangle}{2\pi\sqrt{\det\boldsymbol{\sigma}_0} \langle (\boldsymbol{\sigma}_0)^{-1}(\mathbf{x} - \mathbf{x}_0), (\mathbf{x} - \mathbf{x}_0) \rangle} & \text{if } d = 2, \\ \frac{\langle \mathbf{p}, (\boldsymbol{\sigma}_0)^{-1}(\mathbf{x} - \mathbf{x}_0) \rangle}{4\pi\sqrt{\det\boldsymbol{\sigma}_0} \langle (\boldsymbol{\sigma}_0)^{-1}(\mathbf{x} - \mathbf{x}_0), (\mathbf{x} - \mathbf{x}_0) \rangle^{3/2}} & \text{if } d = 3. \end{cases}$$

Replacing (5.4), (5.5) in (5.3) and using that u_0 satisfies (5.6), we obtain

$$\operatorname{div} [(\boldsymbol{\sigma}_0 + \boldsymbol{\sigma}_s)\nabla(u_0 + u_s)] = \operatorname{div}(\mathbf{p}\delta_{\mathbf{x}_0}) = \operatorname{div}(\boldsymbol{\sigma}_0\nabla u_0),$$

and hence,

$$\operatorname{div}(\boldsymbol{\sigma}\nabla u_s) = \operatorname{div}[(\boldsymbol{\sigma}_0 + \boldsymbol{\sigma}_s)\nabla u_s] = -\operatorname{div}(\boldsymbol{\sigma}_s\nabla u_0).$$

On the other hand, since

$$0 = (\boldsymbol{\sigma}\nabla u) \cdot \mathbf{n} = (\boldsymbol{\sigma}\nabla(u_0 + u_s)) \cdot \mathbf{n} \quad \text{on } \partial\Omega,$$

then we obtain the Neumann boundary condition:

$$(\boldsymbol{\sigma}\nabla u_s) \cdot \mathbf{n} = -(\boldsymbol{\sigma}\nabla u_0) \cdot \mathbf{n} \quad \text{on } \partial\Omega.$$

In conclusion u_0 is known and u_s solves the boundary value problem

$$\begin{cases} \operatorname{div}(\boldsymbol{\sigma}\nabla u_s) = -\operatorname{div}(\boldsymbol{\sigma}_s\nabla u_0) & \text{in } \Omega, \\ (\boldsymbol{\sigma}\nabla u_s) \cdot \mathbf{n} = -(\boldsymbol{\sigma}\nabla u_0) \cdot \mathbf{n} & \text{on } \partial\Omega, \\ \int_{\Omega} u_s = 0. \end{cases} \quad (5.7)$$

The last condition of (5.7) filters out additive constants and therefore is suitable for assuring uniqueness of the solution u_s .

The goal of the reformulation using the explicit representation of u_0 is to obtain a problem with a more regular source, eliminating the singularity at \mathbf{x}_0 : notice that the potential u_0 has a singularity at $\mathbf{x} = \mathbf{x}_0$ but it is smooth for $\mathbf{x} \neq \mathbf{x}_0$. Therefore, the Neumann datum in (5.7) is smooth and moreover, $\boldsymbol{\sigma}_s$ vanishes in Ω_0 which implies that $\boldsymbol{\sigma}_s\nabla u_0 \in L^\infty(\Omega)$.

An alternative approach is the *direct method* studied by Valli in [65] ($d = 3$) and also in the previous chapter of this thesis ($d = 2$). Notice that to prove that the following weak formulation has a unique solution, it is necessary to assume that there exists $r_0 > 0$ such that the entries of $\boldsymbol{\sigma}$ belong to $W^{1,\infty}(B_{r_0}(\mathbf{x}_0))$, where $B_{r_0}(\mathbf{x}_0) := \{\mathbf{x} \in \mathbb{R}^d : |\mathbf{x} - \mathbf{x}_0| < r_0\}$. We recall the weak formulation: find $u \in L^p(\Omega)$ such that

$$\begin{cases} \int_{\Omega} u \operatorname{div}(\boldsymbol{\sigma}\nabla\varphi) = -\mathbf{p} \cdot \nabla\varphi(\mathbf{x}_0) & \forall \varphi \in X_q, \\ \int_{\Omega} u = 0, \end{cases} \quad (5.8)$$

where

$$X_q := \{\varphi \in W^{1,q}(\Omega) : \varphi \in C^1(B_{r^*}(\mathbf{x}_0)), \operatorname{div}(\boldsymbol{\sigma} \nabla \varphi) \in L^q(\Omega), (\boldsymbol{\sigma} \nabla \varphi) \cdot \mathbf{n} = 0 \text{ on } \partial\Omega\},$$

being r^* a fixed number such that $0 < r^* < r_0$. Moreover, here and thereafter $\frac{1}{p} + \frac{1}{q} = 1$.

The following theorem, which is derivated from [65, Remark 3.3], ensures the existence and uniqueness of solution to (5.8) in the three-dimensional case ($d = 3$) and in two-dimensional case ($d = 2$):

Theorem 5.1.1 *For all p with $1 \leq p < 3/2$ if $d = 3$ ($1 \leq p < 2$ if $d = 2$), there exists a unique solution $u \in L^p(\Omega)$ to (5.8), which is the same for all p in this range.*

Another alternative approach, is to use an *approximation of the delta function*

$$\delta_{\epsilon, \mathbf{x}_0} := \chi_{\epsilon} / |B_{\epsilon}(\mathbf{x}_0)| \in L^2(\Omega), \quad (5.9)$$

when solving the discrete problem, where χ_{ϵ} is the characteristic function (equal to one in the ball $B_{\epsilon}(\mathbf{x}_0)$ and zero, otherwise). For simplicity of notation, in this section we define $B_{\epsilon} := B_{\epsilon}(\mathbf{x}_0)$.

In this case, the weak problem corresponds to

find $u^{\epsilon} \in H^1(\Omega)$ such that

$$\begin{cases} \int_{\Omega} \boldsymbol{\sigma} \nabla u^{\epsilon} \cdot \nabla v = \frac{1}{|B_{\epsilon}|} \int_{B_{\epsilon}} \mathbf{p} \cdot \nabla v & \forall \varphi \in H^1(\Omega), \\ \int_{\Omega} u^{\epsilon} = 0, \end{cases} \quad (5.10)$$

for each $\epsilon > 0$. In the following theorem, we prove the convergence of u^{ϵ} to u when ϵ tends to zero. We prove the convergence only in the bidimensional case (but a similar result is true also for $d = 3$).

Theorem 5.1.2 *Let $\sigma_{i,j} \in W^{1,\infty}(B_{r_0})$ for each $i, j = 1, 2$ and $d = 2$. Let u and u^{ϵ} be the respective solutions to problems (5.8) and (5.10) and $r^* > 0$ a fixed number such that $r^* < r_0$. Then if $\epsilon < r^*$ there exist a positive constant C , independent of ϵ such that for all p with $1 \leq p < 2$*

$$\|u - u^{\epsilon}\|_{0,p,\Omega} \leq C\epsilon^{2/p-1}. \quad (5.11)$$

Proof. To find this estimate in $L^p(\Omega)$, with $1 \leq p < 2$, we will use the same duality argument that in Chapter 4. We recall the well-posed auxiliary problem: given $\psi \in L^q(\Omega)$, find $\varphi \in H^1(\Omega)$ such that

$$\begin{cases} \operatorname{div}(\boldsymbol{\sigma} \nabla \varphi) = \psi - \frac{1}{|\Omega|} \int_{\Omega} \psi & \text{in } \Omega, \\ (\boldsymbol{\sigma} \nabla \varphi) \cdot \mathbf{n} = 0 & \text{on } \partial\Omega, \\ \int_{\Omega} \varphi = 0. \end{cases} \quad (5.12)$$

where $\frac{1}{p} + \frac{1}{q} = 1$.

Since $\psi - \frac{1}{|\Omega|} \int_{\Omega} \psi \in L^q(\Omega)$, then the internal regularity results for elliptic problems [37, Section 9.5] yield $\varphi \in W^{2,q}(B_{r^*})$. The Sobolev embedding theorem (see, e.g. [35, Section 5.6.3]) also gives $\varphi \in C^{1,\alpha}(\overline{B_{r^*}})$, with $\alpha = 2/p - 1$. Moreover, $\|\varphi\|_{C^{1,\alpha}(\overline{B_{r^*}})} \leq C\|\varphi\|_{2,q,B_{r^*}} \leq C\|\psi\|_{0,q,\Omega}$, where C depends on σ , r^* , but not on ψ . By using this fact, (5.8), (5.10) and integration by parts, we obtain

$$\begin{aligned}
\int_{\Omega} (u - u^\epsilon)\psi &= \int_{\Omega} (u - u^\epsilon) \left(\operatorname{div}(\sigma \nabla \varphi) + \frac{1}{|\Omega|} \int_{\Omega} \psi \right), \\
&= \int_{\Omega} u \operatorname{div}(\sigma \nabla \varphi) - \int_{\Omega} u^\epsilon \operatorname{div}(\sigma \nabla \varphi) \\
&= -\mathbf{p} \cdot \nabla \varphi(\mathbf{x}_0) + \int_{\Omega} \sigma \nabla u^\epsilon \cdot \nabla \varphi \\
&= -\mathbf{p} \cdot \nabla \varphi(\mathbf{x}_0) + \frac{1}{|B_\epsilon|} \int_{B_\epsilon} \mathbf{p} \cdot \nabla \varphi \\
&= \mathbf{p} \cdot \left(\frac{1}{|B_\epsilon|} \int_{B_\epsilon} \nabla \varphi - \nabla \varphi(\mathbf{x}_0) \right), \\
&\leq |\mathbf{p}| \frac{1}{|B_\epsilon|} \int_{B_\epsilon} |\nabla \varphi - \nabla \varphi(\mathbf{x}_0)| \\
&\leq |\mathbf{p}| \frac{1}{|B_\epsilon|} \int_{B_\epsilon} |\mathbf{x} - \mathbf{x}_0|^\alpha \|\nabla \varphi\|_{C^\alpha(\overline{B_\epsilon})} \\
&\leq C|\mathbf{p}| \|\nabla \varphi\|_{C^{1,\alpha}(\overline{B_\epsilon})} \epsilon^\alpha \\
&\leq C|\mathbf{p}| \|\nabla \varphi\|_{2,q,B_{r^*}} \epsilon^\alpha \\
&\leq C|\mathbf{p}| \|\psi\|_{0,q,\Omega} \epsilon^\alpha.
\end{aligned} \tag{5.13}$$

Therefore we have

$$\|u - u^\epsilon\|_{0,p,\Omega} = \sup_{\psi \in L^q(\Omega)} \frac{\int_{\Omega} (u - u^\epsilon)\psi}{\|\psi\|_{0,q,\Omega}} \leq C\epsilon^{2/p-1}.$$

□

5.1.2 Discrete problem

In all this work, we will use 2D geometries in order to simplify the calculations, since 3D geometries require longer computation times.

We assume that Ω is a Lipschitz polygon. We consider a regular family of triangular meshes \mathcal{T}_h of Ω (see, for instance, [23]). As usual, h denotes the mesh size: $h := \max_{T \in \mathcal{T}_h} h_T$, with h_T being the diameter of T . We consider the space of Lagrange finite elements of degree one:

$$H_h := \{v_h \in C(\Omega) : v_h|_T \in \mathcal{P}_1 \ \forall T \in \mathcal{T}_h\}. \tag{5.14}$$

The finite element approximation of the solution of (5.7) reads: find $u_{s,h} \in H_h$ such that

$$\begin{cases} \int_{\Omega} \boldsymbol{\sigma} \nabla u_{s,h} \cdot \nabla v_h = - \int_{\Omega} \boldsymbol{\sigma}_s \nabla u_0 \cdot \nabla v_h - \int_{\partial\Omega} \boldsymbol{\sigma}_0 \nabla u_0 \cdot \mathbf{n} v_h & \forall v_h \in H_h, \\ \int_{\Omega} u_{s,h} = 0, \end{cases} \quad (5.15)$$

In [67] the convergence of $u_{s,h}$ to u_s has been studied.

The finite element approximation of the direct method reads: find $u_h \in H_h$ such that

$$\begin{cases} \int_{\Omega} \boldsymbol{\sigma} \nabla u_h \cdot \nabla v_h = \mathbf{p} \cdot \nabla (v_h|_{T_0})(\mathbf{x}_0) & \forall v_h \in H_h, \\ \int_{\Omega} u_h = 0, \end{cases} \quad (5.16)$$

where T_0 is any triangle that contains \mathbf{x}_0 . In this case, we have proved an a priori error estimate in Chapter 4, under certain assumptions:

Theorem 5.1.3 *Let \mathcal{T}_h be a quasiuniform family of subdivisions of the convex Lipschitz polygon Ω and assume that $\sigma_{i,j} \in C^1(\overline{\Omega})$ for each $i, j = 1, 2$. Let u and u_h be the respective solutions to problems (5.8) and (5.16). Then there exists $h_0 > 0$ such that*

$$\|u - u_h\|_{0,p,\Omega} \leq Ch^{2/p-1}$$

for all $0 < h < h_0$ and for all p such that $\frac{q_0}{q_0-1} < p < 2$, where q_0 is the maximal regularity exponent such that the solution φ of problem (5.12) belongs to $W^{2,q}(\Omega)$, and moreover satisfies $\|\varphi\|_{2,q,\Omega} \leq C\|\psi\|_{0,q,\Omega}$, with $2 < q < q_0$.

In the case of the approximation of the delta (5.9), we have the following discrete problem: find $u_h^\epsilon \in H_h$ such that

$$\begin{cases} \int_{\Omega} \boldsymbol{\sigma} \nabla u_h^\epsilon \cdot \nabla v_h = \frac{1}{|B_\epsilon|} \int_{B_\epsilon} \mathbf{p} \cdot \nabla v_h & \forall v_h \in H_h, \\ \int_{\Omega} u_h^\epsilon = 0, \end{cases} \quad (5.17)$$

for each $\epsilon > 0$. To give an a priori error estimate of this problem, we need to assume that Ω is a convex Lipschitz polygon, $\sigma_{i,j} \in C^1(\overline{\Omega})$, $i, j = 1, 2$, and more regularity of the source used. Let $\widehat{\delta}_{\epsilon,\mathbf{x}_0}$ be a smoothing of $\delta_{\epsilon,\mathbf{x}_0}|_{B_\epsilon}$ to Ω with support in B_ϵ . Then, $\widehat{\delta}_{\epsilon,\mathbf{x}_0}$ is globally smooth and therefore, $\text{div}(\mathbf{p}\widehat{\delta}_{\epsilon,\mathbf{x}_0}) \in L^\infty(\Omega)$. The solutions of the problems (5.10) and (5.17) with source $\text{div}(\mathbf{p}\widehat{\delta}_{\epsilon,\mathbf{x}_0})$ will be called \widehat{u}^ϵ and \widehat{u}_h^ϵ respectively. It is known that in this case, $\widehat{u}^\epsilon \in H^2(\Omega)$, for each $\epsilon > 0$ and therefore, $\|\widehat{u}^\epsilon - \widehat{u}_h^\epsilon\|_{0,\Omega} \leq Ch^2\|\widehat{u}^\epsilon\|_{2,\Omega}$, for each $\epsilon > 0$. We are interested in to show that \widehat{u}_h^ϵ is converging to u . The following theorem give us an a priori error estimate in this case.

Theorem 5.1.4 *Let Ω be a convex Lipschitz polygon and $\sigma_{i,j} \in C^1(\overline{\Omega})$ for each $i, j = 1, 2$. Let u and \widehat{u}_h^ϵ be the respective solutions to problems (5.8) and the problem (5.17), respectively. The last one, computed with source $\text{div}(\mathbf{p}\widehat{\delta}_{\epsilon, \mathbf{x}_0})$. Then for each $\eta > 0$ there exist $\epsilon_0(\eta)$ and $h_0(\eta)$ such that*

$$\|u - \widehat{u}_h^{\epsilon_0}\|_{0,p,\Omega} \leq \eta, \quad \forall h < h_0(\eta).$$

Proof. From Theorem 5.1.2 and the results above, we know that $\|u - \widehat{u}^\epsilon\|_{0,p,\Omega} \leq C\epsilon^{2/p-1}$ and $\|\widehat{u}^\epsilon - \widehat{u}_h^\epsilon\|_{0,\Omega} \leq Ch^2\|\widehat{u}^\epsilon\|_{2,\Omega}$, for each $\epsilon > 0$. Given $\eta > 0$ we can choose $\epsilon_0 = \epsilon_0(\eta)$ such that $\|u - \widehat{u}^{\epsilon_0}\|_{0,p,\Omega} \leq C\epsilon_0^{2/p-1} < \eta/2$ and $\|\widehat{u}^{\epsilon_0} - \widehat{u}_h^{\epsilon_0}\|_{0,\Omega} \leq Ch^2\|\widehat{u}^{\epsilon_0}\|_{2,\Omega}$. Also, we can choose $h_0 = h_0(\eta)$ such that $\|\widehat{u}^{\epsilon_0} - \widehat{u}_{h_0}^{\epsilon_0}\|_{0,\Omega} \leq Ch_0^2\|\widehat{u}^{\epsilon_0}\|_{2,\Omega} \leq \eta/2$. Then, using that $\|u - \widehat{u}_h^{\epsilon_0}\|_{0,p,\Omega} \leq \|u - \widehat{u}^{\epsilon_0}\|_{0,p,\Omega} + \|\widehat{u}^{\epsilon_0} - \widehat{u}_h^{\epsilon_0}\|_{0,p,\Omega}$ and the fact that $L^2(\Omega) \subset L^p(\Omega)$, $1 \leq p < 2$, we conclude that for each $h < h_0(\eta)$ we have that $\|u - \widehat{u}_h^{\epsilon_0}\|_{0,p,\Omega} \leq \eta$ \square

Notice that to have uniqueness of the problem we can change the second condition in problems (5.15), (5.16) and (5.17). It is enough to set equal to zero the value of the potential u in a point. This new assumption simplifies the computations at computational level. We will consider a reference electrode with given potential, i.e.,

$$u(\mathbf{x}_{ref}) = 0.$$

Moreover, this is a realistic condition since EEG measures electric potential differences respect to a fix electrode.

Notice that, in order to prove existence and uniqueness of solution, in all the preceding sections we have required some regularity of σ in a vicinity of \mathbf{x}_0 . If σ is piecewise regular and \mathbf{x}_0 is on the interface between two regions with different conductivities, we do not know how to formulate the problem in a suitable variational way.

In this chapter we study experimentally the behavior of the methods when \mathbf{x}_0 tends to the interface. The direct approach and the characteristic function approach are well defined if σ is piecewise constant; however, we have not a proof of the convergence of the corresponding finite element solutions. The characteristic function approach is well defined also for \mathbf{x}_0 on the interface. Let us also recall that the error bound in the subtraction approach deteriorates when \mathbf{x}_0 tends to the interface (see [67]).

In Section 5.2 we show that the solution computed with the direct method is more stable than the one computed with the subtraction approach. We also consider the case when \mathbf{x}_0 is on the interface. We use the characteristic function approach (the only one that is well defined in this situation) and we study the behavior when ϵ tends to zero. In Section 5.3 we study the inverse source problem. Also in this case σ is piecewise regular. We analyze the results obtained using the three methods and also the adaptive procedure studied in Chapter 4. We consider

two different situations: a source internal to a regular region and a source close to the interface between two regions. In Section 5.4 we study the case of a distributed source and we compare the lead field matrices in different situations. Also here we are interested in the case when $\boldsymbol{\sigma}$ is piecewise regular. We analyze the results obtained using the methods already presented and two other methods that will be introduced in the same section. We consider the same two situations that in the previous section: a source completely contained in a regular region and a source close to the interface between two regions with different conductivities. Finally, in Section 5.5 we give some conclusions.

5.2 General considerations for \boldsymbol{x}_0 on the interface between two regions with different conductivities

The aim of this section is to investigate the behavior of the different approximation methods, when the source is located very close to the interface between two different regions.

The subtraction method requires to assume that around the source position \boldsymbol{x}_0 we can find a nonempty open subdomain $\Omega_0 \subset \Omega$ with homogeneous constant conductivity $\boldsymbol{\sigma}_0$. This technique has showed to give good results when one solves the inverse problem in a point internal to a regular region [67]. However, if \boldsymbol{x}_0 is a point on the interface between two regions with different conductivities, the fundamental solution cannot be used, and therefore the subtraction technique is not well defined.

Also the solution obtained by means of the direct method has a good behavior when \boldsymbol{x}_0 is an internal point. However, when the point belongs to an interface, it does not seem to be reliable, as it has a different behavior if we take a sequence of locations $\boldsymbol{x}_{0,k}$ converging to \boldsymbol{x}_0 from one side or from the other. An alternative in such case is to consider an approximation of the delta function. In particular, we consider (5.9). This approximation is independent of the mesh, and is well-defined even when \boldsymbol{x}_0 lies on the interface.

The first experiment is performed in order to obtain information on what is happening to the solution obtained by using the subtraction method or the direct method for $\boldsymbol{x}_{0,k}$ tending to \boldsymbol{x}_0 on an interface. In a second test, we analyze the behavior of the characteristic function approach when \boldsymbol{x}_0 is exactly on the interface, considering different choices of the side-length of the square where this function is supported.

5.2.1 Test 1.

This experiment consists in taking two sequences of seven points both of them converging at the same point on the interface, one sequence coming from one region and the other one, coming

from other region. After that, we fix the source on these points and we solve the problem (5.3) with a fixed polarization, by using subtraction method and direct method. We compare the values of both solutions in twelve nodes on the external boundary, that correspond to the nodes in Table 5.1.

Nodes	1	2	3	4	5	6	7	8	9	10	11	12
x	-1	-0.5	0	0.25	0.5	1	1	1	1	1	1	1
y	-1	-1	-1	-1	-1	-1	-0.5	0	0.25	0.5	0.75	1

Table 5.1: Twelve nodes on the external boundary.

The domain Ω is a multi-layer square centered at $(0, 0)$ with side-length 2. It has three different layers: $\bar{\Omega}_1 = \bar{\Omega} \setminus (-0.92, 0.92)^2$, $\bar{\Omega}_2 = [-0.92, 0.92]^2 \setminus (-0.87, 0.87)^2$ and $\bar{\Omega}_3 = [-0.87, 0.87]^2$. The conducting σ is assumed isotropic on each layer and equal to $\sigma|_{\Omega_1} = \sigma|_{\Omega_3} = 0.33$ and $\sigma|_{\Omega_2} = 0.0042$. Notice that the values of the conductivities have not been chosen random. These correspond to real values in the brain.

We focus on the interface between the region 1 and region 2. We consider the points in Table 5.2 that are converging to the point $(0.0012634, 0.92)$. The computations were done in the meshes in Table 5.3.

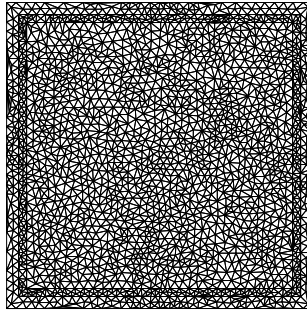


Figure 5.1: Domain Ω .

Notice that each row in Table 5.2 contains a point in region 1 and a point in region 2 which are at the same distance of the point on the interface $(0.0012634, 0.92)$. The points on the first row were chosen at a distance 0.025 to $(0.0012634, 0.92)$, the points on the second row at half of the above distance and so on.

In Table 5.4 we find twelve values for each one of the seven solutions corresponding to dipoles placed at the seven points in region 1 in Table 5.2. The polarization $\mathbf{p} = (-0.2425, 0.9701)$ is the same in all the cases. Moreover, the last row contains the values of the L^p norm of the

Points	Sequence in region 1	Sequence in region 2
1	(0.0012634, 0.945)	(0.0012634, 0.8950)
2	(0.0012634, 0.9325)	(0.0012634, 0.9075)
3	(0.0012634, 0.9263)	(0.0012634, 0.9075)
4	(0.0012634, 0.9232)	(0.0012634, 0.9169)
5	(0.0012634, 0.9216)	(0.0012634, 0.9169)
6	(0.0012634, 0.9208)	(0.0012634, 0.9192)
7	(0.0012634, 0.9204)	(0.0012634, 0.9196)

Table 5.2: The two sequences of points converging to (0.0012634, 0.92).

Mesh	Degrees of freedom	Elements	Elem. region 1	Elem. region 2	Elem. region 3
1	86718	172751	27146	31581	114024
2	544135	1086493	171571	199069	715853

Table 5.3: Meshes used in Tests 1 and 2.

solutions computed in all the domain Ω , with $p = 5/4$. Table 5.5 contains the same information, but the solutions were computed by using direct method. In Tables 5.6 and 5.7 we report the same computations, but now the seven points correspond to the points in region 2. In Tables 5.8, 5.9, 5.10 and 5.11, we repeat the same procedure, but with a finer mesh, mesh 2 in Table 5.3.

Notice that in the direct method, in Tables 5.5, 5.7, 5.9 and 5.11 there are columns that are the same although we are computing the solution using different points as support of the delta. The reason is that some points of the Table 5.2 are contained in a same triangle of the mesh, and the direct method is not reading the exact position of the point, as only considers the triangle that contains it. This method is a little imprecise respect to the position because all the points inside a triangle produce the same solution.

We obtain several conclusions from this experiment: first, the subtraction method has an oscillating behavior when \mathbf{x}_0 gets closer and closer to the interface. This is illustrating in Tables 5.4, 5.6, 5.8 and 5.10. In the coarser mesh the oscillatory behavior is more evident, while in the finer mesh it can be seen only in the last columns, that correspond to the nearest points to the interface. With this experiment, we see the non-robustness of the subtraction approach when \mathbf{x}_0 can be very close to the interface. A theoretical analysis about this statement can be found in [67, Lemma 3.10].

Nodes	Point 1	Point 2	Point 3	Point 4	Point 5	Point 6	Point 7
1	0.3481	0.3338	0.3279	0.3531	0.5448	0.6506	0.0752
2	0.2915	0.2753	0.2685	0.2965	0.5269	0.7037	0.1247
3	0.2398	0.2229	0.2157	0.2445	0.4923	0.7111	0.1538
4	0.2165	0.1997	0.1926	0.2209	0.4684	0.6957	0.1597
5	0.1945	0.1782	0.1713	0.1986	0.4395	0.6672	0.1599
6	0.1555	0.1413	0.1353	0.159	0.3712	0.578	0.1451
7	0.1052	0.0949	0.0904	0.1077	0.2633	0.4183	0.1087
8	0	0	0	0	0	0	0
9	-0.0852	-0.0754	-0.0712	-0.0873	-0.235	-0.3879	-0.1071
10	-0.2029	-0.1782	-0.1676	-0.2082	-0.5822	-0.9743	-0.2744
11	-0.3665	-0.3194	-0.2991	-0.3764	-1.0925	-1.8518	-0.5312
12	-0.5316	-0.4607	-0.4301	-0.5461	-1.6243	-2.7753	-0.8051
$\ u\ _{0,p,\Omega}$	1.4196	1.3727	1.3501	1.3745	2.2112	4.2001	1.5887

Table 5.4: Subtraction method in region 1, using mesh 1.

Nodes	Point 1	Point 2	Point 3	Point 4	Point 5	Point 6	Point 7
1	0.3452	0.3388	0.3216	0.3216	0.3243	0.3243	0.3243
2	0.2882	0.281	0.2613	0.2613	0.2646	0.2646	0.2646
3	0.2363	0.2288	0.2083	0.2083	0.2117	0.2117	0.2117
4	0.213	0.2056	0.1853	0.1853	0.1887	0.1887	0.1887
5	0.1911	0.1839	0.1643	0.1643	0.1676	0.1676	0.1676
6	0.1526	0.1463	0.1291	0.1291	0.132	0.132	0.132
7	0.1031	0.0985	0.086	0.086	0.088	0.088	0.088
8	0	0	0	0	0	0	0
9	-0.0831	-0.0788	-0.067	-0.067	-0.0689	-0.0689	-0.0689
10	-0.1978	-0.1868	-0.1571	-0.1571	-0.1619	-0.1619	-0.1619
11	-0.3567	-0.3358	-0.279	-0.279	-0.288	-0.288	-0.288
12	-0.5168	-0.4852	-0.3999	-0.3999	-0.4133	-0.4133	-0.4133
$\ u\ _{0,p,\Omega}$	1.4222	1.3941	1.3457	1.3457	1.3476	1.3476	1.3476

Table 5.5: Direct method in region 1, using mesh 1.

Nodes	Point 1	Point 2	Point 3	Point 4	Point 5	Point 6	Point 7
1	-6.7323	-6.6863	-6.6744	-7.0787	-10.6393	-19.4138	-28.3595
2	-7.7854	-7.7411	-7.7283	-8.0862	-11.232	-18.9606	-26.8082
3	-8.1971	-8.1531	-8.1389	-8.4487	-11.1721	-17.8444	-24.5941
4	-8.1307	-8.0872	-8.0725	-8.3582	-10.8717	-17.0226	-23.2353
5	-7.8782	-7.8358	-7.8209	-8.0822	-10.3829	-16.0076	-21.6812
6	-6.9044	-6.8668	-6.853	-7.0668	-8.9518	-13.5547	-18.1898
7	-5.0424	-5.0144	-5.0038	-5.1514	-6.4544	-9.633	-12.8291
8	0	0	0	0	0	0	0
9	4.7534	4.7254	4.7141	4.8386	5.9426	8.6302	11.3244
10	12.0118	11.9392	11.9091	12.2105	14.8913	21.4121	27.9406
11	22.9467	22.8044	22.7441	23.2973	28.2308	40.2215	52.212
12	34.501	34.2835	34.19	35.0007	42.2446	59.8415	77.424
$\ u\ _{0,p,\Omega}$	52.5596	78.6864	52.8219	55.3922	61.7053	80.2363	108.0021

Table 5.6: Subtraction method in region 2, using mesh 1.

Nodes	Point 1	Point 2	Point 3	Point 4	Point 5	Point 6	Point 7
1	-6.7504	-6.6292	-6.6869	-6.6327	-6.6327	-6.6613	-6.6613
2	-7.8019	-7.689	-7.7389	-7.6895	-7.6895	-7.7155	-7.7155
3	-8.2128	-8.1022	-8.1497	-8.1018	-8.1018	-8.1269	-8.1269
4	-8.1463	-8.0367	-8.0838	-8.0363	-8.0363	-8.0613	-8.0613
5	-7.8935	-7.7864	-7.8327	-7.7862	-7.7862	-7.8106	-7.8106
6	-6.918	-6.8224	-6.8642	-6.8225	-6.8225	-6.8444	-6.8444
7	-5.0527	-4.9812	-5.0128	-4.9815	-4.9815	-4.998	-4.998
8	0	0	0	0	0	0	0
9	4.7647	4.6914	4.7253	4.6927	4.6927	4.7099	4.7099
10	12.0399	11.8474	11.9384	11.8521	11.8521	11.8976	11.8976
11	23.0075	22.6253	22.8098	22.6369	22.6369	22.7282	22.7282
12	34.5989	34.0097	34.298	34.0299	34.0299	34.1715	34.1715
$\ u\ _{0,p,\Omega}$	51.9	52.3894	54.1701	54.6374	54.6374	55.7171	55.7171

Table 5.7: Direct method in region 2, using mesh 1.

Nodes	Point 1	Point 2	Point 3	Point 4	Point 5	Point 6	Point 7
1	0.3482	0.3339	0.3268	0.3228	0.3144	0.3475	0.6223
2	0.2916	0.2753	0.2673	0.2628	0.2526	0.2835	0.5687
3	0.24	0.2229	0.2145	0.2098	0.1988	0.227	0.5073
4	0.2166	0.1998	0.1915	0.1868	0.1758	0.2023	0.474
5	0.1946	0.1783	0.1703	0.1657	0.1551	0.1797	0.4384
6	0.1556	0.1414	0.1343	0.1304	0.121	0.1416	0.3638
7	0.1053	0.0949	0.0898	0.0869	0.08	0.0944	0.2542
8	0	0	0	0	0	0	0
9	-0.0852	-0.0754	-0.0706	-0.0679	-0.0613	-0.074	-0.2203
10	-0.203	-0.1783	-0.1661	-0.1593	-0.1427	-0.1739	-0.5398
11	-0.3667	-0.3195	-0.2962	-0.2831	-0.2512	-0.3096	-1.0019
12	-0.532	-0.4611	-0.426	-0.4063	-0.3583	-0.4447	-1.4803
$\ u\ _{0,p,\Omega}$	1.4378	1.4333	1.3683	1.3538	1.3472	1.4339	2.2846

Table 5.8: Subtraction method in region 1, using mesh 2.

Nodes	Point 1	Point 2	Point 3	Point 4	Point 5	Point 6	Point 7
1	0.349	0.3323	0.3277	0.3244	0.3219	0.3219	0.3219
2	0.2926	0.2736	0.2684	0.2645	0.2618	0.2618	0.2618
3	0.2409	0.2211	0.2157	0.2116	0.2088	0.2088	0.2088
4	0.2176	0.198	0.1926	0.1886	0.1858	0.1858	0.1858
5	0.1955	0.1766	0.1713	0.1675	0.1648	0.1648	0.1648
6	0.1565	0.1399	0.1353	0.1319	0.1296	0.1296	0.1296
7	0.1059	0.0938	0.0904	0.088	0.0863	0.0863	0.0863
8	0	0	0	0	0	0	0
9	-0.0858	-0.0744	-0.0712	-0.0689	-0.0673	-0.0673	-0.0673
10	-0.2045	-0.1757	-0.1678	-0.162	-0.1578	-0.1578	-0.1578
11	-0.3694	-0.3145	-0.2993	-0.2882	-0.2803	-0.2803	-0.2803
12	-0.5361	-0.4535	-0.4306	-0.414	-0.402	-0.402	-0.402
$\ u\ _{0,p,\Omega}$	1.4355	1.3893	1.3682	1.357	1.3432	1.3432	1.3432

Table 5.9: Direct method in region 1, using mesh 2.

Nodes	Point 1	Point 2	Point 3	Point 4	Point 5	Point 6	Point 7
1	-6.7298	-6.6822	-6.657	-6.6215	-6.1482	-1.8834	11.0224
2	-7.7837	-7.7376	-7.713	-7.6803	-7.262	-3.5241	7.7403
3	-8.1949	-8.1492	-8.1247	-8.0946	-7.732	-4.5192	5.1254
4	-8.1285	-8.0832	-8.0589	-8.0304	-7.6954	-4.7389	4.1212
5	-7.8761	-7.832	-7.8083	-7.7814	-7.4745	-4.7751	3.3033
6	-6.9022	-6.8629	-6.8419	-6.8191	-6.5673	-4.3626	2.2236
7	-5.0399	-5.0107	-4.9951	-4.9788	-4.8046	-3.285	1.2473
8	0	0	0	0	0	0	0
9	4.7519	4.7228	4.7072	4.6921	4.5439	3.2633	-0.5432
10	12.0083	11.9328	11.8922	11.854	11.4937	8.3904	-0.8209
11	22.9412	22.7931	22.7133	22.6405	21.9762	16.2778	-0.6133
12	34.5175	34.291	34.1687	34.059	33.082	24.7214	-0.0381
$\ u\ _{0,p,\Omega}$	52.2292	57.1387	53.8755	55.4943	55.6164	51.5907	64.26

Table 5.10: Subtraction method in region 2, using mesh 2.

Nodes	Point 1	Point 2	Point 3	Point 4	Point 5	Point 6	Point 7
1	-6.7258	-6.6673	-6.6755	-6.644	-6.6505	-6.6316	-6.6316
2	-7.7801	-7.7239	-7.7301	-7.7003	-7.706	-7.6888	-7.6888
3	-8.1915	-8.1358	-8.1414	-8.1121	-8.1175	-8.1008	-8.1008
4	-8.1251	-8.07	-8.0756	-8.0465	-8.0518	-8.0353	-8.0353
5	-7.8728	-7.819	-7.8245	-7.7961	-7.8014	-7.7852	-7.7852
6	-6.8991	-6.8513	-6.8564	-6.8311	-6.8358	-6.8213	-6.8213
7	-5.0376	-5.002	-5.006	-4.9871	-4.9907	-4.9798	-4.9798
8	0	0	0	0	0	0	0
9	4.7496	4.7138	4.7184	4.6991	4.703	4.6916	4.6916
10	12.0019	11.909	11.9217	11.871	11.8813	11.8512	11.8512
11	22.9287	22.7461	22.7726	22.6719	22.6928	22.6325	22.6325
12	34.4987	34.219	34.2613	34.1058	34.1385	34.045	34.045
$\ u\ _{0,p,\Omega}$	52.1918	53.0541	54.1383	55.3545	55.8542	56.0896	56.0896

Table 5.11: Direct method in region 2, using mesh 2.

Nodes	$\epsilon = 0.01$	$\epsilon = 0.001$	$\epsilon = 0.0001$	$\epsilon = 0.00001$
1	-3.1643	-3.1657	-3.1685	-3.1685
2	-3.7218	-3.7229	-3.7254	-3.7254
3	-3.9542	-3.9551	-3.9576	-3.9576
4	-3.9329	-3.9338	-3.9363	-3.9363
5	-3.8182	-3.8191	-3.8215	-3.8215
6	-3.3532	-3.3541	-3.3562	-3.3562
7	-2.4527	-2.4534	-2.4550	-2.4550
8	0	0	0	0
9	2.3180	2.3188	2.3205	2.3205
10	5.8613	5.8634	5.8679	5.8679
11	11.2066	11.2111	11.2201	11.2201
12	16.8581	16.8651	16.8791	16.8791
$\ u\ _{0,p,\Omega}$	26.5281	27.7785	27.9054	27.9054

Table 5.12: Dipole position on the interface, mesh 1.

On the contrary, the direct method is stable when the dipole position is in region 1 or 2, near or far from the interface. We also clearly see that the solution converges to different functions when \mathbf{x}_0 tends to the interface from one side or from the other. This confirms that the variational formulation for \mathbf{x}_0 lying exactly on the interface must have a different structure from the case in which \mathbf{x}_0 is internal to the middle layer. Nevertheless, for that case we can show some numerical results obtained by approximating the delta distribution in a suitable way.

5.2.2 Test 2.

In this test we want to analyze what happens if \mathbf{x}_0 is on the interface. To this end, we consider the approximation of the delta distribution in (5.9). It is supported on a square centered at \mathbf{x}_0 and with side-length 2ϵ , with the same polarization that in the previous test. We solve the problem four times, with four different values of ϵ . As in the previous test, we consider twelve values of the solution corresponding to the same twelve external nodes in Table 5.1 and also we compute the L^p norm in all Ω , with $p = 5/4$. This procedure was done with the two meshes in Table 5.3. In Table 5.12, we find the results corresponding to the mesh 1 and in Table 5.13, to the mesh 2. We can obtain as a conclusion that this approximation performs in a satisfactory way.

Notice that if we take the last column of Tables 5.5 and 5.7 and we do an average, we obtain

Nodes	$\epsilon = 0.01$	$\epsilon = 0.001$	$\epsilon = 0.0001$	$\epsilon = 0.00001$
1	-3.1638	-3.1581	-3.1563	-3.1563
2	-3.7218	-3.7164	-3.7148	-3.7148
3	-3.9541	-3.9488	-3.9473	-3.9473
4	-3.9328	-3.9275	-3.9260	-3.9260
5	-3.8180	-3.8130	-3.8114	-3.8115
6	-3.3529	-3.3483	-3.3470	-3.3470
7	-2.4520	-2.4486	-2.4476	-2.4476
8	0	0	0	0
9	2.3176	2.3141	2.3130	2.3130
10	5.8610	5.8518	5.8490	5.8490
11	11.2048	11.1864	11.1808	11.1808
12	16.8658	16.8374	16.8287	16.8288
$\ u\ _{0,p,\Omega}$	26.6009	28.0923	28.6901	28.6971

Table 5.13: Dipole position on the interface, mesh 2.

a result quite similar to the last column in Table 5.12. The same happens for mesh 2 in Table 5.3.

However from a physiological point of view, people are interested in considering impulses coming from the middle region. Specifically, people study the neuronal impulses which are generated in that region, but close to the interface between regions 1 and 2. Then, from the computational results we can conclude that the subtraction approach in this real situation is not the best one and it is better to choose an alternative approach.

5.3 Inverse problem

In this section we study the inverse problem and specifically, we are interested in finding the localization and the polarization of a dipole source, knowing a priori some measurements on the boundary of the domain. We analyze the case of a single dipole, but in different positions, and present some numerical results.

Since we are interested in a single dipole, we need to find only four parameters that minimize the least-square function

$$\phi(\mathbf{x}, \mathbf{q}_x) = \|\mathbf{m} - \mathbf{m}_{ref}\|_2^2 \quad (5.18)$$

where \mathbf{x} is the coordinates of the dipole location and \mathbf{q}_x is the polarization. We assume that

we can obtain the measurements at some boundary nodes of the domain. In this equation, \mathbf{m} is a n -dimensional vector (with n the number of measurements) which contains the values of the potential computed using FEM, and \mathbf{m}_{ref} is a vector which contains the values of the measured potential (indeed, the measured potential is simulated by using the values computed with one of the aforementioned techniques using FEM in a very fine mesh). It is clear that this problem is non-linear.

For any given dipole location \mathbf{x} we can find the optimal polarization $\mathbf{p}_x = p_1\mathbf{e}_1 + p_2\mathbf{e}_2$ (\mathbf{e}_1 and \mathbf{e}_2 are the cartesian orientations) as follows: we define as $\mathbf{m}_{1,i}$ the value of an approximated solution at the same points P_i , $1 \leq i \leq n$ on $\partial\Omega$ where the solution that produces \mathbf{m}_{ref} is evaluated, obtained by using as localization \mathbf{x} and as polarization \mathbf{e}_1 . Similarly, $\mathbf{m}_{2,i}$ corresponds to the value of an approximated solution at the same points P_i , $1 \leq i \leq n$ on the boundary obtained by using the same localization and as polarization \mathbf{e}_2 . Then, we define the $n \times 2$ matrix $\mathbf{M} := (\mathbf{m}_1 \ \mathbf{m}_2)$. By linearity, the values of the approximated solution corresponding to \mathbf{p}_x are given by

$$\mathbf{m} = \mathbf{M}\mathbf{p}_x.$$

Thus, finding \mathbf{p}_x which minimize $\phi(\mathbf{x}, \mathbf{q}_x) = \|\mathbf{m} - \mathbf{m}_{ref}\|_2^2$ in the least squares sense, is equivalent to solve

$$\mathbf{M}^t \mathbf{M} \mathbf{p}_x = \mathbf{M}^t \mathbf{m}_{ref}. \quad (5.19)$$

After having computed the optimal polarization for each possible dipole position \mathbf{x} , the function ϕ reduces to a least-squares function ψ which is only a function of \mathbf{x} , that is

$$\psi(\mathbf{x}) = \|\mathbf{M}\mathbf{p}_x - \mathbf{m}_{ref}\|_2^2. \quad (5.20)$$

We use the pattern-search optimization method to find the optimum dipole position \mathbf{x} by minimizing the function $\psi(\mathbf{x})$. This minimization algorithm is already implemented in MATLAB and corresponds to the command *patternsearch*.

We are interested in solving the inverse problem by using the aforementioned methods. From Chapter 4 we know that there exists an a posteriori error estimator for the direct method which enables to improve the obtained results. We must recall that this estimator was defined in the case in which the matrix $\boldsymbol{\sigma}$ has entries in $C^1(\overline{\Omega})$. We use the estimator to devise a strategy to solve the inverse problem.

According to Theorem 5.1.1 the solution of problem (5.8) belongs to $L^p(\Omega)$ with $1 \leq p < 2$ when $\boldsymbol{\sigma}$ is regular enough. We will recall the a posteriori error estimator in the $L^p(\Omega)$ -norm for the finite element approximation error $u - u_h$ defined in Chapter 4. We proved the reliability and efficiency of the estimator for a particular range of p .

For all $T \in \mathcal{T}_h$ we define

$$\varepsilon_{T,p} := \left(h_T^{2p} \|\operatorname{div}(\boldsymbol{\sigma} \nabla u_h)\|_{0,p,T}^p + \frac{1}{2} \sum_{\ell \in \mathcal{E}(T) \cap \mathcal{E}_{h,i}} |\ell|^{p+1} \|\llbracket \boldsymbol{\sigma} \nabla u_h \cdot \mathbf{n} \rrbracket\|_{0,p,\ell}^p + \sum_{\ell \in \mathcal{E}(T) \cap \mathcal{E}_{h,e}} |\ell|^{p+1} \|\boldsymbol{\sigma} \nabla u_h \cdot \mathbf{n}\|_{0,p,\ell}^p \right)^{1/p},$$

where $\mathcal{E}_{h,i}$ is the set of all the inner edges of the triangulation \mathcal{T}_h , $\mathcal{E}_{h,e}$ is the set of boundary edges of the triangulation \mathcal{T}_h , $\mathcal{E}(T)$ is the set of the edges of T and $\llbracket g \rrbracket$ denotes the jump of g across an edge. We define the local a posteriori error indicator $\eta_{T,p}$ for all $T \in \mathcal{T}_h$ as follows:

$$\eta_{T,p} := \begin{cases} \left(h_0^{2-p} + \varepsilon_{T,p}^p \right)^{1/p} & \text{if } T = T_0, \\ \varepsilon_{T,p} & \text{otherwise,} \end{cases}$$

where we denote by T_0 the triangle that contains the point \mathbf{x}_0 and by h_0 , its diameter.

Next, we define the global error estimator from these indicators as follows:

$$\eta_p := \left(\sum_{T \in \mathcal{T}_h} \eta_{T,p}^p \right)^{1/p}. \quad (5.21)$$

In Tests 3 and 4 we are interested in finding the localization and polarization of the dipole from certain measurements that have been generated by using the subtraction approach or the direct method (depending if the localization is inside a region or near the interface). The exact solution is computed in the finest mesh in Table 5.14.

5.3.1 Test 3.

This experiment consists in reconstructing the position and the polarization of the dipole source from boundary measurements, by using four different techniques: subtraction approach, direct method, direct method accompanied by an adaptive procedure and the characteristic function approach. We use the same domain Ω in Test 1. We recall that Ω is a multi-layered square as in Figure 5.1, with three regions, the external and internal layers (which correspond to regions 1 and 3, respectively) with conductivities 0.33 and the layer in between (region 2) with conductivity 0.0042. As in the other test, it is important to recall that these values of the conductivity correspond to a real values.

Notice that when we solve the inverse problem by using the direct method (or direct method with adaptivity), the minimization algorithm find a triangle, not a position. Then, we will consider as \mathbf{x}_0 the barycenter of this triangle.

Mesh	Degrees of freedom	Elements	Elem. region 1	Elem. region 2	Elem. region 3
1	362	682	104	120	458
2	2186	4279	653	776	2850
3	544135	1086493	171571	199069	715853

Table 5.14: Meshes used in Tests 3 and 4.

Speaking about the direct method with the adaptive procedure, the strategy that we propose combines the minimization algorithm and the adaptive procedure guided by the a posteriori error estimator defined in (5.21). It consists in the following: the algorithm start minimizing the function ψ using mesh 1 and in this first iteration, it finds a first approximation of the position and the polarization of the source. With these data, the algorithm realize an adaptive procedure guided by the error estimator above; the procedure is applied four times. Then, with this new mesh generated in the previous process, the algorithm restarts the minimization of ψ for another time. The algorithm shows a more precise localization and polarization and with these new data, it realizes the adaptive procedure four times more, and so on. This process is done six times. Therefore, it refines the mesh twenty four times. Thus, the algorithm does seven steps of minimization and the last one is performed in the mesh number twenty five.

In this test, the real location is an internal point in region 2 and the measurements are generated by using the subtraction technique in a fine mesh. We generate the data with mesh 3 in Table 5.14. We consider thirty measurements which correspond to thirty values of the solution in the thirty corresponding nodes on the boundary in Table 5.15. As dipole position we consider $\mathbf{x}_0 = (0.0126, 0.8901)$ which corresponds to a point internal to region 2, and as polarization, $\mathbf{p} = (-0.2425, 0.9701)$.

In Table 5.16 we can find the exact localization and polarization and the results obtained by solving the inverse problem. This problem was solved using four different methods: the subtraction approach (S.A.), the direct method (D.M.), the direct method with an adaptive procedure (D.M.A.) and finally, the characteristic function approach (C.F.A). This last method was realized by using as support a square of length-side 2ϵ , with $\epsilon = 0.01$. Notice that we find two rows with results obtained by D.M.A. in Table 5.16: D.M.A. (1) contains the results obtained in the step number six of minimization and D.M.A. (2) contains the results obtained in the last step of minimization, that is, step number seven of minimization.

We define the relative error \mathbf{e}_r as follows:

$$\mathbf{e}_r := \sqrt{\frac{|\mathbf{x}_0 - \mathbf{x}|^2}{|\mathbf{x}_0|^2} + \frac{|\mathbf{p} - \mathbf{q}|^2}{|\mathbf{p}|^2}},$$

Nodes	x	y	Nodes	x	y	Nodes	x	y
1	0.5	-1	11	-1	-0.25	21	1	0.5
2	-0.5	-1	12	-1	0.75	22	1	-0.5
3	0.25	-1	13	-1	-0.75	23	1	0.25
4	-0.25	-1	14	0	1	24	1	-0.25
5	0.75	-1	15	0.5	1	25	1	0.75
6	-0.75	-1	16	-0.5	1	26	1	-0.75
7	-1	0	17	0.25	1	27	0.75	1
8	-1	0.5	18	-0.25	1	28	0.125	-1
9	-1	-0.5	19	-0.75	1	29	-0.125	-1
10	-1	0.25	20	1	0	30	-1	0.125

Table 5.15: Thirty nodes on the external boundary.

where \mathbf{x} and \mathbf{q} correspond to the approximations of \mathbf{x}_0 and \mathbf{p} obtained by solving the inverse problem using the different approaches.

Solution	\mathbf{x}_0	\mathbf{p}	\mathbf{e}_r	Degrees of freedom
Exact	(0.0126, 0.8901)	(-0.2425, 0.9701)	-	544135
S.A.	(-0.0383, 0.8941)	(1.6646, 0.9545)	1.9081	2186
D.M.	(0.0260, 0.9123)	(-0.2734, 0.9761)	0.0429	2186
D.M.A. (1)	(0.0062, 0.8877)	(-0.0691, 0.9741)	0.1736	1193
D.M.A. (2)	(0.0152, 0.8896)	(-0.2502, 0.9715)	0.0085	3030
C.F.A.	(0.0104, 0.8838)	(-0.3137, 0.9799)	0.0723	2186

Table 5.16: Results obtained by solving the inverse problem.

Notice that the strategy that combines the direct method with the adaptive procedure start from mesh 1 in Table 5.14. In Table 5.17 we see the results given by the minimization algorithm the seven times that the process was done. The last mesh in this iterative process contained 3030 nodes. We see that this strategy is giving a better approximation of the data in the last iteration that in the case of the direct method without an adaptive procedure. However, we want also to underline that the results obtained by means of the direct method with adaptive procedure are somehow oscillating from a refinement step to another. This phenomenon is seen also in the numerical results in Section 5.4. On the other hand, the direct method and the characteristic function approach, are giving good results.

Iteration	\mathbf{x}_0	\mathbf{p}
1	(0.0400, 0.9033)	(0.0796, 0.9896)
2	(0.0288, 0.9143)	(-0.3975, 0.9786)
3	(-0.0211, 0.9114)	(0.1494, 0.9757)
4	(0.0169, 0.8852)	(-0.3318, 0.9766)
5	(0.0169, 0.8852)	(-0.3228, 0.9756)
6	(0.0062, 0.8877)	(-0.0691, 0.97411)
7	(0.0152, 0.8896)	(-0.2503, 0.9716)

Table 5.17: Data found using the direct method with adaptive procedure.

5.3.2 Test 4.

This experiment is similar to Test 3. The difference is the position of the dipole source we want to find. We are interested in the behavior of the four aforementioned methods in Test 3 when we solve the inverse problem with a dipole located very close to the interface. In this test we use the same geometry of Test 3. Since we need to generate the measurements and we know that the subtraction method cannot be used in this situation, we use the direct approach to compute the data in the finest mesh in Table 5.14 (this corresponds to mesh 3). Note that if ϵ is so small that the square centered at \mathbf{x}_0 of side size 2ϵ is inside one triangle, the characteristic function approach is giving the same result. For a larger ϵ , the characteristic function approach has to be used being careful that the square centered in \mathbf{x}_0 and with side-length 2ϵ , is not intersecting the interface, as in Section 5.2. We have seen that the location of the delta function on the interface is giving rise to a problem that is not the one obtained by taking the limit from one or the other side.

The dipole position is $\mathbf{x}_0 = (0.0126, 0.917)$, which belongs to region 2 and it is close to the interface between regions 1 and 2. We consider thirty measurements that correspond to the thirty nodes on the boundary in Table 5.15. The polarization is the same that in the experiment above, i.e., $\mathbf{p} = (-0.2425, 0.9701)$. To compute the inverse problem in the case of the characteristic function approach, we use as support a square of length-side 2ϵ with $\epsilon = 0.003$.

As in the previous experiment, we can find the results in Table 5.18.

From these two experiments, we can conclude that the direct method combined with the adaptive procedure is giving good results in both cases respect to the other methods (despite this estimator is not well suited when the entries of $\boldsymbol{\sigma}$ are piecewise constant). However, this method is giving data that are converging in a oscillatory way, then we have to be careful when we use this technique. On the other hand, the other alternatives that are giving reasonable results

Solution	\mathbf{x}_0	\mathbf{p}	\mathbf{e}_r	Degrees of freedom
Exact	(0.0126, 0.917)	(-0.2425, 0.9701)	-	544135
S.A.	(0.1283, 0.9343)	(-2.1445, -35.6436)	36.6651	2186
D.M.	(-0.0019, 0.9007)	(0.0096, 0.9807)	0.2535	2186
D.M.A. (1)	(0.0183, 0.9141)	(-0.3718, 0.9741)	0.1296	1014
D.M.A. (2)	(0.0108, 0.9159)	(-0.2305, 0.9729)	0.0125	1802
C.F.A.	(0.0127, 0.9039)	(-0.1513, 0.9821)	0.0931	2186

Table 5.18: Results obtained by solving the inverse problem.

Iteration	\mathbf{x}_0	\mathbf{p}
1	(-0.0367, 0.9033)	(-0.1486, 0.9957)
2	(0.0037, 0.9098)	(-0.0294, 0.9837)
3	(0.0158, 0.9098)	(-0.3244, 0.9770)
4	(0.0068, 0.9181)	(-0.1264, 0.9759)
5	(0.0128, 0.9147)	(-0.2422, 0.9758)
6	(0.0183, 0.9141)	(-0.3718, 0.9741)
7	(0.0108, 0.9159)	(-0.2305, 0.9729)

Table 5.19: Data found using the direct method with adaptive procedure.

are the characteristic function approach and the direct method. Notice that the subtraction approach in this last test is giving the worst results.

5.4 Lead field matrix

In the previous section the inverse problem in the case of only one dipole was analyzed (but this analysis can be extended to a small quantity of dipoles). In the standard dipolar method the parameters of the dipoles (location and polarization) are found using a nonlinear leastsquares search. However, there exists another way to study the inverse problem: it is to assume that the current density is a distributed source and, in such case, the measurements are assumed to be generated by many dipoles placed in a certain region of the mesh. We will focus in this point of view.

In the EEG forward model a given primary current density \mathbf{J}_p in the head Ω generates a measurement data vector \mathbf{m} (the electric potential values). In the numerical simulation of the

inverse problem, the unknown is a finite dimensional vector \mathbf{z} , which is linked to the measurement data \mathbf{m} through the system of linear equations $\mathbf{m} = \mathbf{L}\mathbf{z}$, the so-called *lead field matrix* \mathbf{L} .

The goal of this section is to construct the lead field matrix with each one of the methods in Section 5.1 (and with one new method that we add in this section). First, we discuss how to construct this lead field matrix in each case. After that, we want to compare each one of these lead field matrices with a reference lead field matrix.

For a mesh consisting of N nodes, the approximate value of the potential can be expressed as an element of the set H_h defined in (5.14) as follows

$$u_h = \sum_{i=1}^N \alpha_i \lambda_i$$

where λ_i is a basis function in H_h associated with node i , for all $i = 1, \dots, N$. In the most of the subsections, we are interested in analyzing problem (5.2) with

$$\mathbf{J}_p = \sum_{k=1}^M \mathbf{p}_k \delta_{\mathbf{x}_k}, \quad (5.22)$$

where \mathbf{p}_k is a non null vector and \mathbf{x}_k in an inner point of Ω , for all $k = 1, \dots, M$. We will specify when we need to use a different definition for the current density \mathbf{J}_p .

Subtraction method

The vector \mathbf{p}_k in (5.22) can be written in the following way $\mathbf{p}_k = y_1^k \mathbf{e}_1 + y_2^k \mathbf{e}_2$, where \mathbf{e}_1 and \mathbf{e}_2 are the cartesian orientations, for all $k = 1, \dots, M$. Then, the current density also can be written as $\mathbf{J}_p = \sum_{k=1}^M \sum_{j=1}^2 y_j^k \mathbf{e}_j \delta_{\mathbf{x}_k}$ or in a more structured way,

$$\mathbf{J}_p = \sum_{k=1}^{2M} z_k \mathbf{d}_k, \quad (5.23)$$

where

$$z_k := \begin{cases} y_1^k & \text{if } 1 \leq k \leq M, \\ y_2^{k-M} & \text{if } M+1 \leq k \leq 2M, \end{cases} \quad \text{and} \quad \mathbf{d}_k := \begin{cases} \mathbf{e}_1 \delta_{\mathbf{x}_k} & \text{if } 1 \leq k \leq M, \\ \mathbf{e}_2 \delta_{\mathbf{x}_{k-M}} & \text{if } M+1 \leq k \leq 2M. \end{cases} \quad (5.24)$$

Assuming that we can find nonempty subdomains Ω_0^k of Ω around each one of the source positions \mathbf{x}_k with homogeneous constant conductivity $\sigma_{0,k}$, we can solve these $2M$ subproblems by using (5.15) and then we use (5.5) with the corresponding data in each case.

The coefficients α_i , $i = 1, \dots, N$ and z_k , $k = 1, \dots, 2M$ define unknown coordinate vectors $\boldsymbol{\alpha}$ and \mathbf{z} , which satisfy the linear system $\mathbf{S}\boldsymbol{\alpha} = \mathbf{G}_s \mathbf{z}$, where the entries of the matrices \mathbf{S} and \mathbf{G}_s are given by

$$s_{ij} := \int_{\Omega} \boldsymbol{\sigma} \nabla \lambda_i \cdot \nabla \lambda_j,$$

and

$$g_{ik}^s := \begin{cases} - \int_{\Omega} \boldsymbol{\sigma}_{s,k} \nabla u_{0,k}^1 \cdot \nabla \lambda_i - \int_{\partial\Omega} (\boldsymbol{\sigma}_{0,k} \nabla u_{0,k}^1 \cdot \mathbf{n}) \lambda_i & 1 \leq k \leq M, \\ - \int_{\Omega} \boldsymbol{\sigma}_{s,k-M} \nabla u_{0,k-M}^2 \cdot \nabla \lambda_i - \int_{\partial\Omega} (\boldsymbol{\sigma}_{0,k-M} \nabla u_{0,k-M}^2 \cdot \mathbf{n}) \lambda_i & M+1 \leq k \leq 2M, \end{cases}$$

where $\boldsymbol{\sigma}_{s,k} = \boldsymbol{\sigma} - \boldsymbol{\sigma}_{0,k}$, $k = 1, \dots, M$ and we have denoted by $u_{0,k}^j$, $j = 1, 2$ the fundamental solution of this problem:

$$\operatorname{div}(\boldsymbol{\sigma}_{0,k} \nabla u_{0,k}^j) = \operatorname{div}(\mathbf{e}_j \delta_{\mathbf{x}_k}) \text{ in } \Omega, \quad \text{for } j = 1, 2 \text{ and } k = 1, \dots, M.$$

Since we know from (5.5) that the solution can be written as a singular part plus a part obtained by means of FEM, then, we define the N times $2M$ matrix \mathbf{U}_0 whose entries corresponds to

$$u_{ik}^0 := \begin{cases} u_{0,k}^1(\mathbf{x}_i) & 1 \leq k \leq M, \\ u_{0,k-M}^2(\mathbf{x}_i) & M+1 \leq k \leq 2M, \end{cases}$$

for $i = 1, \dots, N$. We assume that the dipole positions are not nodes, so that the fundamental solutions can be evaluated in all the nodes of the mesh. Associating the EEG sensor locations with basis functions $\lambda_{i_1}, \dots, \lambda_{i_L}$ and the zero potential reference with the mean value of the electrode voltages, the EEG lead field matrix is given by $\mathbf{L} = \mathbf{R}(\mathbf{S}^{-1} \mathbf{G}_s + \mathbf{U}_0)$, in which \mathbf{R} is a $L \times N$ restriction matrix with entries

$$r_{sl} := \begin{cases} 1 & \text{if } l = i_s, \\ 0 & \text{if } l \neq i_s, \end{cases}$$

$l = 1, \dots, N$ and $s = 1, \dots, L$.

Direct method

As in the subtraction method, \mathbf{J}_p can be written as above:

$$\mathbf{J}_p = \sum_{k=1}^{2M} z_k \mathbf{d}_k,$$

where z_k and \mathbf{d}_k are defined as in (5.24).

From (5.16), we see that we construct the matrix \mathbf{S} as in the previous case. The entries of \mathbf{G}_d are given by

$$g_{ik}^d := \begin{cases} \mathbf{e}_1 \cdot \nabla(\lambda_i|_{T_{x_k}})(\mathbf{x}_k) & 1 \leq k \leq M, \\ \mathbf{e}_2 \cdot \nabla(\lambda_i|_{T_{x_{k-M}}})(\mathbf{x}_{k-M}) & M+1 \leq k \leq 2M. \end{cases} \quad (5.25)$$

where T_{x_k} is the triangle that contains the point \mathbf{x}_k , $k = 1, \dots, M$.

The lead field matrix in this case corresponds to $\mathbf{L} = \mathbf{R}\mathbf{S}^{-1}\mathbf{G}_d$, where \mathbf{R} is a $L \times N$ restriction matrix.

Characteristic function approach

We define the current density similarly to the previous case, that is, $\mathbf{J}_p := \sum_{k=1}^M \mathbf{p}_k \delta_{\epsilon, \mathbf{x}_k}$ with $\delta_{\epsilon, \mathbf{x}_k}$ as in (5.9) for all $k = 1, \dots, M$.

We can write \mathbf{J}_p as follows

$$\mathbf{J}_p := \sum_{k=1}^{2M} z_k \mathbf{f}_k^\epsilon$$

where if we assume that we can decompose \mathbf{p}_k as above, we define z_k and \mathbf{f}_k^ϵ in a similar way that in the two previous cases

$$z_k := \begin{cases} y_1^k & 1 \leq k \leq M, \\ y_2^{k-M} & M+1 \leq k \leq 2M, \end{cases} \quad \text{and} \quad \mathbf{f}_k^\epsilon := \begin{cases} \mathbf{e}_1 \delta_{\epsilon, \mathbf{x}_k} & 1 \leq k \leq M, \\ \mathbf{e}_2 \delta_{\epsilon, \mathbf{x}_{k-M}} & M+1 \leq k \leq 2M. \end{cases}$$

Notice that, when one changes the source, one has only to change the matrix \mathbf{G}_ϵ . In this case the entries of this matrix are the following

$$g_{ik}^\epsilon := \begin{cases} \frac{1}{|B_{\epsilon, k}|} \int_{S_i \cap B_{\epsilon, k}} \mathbf{e}_1 \cdot \nabla \lambda_i & 1 \leq k \leq M \\ \frac{1}{|B_{\epsilon, k-M}|} \int_{S_i \cap B_{\epsilon, k-M}} \mathbf{e}_2 \cdot \nabla \lambda_i & M+1 \leq k \leq 2M. \end{cases}$$

where $B_{\epsilon, k} := B_\epsilon(\mathbf{x}_k)$, $k = 1, \dots, M$ and $S_i := \text{supp}(\lambda_i)$, with $i = 1, \dots, N$.

Besides these three we propose two other methods. In the first one, the procedure to find the lead field matrix is a little different because the current density is defined in a unusual way. The second one is a variant of the direct method. We will discuss about this two methods in the next two subsections.

Raviart-Thomas source approximation

This approximation was analyzed in [58] and [59]. The current density is approximated as follows:

$$\mathbf{J}_p := \sum_{k=1}^M x_k \mathbf{w}_k,$$

where \mathbf{w}_k is a vector valued finite element basis function defined on a triangular mesh \mathcal{T}_h , specifically, \mathbf{w}_k corresponds to the k th Raviart-Thomas basis function which is supported on two adjacent triangular elements that share the k th edge of the finite element mesh. Here the entries of the matrix \mathbf{G}_r are the following

$$g_{i,k}^r = \int_{\Omega} \mathbf{w}_k \cdot \nabla \lambda_i.$$

As in the direct method or the characteristic function approach, $\mathbf{L} = \mathbf{R}\mathbf{S}^{-1}\mathbf{G}_r$. Notice that, this lead field matrix cannot be comparable with the other ones, because it was constructed in a different way.

In [58], Pursiainen associates each cartesian source element with a single triangle; for each triangle, a dipole position is fixed.

We explain the strategy used in [58]. In a first stage, each basis function \mathbf{w}_k is given a dipole moment by $\mathbf{q}_k = \int_{\Omega} \mathbf{w}_k$ and the dipole position \mathbf{r}_k is defined as the midpoint of the line segment between the two nodes that belong to the support of \mathbf{w}_k but do not belong to the common edge (see point (D) Figure 3 in [59]). The position of the dipole source for a given triangle T is obtained as the mean

$$\mathbf{r} = (\mathbf{r}_1 + \mathbf{r}_2 + \mathbf{r}_3)/3 \quad (5.26)$$

of the dipole positions \mathbf{r}_1 , \mathbf{r}_2 and \mathbf{r}_3 corresponding to the basis functions \mathbf{w}_1 , \mathbf{w}_2 and \mathbf{w}_3 supported on T , respectively. Notice that in a uniform mesh \mathbf{r} coincides with the barycenter of the triangle T .

We denote by $\tilde{\mathbf{v}}_1$, $\tilde{\mathbf{v}}_2$ and $\tilde{\mathbf{v}}_3$ the simulated data vectors obtained by solving (5.3) with \mathbf{J}_p corresponding to \mathbf{w}_1 , \mathbf{w}_2 and \mathbf{w}_3 , respectively. The simulated dipole data associated with T are given by

$$[\mathbf{v}_1 \ \mathbf{v}_2] = [\tilde{\mathbf{v}}_1 \ \tilde{\mathbf{v}}_2 \ \tilde{\mathbf{v}}_3][\mathbf{q}_1 \ \mathbf{q}_2 \ \mathbf{q}_3]^{\perp} \quad (5.27)$$

in which \perp denotes the Moore-Penrose pseudo-inverse and \mathbf{v}_1 and \mathbf{v}_2 form the final data for the perpendicular directions \mathbf{e}_1 and \mathbf{e}_2 , respectively. In simple words, in (5.27) was used a “base change”. Thus, it is possible to obtain a lead field matrix comparable with the others through the lead field matrix computed by means of the Raviart-Thomas sources.

Direct method with adaptive procedure

To find the lead field matrix, we use \mathbf{J}_p as in the subsection Direct method and to improve the way of solving the $2M$ problems, we use an adaptive procedure guided by the a posteriori error estimator in (5.21). We explain later on the strategy used in this method.

Now, we are in a position to give some numerical results. Before starting with the experiments, we give some definitions. With each method, one lead field matrix of the form $\mathbf{L} = (\mathbf{I}_1, \mathbf{I}_2, \dots, \mathbf{I}_{2M})$ is produced. For $1 \leq k \leq M$, the column \mathbf{I}_k of \mathbf{L} corresponds to a

single source location \mathbf{x}_k and the cartesian orientation \mathbf{e}_1 . If $M + 1 \leq k \leq 2M$, the column \mathbf{I}_k corresponds also to a single source location, \mathbf{x}_{k-M} and the cartesian orientation, \mathbf{e}_2 .

The relative error (RE) is defined as follows:

$$\text{RE} := \sqrt{\frac{\sum_{k=1}^{2M} \|\mathbf{I}_k - \mathbf{I}_k^{ref}\|_2^2}{\sum_{k=1}^{2M} \|\mathbf{I}_k^{ref}\|_2^2}},$$

where $\mathbf{L}_{ref} = (\mathbf{I}_1^{ref}, \mathbf{I}_2^{ref}, \dots, \mathbf{I}_{2M}^{ref})$ is a reference lead field matrix computed by some of the above methods (which will be indicated case by case) in the finest mesh in Table 5.21.

We define by RE_1 , RE_2 , RE_3 , RE_4 and RE_5 the relative errors computed between a reference lead field matrix and the lead field matrices obtained using the subtraction approach, the direct method, the characteristic function approach, the Raviart-Thomas source approximation and the direct method with adaptive procedure, respectively.

5.4.1 Test 5.

In this test we are interested in analyzing the lead field matrix constructed by using the direct method with an adaptive procedure respect to the lead field constructed by means of the subtraction approach in two different situations: constant conductivity and piecewise constant conductivity in the domain Ω .

The domain Ω is a square centered at $(0.5, 0.5)$ with side-length 1. As in the previous tests, this domain consists of layers formed by squares completely contained in Ω . It has three different layers: $\bar{\Omega}_1 = \bar{\Omega} \setminus (0.2, 0.8)^2$, $\bar{\Omega}_2 = [0.2, 0.8]^2 \setminus (0.4, 0.6)^2$ and $\bar{\Omega}_3 = [0.4, 0.6]^2$. Unlike the other tests, the meshes in Table 5.21 are uniform meshes. A property of these meshes is that the barycenter of each one of the triangles in mesh 1 are barycenters of some triangles in the following meshes. It is the same for mesh 2, and so on. Henceforth, we consider the locations of the dipoles only in region 2.

For this test, we consider only one point and the cartesian orientations \mathbf{e}_1 and \mathbf{e}_2 as the polarizations. The point considered $\mathbf{x}_0 = (0.2417, 0.4333)$ corresponds to an internal point in region 2 which is a barycenter of a triangle in mesh 1. In this first experiment, we consider a constant conductivity equal to one in the three regions.

In Table 5.22, we found the relative errors RE_1 and RE_5 , computed using the lead field matrices calculated by means of the subtraction approach and the direct method with adaptive procedure in meshes 1, 2 and 3 in Table 5.21. In the first column we compute RE_1 defined above, considering as the reference lead field matrix the one computed by means of the direct

method with adaptive procedure. Notice that the strategy consists in starting with a coarse initial mesh (mesh 1 in Table 5.21) and by means of an adaptive procedure to refine the mesh using as stopping criterion the quantity of d.o.f. In this case, the adaptive procedure stops when the d.o.f. overtake the d.o.f. of mesh 3 in Table 5.21. On the other hand, in the second column we compute RE_5 using as reference lead field matrix the one computed by using the subtraction method in the finest mesh, that is, mesh 5 in Table 5.21. In this case the adaptive procedure stops when the d.o.f. overtake the d.o.f. of the mesh we use to compare the relative errors. Notice that, since the adaptive procedure starts refining mesh 1, the first relative error in the second column in Table 5.22 was computed without refinement.

We consider twelve “measurements” on the boundary of Ω computed in the twelve nodes in Table 5.20. So in each case, the lead field matrix is a 12×2 matrix.

Nodes	1	2	3	4	5	6	7	8	9	10	11	12
x	0	0.2	0.4	0.6	0.8	0.8	1	1	1	1	1	1
y	0	0	0	0	0	1	0	0.2	0.4	0.6	0.8	1

Table 5.20: Twelve nodes on the external boundary.

Mesh	Degrees of freedom	Elements	Elem. region 1	Elem. region 2	Elem. region 3
1	1681	3200	2048	1024	128
2	6561	12800	8192	4096	512
3	25921	51200	32768	16384	2048
4	103041	204800	131072	65536	8192
5	410881	819200	524288	262144	32768

Table 5.21: Meshes used in Tests 5, 6 and 7.

Mesh	RE_1	RE_5
1	0.0010	0.0273
2	0.0004	0.0004
3	0.0002	0.0002

Table 5.22: Subtraction approach versus direct method with adaptive procedure.

In Table 5.23 we find the references lead field matrices. L_1 corresponds to the lead field

\mathbf{L}_1	\mathbf{L}_5
-0.7755 -0.6768	-0.7754 -0.6768
-0.5840 -0.6507	-0.5839 -0.6509
-0.2403 -0.4596	-0.2403 -0.4597
-0.0596 -0.2042	-0.0594 -0.2041
-0.0088 -0.0480	-0.0087 -0.0479
-0.0752 0.4747	-0.0751 0.4747
0 0	0 0
0.0055 0.0453	0.0055 0.0453
0.0077 0.1632	0.0077 0.1632
-0.0124 0.3016	-0.0124 0.3017
-0.0436 0.4030	-0.0436 0.4030
-0.0583 0.4387	-0.0583 0.4387

Table 5.23: Reference lead field matrices.

matrix computed by means of subtraction approach and \mathbf{L}_5 to the lead field matrix computed using the direct method with the adaptive procedure. Notice that both solutions are similar.

Now, we focus on the case of a piecewise constant conductivity. Henceforth, the conducting σ is assumed isotropic on each layer and equal to $\sigma|_{\Omega_1} = \sigma|_{\Omega_3} = 0.33$ and $\sigma|_{\Omega_2} = 0.0042$. This experiment is similar to the previous one. We consider an internal point in region 2, $\mathbf{x}_0 = (0.3667, 0.3833)$ which is a barycenter of a triangle of mesh 1 in Table 5.21. As in the previous case, we compute a reference lead field matrix by means of the subtraction approach in the finest mesh and by means of the direct method with adaptive procedure starting with mesh 1 but now using as stopping criterion 30.000 d.o.f. We can see these reference matrices in Table 5.25.

In Table 5.24 we find in the first two columns the relative errors RE_1 and RE_5 computed by using as reference lead field matrix the one obtained by the subtraction approach that corresponds to \mathbf{L}_1 in Table 5.25. The other columns correspond to compute the same relative errors RE_1 and RE_5 , but now considering as the reference lead field matrix the one obtained by means of the direct method with adaptive procedure. This matrix corresponds to \mathbf{L}_5 in Table 5.25. All these computations were done in the first three meshes in Table 5.21.

We can see from Table 5.24 that the relative error in the case of the direct method with adaptive procedure is increasing in the last mesh. We see a non-monotone behavior of this method. It is important to recall that here we are using this estimator even if it is not proved

S.A.		D.M.A.	
RE ₁	RE ₅	RE ₁	RE ₅
0.0349	0.1001	0.0358	0.1014
0.0125	0.0011	0.0136	0.0027
0.0046	0.0231	0.0061	0.0259

Table 5.24: Subtraction approach versus direct method with adaptive procedure.

L_1		L_5	
-13.7644	-6.0037	-13.7540	-6.0048
-12.3147	-6.9000	-12.3073	-6.8986
-8.2128	-7.2754	-8.2065	-7.2705
-3.8710	-4.5372	-3.8669	-4.5305
-1.0194	-1.3208	-1.0175	-1.3173
2.4304	7.8903	2.4278	7.8388
0	0	0	0
0.9520	1.2863	0.9512	1.2829
2.7839	4.0433	2.7812	4.0326
3.5683	6.1806	3.5643	6.1584
3.1712	7.2751	3.1676	7.2379
2.8320	7.6067	2.8286	7.5617

Table 5.25: Reference lead field matrices.

to be suitable when the conductivity is piecewise constant.

5.4.2 Test 6.

In this test we are interested in analyzing the behavior of the first four methods in this section, when the conductivity is a piecewise constant and the localizations of the dipoles are inside region 2 and far enough from the interface. Since the points are inside region 2 and we have seen that in this situation the subtraction approach has shown to be quite efficient, we consider as reference lead field matrix the one computed by using the subtraction approach in the finest mesh in Table 5.21, that corresponds to mesh 5.

First, we consider only one point $\mathbf{x}_0 = (0.3667, 0.3833)$ which corresponds to a barycenter of a triangle of mesh 1. In Table 5.26 we can see the relative errors RE₁, RE₂, RE₃ and RE₄

Mesh	RE ₁	RE ₂	RE ₃	RE ₄
1	0.0349	0.1001	0.1001	0.1673
2	0.0125	0.0595	0.0595	0.0332
3	0.0046	0.0205	0.0134	0.0243
4	0.0014	0.0127	0.0016	0.0083

Table 5.26: Relatives errors using one dipole.

Mesh	RE ₁	RE ₂	RE ₃	RE ₄
1	0.2468	0.0671	0.0671	0.0532
2	0.0643	0.0312	0.0312	0.0362
3	0.0143	0.0150	0.0109	0.0121
4	0.0027	0.0072	0.0023	0.0060

Table 5.27: Relative errors using fifty dipoles.

in the first four meshes in Table 5.21. It is important to note that it is possible to work with the Raviart-Thomas source approximation because we are in a uniform mesh, and therefore the localization \mathbf{r} defined in (5.26) for each triangle corresponds to the barycenter; thus we are sure that the lead field matrices are constructed with the same localization points. When the mesh is not uniform, we cannot compare this method with the other ones in this way.

Notice that the support of the characteristic function used to compute RE₃ in Table 5.26 is a square of side-length 2ϵ . We consider $\epsilon = 0.002$ in the four cases. Notice that ϵ can be chosen in different ways. We seen a dependence on that choice. The options of choice is something we have not considered.

We follow the same procedure, but now we consider fifty points that corresponds to fifty barycenters of fifty triangles inside the region 2 in mesh 1. The relative errors in this case are reported in Table 5.27. To compute RE₃ we use the same choice that in Table 5.26.

In Tables 5.26 and 5.27 we can see that the characteristic function approach gives good results, similar to those of the subtraction approach. The other two methods are performing reasonably well, though not at the same level of precision of the first two methods.

5.4.3 Test 7.

This experiment is similar to the previous one. The difference here is that now we are considering points inside region 2, but close to the interface between region 1 and region 2. Since the points are near the boundary, we consider as the reference lead field matrix the one computed by means of the direct method. We compute this matrix in the finest mesh in Table 5.21, that is, mesh 5.

As in the previous experiment, first we consider only one position $\mathbf{x}_0 = (0.2083, 0.2042)$ which corresponds to a barycenter of a triangle in mesh 2 of Table 5.21, with an edge belonging to the interface. We can see the relatives errors RE₁, RE₂, RE₃ and RE₄ computed in Table 5.28. RE₃ was computed by using ϵ as in the previous experiment. We use this choice to be

Mesh	RE ₁	RE ₂	RE ₃	RE ₄
1	7.3765	0.3050	0.3050	-
2	3.8599	0.1712	0.1712	0.2295
3	1.2979	0.0293	0.0351	0.0936
4	0.3232	0.0547	0.0182	0.0107

Table 5.28: Relative errors with one dipole.

Mesh	RE ₁	RE ₂	RE ₃	RE ₄
1	3.5643	0.0993	0.0993	-
2	1.2753	0.0454	0.0454	0.2191
3	0.2471	0.0144	0.0104	0.0233
4	0.0596	0.0149	0.0036	0.0037

Table 5.29: Relative errors with fifty dipoles.

sure that the support of the characteristic function is contained in region 2. Notice that \mathbf{x}_0 is a barycenter of a triangle in mesh 2 and therefore, it is not a barycenter of a triangle in mesh 1. Then, we have not computed RE₄ in mesh 1.

We repeat this experiment considering fifty barycenters of fifty triangles in mesh 2, close to the interface between regions 1 and 2. We compute RE₃ with the same ϵ than before since we are sure that in the fifty problems, the supports of the characteristic function are inside region 2. We can see the results in Table 5.29.

From Tables 5.28 and 5.29 we can conclude that as in the case before, the best results are achieved by the characteristic function approach and the Raviart-Thomas source approximation. As conclusion, we see that the subtraction approach is always giving the worst performance, and sometimes its relative error is one order of magnitude larger than the other relative errors. This leads to say that, when the locations of \mathbf{x}_0 are close to the interface, it is better to resort to a different approach, for instance to the characteristic function approach or the other methods.

5.5 Conclusions

It is important to recall that all the methods here introduced require more regularity of σ in a vicinity of the dipole position. We are testing what happens if we do not consider this restriction and, despite this fact, which method can still give good results.

From Section 5.2, we can conclude that when the dipole source is located close to the interface, the solution obtained by means of subtraction approach is not robust. These computational results are backed by the theory in [67]. On the other hand, the direct method is stable when the locations are closer and closer to the interface; however, the results obtained in that section, clearly show that a discontinuity occurs there, namely, approaching the interface from different sides gives quite different results. When the source is exactly on the interface, there is only one method that is well defined: the characteristic function approach. We have seen that this method gives reasonable results in that specific case.

In Section 5.3 we have seen that it is possible to reconstruct the localization and the polarization using the direct method; however, we can obtain better results when we use the direct method with the adaptive procedure. However, we want also to underline that the results obtained by means of this method are somehow oscillating from a refinement step to another. Another competitive method is the characteristic function approach, which has given accurate results. The subtraction approach is not performing well, especially when the location \boldsymbol{x}_0 is close to the interface between two regions with different conductivities.

In Section 5.4, we see that, when the conductivity is constant, the lead field matrix computed by using the direct method with an adaptive procedure is similar to the lead field matrix constructed by means of the subtraction approach; in particular, the relative errors are falling down in the same way when we use a finer mesh. When the conductivity is piecewise constant, we conclude that, when the dipole positions are inside a region, the best results are given by the characteristic function approach and the subtraction approach; the other techniques are also giving good results. When the points are close to the interface we can conclude that the relative errors have a different behavior, and the subtraction approach does not seem to be very reliable. Instead, the characteristic function approach is always furnishing good results, as well as the Raviart-Thomas source approximation.

Chapter 6

Analysis of a FEM-BEM model posed on the conducting domain for the time-dependent eddy current problem

6.1 Introduction

The eddy current model is commonly used in many problems in sciences and industry, for example, in induction heating, electromagnetic braking, electric generation, etc. An overview of the mathematical analysis of the eddy current model and its numerical solution in harmonic regime can be found in the recent book [5], which provides a large list of references on this subject.

In this chapter, we deal with the numerical solution of the time-dependent eddy current problem, which is naturally formulated in the whole space, with adequate decay conditions at infinity. The literature on the numerical analysis of time-dependent problems of this kind is more scarce. Among the few papers devoted to this subject, both in bounded and unbounded domains, by using finite element (FEM), boundary element (BEM) or coupled FEM-BEM methods, we can mention [1, 2, 42, 43, 47, 49, 69]. These articles differ from each other by the physical quantities chosen for the formulation (magnetic field, electric field or different kind of potentials) and by the way of treating the decay condition to reduce the problem to a bounded domain.

We consider a FEM-BEM method to compute the eddy currents generated in a three-dimensional conductor Ω_C by a time-dependent source current. The problem is reformulated

by expressing the magnetic and the electric fields in terms of convenient new variables. We use FEM only on the conducting domain Ω_C , the integral conditions being imposed on its boundary $\partial\Omega_C$. Therefore, the domain where FEM is used results as small as possible, leading to a more efficient method as compared, for instance, with [1, 2], where similar formulations but involving FEM in part of the dielectric domain are considered. Another important feature of this approach is that it preserves the coercivity of the original problem. The purpose of this chapter is to analyze the convergence of a fully discrete FEM-BEM scheme for this formulation and to investigate the convergence order.

The chapter is organized as follows. In Section 6.2 we give some basic definitions. In Section 6.3 we introduce the model problem and the assumptions over the data. Then, we introduce a new variable, the time-primitive of the electric field, which plays the role of a vector potential for the magnetic field. In Section 6.4 we introduce the integral operators and recall their properties. Then, we derive the FEM-BEM formulation and show the existence and uniqueness of the solution to the problem. In Section 6.5, we introduce a space-discretization of the problem based on Nédélec edge elements in Ω_C and piecewise linear continuous elements for the variable on $\partial\Omega_C$ arising from the integral equations. Then, a backward Euler method is employed for the time discretization. Finally, the results presented in Section 6.6 prove that the proposed fully discrete scheme is convergent with optimal order.

6.2 Preliminaries

In the sequel we deal with real valued functions. Boldface letters will denote vectors (in \mathbb{R}^n) or vector-valued functions, as well as matrices. The symbol $|\cdot|$ will represent the Euclidean norm for n -dimensional vectors:

$$|\mathbf{v}|^2 = \mathbf{v} \cdot \mathbf{v} := \sum_{i=1}^n v_i^2.$$

In all the chapter the conductor $\Omega_C \subset \mathbb{R}^3$ is a bounded connected polyhedron, with a Lipschitz-continuous connected boundary $\Gamma := \partial\Omega_C$, so that the insulator $\Omega_I := \mathbb{R}^3 \setminus \bar{\Omega}_C$ is also connected.

We remark that, under the above conditions, Ω_C and Ω_I have the same number of non-bounding cycles L ; namely, there exist L disjoint connected open “cutting” surfaces $\Sigma_j^{\text{int}} \subset \Omega_C$ (respectively $\Sigma_j^{\text{ext}} \subset \Omega_I$), $j = 1, \dots, L$, such that $\tilde{\Omega}_C := \Omega_C \setminus \bigcup_{j=1}^L \Sigma_j^{\text{int}}$ (respectively $\tilde{\Omega}_I := \Omega_I \setminus \bigcup_{j=1}^L \Sigma_j^{\text{ext}}$) is simply connected. The boundary curves $\partial\Sigma_j^{\text{int}}$ and $\partial\Sigma_j^{\text{ext}}$ lie on Γ .

We denote by

$$(f, g)_{0, \Omega_*} := \int_{\Omega_*} fg \, d\mathbf{x}$$

the inner product in $L^2(\Omega_*)$ and $\|\cdot\|_{0,\Omega_*}$ the corresponding norm with $*$ $\in \{C, I\}$. As usual, $\|\cdot\|_{s,\Omega_C}$ stands for the norm of the Hilbertian Sobolev spaces $H^s(\Omega_C)$ for all $s \in \mathbb{R}$. We recall that, for $s \in (0, 1)$, the space $H^s(\Gamma)$ has an intrinsic definition (by localization) on the Lipschitz surface Γ due to their invariance under Lipschitz coordinate transformations. We denote by $\|\cdot\|_{s,\Gamma}$ the norm in $H^s(\Gamma)$. Moreover, $H^{-s}(\Gamma)$ denotes the corresponding dual space.

In this chapter, the spaces that are product of function spaces are endowed with the natural product norms and duality pairings without changing the notations; it will be clear from the context when scalar or vector functions are used.

Finally, we introduce the functional spaces

$$\begin{aligned} H(\text{curl}; \Omega_C) &:= \{ \mathbf{v} \in (L^2(\Omega_C))^3 : \text{curl } \mathbf{v} \in (L^2(\Omega_C))^3 \}, \\ H(\text{div}; \Omega_C) &:= \{ \mathbf{v} \in (L^2(\Omega_C))^3 : \text{div } \mathbf{v} \in L^2(\Omega_C) \}, \end{aligned}$$

endowed with their natural norms $\|\mathbf{v}\|_{H(\text{curl}; \Omega_C)}^2 := \|\mathbf{v}\|_{0,\Omega_C}^2 + \|\text{curl } \mathbf{v}\|_{0,\Omega_C}^2$ and $\|\mathbf{v}\|_{H(\text{div}; \Omega_C)}^2 := \|\mathbf{v}\|_{0,\Omega_C}^2 + \|\text{div } \mathbf{v}\|_{0,\Omega_C}^2$, respectively.

6.2.1 Basic spaces for time dependent problems

Since we will deal with a time-dependent problem, we will use spaces of functions defined on a bounded interval $[0, T]$ and with values in a separable Hilbert space V whose norm is denoted here by $\|\cdot\|_V$. We use the notation $\mathcal{C}^0([0, T]; V)$ for the Banach space consisting of all continuous functions $f : [0, T] \rightarrow V$. More generally, for any $k \in \mathbb{N}$, $\mathcal{C}^k([0, T]; V)$ denotes the subspace of $\mathcal{C}^0([0, T]; V)$ of all functions f with (strong) derivatives $d^j f/dt^j$ in $\mathcal{C}^0([0, T]; V)$ for all $j = 1, \dots, k$. In the sequel, we will use indistinctly the notations $\partial_t f = df/dt$ to express the derivative with respect to t .

We also consider the space $L^2(0, T; V)$ of classes of functions $f : (0, T) \rightarrow V$ that are Böchner-measurable and such that

$$\|f\|_{L^2(0, T; V)}^2 := \int_0^T \|f(t)\|_V^2 dt < +\infty.$$

Furthermore, we will use

$$H^1(0, T; V) := \{ f \in L^2(0, T; V) : \partial_t f \in L^2(0, T; V) \}.$$

Analogously, we define $H^k(0, T; V)$ for all $k \in \mathbb{N}$.

6.3 The model problem

The unit normal vector on Γ that points from Ω_C to Ω_I (respectively from Ω_I to Ω_C) is denoted by \mathbf{n}_C (respectively $\mathbf{n}_I = -\mathbf{n}_C$).

Let $\mathbf{E}(\mathbf{x}, t)$ be the electric field and $\mathbf{H}(\mathbf{x}, t)$ the magnetic field. Given a time-dependent compactly supported current density \mathbf{J} , our aim is to furnish an approximate solution to the problem below:

$$\begin{aligned}
\partial_t(\boldsymbol{\mu}\mathbf{H}) + \operatorname{curl} \mathbf{E} &= \mathbf{0} && \text{in } \mathbb{R}^3 \times (0, T), \\
\operatorname{curl} \mathbf{H} - \boldsymbol{\sigma}\mathbf{E} &= \mathbf{J} && \text{in } \mathbb{R}^3 \times [0, T], \\
\operatorname{div}(\boldsymbol{\varepsilon}\mathbf{E}) &= 0 && \text{in } \Omega_I \times [0, T], \\
\mathbf{H}(\mathbf{x}, t), \mathbf{E}(\mathbf{x}, t) &= \mathcal{O}(|\mathbf{x}|^{-1}) && \text{as } |\mathbf{x}| \rightarrow \infty, \\
\mathbf{H}(\mathbf{x}, 0) &= \mathbf{H}_0(\mathbf{x}) && \mathbf{x} \in \mathbb{R}^3,
\end{aligned} \tag{6.1}$$

where the asymptotic behavior (6.1)₄ holds uniformly in $[0, T]$.

The initial data $\mathbf{H}_0 \in (L^2(\mathbb{R}^3))^3$ has to satisfy $\operatorname{div}(\boldsymbol{\mu}\mathbf{H}_0) = 0$ in \mathbb{R}^3 . Coefficients $\boldsymbol{\sigma}$, $\boldsymbol{\mu}$ and $\boldsymbol{\varepsilon}$ are assumed to be symmetric matrices with bounded entries. The electric conductivity $\boldsymbol{\sigma}$ is positive definite in Ω_C and vanishes in Ω_I . The magnetic permeability $\boldsymbol{\mu}$ is positive definite in all \mathbb{R}^3 and satisfies $\boldsymbol{\mu} = \mu_0\mathbf{I}$ in Ω_I (\mathbf{I} being the identity matrix). The electric permittivity $\boldsymbol{\varepsilon}$ is only needed in the dielectric domain in this formulation and we assume it satisfies $\boldsymbol{\varepsilon} = \varepsilon_0\mathbf{I}$ in Ω_I ; μ_0 and ε_0 being the corresponding coefficients in vacuum. Finally, we assume that the source current is supported in Ω_C . Moreover, we consider $\mathbf{J} \in L^2(0, T; (L^2(\Omega_C))^3)$.

We define $\mathbf{H}_C := \mathbf{H}|_{\Omega_C}$ and $\mathbf{H}_I := \mathbf{H}|_{\Omega_I}$; analogously, $\mathbf{H}_{C,0} := \mathbf{H}_0|_{\Omega_C}$, $\mathbf{H}_{I,0} := \mathbf{H}_0|_{\Omega_I}$, $\mathbf{E}_C := \mathbf{E}|_{\Omega_C}$, $\mathbf{E}_I := \mathbf{E}|_{\Omega_I}$, etc.

We consider the space $\mathbb{H}(\Omega_C)$, defined as

$$\mathbb{H}(\Omega_C) := \{ \mathbf{v} \in (L^2(\Omega_C))^3 : \operatorname{curl} \mathbf{v} = \mathbf{0}, \operatorname{div}(\boldsymbol{\sigma}\mathbf{v}) = 0, \boldsymbol{\sigma}\mathbf{v} \cdot \mathbf{n}_C = 0 \text{ on } \Gamma \}.$$

We recall that each cutting surface Σ_j^{int} , $j = 1, \dots, L$, ‘‘cuts’’ an independent non-bounding cycle in Ω_C . They are connected orientable Lipschitz surfaces with $\partial\Sigma_j^{\text{int}} \subset \Gamma$, such that every curl-free vector field in Ω_C has a global potential in $\tilde{\Omega}_C$. A basis of $\mathbb{H}(\Omega_C)$ is given by the functions $\boldsymbol{\omega}_j$ which are the $(L^2(\Omega_C))^3$ -extension of ∇p_j , where $p_j \in H^1(\Omega_C \setminus \Sigma_j^{\text{int}})$ is the solution of the problem

$$\begin{aligned}
\operatorname{div}(\boldsymbol{\sigma}\nabla p_j) &= 0 && \text{in } \Omega_C \setminus \Sigma_j^{\text{int}}, \\
\boldsymbol{\sigma}\nabla p_j \cdot \mathbf{n}_C &= 0 && \text{on } \Gamma \setminus \partial\Sigma_j^{\text{int}}, \\
[[\boldsymbol{\sigma}\nabla p_j \cdot \mathbf{n}_j^{\text{int}}]]_{\Sigma_j^{\text{int}}} &= 0, && j = 1, \dots, L, \\
[[p_j]]_{\Sigma_j^{\text{int}}} &= 1, && j = 1, \dots, L,
\end{aligned}$$

having denoted by $[[\cdot]]_{\Sigma_j^{\text{int}}}$ the jump across the surface Σ_j^{int} and by $\mathbf{n}_j^{\text{int}}$ a unit normal vector on Σ_j^{int} .

In order to obtain a suitable formulation for problem (6.1), we introduce the variable

$$\mathbf{A}_C(\mathbf{x}, t) := - \int_0^t \mathbf{E}_C(\mathbf{x}, s) + \mathbf{A}_{C,0}(\mathbf{x}) \tag{6.2}$$

where $\mathbf{A}_{C,0}$ is a vector potential of $\boldsymbol{\mu}_C \mathbf{H}_{C,0}$; namely, a vector field such that

$$\operatorname{curl} \mathbf{A}_{C,0} = \boldsymbol{\mu}_C \mathbf{H}_{C,0} \quad \text{in } \Omega_C, \quad (6.3)$$

which is well known to exist because $\operatorname{div}(\boldsymbol{\mu}_C \mathbf{H}_{C,0}) = 0$ in Ω_C (see, for instance, [13, Lemma 3.5]).

In practice, $\mathbf{A}_{C,0}$ can be found, for instance, by solving the following problem:

$$\begin{aligned} \operatorname{curl} \mathbf{A}_{C,0} &= \boldsymbol{\mu}_C \mathbf{H}_{C,0} && \text{in } \Omega_C, \\ \operatorname{div}(\boldsymbol{\sigma} \mathbf{A}_{C,0}) &= 0 && \text{in } \Omega_C, \\ \boldsymbol{\sigma} \mathbf{A}_{C,0} \cdot \mathbf{n}_C &= 0 && \text{on } \Gamma, \\ \int_{\Omega_C} \boldsymbol{\sigma} \mathbf{A}_{C,0} \cdot \boldsymbol{\omega}_j \, d\mathbf{x} &= 0, && j = 1, \dots, L. \end{aligned}$$

We obtain directly from (6.2) that $\mathbf{E}_C = -\partial_t \mathbf{A}_C$ in $\Omega_C \times (0, T)$. Moreover, if we apply curl to (6.2) and use (6.1)₁ and (6.3), we also deduce that $\boldsymbol{\mu}_C \mathbf{H}_C = \operatorname{curl} \mathbf{A}_C$ in $\Omega_C \times [0, T]$ and, replacing the new equalities in (6.1)₂, we have

$$\boldsymbol{\sigma} \partial_t \mathbf{A}_C + \operatorname{curl}(\boldsymbol{\mu}_C^{-1} \operatorname{curl} \mathbf{A}_C) = \mathbf{J} \quad \text{in } \Omega_C \times (0, T).$$

We introduce the Beppo Levi space

$$W^1(\Omega_I) := \left\{ \varphi \in L^2_{\text{loc}}(\Omega_I) : \frac{\varphi}{\sqrt{1+|\mathbf{x}|^2}} \in L^2(\Omega_I), \nabla \varphi \in (L^2(\Omega_I))^3 \right\}$$

and recall that the seminorm $\|\nabla(\cdot)\|_{0,\Omega_I}$ is a norm in $W^1(\Omega_I)$ equivalent to the natural norm; i.e., there exists a constant $C > 0$ such that (see, e.g., [52]):

$$\left\| \frac{\varphi}{\sqrt{1+|\mathbf{x}|^2}} \right\|_{0,\Omega_I}^2 \leq C \|\nabla \varphi\|_{0,\Omega_I}^2 \quad \forall \varphi \in W^1(\Omega_I).$$

Moreover we define the harmonic Neumann vector-fields in Ω_I by

$$\mathbb{H}(\Omega_I) := \{ \mathbf{v} \in (L^2(\Omega_I))^3 : \operatorname{curl} \mathbf{v} = \mathbf{0}, \operatorname{div} \mathbf{v} = 0, \mathbf{v} \cdot \mathbf{n}_I = 0 \text{ on } \Gamma \}.$$

We will also need a basis of the finite dimensional space $\mathbb{H}(\Omega_I)$. To this end, let $\Sigma_j^{\text{ext}}, j = 1, \dots, L$, be the orientable cutting surfaces in Ω_I introduced above. We fix a unit normal $\mathbf{n}_j^{\text{ext}}$ on each Σ_j^{ext} . Then, for each $j = 1, \dots, L$, consider the following problem, which admits a unique solution: Find $z_j \in W^1(\Omega_I \setminus \Sigma_j^{\text{ext}})$ such that

$$\begin{aligned} \Delta z_j &= 0 && \text{in } \Omega_I \setminus \Sigma_j^{\text{ext}}, \\ \nabla z_j \cdot \mathbf{n}_I &= 0 && \text{on } \Gamma \setminus \partial \Sigma_j^{\text{ext}}, \\ \llbracket \nabla z_j \cdot \mathbf{n}_j^{\text{ext}} \rrbracket_{\Sigma_j^{\text{ext}}} &= 0, \\ \llbracket z_j \rrbracket_{\Sigma_j^{\text{ext}}} &= 1. \end{aligned} \quad (6.4)$$

The set $\{\tilde{\nabla}z_j : j = 1, \dots, L\}$, where $\tilde{\nabla}z_j$ are the $(L^2(\Omega_I))^3$ -extension of ∇z_j , is a basis of $\mathbb{H}(\Omega_I)$ (see, for instance, [49]).

We have the following representation of curl-free vector-fields in Ω_I (see, e.g., [32, Remark 7]).

Lemma 6.3.1 *There holds*

$$\{\mathbf{u} \in (L^2(\Omega_I))^3 : \operatorname{curl} \mathbf{u} = \mathbf{0} \text{ in } \Omega_I\} = \nabla(W^1(\Omega_I)) \oplus \mathbb{H}(\Omega_I).$$

Moreover, this is an $L^2(\Omega_I)$ -orthogonal decomposition.

We know from (6.1)₂ that $\operatorname{curl} \mathbf{H}_I = \mathbf{0}$ in Ω_I at all time $t \in [0, T]$. Then, the previous lemma ensures the existence, at each time $t \in [0, T]$, of a function $\psi_I(t)$ in $W^1(\Omega_I)$ and real constants $\{\alpha_j(t)\}_{j=1}^L$ such that

$$\mathbf{H}_I(\mathbf{x}, t) = \nabla\psi_I(\mathbf{x}, t) + \sum_{j=1}^L \alpha_j(t) \tilde{\nabla}z_j(\mathbf{x}) \quad \text{in } \Omega_I \times [0, T]. \quad (6.5)$$

Moreover, taking divergence in the equation (6.1)₁ and using that $\boldsymbol{\mu} = \mu_0 \mathbf{I}$ in Ω_I , we obtain that $\partial_t(\operatorname{div} \mathbf{H}_I) = 0$ in $\Omega_I \times (0, T)$. Hence, since we know that $\operatorname{div} \mathbf{H}_I(\mathbf{x}, 0) = \operatorname{div} \mathbf{H}_{I,0} = 0$ in Ω_I , we conclude that $\operatorname{div} \mathbf{H}_I = 0$ in $\Omega_I \times [0, T]$. Then, using (6.5) and (6.4)₁, we obtain that

$$\Delta\psi_I = 0 \quad \text{in } \Omega_I \times [0, T].$$

On the other hand, multiplying (6.1)₁ by $\tilde{\nabla}z_i$, using a Green's formula and the fact that $\mathbf{E}_I \times \mathbf{n}_I = -\mathbf{E}_C \times \mathbf{n}_C$, we obtain

$$\int_{\Omega_I} \partial_t(\mu_0 \mathbf{H}_I) \cdot \tilde{\nabla}z_i \, d\mathbf{x} = - \int_{\Gamma} \mathbf{E}_C \times \mathbf{n}_C \cdot \tilde{\nabla}z_i \, d\zeta, \quad i = 1, \dots, L.$$

Replacing \mathbf{H}_I by $\nabla\psi_I + \sum_{j=1}^L \alpha_j \tilde{\nabla}z_j$ and \mathbf{E}_C by $-\partial_t \mathbf{A}_C$, using the orthogonality between $\nabla W^1(\Omega_I)$ and $\mathbb{H}(\Omega_I)$ and integrating by parts in Ω_I , we obtain

$$\mu_0 \sum_{j=1}^L \alpha'_j(t) \int_{\Omega_I} \tilde{\nabla}z_j \cdot \tilde{\nabla}z_i \, d\mathbf{x} = \int_{\Gamma} \partial_t \mathbf{A}_C(t) \times \mathbf{n}_C \cdot \tilde{\nabla}z_i \, d\zeta, \quad i = 1, \dots, L.$$

Next, integrating in time between 0 and s ($0 < s < T$) and recalling that $\mathbf{A}_C(\mathbf{x}, 0) = \mathbf{A}_{C,0}(\mathbf{x})$, we obtain

$$\begin{aligned} \mu_0 \sum_{j=1}^L \alpha_j(s) \int_{\Omega_I} \tilde{\nabla}z_j \cdot \tilde{\nabla}z_i \, d\mathbf{x} - \int_{\Gamma} \mathbf{A}_C(s) \times \mathbf{n}_C \cdot \tilde{\nabla}z_i \, d\zeta \\ = \mu_0 \sum_{j=1}^L \alpha_j(0) \int_{\Omega_I} \tilde{\nabla}z_j \cdot \tilde{\nabla}z_i \, d\mathbf{x} - \int_{\Gamma} \mathbf{A}_{C,0} \times \mathbf{n}_C \cdot \tilde{\nabla}z_i \, d\zeta, \end{aligned} \quad (6.6)$$

with $i = 1, \dots, L$. From (6.4), Green's formula yields

$$\int_{\Omega_I} \tilde{\nabla} z_j \cdot \tilde{\nabla} z_i \, d\mathbf{x} = \int_{\Sigma_j^{\text{ext}}} \frac{\partial z_i}{\partial \mathbf{n}_j} \, d\zeta,$$

for all $i, j = 1, \dots, L$. Then, we introduce the matrix

$$\mathbf{N} := \left(\int_{\Sigma_j^{\text{ext}}} \frac{\partial z_i}{\partial \mathbf{n}_j} \, d\zeta \right)_{1 \leq i, j \leq L}. \quad (6.7)$$

It is clear that \mathbf{N} is symmetric and positive definite. We also define the matrix \mathbf{Z} and the vector $\boldsymbol{\alpha}$ by

$$\mathbf{Z} := [\tilde{\nabla} z_1 \quad \dots \quad \tilde{\nabla} z_L]^t \quad \text{and} \quad \boldsymbol{\alpha} := [\alpha_1 \quad \dots \quad \alpha_L]^t. \quad (6.8)$$

Thus, we can write equation (6.6) as follows:

$$\mu_0 \mathbf{N} \boldsymbol{\alpha} - \int_{\Gamma} \mathbf{Z} (\mathbf{A}_C \times \mathbf{n}_C) \, d\zeta = \mu_0 \mathbf{N} \boldsymbol{\alpha}_0 - \int_{\Gamma} \mathbf{Z} (\mathbf{A}_{C,0} \times \mathbf{n}_C) \, d\zeta,$$

where $\boldsymbol{\alpha}_0 := \boldsymbol{\alpha}(0)$ is known.

In conclusion, we are led to the following problem:

Find $\mathbf{A}_C \in L^2(0, T; H(\text{curl}; \Omega_C)) \cap H^1(0, T; (L^2(\Omega_C))^3)$, $\psi_I \in L^2(0, T; W^1(\Omega_I))$ and $\boldsymbol{\alpha} \in L^2(0, T; \mathbb{R}^L)$ such that

$$\begin{aligned} \sigma \partial_t \mathbf{A}_C + \text{curl}(\boldsymbol{\mu}_C^{-1} \text{curl} \mathbf{A}_C) &= \mathbf{J} && \text{in } \Omega_C \times (0, T), \\ \mu_0 \mathbf{N} \boldsymbol{\alpha} - \int_{\Gamma} \mathbf{Z} (\mathbf{A}_C \times \mathbf{n}_C) \, d\zeta &= \mu_0 \mathbf{N} \boldsymbol{\alpha}_0 - \int_{\Gamma} \mathbf{Z} (\mathbf{A}_{C,0} \times \mathbf{n}_C) \, d\zeta, \\ \Delta \psi_I &= 0 && \text{in } \Omega_I \times [0, T], \\ (\boldsymbol{\mu}_C^{-1} \text{curl} \mathbf{A}_C) \times \mathbf{n}_C + (\nabla \psi_I + \mathbf{Z}^t \boldsymbol{\alpha}) \times \mathbf{n}_I &= \mathbf{0} && \text{on } \Gamma \times [0, T], \\ \text{curl} \mathbf{A}_C \cdot \mathbf{n}_C + \mu_0 \nabla \psi_I \cdot \mathbf{n}_I &= 0 && \text{on } \Gamma \times [0, T], \\ \mathbf{A}_C(\mathbf{x}, 0) &= \mathbf{A}_{C,0} && \text{in } \Omega_C. \end{aligned} \quad (6.9)$$

Equations (6.9)₄ and (6.9)₅ come from the fact that $\mathbf{H} \in H(\text{curl}; \mathbb{R}^3)$ and $\boldsymbol{\mu} \mathbf{H} \in H(\text{div}; \mathbb{R}^3)$ and, hence, $\mathbf{H}_C \times \mathbf{n}_C = -\mathbf{H}_I \times \mathbf{n}_I$ and $\boldsymbol{\mu}_C \mathbf{H}_C \cdot \mathbf{n}_C = -\mu_0 \mathbf{H}_I \cdot \mathbf{n}_I$ on Γ , respectively.

6.4 A FEM-BEM coupling variational formulation

In what follows we reduce problem (6.9) to the bounded domain Ω_C . To do this we will use Costabel's symmetric FEM-BEM coupling technique (cf. [25, 26]). We introduce on Γ the single and double layer potentials, which are formally defined by

$$\begin{aligned} \mathcal{S} : H^{-1/2}(\Gamma) &\rightarrow H^{1/2}(\Gamma), & \mathcal{S}(\xi)(\mathbf{x}) &:= \int_{\Gamma} \frac{1}{4\pi |\mathbf{x} - \mathbf{y}|} \xi(\mathbf{y}) \, d\zeta_{\mathbf{y}}, \\ \mathcal{D} : H^{1/2}(\Gamma) &\rightarrow H^{1/2}(\Gamma), & \mathcal{D}(\eta)(\mathbf{x}) &:= \int_{\Gamma} \frac{\mathbf{x} - \mathbf{y}}{4\pi |\mathbf{x} - \mathbf{y}|^3} \cdot \eta(\mathbf{y}) \mathbf{n}_C(\mathbf{y}) \, d\zeta_{\mathbf{y}}, \end{aligned}$$

respectively, and the hypersingular operator $\mathcal{H} : H^{1/2}(\Gamma) \rightarrow H^{-1/2}(\Gamma)$, which is formally defined as the following normal derivative:

$$\mathcal{H}(\eta)(\mathbf{x}) := -\nabla_{\mathbf{x}} \left(\int_{\Gamma} \frac{\mathbf{x} - \mathbf{y}}{4\pi |\mathbf{x} - \mathbf{y}|^3} \cdot \eta(\mathbf{y}) \mathbf{n}_C(\mathbf{y}) \, d\zeta_{\mathbf{y}} \right) \cdot \mathbf{n}_C(\mathbf{x}).$$

Let us remark that the restrictions to the boundary as well as the normal derivative above have to be understood in a weak sense; for rigorous definitions see, for instance, McLean [48]. The three operators are linear and bounded. Let $\mathcal{D}' : H^{-1/2}(\Gamma) \rightarrow H^{-1/2}(\Gamma)$ denote the adjoint operator of \mathcal{D} .

In what follows, we recall some basics properties of these operators (see, e.g., McLean [48] and Nédélec [52] for the corresponding proofs).

Theorem 6.4.1 *Let $\varphi \in W^1(\Omega_I)$ be a harmonic function. Then, the following identities hold on Γ :*

$$\begin{aligned} \left(\frac{1}{2}\mathcal{I} - \mathcal{D} \right) (\varphi|_{\Gamma}) - \mathcal{S} \left(\frac{\partial \varphi}{\partial \mathbf{n}_I} \right) &= 0, \\ - \left(\frac{1}{2}\mathcal{I} + \mathcal{D}' \right) \left(\frac{\partial \varphi}{\partial \mathbf{n}_I} \right) + \mathcal{H}(\varphi|_{\Gamma}) &= 0. \end{aligned}$$

Lemma 6.4.1 (i) *There exists $k_1 > 0$ such that*

$$\int_{\Gamma} \mathcal{S}(\eta)\eta \, d\zeta \geq k_1 \|\eta\|_{-1/2,\Gamma}^2 \quad \forall \eta \in H^{-1/2}(\Gamma).$$

(ii) *There exists $k_2 > 0$ such that*

$$\int_{\Gamma} \mathcal{H}(\varphi)\varphi \, d\zeta \geq k_2 \|\varphi\|_{1/2,\Gamma}^2 \quad \forall \varphi \in H_0^{1/2}(\Gamma),$$

where

$$H_0^{1/2}(\Gamma) := \left\{ \varphi \in H^{1/2}(\Gamma) : \int_{\Gamma} \varphi \, d\zeta = 0 \right\}.$$

Lemma 6.4.2 $\mathcal{H}(1) = 0$, $\mathcal{D}(1) = -1/2$ and $\int_{\Gamma} \mathcal{H}(\eta) \, d\zeta = 0 \quad \forall \eta \in H^{1/2}(\Gamma)$.

Here and thereafter, for the ease of notation, we use the integration symbol on Γ instead of the duality pairing between $H^{-1/2}(\Gamma)$ and $H^{1/2}(\Gamma)$; namely, $\int_{\Gamma} \mathcal{H}(\eta) \, d\zeta = \langle \mathcal{H}(\eta), 1 \rangle_{H^{-1/2}(\Gamma) \times H^{1/2}(\Gamma)}$.

Theorem 6.4.2 *The linear operator $\mathcal{H} : H^{1/2}(\Gamma)/\mathbb{R} \rightarrow H_0^{-1/2}(\Gamma)$, where*

$$H_0^{-1/2}(\Gamma) := \left\{ \eta \in H^{-1/2}(\Gamma) : \int_{\Gamma} \eta \, d\zeta = 0 \right\},$$

defines an isomorphism.

Let $(\mathbf{A}_C, \psi_I, \boldsymbol{\alpha})$ satisfying (6.9). Let $\psi(t) := \psi_I|_\Gamma(t) - c(t)$, where $c : [0, T] \rightarrow \mathbb{R}$ is such that $\psi(t) \in H_0^{1/2}(\Gamma)$. By using (6.9)₃ and (6.9)₅, according to Theorem 6.4.1 and Lemma 6.4.2, for all $t \in [0, T]$ we have

$$-\frac{1}{2}\psi - \mathcal{D}(\psi) + \frac{1}{\mu_0}\mathcal{S}(\text{curl } \mathbf{A}_C \cdot \mathbf{n}_C) = -\psi_I \quad \text{on } \Gamma, \quad (6.10)$$

$$\frac{1}{2\mu_0}\text{curl } \mathbf{A}_C \cdot \mathbf{n}_C + \frac{1}{\mu_0}\mathcal{D}'(\text{curl } \mathbf{A}_C \cdot \mathbf{n}_C) + \mathcal{H}(\psi) = 0 \quad \text{on } \Gamma. \quad (6.11)$$

The following is a variational formulation of problem (6.9), where

$$\mathcal{V} := H(\text{curl}; \Omega_C).$$

Find $\mathbf{A}_C \in L^2(0, T; \mathcal{V}) \cap H^1(0, T; (L^2(\Omega_C))^3)$, $\psi \in L^2(0, T; H_0^{1/2}(\Gamma))$ and $\boldsymbol{\alpha} \in L^2(0, T; \mathbb{R}^L)$ such that

$$\begin{aligned} & \frac{d}{dt} \int_{\Omega_C} \boldsymbol{\sigma} \mathbf{A}_C \cdot \mathbf{w}_C \, d\mathbf{x} + \int_{\Omega_C} \boldsymbol{\mu}_C^{-1} \text{curl } \mathbf{A}_C \cdot \text{curl } \mathbf{w}_C \, d\mathbf{x} \\ & + \int_{\Gamma} \left[-\frac{1}{2}\psi - \mathcal{D}(\psi) + \frac{1}{\mu_0}\mathcal{S}(\text{curl } \mathbf{A}_C \cdot \mathbf{n}_C) \right] \text{curl } \mathbf{w}_C \cdot \mathbf{n}_C \, d\zeta \\ & + \boldsymbol{\alpha}^t \int_{\Gamma} \mathbf{Z}(\mathbf{w}_C \times \mathbf{n}_C) \, d\zeta = \int_{\Omega_C} \mathbf{J} \cdot \mathbf{w}_C \, d\mathbf{x}, \quad (6.12) \\ & \int_{\Gamma} \left[\frac{1}{2}\text{curl } \mathbf{A}_C \cdot \mathbf{n}_C + \mathcal{D}'(\text{curl } \mathbf{A}_C \cdot \mathbf{n}_C) + \mu_0 \mathcal{H}(\psi) \right] \eta \, d\zeta = 0, \\ & \mu_0 \boldsymbol{\beta}^t \mathbf{N} \boldsymbol{\alpha} - \boldsymbol{\beta}^t \int_{\Gamma} \mathbf{Z}(\mathbf{A}_C \times \mathbf{n}_C) \, d\zeta = \mu_0 \boldsymbol{\beta}^t \mathbf{N} \boldsymbol{\alpha}_0 - \boldsymbol{\beta}^t \int_{\Gamma} \mathbf{Z}(\mathbf{A}_{C,0} \times \mathbf{n}_C) \, d\zeta, \end{aligned}$$

for all $\mathbf{w}_C \in \mathcal{V}$, $\eta \in H_0^{1/2}(\Gamma)$ and $\boldsymbol{\beta} \in \mathbb{R}^L$, with

$$\mathbf{A}_C(0) = \mathbf{A}_{C,0} \quad \text{in } \Omega_C.$$

In fact, to derive (6.12)₁, we have multiplied (6.9)₁ by \mathbf{w}_C , integrated by parts in Ω_C and used (6.9)₄, the identity

$$\int_{\Gamma} \mathbf{n}_I \times \nabla \psi_I \cdot \mathbf{w}_C \, d\zeta = \int_{\Gamma} \psi_I \text{curl } \mathbf{w}_C \cdot \mathbf{n}_C \, d\zeta, \quad (6.13)$$

(which in its turn follows by integration by parts, too) and (6.10). On the other hand, Eqs. (6.12)₂ and (6.12)₃ follow directly from (6.11) and (6.9)₂.

For the theoretical analysis it is convenient to eliminate $\boldsymbol{\alpha}$ and ψ from the previous formulation. With this aim, we introduce the linear operator $\mathbb{T} : \mathcal{V} \rightarrow \mathbb{R}^L$ defined by

$$\mathbb{T}(\mathbf{w}_C) := \int_{\Gamma} \mathbf{Z}(\mathbf{w}_C \times \mathbf{n}_C) \, d\zeta.$$

We eliminate $\boldsymbol{\alpha}$ from (6.12)₃ and replace it in (6.12)₁. Then, the fourth term of this equation reads

$$\begin{aligned} \boldsymbol{\alpha}^\dagger \int_{\Gamma} \mathbf{Z}(\mathbf{w}_C \times \mathbf{n}_C) \, d\zeta &= (\mathbb{T}(\mathbf{w}_C))^\dagger \boldsymbol{\alpha} \\ &= \mu_0^{-1} (\mathbb{T}(\mathbf{w}_C))^\dagger \mathbf{N}^{-1} \mathbb{T}(\mathbf{A}_C) + (\mathbb{T}(\mathbf{w}_C))^\dagger \boldsymbol{\alpha}_0 \\ &\quad - \mu_0^{-1} (\mathbb{T}(\mathbf{w}_C))^\dagger \mathbf{N}^{-1} \mathbb{T}(\mathbf{A}_{C,0}). \end{aligned}$$

Moreover, we introduce the operator $\mathcal{R} : H_0^{-1/2}(\Gamma) \rightarrow H_0^{1/2}(\Gamma)$ given by

$$\int_{\Gamma} \mathcal{H}(\mathcal{R}(\xi)) \eta \, d\zeta = \int_{\Gamma} \xi \eta \, d\zeta \quad \forall \eta \in H_0^{1/2}(\Gamma), \quad \forall \xi \in H_0^{-1/2}(\Gamma). \quad (6.14)$$

It is straightforward to show, from Lemma 6.4.1(ii) and the Lax-Milgram lemma, that \mathcal{R} is well defined and bounded. Therefore, the second equation of (6.12) may be equivalently written

$$\psi = -\mu_0^{-1} \mathcal{R} \left(\frac{1}{2} \operatorname{curl} \mathbf{A}_C \cdot \mathbf{n}_C + \mathcal{D}'(\operatorname{curl} \mathbf{A}_C \cdot \mathbf{n}_C) \right).$$

Consequently, (6.12) admits the following equivalent reduced form:

Find $\mathbf{A}_C \in L^2(0, T; \mathcal{V}) \cap H^1(0, T; (L^2(\Omega_C))^3)$ such that

$$\frac{d}{dt} (\mathbf{A}_C(t), \mathbf{w}_C)_\sigma + \mathcal{A}(\mathbf{A}_C(t), \mathbf{w}_C) + \mathcal{B}(\mathbf{A}_C(t), \mathbf{w}_C) = (\mathbf{J}(t), \mathbf{w}_C)_{0, \Omega_C} + \mathbf{g}(\mathbf{w}_C) \quad (6.15)$$

for all $\mathbf{w}_C \in \mathcal{V}$, with

$$\mathbf{A}_C(0) = \mathbf{A}_{C,0} \quad \text{in } \Omega_C,$$

where

$$(\mathbf{H}, \mathbf{G})_\sigma := \int_{\Omega_C} \boldsymbol{\sigma} \mathbf{H} \cdot \mathbf{G} \, d\mathbf{x} \quad \forall \mathbf{H}, \mathbf{G} \in (L^2(\Omega_C))^3,$$

$$\begin{aligned} \mathcal{A} : \mathcal{V} \times \mathcal{V} &\rightarrow \mathbb{R}, & \mathcal{A}(\mathbf{H}, \mathbf{G}) &:= \int_{\Omega_C} \mu_C^{-1} \operatorname{curl} \mathbf{H} \cdot \operatorname{curl} \mathbf{G} \, d\mathbf{x} \\ & & &+ \mu_0^{-1} \int_{\Gamma} \mathcal{S}(\operatorname{curl} \mathbf{H} \cdot \mathbf{n}_C) \operatorname{curl} \mathbf{G} \cdot \mathbf{n}_C \, d\zeta, \end{aligned}$$

$$\begin{aligned} \mathcal{B} : \mathcal{V} \times \mathcal{V} &\rightarrow \mathbb{R}, & \mathcal{B}(\mathbf{H}, \mathbf{G}) &:= \mu_0^{-1} \int_{\Gamma} \mathcal{K}(\mathbf{G}) \mathcal{R}(\mathcal{K}(\mathbf{H})) \, d\zeta \\ & & &+ \mu_0^{-1} (\mathbb{T}(\mathbf{G}))^\dagger \mathbf{N}^{-1} \mathbb{T}(\mathbf{H}), \end{aligned}$$

$$\mathcal{K} : \mathcal{V} \rightarrow H_0^{-1/2}(\Gamma), \quad \mathcal{K}(\mathbf{H}) := \frac{1}{2} \operatorname{curl} \mathbf{H} \cdot \mathbf{n}_C + \mathcal{D}'(\operatorname{curl} \mathbf{H} \cdot \mathbf{n}_C),$$

$$\mathbf{g} : \mathcal{V} \rightarrow \mathbb{R}, \quad \mathbf{g}(\mathbf{H}) := \mu_0^{-1} (\mathbb{T}(\mathbf{H}))^\dagger \mathbf{N}^{-1} \mathbb{T}(\mathbf{A}_{C,0}) - (\mathbb{T}(\mathbf{H}))^\dagger \boldsymbol{\alpha}_0.$$

Notice that \mathcal{A} and \mathcal{B} are bounded, symmetric and non-negative definite bilinear forms.

Remark 6.4.1 *The norm $\|\cdot\|_{0, \Omega_C}$ is equivalent to $\|\cdot\|_\sigma$ and, therefore, $\|\cdot\|_{\mathcal{V}}$ is equivalent to $\|\cdot\|_\sigma + \|\operatorname{curl}(\cdot)\|_{0, \Omega_C}$.*

6.4.1 Existence and Uniqueness.

As shown in the following lemma, problem (6.15) is well posed.

Lemma 6.4.3 *There exists a unique solution to (6.15) and*

$$\begin{aligned} \|\mathbf{A}_C\|_{L^\infty(0,T;\mathcal{V})}^2 + \|\partial_t \mathbf{A}_C\|_{L^2(0,T;(L^2(\Omega_C))^3)}^2 \\ \leq C \left\{ \|\mathbf{J}\|_{L^2(0,T;(L^2(\Omega_C))^3)}^2 + \|\mathbf{A}_{C,0}\|_{\mathcal{V}}^2 + |\boldsymbol{\alpha}_0|^2 \right\} \end{aligned} \quad (6.16)$$

for some constant $C > 0$, independent of the problem data \mathbf{J} , $\mathbf{A}_{C,0}$ and $\boldsymbol{\alpha}_0$.

Proof. The classical theory for parabolic problems (see, for instance, [32]) allows us to show that Problem (6.15) has a unique solution $\mathbf{A}_C \in L^2(0,T;\mathcal{V}) \cap H^1(0,T;\mathcal{V}')$. Moreover, since $\mathbf{A}_{C,0} \in \mathcal{V}$ and the right hand side of (6.15) is the sum of two terms, $(\mathbf{J}(t), \mathbf{w}_C)_{0,\Omega_C}$ with $\mathbf{J} \in L^2(0,T;(L^2(\Omega_C))^3)$ and $\mathbf{g}(\mathbf{w}_C)$ with $\mathbf{g} \in \mathcal{V}'$ independent of t , it is straightforward to show that actually $\partial_t \mathbf{A}_C \in L^2(0,T;(L^2(\Omega_C))^3)$ and the estimate (6.16) holds true (In fact, we may proceed as in the proof of Theorem 7.1.5 from [35] for the first term, and use Theorem A.1 from [17] for the second one). \square

Remark 6.4.2 *Problems (6.12) and (6.15) are actually equivalent. In fact, for \mathbf{A}_C being a solution of (6.15), if we define $\psi := -\mu_0^{-1} \mathcal{R}(\mathcal{K}(\mathbf{A}_C))$ and $\boldsymbol{\alpha} := \boldsymbol{\alpha}_0 + \mu_0^{-1} \mathbf{N}^{-1}(\mathbb{T}(\mathbf{A}_C) - \mathbb{T}(\mathbf{A}_{C,0}))$, then $(\mathbf{A}_C, \psi, \boldsymbol{\alpha})$ is a solution of (6.12). Moreover this problem has a unique solution, because \mathbf{A}_C has to be the unique solution of (6.15) and ψ and $\boldsymbol{\alpha}$ are determined via (6.12)₂ and (6.12)₃, respectively.*

Problems (6.9) and (6.12) are also equivalent. In fact, we derived (6.12) from (6.9). In what follows, we show the converse implication:

Theorem 6.4.3 *Let $(\mathbf{A}_C, \psi, \boldsymbol{\alpha})$ be the solution to problem (6.12). Then, there exists $\psi_I \in L^2(0,T;W^1(\Omega_I))$ and a function $c : [0,T] \rightarrow \mathbb{R}$ such that $\psi = \psi_I|_\Gamma - c$ and $(\mathbf{A}_C, \psi_I, \boldsymbol{\alpha})$ satisfies (6.9).*

Proof. Testing (6.12)₁ with $\mathbf{w}_C \in (C_0^\infty(\Omega_C))^3$ we obtain

$$\boldsymbol{\sigma} \partial_t \mathbf{A}_C + \text{curl}(\boldsymbol{\mu}_C^{-1} \text{curl} \mathbf{A}_C) = \mathbf{J} \quad \text{in } \Omega_C \quad (6.17)$$

a.e. in $[0,T]$. Then, testing (6.12)₂ with $\eta \in H^{1/2}(\Gamma)$ and using Lemma 6.4.2 we have

$$\frac{1}{2} \text{curl} \mathbf{A}_C \cdot \mathbf{n}_C + \mathcal{D}'(\text{curl} \mathbf{A}_C \cdot \mathbf{n}_C) + \mu_0 \mathcal{H}(\psi) = 0 \quad \text{on } \Gamma. \quad (6.18)$$

Now, let $\psi_I \in W^1(\Omega_I)$ be the solution of the following problem:

$$\begin{aligned} \Delta\psi_I &= 0 && \text{in } \Omega_I, \\ \mu_0 \nabla\psi_I \cdot \mathbf{n}_I &= -\operatorname{curl} \mathbf{A}_C \cdot \mathbf{n}_C && \text{on } \Gamma. \end{aligned} \tag{6.19}$$

Since $\psi_I \in W^1(\Omega_I)$ is a harmonic function, Theorem 6.4.1 ensures that

$$\begin{aligned} \frac{1}{2}\psi_I|_\Gamma - \mathcal{D}(\psi_I|_\Gamma) + \frac{1}{\mu_0}\mathcal{S}(\operatorname{curl} \mathbf{A}_C \cdot \mathbf{n}_C) &= 0, \\ \frac{1}{2}\operatorname{curl} \mathbf{A}_C \cdot \mathbf{n}_C + \mathcal{D}'(\operatorname{curl} \mathbf{A}_C \cdot \mathbf{n}_C) + \mu_0\mathcal{H}(\psi_I|_\Gamma) &= 0. \end{aligned} \tag{6.20}$$

Subtracting (6.18) from (6.20)₂, we obtain $\mathcal{H}(\psi - \psi_I) = 0$ on Γ . Therefore, we conclude from Theorem 6.4.2 that $\psi_I(t) = \psi(t) + c(t)$ on Γ , where, for each $t \in [0, T]$, $c(t)$ is a constant. As a consequence, from (6.20)₁ we have

$$\begin{aligned} -\frac{1}{2}\psi|_\Gamma - \mathcal{D}(\psi|_\Gamma) + \frac{1}{\mu_0}\mathcal{S}(\operatorname{curl} \mathbf{A}_C \cdot \mathbf{n}_C) \\ = -\frac{1}{2}(\psi_I|_\Gamma - c) - \mathcal{D}(\psi_I|_\Gamma - c) + \frac{1}{\mu_0}\mathcal{S}(\operatorname{curl} \mathbf{A}_C \cdot \mathbf{n}_C) = -\psi_I|_\Gamma. \end{aligned}$$

Now, replacing this equality in (6.12)₁, using (6.13) and testing with $\mathbf{w}_C \in H(\operatorname{curl}; \Omega_C)$, we obtain

$$(\boldsymbol{\mu}_C^{-1} \operatorname{curl} \mathbf{A}_C) \times \mathbf{n}_C + (\nabla\psi_I + \mathbf{Z}^t \boldsymbol{\alpha}) \times \mathbf{n}_I = \mathbf{0} \quad \text{on } \Gamma.$$

Let us emphasize that the first term on the left hand side is well defined in $H^{-1/2}(\Gamma)$, since $\boldsymbol{\mu}_C^{-1} \operatorname{curl} \mathbf{A}_C \in H(\operatorname{curl}; \Omega_C)$, which in turn follows because of (6.17) and the facts that $\mathbf{J} \in L^2(0, T; (L^2(\Omega_C))^3)$ and the solution to Problem (6.12) satisfies $\partial_t \mathbf{A}_C \in L^2(0, T; (L^2(\Omega_C))^3)$. Finally (6.9)₂ and (6.9)₃ follows from (6.12)₃ and the initial condition of problem (6.12), respectively. \square

6.5 Fully-discrete scheme

Let $\{\mathcal{T}_h(\Omega_C)\}_h$ be a regular family of tetrahedral meshes of Ω_C . As usual, h stands for the largest diameter of the tetrahedra K in $\mathcal{T}_h(\Omega_C)$. Furthermore, we consider the corresponding family of triangulations induced on Γ , $\{\mathcal{T}_h(\Gamma)\}_h$. Let $N \in \mathbb{N}$, $\Delta t := T/N$ and $t_n = n\Delta t$, $n = 0, \dots, N$.

We define a fully-discrete version of (6.12) by means of Nédélec finite elements. The local representation on K of the lowest-order Nédélec finite element is given by

$$\mathcal{N}(K) := \{\mathbf{a} \times \mathbf{x} + \mathbf{b} : \mathbf{a}, \mathbf{b} \in \mathbb{R}^3, \mathbf{x} \in K\}.$$

The corresponding global space \mathbf{V}_h is the space of vector fields that are locally in $\mathcal{N}(K)$ for all K in Ω_C and globally in $\mathbf{V} = H(\text{curl}; \Omega_C)$. Moreover, we define

$$\mathcal{L}_h(\Gamma) := \left\{ \eta \in H_0^{1/2}(\Gamma) : \eta|_F \in \mathbb{P}_1(F) \quad \forall F \in \mathcal{T}_h(\Gamma) \right\},$$

which approximates the space $H_0^{1/2}(\Gamma)$, where $\mathbb{P}_k(F)$ is the set of polynomial functions defined in F of degree not greater than k .

When Ω_C is not simply connected, problem (6.12) involves the matrices \mathbf{N} and \mathbf{Z} defined by (6.7) and (6.8), respectively. To compute these matrices we also need to approximate numerically the basis $\{\tilde{\nabla} z_k\}_{k=1}^L$ of the harmonic Neumann vector-fields space $\mathbb{H}(\Omega_I)$. A similar need arose in [49], where the authors proposed a coupled FEM-BEM method to compute the entries of a matrix \mathbf{N}_h approximating \mathbf{N} . For the sake of completeness, in what follows, we briefly describe the method introduced in [49] to approximate \mathbf{N} and the corresponding error estimate proved in this reference.

Consider a convex polyhedron Ω such that $\bar{\Omega}_C \cup \left(\bigcup_{k=1}^L \bar{\Sigma}_k^{\text{ext}} \right) \subset \Omega$. Set

$$\mathcal{Q}^0 := \Omega \setminus \left\{ \bar{\Omega}_C \cup \left(\bigcup_{k=1}^L \bar{\Sigma}_k^{\text{ext}} \right) \right\}, \quad \mathcal{Q} := \Omega \setminus \bar{\Omega}_C \quad \text{and} \quad \Lambda := \partial\Omega.$$

From (6.4), $\mathbf{p}_k := \tilde{\nabla} z_k|_{\mathcal{Q}}$, $k = 1, \dots, L$, belong to the closed subspace of $H(\text{div}; \mathcal{Q})$

$$\mathcal{Y} := \left\{ \mathbf{q} \in (L^2(\mathcal{Q}))^3 : \text{div } \mathbf{q} = 0 \text{ in } \mathcal{Q} \text{ and } \mathbf{q} \cdot \mathbf{n}_I = 0 \text{ on } \Gamma \right\}$$

and satisfies the variational equation

$$\int_{\mathcal{Q}} \mathbf{p}_k \cdot \mathbf{q} \, d\mathbf{x} - \int_{\Sigma_k^{\text{ext}}} \mathbf{q} \cdot \mathbf{n}_k \, d\zeta + \int_{\Lambda} \mathbf{q} \cdot \mathbf{n} z_k \, d\zeta \quad \forall \mathbf{q} \in \mathcal{Y},$$

where \mathbf{n} correspond to the unit normal vector on Λ outer to \mathcal{Q} . Furthermore, as z_k is harmonic in $\mathbb{R}^3 \setminus \bar{\Omega}$, the last equation may be coupled with boundary integral equations relating z_k and its normal derivative $\mathbf{p}_k \cdot \mathbf{n}$ on Λ . This leads to the following weak formulation (see [50] for more details)

Find $\mathbf{p}_k \in \mathcal{Y}$ and $\phi_k \in H^{1/2}(\Lambda)/\mathbb{R}$ such that

$$\begin{aligned} & \int_{\mathcal{Q}} \mathbf{p}_k \cdot \mathbf{q} \, d\mathbf{x} + \int_{\Lambda} \mathcal{S}(\mathbf{p}_k \cdot \mathbf{n}) \mathbf{q} \cdot \mathbf{n} \, d\zeta - \int_{\Lambda} \left[\frac{1}{2} \phi_k + \mathcal{D}(\phi_k) \right] \mathbf{q} \cdot \mathbf{n} \, d\zeta \\ & = \int_{\Sigma_k^{\text{ext}}} \mathbf{q} \cdot \mathbf{n}_k \, d\zeta, \\ & \int_{\Lambda} \left[\frac{1}{2} \chi + \mathcal{D}(\chi) \right] \mathbf{p}_k \cdot \mathbf{n} \, d\zeta + \int_{\Lambda} \mathcal{H}(\phi_k) \chi \, d\zeta = 0, \end{aligned} \tag{6.21}$$

for all functions $\mathbf{q} \in \mathcal{Y}$ and $\chi \in H^{1/2}(\Lambda)/\mathbb{R}$. The variable ϕ_k represents (up to an additive constant) the trace of z_k on Λ . Now, consider a regular family of triangulations $\{\mathcal{T}_h(\mathcal{Q})\}_h$ of \mathcal{Q} by

tetrahedra K of diameter no greater than $h > 0$. Assume that, for any h , the set $\mathcal{T}_h(\Omega_C) \cup \mathcal{T}_h(\mathcal{Q})$ is a triangulation of Ω . This implies that the triangulation induced by $\mathcal{T}_h(\mathcal{Q})$ on Γ is identical to $\mathcal{T}_h(\Gamma)$. It can be assumed, without loss of generality, that, for each mesh, the cutting surfaces Σ_k^{ext} are union of faces of tetrahedra in $\mathcal{T}_h(\mathcal{Q})$. Finally, denote by $\mathcal{T}_h(\Lambda)$ the triangulation induced by $\mathcal{T}_h(\mathcal{Q})$ on Λ .

Consider a conforming discretization of $H(\text{div}; \mathcal{Q})$:

$$\mathcal{RT}_h(\mathcal{Q}) := \{\mathbf{q} \in H(\text{div}; \mathcal{Q}) : \mathbf{q}|_K \in \mathcal{RT}(K) \quad \forall K \in \mathcal{T}_h(\mathcal{Q})\},$$

$\mathcal{RT}(K) := \{a\mathbf{x} + \mathbf{b} : a \in \mathbb{R}, \mathbf{b} \in \mathbb{R}^3, \mathbf{x} \in K\}$ being the lowest-order Raviart-Thomas element. The following is a convenient way of discretizing problem (6.21) (for more details, see [49]):

Find $\mathbf{p}_{kh} \in \mathcal{RT}_h^0(\mathcal{Q})$, $\phi_{kh} \in \Phi_h/\mathbb{R}$ and $\beta_{kh} \in M_h$ such that

$$\begin{aligned} & \int_{\mathcal{Q}} \mathbf{p}_{kh} \cdot \mathbf{q} \, d\mathbf{x} + \int_{\Lambda} \mathcal{S}(\mathbf{p}_{kh} \cdot \mathbf{n}) \mathbf{q} \cdot \mathbf{n} \, d\zeta - \int_{\Lambda} \left[\frac{1}{2} \phi_{kh} + \mathcal{D}(\phi_{kh}) \right] \mathbf{q} \cdot \mathbf{n} \, d\zeta \\ & + \int_{\mathcal{Q}} \beta_{kh} \text{div} \mathbf{q} \, d\mathbf{x} = \int_{\Sigma_k^{\text{ext}}} \mathbf{q} \cdot \mathbf{n}_k \, d\zeta, \\ & \int_{\Lambda} \left[\frac{1}{2} \chi + \mathcal{D}(\chi) \right] \mathbf{p}_{kh} \cdot \mathbf{n} \, d\zeta + \int_{\Lambda} \mathcal{S}(\text{curl}_{\tau} \phi_{kh}) \text{curl}_{\tau} \chi \, d\zeta = 0, \\ & \int_{\mathcal{Q}} \text{div} \mathbf{p}_{kh} v \, d\mathbf{x} = 0, \end{aligned} \tag{6.22}$$

for all functions $\mathbf{q} \in \mathcal{RT}_h^0(\mathcal{Q})$, $\chi \in \Phi_h/\mathbb{R}$ and $v \in M_h$, where

$$\begin{aligned} \mathcal{RT}_h^0(\mathcal{Q}) &:= \{\mathbf{q} \in \mathcal{RT}_h(\mathcal{Q}) : \mathbf{q}|_{\Gamma} \cdot \mathbf{n}_I = 0\}, \\ \Phi_h &:= \{\eta \in \mathcal{C}^0(\Lambda) : \eta|_F \in \mathbb{P}_1(F) \quad \forall F \in \mathcal{T}_h(\Lambda)\}, \\ M_h &:= \{v \in L^2(\mathcal{Q}) : v|_K \in \mathbb{P}_0(K) \quad \forall K \in \mathcal{T}_h(\mathcal{Q})\}. \end{aligned}$$

Moreover, curl_{τ} denotes the surface curl on Λ (see, for instance, [5, Section A.1]).

We know from [50] that (6.22) is a well posed problem. Once the functions \mathbf{p}_{kh} , $1 \leq k \leq L$, are computed, the matrix \mathbf{N} can be approximated by

$$\mathbf{N}_h := \left(\int_{\Sigma_j^{\text{ext}}} \mathbf{p}_{kh} \cdot \mathbf{n}_j \, d\zeta \right)_{1 \leq k, j \leq L}. \tag{6.23}$$

Note that this matrix is symmetric and positive definite. Error estimates for the approximation \mathbf{N}_h of \mathbf{N} has been obtained in [49]. With this end, an additional regularity result has been also proved therein. In the sequel, we denote by $s_{\mathcal{Q}} \in (1/2, 1)$ the exponent of maximal regularity in \mathcal{Q} of the solution of the Laplace operator with $L^2(\mathcal{Q})$ right-hand side and homogeneous Neumann boundary data.

Theorem 6.5.1 *If (\mathbf{p}_k, ϕ_k) is the solution to problem (6.21), $k = 1, \dots, L$, then $\mathbf{p}_k \in (H^s(\mathcal{Q}))^3$ for all $s \in (1/2, s_{\mathcal{Q}})$.*

Proof. See [49, Theorem 7.1]. \square

Finally we recall the error estimates obtained in [49]. Here and thereafter C denotes a generic positive constant not necessarily the same at each occurrence, but always independent of the mesh size h and the time step Δt .

Theorem 6.5.2 *Problems (6.21) and (6.22) are well posed and*

$$\|\mathbf{p}_k - \mathbf{p}_{kh}\|_{0,\mathcal{Q}} + \|\phi_k - \phi_{kh}\|_{H^{1/2}(\Lambda)/\mathbb{R}} \leq Ch^s \left\{ \|\mathbf{p}_k\|_{s,\mathcal{Q}} + \|\phi_k\|_{s+1/2,\Lambda} \right\}$$

holds, with s as in Theorem 6.5.1.

Proof. See [49, Theorem 7.2]. \square

Theorem 6.5.3 *There exists $h_0 > 0$ such that \mathbf{N}_h is invertible for all $h \in (0, h_0)$. Moreover, the error estimate*

$$\|\mathbf{N} - \mathbf{N}_h\| + \|\mathbf{N}^{-1} - \mathbf{N}_h^{-1}\| \leq Ch^s \max_{1 \leq k \leq L} \left\{ \|\mathbf{p}_k\|_{s,\mathcal{Q}} + \|\phi_k\|_{s+1/2,\Lambda} \right\}$$

holds, with s as in Theorem 6.5.1.

Proof. See [49, Corollary 7.3]. \square

Notice that $\|\phi_k\|_{s+1/2,\Lambda}$ is clearly bounded, since ϕ_k is the trace on Λ of the solution z_k to problem 6.4.

To compute an approximation of the entries of \mathbf{Z} , we need to resort to a different strategy. In fact, the previous methods yields good approximation of $\mathbf{p}_k|_{\Gamma} \cdot \mathbf{n}_I = \tilde{\nabla} z_k|_{\Gamma} \cdot \mathbf{n}_I$, but not of $\tilde{\nabla} z_k|_{\Gamma} \times \mathbf{n}_I$ (which are the terms defining the entries of \mathbf{Z}). A similar situation happened in [49], too. However, in this case, we follow an alternative approach that we think is simpler.

It is easy to show that the solution of (6.4) satisfies the following variational formulation:

Find $z_k \in H^1(\mathcal{Q} \setminus \Sigma_k^{\text{ext}})/\mathbb{R}$ such that $\llbracket z_k \rrbracket_{\Sigma_k^{\text{ext}}} = 1$ and

$$\int_{\mathcal{Q} \setminus \Sigma_k^{\text{ext}}} \nabla z_k \cdot \nabla \varphi \, d\mathbf{x} = \int_{\Lambda} \mathbf{p}_k \cdot \mathbf{n} \varphi \, d\zeta \quad \forall \varphi \in H^1(\mathcal{Q})/\mathbb{R}. \quad (6.24)$$

We introduce

$$\begin{aligned} \mathcal{L}_h(\mathcal{Q}) &:= \{ \theta \in H^1(\mathcal{Q}) : \theta|_K \in \mathbb{P}_1(K) \quad \forall K \in \mathcal{T}_h(\mathcal{Q}) \}, \\ \mathcal{L}_h(\mathcal{Q} \setminus \Sigma_k^{\text{ext}}) &:= \{ \theta \in H^1(\mathcal{Q} \setminus \Sigma_k^{\text{ext}}) : \theta|_K \in \mathbb{P}_1(K) \quad \forall K \in \mathcal{T}_h(\mathcal{Q}) \} \end{aligned}$$

and consider the following discrete version of problem (6.24):

Find $z_{kh} \in \mathcal{L}_h(\mathcal{Q} \setminus \Sigma_k^{\text{ext}})/\mathbb{R}$ such that $[[z_{kh}]]_{\Sigma_k^{\text{ext}}} = 1$ and

$$\int_{\mathcal{Q} \setminus \Sigma_k^{\text{ext}}} \nabla z_{kh} \cdot \nabla \varphi \, d\mathbf{x} = \int_{\Lambda} \mathbf{p}_{kh} \cdot \mathbf{n} \varphi \, d\zeta \quad \forall \varphi \in \mathcal{L}_h(\mathcal{Q})/\mathbb{R}. \quad (6.25)$$

Lemma 6.5.1 *Let z_k and z_{kh} be the solutions to problems (6.24) and (6.25), respectively. Then*

$$\|\tilde{\nabla} z_k - \tilde{\nabla} z_{kh}\|_{0,\mathcal{Q}} \leq Ch^s,$$

with s as in Theorem 6.5.1.

Proof. Let $\hat{z}_k \in C^\infty(\mathcal{Q} \setminus \Sigma_k^{\text{ext}})$ be such that $[[\hat{z}_k]]_{\Sigma_k^{\text{ext}}} = 1$. Let \hat{z}_k^I be the Lagrange interpolant of \hat{z}_k in $\mathcal{Q} \setminus \Sigma_k^{\text{ext}}$. Notice that $[[\hat{z}_k^I]]_{\Sigma_k^{\text{ext}}} = 1$, too. We write

$$z_k = \hat{z}_k + \bar{z}_k \quad \text{and} \quad z_{kh} = \hat{z}_k^I + \bar{z}_{kh},$$

with $\bar{z}_k \in H^1(\mathcal{Q})/\mathbb{R}$ and $\bar{z}_{kh} \in \mathcal{L}_h(\mathcal{Q})/\mathbb{R}$. Substituting these expressions in problems (6.24) and (6.25), respectively, and using the first Strang lemma (see, for instance, [23, Theorem 4.4.1]), we obtain

$$\begin{aligned} \|\nabla \bar{z}_k - \nabla \bar{z}_{kh}\|_{0,\mathcal{Q}} &\leq C \inf_{\varphi \in \mathcal{L}_h(\mathcal{Q})/\mathbb{R}} \|\nabla \bar{z}_k - \nabla \varphi\|_{0,\mathcal{Q}} \\ &\quad + C \sup_{\varphi \in \mathcal{L}_h(\mathcal{Q})/\mathbb{R}} \frac{\left| -\int_{\mathcal{Q} \setminus \Sigma_k^{\text{ext}}} \nabla(\hat{z}_k - \hat{z}_k^I) \cdot \nabla \varphi \, d\mathbf{x} + \int_{\Lambda} (\mathbf{p}_k - \mathbf{p}_{kh}) \cdot \mathbf{n} \varphi \, d\zeta \right|}{\|\nabla \varphi\|_{0,\mathcal{Q}}}. \end{aligned}$$

The second term on the right-hand side above is bounded as follows:

$$\begin{aligned} &\left| -\int_{\mathcal{Q} \setminus \Sigma_k^{\text{ext}}} \nabla(\hat{z}_k - \hat{z}_k^I) \cdot \nabla \varphi \, d\mathbf{x} + \int_{\Lambda} (\mathbf{p}_k - \mathbf{p}_{kh}) \cdot \mathbf{n} \varphi \, d\zeta \right| \\ &\leq \|\nabla \hat{z}_k - \nabla \hat{z}_k^I\|_{0,\mathcal{Q} \setminus \Sigma_j^{\text{ext}}} \|\nabla \varphi\|_{0,\mathcal{Q}} + C \|\mathbf{p}_k - \mathbf{p}_{kh}\|_{0,\mathcal{Q}} \|\nabla \varphi\|_{0,\mathcal{Q}}, \end{aligned}$$

where we have used that $\text{div } \mathbf{p}_k = \text{div } \mathbf{p}_{kh} = 0$ in \mathcal{Q} and the fact that $\|\nabla(\cdot)\|_{0,\mathcal{Q}}$ is equivalent to $\|\cdot\|_{1,\mathcal{Q}}$ on $H^1(\mathcal{Q})/\mathbb{R}$.

On the other hand, from Theorem 6.5.1 we know that $\nabla \bar{z}_k|_{\mathcal{Q}} \in (H^s(\mathcal{Q}))^3$. Hence,

$$\inf_{\varphi \in \mathcal{L}_h(\mathcal{Q})/\mathbb{R}} \|\nabla \bar{z}_k - \nabla \varphi\|_{0,\mathcal{Q}} \leq \|\nabla \bar{z}_k - \nabla \bar{z}_k^I\|_{0,\mathcal{Q}} \leq Ch^s \|\nabla \bar{z}_k\|_{s,\mathcal{Q}}.$$

Thus, using the last two estimates and Theorem 6.5.2, we obtain

$$\|\nabla \bar{z}_k - \nabla \bar{z}_{kh}\|_{0,\mathcal{Q}} \leq Ch^s \left\{ \|\nabla \hat{z}_k\|_{s,\mathcal{Q} \setminus \Sigma_k^{\text{ext}}} + \|\mathbf{p}_k\|_{s,\mathcal{Q}} + \|\phi_k\|_{s+1/2,\Lambda} + \|\nabla \bar{z}_k\|_{s,\mathcal{Q}} \right\}.$$

Therefore, as a consequence of Theorem 6.5.1,

$$\|\tilde{\nabla} z_k - \tilde{\nabla} z_{kh}\|_{0,\mathcal{Q}} \leq Ch^s$$

and we conclude the proof. \square

Now, we are in a position to introduce the following full discretization of problem (6.12):

For $n = 1, \dots, N$, find $(\mathbf{A}_{Ch}^n, \psi_h^n, \boldsymbol{\alpha}_h^n) \in \mathbf{V}_h \times \mathcal{L}_h(\Gamma) \times \mathbb{R}^L$ such that

$$\begin{aligned} & \int_{\Omega_C} \boldsymbol{\sigma} \bar{\partial} \mathbf{A}_{Ch}^n \cdot \mathbf{w}_C \, d\mathbf{x} + \int_{\Omega_C} \boldsymbol{\mu}_C^{-1} \operatorname{curl} \mathbf{A}_{Ch}^n \cdot \operatorname{curl} \mathbf{w}_C \, d\mathbf{x} \\ & + \int_{\Gamma} \left[-\frac{1}{2} \psi_h^n - \mathcal{D}(\psi_h^n) + \frac{1}{\mu_0} \mathcal{S}(\operatorname{curl} \mathbf{A}_{Ch}^n \cdot \mathbf{n}_C) \right] \operatorname{curl} \mathbf{w}_C \cdot \mathbf{n}_C \, d\zeta \\ & + (\boldsymbol{\alpha}_h^n)^t \mathbb{T}_h(\mathbf{w}_C) = \int_{\Omega_C} \mathbf{J}(t_n) \cdot \mathbf{w}_C \, d\mathbf{x}, \end{aligned} \quad (6.26)$$

$$\int_{\Gamma} \left[\frac{1}{2} \operatorname{curl} \mathbf{A}_{Ch}^n \cdot \mathbf{n}_C + \mathcal{D}'(\operatorname{curl} \mathbf{A}_{Ch}^n \cdot \mathbf{n}_C) + \mu_0 \mathcal{H}(\psi_h^n) \right] \eta \, d\zeta = 0,$$

$$\mu_0 \boldsymbol{\beta}^t \mathbf{N}_h \boldsymbol{\alpha}_h^n - \boldsymbol{\beta}^t \mathbb{T}_h(\mathbf{A}_{Ch}^n) = \mu_0 \boldsymbol{\beta}^t \mathbf{N}_h \boldsymbol{\alpha}_0 - \boldsymbol{\beta}^t \mathbb{T}_h(\mathbf{A}_{C,0}),$$

for all $(\mathbf{w}_C, \eta, \boldsymbol{\beta}) \in \mathbf{V}_h \times \mathcal{L}_h(\Gamma) \times \mathbb{R}^L$, with

$$\mathbf{A}_{Ch}^0 = \mathbf{A}_{Ch,0} \quad \text{in } \Omega_C,$$

where $\mathbf{A}_{Ch,0} \in \mathbf{V}_h$ is an approximation of $\mathbf{A}_{C,0}$, $\bar{\partial} \mathbf{A}_{Ch}^n := (\mathbf{A}_{Ch}^n - \mathbf{A}_{Ch}^{n-1})/\Delta t$ and the linear and continuous operator $\mathbb{T}_h : \mathbf{V} \rightarrow \mathbb{R}^L$ is defined by

$$\mathbb{T}_h(\mathbf{w}) := \int_{\Gamma} \mathbf{Z}_h(\mathbf{w} \times \mathbf{n}_C) \, d\zeta, \quad \text{with } \mathbf{Z}_h := \left[\tilde{\nabla} z_{1h} \quad \cdots \quad \tilde{\nabla} z_{Lh} \right]^t.$$

To prove the existence and uniqueness of solution to (6.26), first we proceed as in the continuous case and obtain a discrete form of Problem (6.15). Let $\mathcal{R}_h : H_0^{-1/2}(\Gamma) \rightarrow \mathcal{L}_h(\Gamma)$ be the operator defined by

$$\int_{\Gamma} \mathcal{H}(\mathcal{R}_h(\xi)) \eta \, d\zeta = \int_{\Gamma} \xi \eta \, d\zeta \quad \forall \eta \in \mathcal{L}_h(\Gamma), \quad \forall \xi \in H_0^{-1/2}(\Gamma).$$

Note that this is a Galerkin discretization of the elliptic problem (6.14). Consequently, using the Galerkin orthogonality and the continuity and ellipticity of \mathcal{H} (cf. Lemma 6.4.1(ii)), we have the following Cea estimate:

$$\|\mathcal{R}\xi - \mathcal{R}_h\xi\|_{1/2,\Gamma} \leq C \inf_{\eta \in \mathcal{L}_h(\Gamma)} \|\mathcal{R}\xi - \eta\|_{1/2,\Gamma} \quad \forall \xi \in H_0^{-1/2}(\Gamma). \quad (6.27)$$

Now, using again that $\psi_h^n := -\mu_0^{-1} \mathcal{R}_h(\mathcal{K}(\mathbf{A}_{Ch}^n))$ (cf. (6.26)₂) we obtain the following equivalent formulation of (6.26):

For $n = 1, \dots, N$, find $\mathbf{A}_{Ch}^n \in \mathbf{V}_h$ such that

$$(\bar{\partial} \mathbf{A}_{Ch}^n, \mathbf{w}_C)_\sigma + \mathcal{A}(\mathbf{A}_{Ch}^n, \mathbf{w}_C) + \mathcal{B}_h(\mathbf{A}_{Ch}^n, \mathbf{w}_C) = (\mathbf{J}(t_n), \mathbf{w}_C)_{0, \Omega_C} + \mathbf{g}_h(\mathbf{w}_C) \quad (6.28)$$

for all $\mathbf{w}_C \in \mathbf{V}_h$, with

$$\mathbf{A}_{Ch}^0 = \mathbf{A}_{Ch,0} \quad \text{in } \Omega_C,$$

where

$$\begin{aligned} \mathcal{B}_h : \mathbf{V}_h \times \mathbf{V}_h &\rightarrow \mathbb{R}, & \mathcal{B}_h(\mathbf{H}, \mathbf{G}) &:= \mu_0^{-1} \int_{\Gamma} \mathcal{K}(\mathbf{G}) \mathcal{R}_h(\mathcal{K}(\mathbf{H})) \, d\zeta \\ & & &+ \mu_0 (\mathbb{T}_h(\mathbf{G}))^\dagger \mathbf{N}_h^{-1} \mathbb{T}_h(\mathbf{H}), \\ \mathbf{g}_h : \mathbf{V}_h &\rightarrow \mathbb{R}, & \mathbf{g}_h(\mathbf{H}) &:= \mu_0^{-1} (\mathbb{T}_h(\mathbf{H}))^\dagger \mathbf{N}_h^{-1} \mathbb{T}_h(\mathbf{A}_{C,0}) - (\mathbb{T}_h(\mathbf{H}))^\dagger \boldsymbol{\alpha}_0. \end{aligned}$$

Hence, at each iteration, we have to find $\mathbf{A}_{Ch}^n \in \mathbf{V}_h$ such that

$$\begin{aligned} (\mathbf{A}_{Ch}^n, \mathbf{w}_C)_\sigma + \Delta t [\mathcal{A}(\mathbf{A}_{Ch}^n, \mathbf{w}_C) + \mathcal{B}_h(\mathbf{A}_{Ch}^n, \mathbf{w}_C)] \\ = \Delta t \left[(\mathbf{J}(t_n), \mathbf{w}_C)_{0, \Omega_C} + \mathbf{g}_h(\mathbf{w}_C) \right] + (\mathbf{A}_{Ch}^{n-1}, \mathbf{w}_C)_\sigma. \end{aligned} \quad (6.29)$$

Since \mathcal{B}_h and \mathcal{A} are non-negative definite, the existence and uniqueness of \mathbf{A}_{Ch}^n , $n = 1, \dots, N$, is immediate.

Remark 6.5.1 *It is easy to prove that if $\psi_h^n := -\mu_0^{-1} \mathcal{R}_h(\mathcal{K}(\mathbf{A}_{Ch}^n))$ as defined above and $\boldsymbol{\alpha}_h^n := \boldsymbol{\alpha}_0 + \mu_0^{-1} \mathbf{N}_h^{-1} (\mathbb{T}_h(\mathbf{A}_{Ch}^n) - \mathbb{T}_h(\mathbf{A}_{C,0}))$, then $(\mathbf{A}_{Ch}^n, \psi_h^n, \boldsymbol{\alpha}_h^n)$ is a solution of (6.26). This solution is unique, because \mathcal{H} is elliptic in $\mathcal{L}_h(\Gamma) \subset H_0^{1/2}(\Gamma)$ and \mathbf{N}_h is a symmetric and positive definite matrix.*

6.5.1 Matrix form

To have it clear the kind of problem we have to solve in practice, we will write the fully discrete scheme (6.26) in matrix form. Let $\{\phi_1, \dots, \phi_J\}$ and $\{\lambda_1, \dots, \lambda_M\}$ be bases of \mathbf{V}_h and $\mathcal{L}_h(\Gamma)$, respectively, and $\{\mathbf{e}_1, \dots, \mathbf{e}_L\}$ the canonical basis of \mathbb{R}^L . We write the solution $(\mathbf{A}_{Ch}^n, \psi_h^n, \boldsymbol{\alpha}_h^n)$, $n = 1, \dots, N$, to problem (6.26), in these bases:

$$\mathbf{A}_{Ch}^n = \sum_{j=1}^J a_j^n \phi_j, \quad \psi_h^n = \sum_{j=1}^M b_j^n \lambda_j, \quad \boldsymbol{\alpha}_h^n = \sum_{j=1}^L c_j^n \mathbf{e}_j, \quad n = 1, \dots, N.$$

Analogously, we write

$$\mathbf{A}_{Ch,0} = \sum_{j=1}^J a_j^0 \phi_j \quad \text{and} \quad \boldsymbol{\alpha}_0 = \sum_{j=1}^L c_j^0 \mathbf{e}_j.$$

We set $\mathbf{a}^n := (a_i^n)_{1 \leq i \leq J}$, $\mathbf{c}^n := (c_i^n)_{1 \leq i \leq L}$, with $n = 0, \dots, N$, and $\mathbf{b}^n := (b_i^n)_{1 \leq i \leq M}$, with $n = 1, \dots, N$. We also set $\mathbf{F}^n := (F_i^n)_{1 \leq i \leq J}$, where

$$F_i^n := \int_{\Omega_C} \mathbf{J}(t_n) \cdot \boldsymbol{\phi}_i \, d\mathbf{x}.$$

We introduce the matrices $\mathbf{W} := (W_{ij})_{1 \leq i, j \leq J}$, $\mathbf{D} := (D_{ij})_{1 \leq i \leq J, 1 \leq j \leq M}$, $\mathbf{H} := (H_{ij})_{1 \leq i, j \leq M}$, $\mathbf{R} := (R_{ij})_{1 \leq i, j \leq J}$, $\mathbf{Q} := (Q_{ij})_{1 \leq i \leq J, 1 \leq j \leq L}$ and $\mathbf{S} := (S_{ij})_{1 \leq i, j \leq J}$, where

$$\begin{aligned} W_{ij} &:= \int_{\Omega_C} \boldsymbol{\sigma} \boldsymbol{\phi}_i \cdot \boldsymbol{\phi}_j \, d\mathbf{x}, & D_{ij} &:= \int_{\Gamma} \left[-\frac{1}{2} \lambda_j - \mathcal{D}(\lambda_j) \right] \operatorname{curl} \boldsymbol{\phi}_i \cdot \mathbf{n}_C \, d\zeta, \\ H_{ij} &:= \int_{\Gamma} \mathcal{H}(\lambda_i) \lambda_j \, d\zeta, & R_{ij} &:= \int_{\Omega_C} \boldsymbol{\mu}_C^{-1} \operatorname{curl} \boldsymbol{\phi}_i \cdot \operatorname{curl} \boldsymbol{\phi}_j \, d\mathbf{x}, \\ Q_{ij} &:= \mathbf{e}_j^t \int_{\Gamma} \mathbf{Z}_h(\boldsymbol{\phi}_i \times \mathbf{n}_C) \, d\zeta, & S_{ij} &:= \int_{\Gamma} \mathcal{S}(\operatorname{curl} \boldsymbol{\phi}_i \cdot \mathbf{n}_C) \operatorname{curl} \boldsymbol{\phi}_j \cdot \mathbf{n}_C \, d\zeta. \end{aligned}$$

Hence, we write problem (6.26) in block matrix form as follows:

$$\begin{bmatrix} \mathbf{W} + \Delta t(\mathbf{R} + \mathbf{S}) & \Delta t \mathbf{D} & \Delta t \mathbf{Q} \\ \Delta t \mathbf{D}^t & -\Delta t \mathbf{H} & \mathbf{O} \\ \Delta t \mathbf{Q}^t & \mathbf{O} & -\Delta t \mathbf{N}_h \end{bmatrix} \begin{bmatrix} \mathbf{a}^n \\ \mathbf{b}^n \\ \mathbf{c}^n \end{bmatrix} = \begin{bmatrix} \Delta t \mathbf{F}^n + \mathbf{W} \mathbf{a}^{n-1} \\ \mathbf{O} \\ \Delta t (\mathbf{Q}^t \mathbf{a}^0 - \mathbf{N}_h \mathbf{c}^0) \end{bmatrix}.$$

As already mentioned in Remark 6.5.1, problem (6.26) has a unique solution, so that the matrix on the left hand side is non singular.

Matrices \mathbf{Z}_h and \mathbf{N}_h are both readily obtained once the solution \mathbf{p}_{kh} to problem (6.22) is computed. In what follows we write down the matrix form of this problem. Let $\{\mathbf{u}_1, \dots, \mathbf{u}_A\}$, $\{v_1, \dots, v_B\}$ and $\{w_1, \dots, w_C\}$ be bases of $\mathcal{RT}_h^0(\mathcal{Q})$, Φ_h/\mathbb{R} and M_h , respectively. Then, we write the solution of problem (6.22) in these bases as follows:

$$\mathbf{p}_{kh} = \sum_{j=1}^A \varphi_{kj} \mathbf{u}_j, \quad \phi_{kh} = \sum_{j=1}^B \gamma_{kj} v_j \quad \text{and} \quad \beta_{kh} = \sum_{j=1}^C \eta_{kj} w_j.$$

Next, we define $\boldsymbol{\varphi}_k := (\varphi_{ki})_{1 \leq i \leq A}$, $\boldsymbol{\gamma}_k := (\gamma_{ki})_{1 \leq i \leq B}$, $\boldsymbol{\eta}_k := (\eta_{ki})_{1 \leq i \leq C}$ and $\mathbf{G} := (G_i)_{1 \leq i \leq A}$, where

$$G_i := \int_{\Sigma_k^{\text{ext}}} \mathbf{u}_i \cdot \mathbf{n}_k \, d\zeta.$$

Moreover, we introduce the matrices $\mathbf{U} := (U_{ij})_{1 \leq i, j \leq A}$, $\mathbf{V} := (V_{ij})_{1 \leq i, j \leq A}$, $\mathbf{K} := (K_{ij})_{1 \leq i \leq A, 1 \leq j \leq B}$, $\mathbf{E} := (E_{ij})_{1 \leq i \leq A, 1 \leq j \leq C}$ and $\mathbf{T} := (T_{ij})_{1 \leq i, j \leq A}$, where

$$\begin{aligned} U_{ij} &:= \int_{\mathcal{Q}} \mathbf{u}_i \cdot \mathbf{u}_j \, d\mathbf{x}, & V_{ij} &:= \int_{\Lambda} \mathcal{S}(\mathbf{u}_i \cdot \mathbf{n}) \mathbf{u}_j \cdot \mathbf{n} \, d\zeta, \\ K_{ij} &:= - \int_{\Lambda} \left[\frac{1}{2} v_j + \mathcal{D}(v_j) \right] \mathbf{u}_i \cdot \mathbf{n} \, d\zeta, & E_{ij} &:= \int_{\mathcal{Q}} w_j \operatorname{div} \mathbf{u}_i \, d\mathbf{x}, \\ T_{ij} &:= \int_{\Lambda} \mathcal{S} \left(\operatorname{curl}_{\tau} v_j \right) \operatorname{curl}_{\tau} v_i \, d\zeta. \end{aligned}$$

Then, Problem (6.22) reads

$$\begin{bmatrix} \mathbf{U} + \mathbf{V} & \mathbf{K} & \mathbf{E} \\ \mathbf{K}^t & -\mathbf{T} & \mathbf{O} \\ \mathbf{E}^t & \mathbf{O} & \mathbf{O} \end{bmatrix} \begin{bmatrix} \varphi_k \\ \gamma_k \\ \boldsymbol{\eta}_k \end{bmatrix} = \begin{bmatrix} \mathbf{G} \\ \mathbf{O} \\ \mathbf{O} \end{bmatrix}.$$

It is proved in [50] that the matrix of the left hand side above is invertible. Finally, for a discussion on the efficient computation of all the singular integrals appearing above, we refer to [63].

As a conclusion, we have that problem (6.26) is actually solvable. Although it involves the solution of the auxiliary problem (6.22), this can be made off-line since it does not depend on time. Once it is solved, the time domain problem (6.26) involves only a vector field on the conducting domain and a scalar field on its boundary. Therefore, this approach allows to minimizing the number of degrees of freedom needed in the discretization.

6.6 Error estimates

For any $s \geq 0$, we consider the space

$$H^s(\text{curl}; \Omega_C) := \{ \mathbf{v} \in (H^s(\Omega_C))^3 : \text{curl } \mathbf{v} \in (H^s(\Omega_C))^3 \}$$

endowed with the norm $\|\mathbf{v}\|_{H^s(\text{curl}; \Omega_C)}^2 := \|\mathbf{v}\|_{s, \Omega_C}^2 + \|\text{curl } \mathbf{v}\|_{s, \Omega_C}^2$. It is well known that the Nédélec interpolation operator $\mathcal{I}_h^N \mathbf{v} \in \mathbf{V}_h$ is well defined for any $\mathbf{v} \in H^s(\text{curl}; \Omega_C)$, with $s > 1/2$ (see, for instance, Lemma 4.7 of [13]). Moreover, for $1/2 < s \leq 1$, the following interpolation error estimate holds true (see Proposition 5.6 of [6]):

$$\|\mathbf{v} - \mathcal{I}_h^N \mathbf{v}\|_{\mathbf{V}} \leq Ch^s \|\mathbf{v}\|_{H^s(\text{curl}; \Omega_C)} \quad \forall \mathbf{v} \in H^s(\text{curl}; \Omega_C). \quad (6.30)$$

To simplify the notation, we introduce for any $\mathbf{w} \in \mathbf{V}$

$$\mathcal{G}_h(\mathbf{w}) := \|(\mathcal{R} - \mathcal{R}_h) \mathcal{K}(\mathbf{w})\|_{1/2, \Gamma}.$$

Lemma 6.6.1 *Let $(\mathbf{A}_C, \psi, \boldsymbol{\alpha})$ and $(\mathbf{A}_{Ch}^n, \psi_h^n, \boldsymbol{\alpha}_h^n)$ be the solutions to problems (6.12) and (6.26), respectively, the latter with initial data $\mathbf{A}_{Ch}^0 := \mathcal{I}_h^N(\mathbf{A}_{C,0})$. Assume that $\mathbf{A}_C \in \mathcal{C}^1([0, T]; \mathbf{V}) \cap \mathcal{C}^0([0, T]; H^s(\text{curl}; \Omega_C))$, with $s > 1/2$. Moreover, let $\boldsymbol{\rho}^n := \mathbf{A}_C(t_n) - \mathcal{I}_h^N \mathbf{A}_C(t_n)$, $\boldsymbol{\delta}^n := \mathcal{I}_h^N \mathbf{A}_C(t_n) - \mathbf{A}_{Ch}^n$ and $\boldsymbol{\tau}^n := \bar{\partial} \mathbf{A}_C(t_n) - \partial_t \mathbf{A}_C(t_n)$. Then, there exists $C > 0$, independent of h and Δt , such*

that

$$\begin{aligned}
& \max_{1 \leq k \leq n} \|\delta^k\|_{\mathbf{V}}^2 + \Delta t \sum_{k=1}^n \|\bar{\partial} \delta^k\|_{\sigma}^2 \\
& \leq C \left\{ \Delta t \sum_{k=1}^n \left[\|\bar{\partial} \rho^k\|_{\mathbf{V}}^2 + \|\tau^k\|_{\mathbf{V}}^2 + \mathcal{G}_h(\partial_t \mathbf{A}_C(t_k))^2 \right. \right. \\
& \quad + \left(\|\mathbf{A}_C(t_k)\|_{\mathbf{V}}^2 + \|\partial_t \mathbf{A}_C(t_k)\|_{\mathbf{V}}^2 \right) \left(\max_{1 \leq i \leq L} \|\tilde{\nabla} z_i - \tilde{\nabla} z_{ih}\|_{0, \mathcal{Q}}^2 + \|\mathbf{N}^{-1} - \mathbf{N}_h^{-1}\|^2 \right) \\
& \quad + \left(\|\mathbf{A}_{C,0}\|_{\mathbf{V}}^2 + |\alpha_0|^2 \right) \left(\max_{1 \leq i \leq L} \|\tilde{\nabla} z_i - \tilde{\nabla} z_{ih}\|_{0, \mathcal{Q}}^2 + \|\mathbf{N}^{-1} - \mathbf{N}_h^{-1}\|^2 \right) \\
& \quad \left. \left. + \max_{0 \leq k \leq n} \|\rho^k\|_{\mathbf{V}}^2 + \max_{0 \leq k \leq n} \mathcal{G}_h(\mathbf{A}_C(t_k))^2 \right\}.
\end{aligned}$$

Proof. It is straightforward to show that

$$\begin{aligned}
& \left(\bar{\partial} \delta^k, \mathbf{v} \right)_{\sigma} + \mathcal{A}(\delta^k, \mathbf{v}) + \mathcal{B}_h(\delta^k, \mathbf{v}) \\
& = - \left(\bar{\partial} \rho^k, \mathbf{v} \right)_{\sigma} + \left(\tau^k, \mathbf{v} \right)_{\sigma} - \mathcal{A}(\rho^k, \mathbf{v}) - \mathcal{B}_h(\rho^k, \mathbf{v}) \\
& \quad + \mathcal{B}_h(\mathbf{A}_C(t_k), \mathbf{v}) - \mathcal{B}(\mathbf{A}_C(t_k), \mathbf{v}) + \mathbf{g}(\mathbf{v}) - \mathbf{g}_h(\mathbf{v}) \quad \forall \mathbf{v} \in \mathbf{V}_h,
\end{aligned} \tag{6.31}$$

as well as the following inequalities:

$$\begin{aligned}
& \left(\bar{\partial} \delta^k, \delta^k \right)_{\sigma} \geq \frac{1}{2\Delta t} \left(\|\delta^k\|_{\sigma}^2 - \|\delta^{k-1}\|_{\sigma}^2 \right), \\
& \mathcal{A}(\delta^k, \delta^k) \geq \mu_1^{-1} \left\| \text{curl } \delta^k \right\|_{0, \Omega_C}^2, \\
& \mathcal{B}(\mathbf{A}_C(t_k), \delta^k) - \mathcal{B}_h(\mathbf{A}_C(t_k), \delta^k) \\
& \leq C \|\mathbf{A}_C(t_k)\|_{\mathbf{V}} \|\delta^k\|_{\mathbf{V}} \left(\max_{1 \leq i \leq L} \|\tilde{\nabla} z_i - \tilde{\nabla} z_{ih}\|_{0, \mathcal{Q}} + \|\mathbf{N}^{-1} - \mathbf{N}_h^{-1}\| \right) \\
& \quad + C \left\| \text{curl } \delta^k \right\|_{0, \Omega_C} \mathcal{G}_h(\mathbf{A}_C(t_k)), \\
& \mathbf{g}(\delta^k) - \mathbf{g}_h(\delta^k) \\
& \leq C \left(\|\mathbf{A}_{C,0}\|_{\mathbf{V}} + |\alpha_0| \right) \|\delta^k\|_{\mathbf{V}} \left(\max_{1 \leq i \leq L} \|\tilde{\nabla} z_i - \tilde{\nabla} z_{ih}\|_{0, \mathcal{Q}} + \|\mathbf{N}^{-1} - \mathbf{N}_h^{-1}\| \right).
\end{aligned}$$

Constant μ_1 on the second inequality is an upper bound in Ω_C of the largest eigenvalue of $\boldsymbol{\mu}_C$. Hence, choosing $\mathbf{v} = \delta^k$ in (6.31) and using that \mathcal{B}_h is non-negative, Cauchy-Schwarz inequality, Remark 6.4.1 and Young's inequality lead us to the following estimate:

$$\begin{aligned}
& \|\delta^k\|_{\sigma}^2 - \|\delta^{k-1}\|_{\sigma}^2 + \Delta t \mu_1^{-1} \left\| \text{curl } \delta^k \right\|_{0, \Omega_C}^2 \\
& \leq \frac{\Delta t}{2T} \|\delta^k\|_{\sigma}^2 + C \Delta t \left[\|\bar{\partial} \rho^k\|_{\sigma}^2 + \|\tau^k\|_{\sigma}^2 + \|\rho^k\|_{\mathbf{V}}^2 + \mathcal{G}_h(\mathbf{A}_C(t_k))^2 \right. \\
& \quad + \|\mathbf{A}_C(t_k)\|_{\mathbf{V}}^2 \left(\max_{1 \leq i \leq L} \|\tilde{\nabla} z_i - \tilde{\nabla} z_{ih}\|_{0, \mathcal{Q}}^2 + \|\mathbf{N}^{-1} - \mathbf{N}_h^{-1}\|^2 \right) \\
& \quad \left. + \left(\|\mathbf{A}_{C,0}\|_{\mathbf{V}}^2 + |\alpha_0|^2 \right) \left(\max_{1 \leq i \leq L} \|\tilde{\nabla} z_i - \tilde{\nabla} z_{ih}\|_{0, \mathcal{Q}}^2 + \|\mathbf{N}^{-1} - \mathbf{N}_h^{-1}\|^2 \right) \right].
\end{aligned} \tag{6.32}$$

Then, summing over k , using the discrete Gronwall's lemma (see, for instance, [60, Lemma 1.4.2]) and taking into account that $\boldsymbol{\delta}^0 = \mathbf{0}$, we obtain

$$\begin{aligned} \|\boldsymbol{\delta}^n\|_{\boldsymbol{\sigma}}^2 \leq C & \left\{ \Delta t \sum_{k=1}^n \left[\|\bar{\boldsymbol{\rho}}^k\|_{\boldsymbol{\sigma}}^2 + \|\boldsymbol{\tau}^k\|_{\boldsymbol{\sigma}}^2 + \|\boldsymbol{\rho}^k\|_{\mathbf{V}}^2 + \mathcal{G}_h(\mathbf{A}_C(t_k))^2 \right. \right. \\ & \left. \left. + \|\mathbf{A}_C(t_k)\|_{\mathbf{V}}^2 \left(\max_{1 \leq i \leq L} \|\tilde{\nabla} z_i - \tilde{\nabla} z_{ih}\|_{0,\mathcal{Q}}^2 + \|\mathbf{N}^{-1} - \mathbf{N}_h^{-1}\|^2 \right) \right] \right. \\ & \left. + \left(\|\mathbf{A}_{C,0}\|_{\mathbf{V}}^2 + |\boldsymbol{\alpha}_0|^2 \right) \left(\max_{1 \leq i \leq L} \|\tilde{\nabla} z_i - \tilde{\nabla} z_{ih}\|_{0,\mathcal{Q}}^2 + \|\mathbf{N}^{-1} - \mathbf{N}_h^{-1}\|^2 \right) \right\} \end{aligned}$$

for $n = 1, \dots, N$. Inserting the last inequality in (6.32) and summing over k we have the estimate

$$\begin{aligned} & \|\boldsymbol{\delta}^n\|_{\boldsymbol{\sigma}}^2 + \Delta t \sum_{k=1}^n \|\operatorname{curl} \boldsymbol{\delta}^k\|_{0,\Omega_C}^2 \\ & \leq C \left\{ \Delta t \sum_{k=1}^n \left[\|\bar{\boldsymbol{\rho}}^k\|_{\boldsymbol{\sigma}}^2 + \|\boldsymbol{\tau}^k\|_{\boldsymbol{\sigma}}^2 + \|\boldsymbol{\rho}^k\|_{\mathbf{V}}^2 + \mathcal{G}_h(\mathbf{A}_C(t_k))^2 \right. \right. \\ & \quad \left. \left. + \|\mathbf{A}_C(t_k)\|_{\mathbf{V}}^2 \left(\max_{1 \leq i \leq L} \|\tilde{\nabla} z_i - \tilde{\nabla} z_{ih}\|_{0,\mathcal{Q}}^2 + \|\mathbf{N}^{-1} - \mathbf{N}_h^{-1}\|^2 \right) \right] \right. \\ & \quad \left. + \left(\|\mathbf{A}_{C,0}\|_{\mathbf{V}}^2 + |\boldsymbol{\alpha}_0|^2 \right) \left(\max_{1 \leq i \leq L} \|\tilde{\nabla} z_i - \tilde{\nabla} z_{ih}\|_{0,\mathcal{Q}}^2 + \|\mathbf{N}^{-1} - \mathbf{N}_h^{-1}\|^2 \right) \right\}. \end{aligned} \tag{6.33}$$

Let us now take $\mathbf{v} = \bar{\boldsymbol{\rho}} \boldsymbol{\delta}^k$ in (6.31). We have

$$\begin{aligned} & \|\bar{\boldsymbol{\rho}} \boldsymbol{\delta}^k\|_{\boldsymbol{\sigma}}^2 + \mathcal{A}(\boldsymbol{\delta}^k, \bar{\boldsymbol{\rho}} \boldsymbol{\delta}^k) + \mathcal{B}_h(\boldsymbol{\delta}^k, \bar{\boldsymbol{\rho}} \boldsymbol{\delta}^k) \\ & = - \left(\bar{\boldsymbol{\rho}}^k, \bar{\boldsymbol{\rho}} \boldsymbol{\delta}^k \right)_{\boldsymbol{\sigma}} + \left(\boldsymbol{\tau}^k, \bar{\boldsymbol{\rho}} \boldsymbol{\delta}^k \right)_{\boldsymbol{\sigma}} + \mathcal{A}(\bar{\boldsymbol{\rho}}^k, \boldsymbol{\delta}^{k-1}) + \mathcal{B}_h(\bar{\boldsymbol{\rho}}^k, \boldsymbol{\delta}^{k-1}) \\ & \quad + \mathcal{B}(\boldsymbol{\tau}^k, \boldsymbol{\delta}^{k-1}) - \mathcal{B}_h(\boldsymbol{\tau}^k, \boldsymbol{\delta}^{k-1}) + \mathcal{B}(\partial_t \mathbf{A}_C(t_k), \boldsymbol{\delta}^{k-1}) \\ & \quad - \mathcal{B}_h(\partial_t \mathbf{A}_C(t_k), \boldsymbol{\delta}^{k-1}) + \mathbf{g}(\bar{\boldsymbol{\rho}} \boldsymbol{\delta}^k) - \mathbf{g}_h(\bar{\boldsymbol{\rho}} \boldsymbol{\delta}^k) - \frac{1}{\Delta t} (\gamma_k - \gamma_{k-1}), \end{aligned} \tag{6.34}$$

where $\gamma_k := \mathcal{A}(\boldsymbol{\rho}^k, \boldsymbol{\delta}^k) + \mathcal{B}_h(\boldsymbol{\rho}^k, \boldsymbol{\delta}^k) - \mathcal{B}_h(\mathbf{A}_C(t_k), \boldsymbol{\delta}^k) + \mathcal{B}(\mathbf{A}_C(t_k), \boldsymbol{\delta}^k)$.

On the other hand, since \mathcal{A} is non-negative definite and symmetric, it is easy to check that

$$\mathcal{A}(\boldsymbol{\delta}^k, \bar{\boldsymbol{\rho}} \boldsymbol{\delta}^k) \geq \frac{1}{2\Delta t} \left[\mathcal{A}(\boldsymbol{\delta}^k, \boldsymbol{\delta}^k) - \mathcal{A}(\boldsymbol{\delta}^{k-1}, \boldsymbol{\delta}^{k-1}) \right]$$

and similarly for \mathcal{B}_h . Using these inequalities in (6.34) together with Cauchy-Schwarz inequality, and, then, summing over k and recalling that \mathcal{B}_h is non-negative, we deduce that

$$\begin{aligned}
& \frac{1}{2} \sum_{k=1}^n \left\| \bar{\partial} \boldsymbol{\delta}^k \right\|_{\boldsymbol{\sigma}}^2 + \frac{1}{2\Delta t} \mu_1^{-1} \left\| \operatorname{curl} \boldsymbol{\delta}^n \right\|_{0, \Omega_C}^2 \\
& \leq \sum_{k=1}^n \left[\left\| \bar{\partial} \boldsymbol{\rho}^k \right\|_{\boldsymbol{\sigma}}^2 + \left\| \boldsymbol{\tau}^k \right\|_{\boldsymbol{\sigma}}^2 \right] \\
& \quad + \sum_{k=1}^n \left[\left| \mathcal{A}(\bar{\partial} \boldsymbol{\rho}^k, \boldsymbol{\delta}^{k-1}) \right| + \left| \mathcal{B}_h(\bar{\partial} \boldsymbol{\rho}^k, \boldsymbol{\delta}^{k-1}) \right| + \left| \mathcal{B}(\boldsymbol{\tau}^k, \boldsymbol{\delta}^{k-1}) - \mathcal{B}_h(\boldsymbol{\tau}^k, \boldsymbol{\delta}^{k-1}) \right| \right. \\
& \quad \quad \left. + \left| \mathcal{B}(\partial_t \mathbf{A}_C(t_k), \boldsymbol{\delta}^{k-1}) - \mathcal{B}_h(\partial_t \mathbf{A}_C(t_k), \boldsymbol{\delta}^{k-1}) \right| \right] \\
& \quad + \frac{1}{\Delta t} \left| \mathbf{g}(\boldsymbol{\delta}^n) - \mathbf{g}_h(\boldsymbol{\delta}^n) \right| + \frac{1}{\Delta t} |\gamma_n|.
\end{aligned} \tag{6.35}$$

The following bounds are easy to obtain from Young's inequality and Remark 6.4.1:

$$\begin{aligned}
& \sum_{k=1}^n \left| \mathcal{A}(\bar{\partial} \boldsymbol{\rho}^k, \boldsymbol{\delta}^{k-1}) \right| \leq \sum_{k=1}^n \left\| \operatorname{curl} \boldsymbol{\delta}^{k-1} \right\|_{0, \Omega_C}^2 + C \sum_{k=1}^n \left\| \operatorname{curl} \bar{\partial} \boldsymbol{\rho}^k \right\|_{0, \Omega_C}^2, \\
& \sum_{k=1}^n \left| \mathcal{B}_h(\bar{\partial} \boldsymbol{\rho}^k, \boldsymbol{\delta}^{k-1}) \right| \leq \sum_{k=1}^n \left\| \operatorname{curl} \boldsymbol{\delta}^{k-1} \right\|_{0, \Omega_C}^2 + \sum_{k=1}^n \left\| \boldsymbol{\delta}^{k-1} \right\|_{\boldsymbol{\sigma}}^2 + C \sum_{k=1}^n \left\| \bar{\partial} \boldsymbol{\rho}^k \right\|_{\mathbf{V}}^2, \\
& \sum_{k=1}^n \left| \mathcal{B}(\boldsymbol{\tau}^k, \boldsymbol{\delta}^{k-1}) - \mathcal{B}_h(\boldsymbol{\tau}^k, \boldsymbol{\delta}^{k-1}) \right| \\
& \quad \leq \sum_{k=1}^n \left\| \operatorname{curl} \boldsymbol{\delta}^{k-1} \right\|_{0, \Omega_C}^2 + \sum_{k=1}^n \left\| \boldsymbol{\delta}^{k-1} \right\|_{\boldsymbol{\sigma}}^2 + C \sum_{k=1}^n \left\| \boldsymbol{\tau}^k \right\|_{\mathbf{V}}^2, \\
& \sum_{k=1}^n \left| \mathcal{B}(\partial_t \mathbf{A}_C(t_k), \boldsymbol{\delta}^{k-1}) - \mathcal{B}_h(\partial_t \mathbf{A}_C(t_k), \boldsymbol{\delta}^{k-1}) \right| \\
& \quad \leq \sum_{k=1}^n \left\| \operatorname{curl} \boldsymbol{\delta}^{k-1} \right\|_{0, \Omega_C}^2 + \sum_{k=1}^n \left\| \boldsymbol{\delta}^{k-1} \right\|_{\boldsymbol{\sigma}}^2 + C \sum_{k=1}^n \mathcal{G}_h(\partial_t \mathbf{A}_C(t_k))^2 \\
& \quad \quad + C \sum_{k=1}^n \left\| \partial_t \mathbf{A}_C(t_k) \right\|_{\mathbf{V}}^2 \left(\max_{1 \leq i \leq L} \left\| \tilde{\nabla} z_i - \tilde{\nabla} z_{ih} \right\|_{0, \mathcal{Q}}^2 + \left\| \mathbf{N}^{-1} - \mathbf{N}_h^{-1} \right\|^2 \right),
\end{aligned}$$

and

$$\begin{aligned}
& \left| \mathbf{g}(\boldsymbol{\delta}^n) - \mathbf{g}_h(\boldsymbol{\delta}^n) \right| \\
& \leq C \left(\left\| \mathbf{A}_{C,0} \right\|_{\mathbf{V}}^2 + |\boldsymbol{\alpha}_0|^2 \right) \left(\max_{1 \leq i \leq L} \left\| \tilde{\nabla} z_i - \tilde{\nabla} z_{ih} \right\|_{0, \mathcal{Q}}^2 + \left\| \mathbf{N}^{-1} - \mathbf{N}_h^{-1} \right\|^2 \right) \\
& \quad + \frac{1}{8} \mu_1^{-1} \left\| \operatorname{curl} \boldsymbol{\delta}^n \right\|_{0, \Omega_C}^2 + \left\| \boldsymbol{\delta}^n \right\|_{\boldsymbol{\sigma}}^2, \\
& |\gamma_n| \leq \frac{1}{8} \mu_1^{-1} \left\| \operatorname{curl} \boldsymbol{\delta}^n \right\|_{0, \Omega_C}^2 + \left\| \boldsymbol{\delta}^n \right\|_{\boldsymbol{\sigma}}^2 \\
& \quad + C \left[\left\| \boldsymbol{\rho}^n \right\|_{\mathbf{V}}^2 + \left\| \mathbf{A}_C(t_n) \right\|_{\mathbf{V}}^2 \left(\max_{1 \leq i \leq L} \left\| \tilde{\nabla} z_i - \tilde{\nabla} z_{ih} \right\|_{0, \mathcal{Q}}^2 + \left\| \mathbf{N}^{-1} - \mathbf{N}_h^{-1} \right\|^2 \right) \right].
\end{aligned}$$

Substituting all these inequalities in (6.35), using (6.33) and Remark 6.4.1, we obtain

$$\begin{aligned}
& \Delta t \sum_{k=1}^n \left\| \bar{\partial} \delta_C^k \right\|_{\boldsymbol{\sigma}}^2 + \|\operatorname{curl} \delta_C^n\|_{0, \Omega_C}^2 \\
& \leq C \left\{ \Delta t \sum_{k=1}^n \left[\left\| \bar{\partial} \boldsymbol{\rho}^k \right\|_{\mathbf{V}}^2 + \left\| \boldsymbol{\tau}^k \right\|_{\mathbf{V}}^2 + \mathcal{G}_h(\partial_t(\mathbf{A}_C(t_k)))^2 + \left\| \boldsymbol{\rho}^k \right\|_{\mathbf{V}}^2 \right. \right. \\
& \quad + \left\| \mathbf{A}_C(t_k) \right\|_{\mathbf{V}}^2 \left(\max_{1 \leq i \leq L} \left\| \tilde{\nabla} z_i - \tilde{\nabla} z_{ih} \right\|_{0, \mathcal{Q}}^2 + \left\| \mathbf{N}^{-1} - \mathbf{N}_h^{-1} \right\|^2 \right) \\
& \quad + \left\| \partial_t \mathbf{A}_C(t_k) \right\|_{\mathbf{V}}^2 \left(\max_{1 \leq i \leq L} \left\| \tilde{\nabla} z_i - \tilde{\nabla} z_{ih} \right\|_{0, \mathcal{Q}}^2 + \left\| \mathbf{N}^{-1} - \mathbf{N}_h^{-1} \right\|^2 \right) \left. \right] \\
& \quad + \left(\left\| \mathbf{A}_{C,0} \right\|_{\mathbf{V}}^2 + |\boldsymbol{\alpha}_0|^2 \right) \left(\max_{1 \leq i \leq L} \left\| \tilde{\nabla} z_i - \tilde{\nabla} z_{ih} \right\|_{0, \mathcal{Q}}^2 + \left\| \mathbf{N}^{-1} - \mathbf{N}_h^{-1} \right\|^2 \right) \\
& \quad \left. + \left\| \boldsymbol{\rho}^n \right\|_{\mathbf{V}}^2 + \mathcal{G}_h(\mathbf{A}_C(t_n))^2 \right\}
\end{aligned}$$

Combining this inequality with (6.33) and Remark 6.4.1, we end the proof. \square

Lemma 6.6.2 *Let $(\mathbf{A}_C, \psi, \boldsymbol{\alpha})$ be the solution of (6.12). If we assume that $\mathbf{A}_C \in H^1(0, T; H^s(\operatorname{curl}; \Omega_C))$, $1/2 < s < s_{\mathcal{Q}}$, then $\psi \in H^1(0, T; H^{s+1/2}(\Gamma))$ and the following estimates hold true:*

$$\inf_{\eta \in \mathcal{L}_h(\Gamma)} \|\psi(t) - \eta\|_{1/2, \Gamma} \leq Ch^s \|\operatorname{curl} \mathbf{A}_C(t)\|_{s, \Omega_C}, \quad (6.36)$$

$$\inf_{\eta \in \mathcal{L}_h(\Gamma)} \|\partial_t \psi(t) - \eta\|_{1/2, \Gamma} \leq Ch^s \|\partial_t(\operatorname{curl} \mathbf{A}_C(t))\|_{s, \Omega_C}. \quad (6.37)$$

Proof. Let $(\mathbf{A}_C, \psi, \boldsymbol{\alpha})$ be the unique solution of (6.12). Let ψ_I be as in Theorem 6.4.3. As shown in that theorem, $\psi_I(t) = \psi(t) + c(t)$ with $c(t) \in \mathbb{R}$ and $t \in [0, T]$. Moreover, a.e. in $[0, T]$, $\psi_I|_{\mathcal{Q}}$ is the solution to

$$\begin{aligned}
& -\Delta \psi_I = 0 && \text{in } \mathcal{Q}, \\
& \mu_0 \frac{\partial \psi_I}{\partial \mathbf{n}_I} = -\operatorname{curl} \mathbf{A}_C \cdot \mathbf{n}_C && \text{on } \Gamma, \\
& \psi_I|_{\Lambda} \in \mathcal{C}^\infty(\Lambda).
\end{aligned} \quad (6.38)$$

Since $\mathbf{A}_C \in C^0([0, T]; H^s(\operatorname{curl}; \Omega_C))$ with $1/2 < s < s_{\mathcal{Q}}$ and Λ is the boundary of a convex polyhedron, by applying classical results for the Laplace equation (see [38]) we have that $\psi_I \in H^{s+1}(\mathcal{Q})$ and

$$\|\psi_I\|_{s+1, \mathcal{Q}} \leq C \|\operatorname{curl} \mathbf{A}_C \cdot \mathbf{n}_C\|_{s-1/2, \Gamma} \leq C \|\operatorname{curl} \mathbf{A}_C\|_{s, \Omega_C}. \quad (6.39)$$

Since $s > 1/2$, the Lagrange interpolant ψ_I^I of ψ_I is well defined. Moreover, since ψ_I and ψ only differ in a constant,

$$(\psi_I - \psi_I^I)|_{\Gamma} = \psi - \psi^I_{\Gamma},$$

where $\psi^{I\Gamma} \in \mathcal{L}_h(\Gamma)$ denotes the 2D Lagrange surface interpolant on Γ . Therefore, because of the trace theorem, standard estimates for the 3D Lagrange interpolant and (6.39), we have

$$\|\psi - \psi^{I\Gamma}\|_{1/2,\Gamma} \leq C \|\psi_I - \psi_I^I\|_{1,\mathcal{Q}} \leq Ch^s \|\psi_I\|_{s+1,\mathcal{Q}} \leq Ch^s \|\operatorname{curl} \mathbf{A}_C\|_{s,\Omega_C}.$$

Thus, we conclude (6.36).

To prove (6.37), we recall that ψ_I is the solution to problem (6.19) (cf. the proof of Theorem 6.4.3). Then, since $\mathbf{A}_C \in H^1(0, T; H^s(\operatorname{curl}; \Omega_C))$, differentiating in time each equation in (6.19), we obtain an estimate analogous to (6.39) for $\partial_t \psi_I$. On the other hand, since $\psi_I(t) = \psi(t) + c(t)$ with

$$c(t) = \frac{1}{|\Gamma|} \int_{\Gamma} \psi_I(t) \, d\zeta,$$

we have that $\partial_t \psi(t) = \partial_t \psi_I(t) - c'(t)$. Hence, the rest of the proof follows identically as above. \square

Now we are in a position to conclude the following asymptotic error estimate for the fully discrete scheme.

Theorem 6.6.1 *Let $(\mathbf{A}_C, \psi, \boldsymbol{\alpha})$ and $(\mathbf{A}_{Ch}^n, \psi_h^n, \boldsymbol{\alpha}_h^n)$, $n = 1, \dots, N$, be the solutions to problem (6.12) and (6.26), respectively. Let us assume that $\mathbf{A}_C \in H^1(0, T; H^s(\operatorname{curl}; \Omega_C)) \cap H^2(0, T; H(\operatorname{curl}; \Omega_C))$ with $s \in (1/2, s_Q)$. Then, there exists $h_0 > 0$ such that, for all $h \in (0, h_0)$, the following estimate holds:*

$$\begin{aligned} & \max_{1 \leq n \leq N} \|\mathbf{A}_C(t_n) - \mathbf{A}_{Ch}^n\|_{\mathbf{V}}^2 + \Delta t \sum_{n=1}^N \|\bar{\partial}(\mathbf{A}_C(t_n) - \mathbf{A}_{Ch}^n)\|_{\boldsymbol{\sigma}}^2 \\ & \leq Ch^{2s} \left\{ \int_0^T \|\partial_t \mathbf{A}_C(t)\|_{H^s(\operatorname{curl}; \Omega_C)}^2 \, dt + \max_{1 \leq n \leq N} \|\partial_t(\operatorname{curl} \mathbf{A}_C(t_n))\|_{s, \Omega_C}^2 \right. \\ & \quad + \max_{1 \leq n \leq N} \left(\|\mathbf{A}_C(t_n)\|_{\mathbf{V}}^2 + \|\partial_t \mathbf{A}_C(t_n)\|_{\mathbf{V}}^2 \right) \left(\max_{1 \leq k \leq L} \|\tilde{\nabla} z_k\|_{s, \mathcal{Q}}^2 + \|z_k\|_{s+1/2, \Lambda}^2 \right) \\ & \quad + \left(\|\mathbf{A}_{C,0}\|_{\mathbf{V}}^2 + |\boldsymbol{\alpha}_0|^2 \right) \left(\max_{1 \leq k \leq L} \|\tilde{\nabla} z_k\|_{s, \mathcal{Q}}^2 + \|z_k\|_{s+1/2, \Lambda}^2 \right) \\ & \quad \left. + \max_{1 \leq n \leq N} \|\mathbf{A}_C(t_n)\|_{H^s(\operatorname{curl}; \Omega_C)}^2 \right\} + (\Delta t)^2 \int_0^T \|\partial_{tt} \mathbf{A}_C(t)\|_{\mathbf{V}}^2 \, dt \\ & \leq C [(\Delta t)^2 + h^{2s}] \left(\|\mathbf{A}_C\|_{H^2(0, T; H^s(\operatorname{curl}; \Omega_C))}^2 + |\boldsymbol{\alpha}_0|^2 \right), \end{aligned}$$

where z_k is the solution of problem (6.4), $k = 1, \dots, L$.

Proof. A Taylor expansion shows that

$$\bar{\partial} \mathbf{A}_C(t_k) = \partial_t \mathbf{A}_C(t_k) + \frac{1}{\Delta t} \int_{t_{k-1}}^{t_k} (t_{k-1} - t) \partial_{tt} \mathbf{A}_C(t) \, dt.$$

Consequently,

$$\sum_{k=1}^n \|\boldsymbol{\tau}^k\|_{\mathbf{V}}^2 \leq \Delta t \int_0^T \|\partial_{tt} \mathbf{A}_C(t)\|_{\mathbf{V}}^2 \, dt.$$

Moreover, we have from (6.30),

$$\begin{aligned} \sum_{k=1}^n \left\| \bar{\partial} \boldsymbol{\rho}^k \right\|_{\mathbf{V}}^2 &\leq \frac{1}{\Delta t} \sum_{k=1}^n \int_{t_{k-1}}^{t_k} \left\| \partial_t (I - \mathcal{I}_h^{\mathcal{N}}) \mathbf{A}_C(t) \right\|_{\mathbf{V}}^2 dt \\ &\leq \frac{Ch^{2s}}{\Delta t} \int_0^T \left\| \partial_t \mathbf{A}_C(t) \right\|_{H^s(\text{curl}; \Omega_C)}^2 dt. \end{aligned}$$

We recall that $\psi(t) = -\mu_0^{-1} \mathcal{R}(\mathcal{K}(\mathbf{A}_C(t)))$ (cf. Remark 6.4.2). It follows from (6.27) that

$$\begin{aligned} \mathcal{G}_h(\mathbf{A}_C(t_n)) &\leq \inf_{\eta \in \mathcal{L}_h(\Gamma)} \left\| \psi(t_n) - \eta \right\|_{1/2, \Gamma}^2, \\ \mathcal{G}_h(\partial_t \mathbf{A}_C(t_n)) &\leq \inf_{\eta \in \mathcal{L}_h(\Gamma)} \left\| \partial_t \psi(t_n) - \eta \right\|_{1/2, \Gamma}^2. \end{aligned}$$

Thus, using Lemma 6.6.2, we obtain

$$\begin{aligned} \mathcal{G}_h(\mathbf{A}_C(t_n)) &\leq Ch^s \left\| \text{curl} \mathbf{A}_C(t_n) \right\|_{s, \Omega_C}, \\ \mathcal{G}_h(\partial_t \mathbf{A}_C(t_n)) &\leq Ch^s \left\| \partial_t (\text{curl} \mathbf{A}_C(t_n)) \right\|_{s, \Omega_C}. \end{aligned} \tag{6.40}$$

Hence, the results follows by writing $\mathbf{A}_C(t_n) - \mathbf{A}_{Ch}^n = \boldsymbol{\delta}^n + \boldsymbol{\rho}^n$ and using Lemma 6.6.1, Lemma 6.5.1, Theorem 6.5.3 and (6.30). \square

Remark 6.6.1 *Let us recall that $\psi(t_n) = -\mu_0^{-1} \mathcal{R}(\mathcal{K}(\mathbf{A}_C(t_n)))$ and $\psi_h^n = -\mu_0^{-1} \mathcal{R}_h(\mathcal{K}(\mathbf{A}_{Ch}^n))$. Therefore, using (6.40) and the uniform boundedness of \mathcal{R}_h with respect to h , we obtain*

$$\begin{aligned} \left\| \psi(t_n) - \psi_h^n \right\|_{1/2, \Gamma} &\leq \mathcal{G}_h(\mathbf{A}_C(t_n)) + \left\| \mathcal{R}_h(\mathcal{K}(\mathbf{A}_C(t_n) - \mathbf{A}_{Ch}^n)) \right\|_{1/2, \Gamma} \\ &\leq C \left\{ h^s \left\| \text{curl} \mathbf{A}_C(t_n) \right\|_{s, \Omega_C} + \left\| \mathbf{A}_C(t_n) - \mathbf{A}_{Ch}^n \right\|_{\mathbf{V}} \right\}. \end{aligned}$$

Then, using Lemma 6.6.2 and Theorem 6.6.1, under the assumptions of the latter, we conclude that

$$\Delta t \sum_{n=1}^N \left\| \psi(t_n) - \psi_h^n \right\|_{1/2, \Gamma}^2 \leq C \left[h^{2s} + (\Delta t)^2 \right].$$

Moreover under the same assumptions, since $\boldsymbol{\alpha}(t_n) = \boldsymbol{\alpha}_0 - \mu_0^{-1} \mathbf{N}^{-1}(\mathbb{T}(\mathbf{A}_C(t_n) - \mathbf{A}_{C,0}))$ and $\boldsymbol{\alpha}_h^n = \boldsymbol{\alpha}_0 - \mu_0^{-1} \mathbf{N}_h^{-1}(\mathbb{T}_h(\mathbf{A}_{Ch}^n - \mathbf{A}_{C,0}))$, from Theorem 6.5.3, Lemma 6.5.1 and Theorem 6.6.1, we also conclude that

$$\max_{1 \leq n \leq N} \left| \boldsymbol{\alpha}(t_n) - \boldsymbol{\alpha}_h^n \right|^2 \leq C \left[h^{2s} + (\Delta t)^2 \right].$$

Chapter 7

Conclusiones y trabajo futuro

7.1 Conclusiones

El objetivo principal de la tesis presentada ha sido analizar y proponer nuevos modelos en el estudio matemático de la electroencefalografía y la magnetoencefalografía. Se estudia inicialmente el modelo de corrientes inducidas como alternativa a los modelos usados clásicamente para estudiar este tema. Para el modelo electrostático, se ha desarrollado un análisis a priori y a posteriori del error en la aproximación mediante elementos finitos. Se ha utilizado tal estimador para idear una estrategia computacional eficiente en la resolución del problema inverso. También se han hecho comparaciones a nivel computacional en cuanto a la eficiencia de los diversos métodos presentes en la literatura y los nuevos métodos propuestos respecto del problema directo e inverso.

Las conclusiones principales de esta tesis, en orden de desarrollo, son:

1. Se propone una alternativa a los modelos ya existentes que abordan el estudio de la electroencefalografía y la magnetoencefalografía: el modelo de corrientes inducidas. Se ha estudiado desde un punto de vista teórico el problema inverso con este modelo. Como fuente de corriente, se estudiaron tres casos: fuente distribuida, fuente superficial y fuente dipolar. Se probó que en el caso de una fuente distribuida, no hay una única solución y se caracterizó el espacio de fuentes no radiantes. En los otros dos casos se demostró que la componente tangencial del campo eléctrico en toda la frontera del dominio determina de forma única la fuente. En el caso de una fuente dipolar, se ha encontrado una fórmula mediante la cual es posible recobrar la posición dipolar y la polarización. También se estudia cómo recobrar la componente tangencial del campo eléctrico a partir de mediciones que se pueden obtener mediante un electroencefalograma y un magnetoencefalograma.

2. Se estudia el modelo electrostático en dominios bidimensionales y tridimensionales. En ambos casos se demuestra una estima a priori y a posteriori bajo ciertas restricciones de las geometrías y conductividades. Se demuestra que tal estimador es confiable y eficiente y finalmente, el estimador se usa para guiar un procedimiento adaptativo en un dominio bidimensional y se prueba experimentalmente, un orden óptimo de convergencia.
3. Se comparan la solución aproximada que se obtiene mediante el problema directo usando el método de substracción y el método directo en el caso de un dominio con varias regiones con distintas conductividades. El método de substracción destaca por ser un método que tiene un buen comportamiento cuando la posición del dipolo está totalmente contenida en una región. Sin embargo, de esta comparación se concluye que cuando el dipolo se ubica cerca de una interfaz, el método de substracción no es robusto y el método directo, sí. También se estudia el problema directo cuando la fuente dipolar se localiza en la interfaz. En este caso particular, ninguno de los métodos ya mencionados está bien definido y por tanto, se utiliza un aproximante de la delta que da mejores resultados. También se estudia el problema inverso. Se comparan los tres métodos mencionados y un último método que combina el método directo con un procedimiento adaptativo guiado por el estimador encontrado en el Capítulo 4 de esta tesis, en dos situaciones diferentes: cuando la posición del dipolo esta completamente contenida en una región homogénea y cuando es cercana a una interfaz. Se concluye que el método directo combinado con adaptatividad supera al método directo sin adaptatividad en ambas situaciones. Sin embargo hay que destacar que los resultados que se obtuvieron utilizando este método oscilan de un refinamiento a otro. Por otra parte, se observa que el método del aproximante de la delta también es competitivo en ambas situaciones. Por último se analiza el caso de una fuente distribuida y se estudian las matrices de influencia en dos situaciones: cuando la fuente distribuida está totalmente incluida en una región homogénea o cuando tal fuente es cercana a una interfaz. En ambas situaciones se comparan errores relativos respecto de una matriz de influencia de referencia. Primero se hace una comparación entre el método de substracción y el método directo con adaptatividad y se observa que la convergencia en el caso de este último, no tiene un comportamiento monótono. Por otra parte, se observa que el aproximante de la delta va convergiendo más rápidamente que los demás métodos estudiados en este capítulo a medida que la malla es más fina.
4. Se introduce un nuevo método numérico para las ecuaciones de corrientes inducidas dependientes del tiempo en un dominio conductor acotado, contenido en \mathbb{R}^3 . Se reformula el problema en término de nuevas variables y finalmente se deriva una formulación FEM-BEM.

Se demuestra existencia y unicidad de solución del problema. Se discretiza el problema usando en la discretización temporal un método backward Euler. También se demuestra un orden óptimo de convergencia a la solución.

7.2 Trabajo futuro

1. En el Capítulo 3, se ha encontrado una fórmula de representación mediante la cual, bajo ciertas suposiciones de las cantidades físicas y asumiendo que la densidad de corriente es una fuente dipolar y que se conocen las mediciones, es posible encontrar la localización y polarización. Se implementará dicha fórmula, lo cual implica implementar el operador de Laplace Beltrami en superficies.

Por otra parte, dentro de este mismo capítulo se probó existencia y unicidad del problema directo usando las ecuaciones de corrientes inducidas con fuente dipolar bajo la hipótesis de homogeneidad de la permeabilidad magnética y de la conductividad. También se estudiará la posibilidad de probar existencia y unicidad de tal problema, sin la necesidad de usar esa hipótesis.

2. Se estudiará la posibilidad de encontrar un estimador a posteriori que sea confiable y eficiente en relación a algunos de los métodos numéricos ya mencionados en Capítulo 5 para resolver el problema electrostático con fuente de corriente dipolar tales como el método de substracción [67] o el usar un aproximante de la delta que sea suave.
3. La ley de Biot-Savart permite encontrar el campo magnético a partir del conocimiento previo de la fuente de corriente y el potencial eléctrico. Se verá cómo aplicar los resultados obtenidos en esta tesis para el estudio del problema inverso de la MEG desde el punto de vista teórico y computacional.

Bibliography

- [1] R. ACEVEDO AND S. MEDDAHI, *An E-based mixed FEM and BEM coupling for a time-dependent eddy current problem*. IMA Journal of Numerical Analysis, vol. 31,2,pp.667-697, (2011).
- [2] R. ACEVEDO, S. MEDDAHI AND R. RODRÍGUEZ, *An E-based mixed formulation for a time-dependent eddy current problem*. Computational Geosciences, vol. 11, 3, pp. 207-218, (2007).
- [3] R. ALBANESE AND P. B. MONK, *The inverse source problem for Maxwell's equations*. Inverse Problems, vol. 22, 3, pp. 1023-1035, (2006).
- [4] A. ALONSO RODRÍGUEZ, J. CAMAÑO AND A. VALLI, *A justification of eddy currents model for the Maxwell equations*. Inverse Problems, vol. 28, 1, 015001 (24pp), (2012).
- [5] A. ALONSO RODRÍGUEZ AND A. VALLI, *Eddy Current Approximation of Maxwell Equations*. Modeling, Simulation and Applications, Springer-Verlag Italia, Milan, vol. 4, (2010).
- [6] A. ALONSO RODRÍGUEZ AND A. VALLI, *An optimal domain decomposition preconditioner for low-frequency time-harmonic Maxwell equations*. Mathematics of Computation, vol. 68, 226, pp.607-631, (1999).
- [7] H. AMMARI, G. BAO AND J. L. FLEMING, *An inverse source problem for Maxwell's equations in magnetoencephalography*. SIAM Journal on Applied Mathematics, vol. 62, 4, pp. 1369-1382, (2002).
- [8] H. AMMARI, A. BUFFA AND J.-C. NÉDÉLEC, *A justification of eddy currents model for the Maxwell equations*. SIAM Journal on Numerical Analysis, vol. 60, 5, pp. 1805-1823, (2000).
- [9] H. AMMARI AND H. KANG, *Reconstruction of small inhomogeneities from boundary measurements*. Lecture Notes in Mathematics. Springer-Verlag, Berlin, vol. 1846, pp. x=238, 2004.

-
- [10] H. AMMARI, E. LAKOVLEVA, DOMINIQUE L. AND GAËLE P., *MUSIC-type electromagnetic imaging of a collection of small three-dimensional inclusions*. SIAM Journal on Scientific Computing, vol. 29, 2, pp. 674-709, (2007).
- [11] H. AMMARI, S. MOSCOW AND M. S. VOGELIUS, *Boundary integral formulae for the reconstruction of electric and electromagnetic inhomogeneities of small volume*. ESAIM: Control, Optimisation and Calculus of Variations, vol. 9, pp. 49-66, (2003).
- [12] H. AMMARI, M. S. VOGELIUS AND D. VOLKOV, *Asymptotic formulas for perturbations in the electromagnetic fields due to the presence of inhomogeneities of small diameter. II. The full Maxwell equations*. Journal de Mathématiques Pures et Appliquées. Neuvième Série, vol. 80, 8, pp. 769-814, (2001).
- [13] C. AMROUCHE, C. BERNARDI, M. DAUGE AND V. GIRAULT, *Vector potentials in three-dimensional non-smooth domains*. Mathematical Methods in the Applied Sciences, vol. 21, 9, pp. 823-864, (1998).
- [14] S. ANDRIEUX AND A. BEN ABDA, *Identification of planar cracks by complete overdetermined data: inversion formulae*. Inverse Problems, vol. 12, 5, pp. 553-563, (1996).
- [15] R. ARAYA, E. BEHRENS AND R. RODRÍGUEZ, *A posteriori error estimates for elliptic problems with Dirac delta source terms*. Numerische Mathematik, vol. 105, 2, pp.193-216, (2006).
- [16] K. A. AWADA, D.R. JACKSON, J. T. WILLIAMS, D. R. WILTON, S.B. BAUMANN AND A. C. PAPANICOLAOU, *Computational aspects of finite element modeling in EEG source localization*. IEEE Transactions on Biomedical Engineering, vol. 44, pp.736-752, (1197).
- [17] A. BERMÚDEZ, B. LÓPEZ-RODRÍGUEZ, R. RODRÍGUEZ AND P. SALGADO, *Numerical solution of transient eddy current problems with input current intensities as boundary data*. IMA Journal of Numerical Analysis, vol. 32, 3, pp. 1001-1029, (2012).
- [18] N. BLEISTEIN AND J. K. COHEN, *Nonuniqueness in the inverse source problem in acoustics and electromagnetics*. Journal of Mathematical Physics, vol. 18, 2, pp. 194-201, (1977).
- [19] A. BOSSAVIT, *What do voltmeters measure?.* COMPEL. The International Journal for Computation and Mathematics in Electrical and Electronic Engineering, vol. 27, 1, pp. 9-16, (2008).
- [20] S. C. BRENNER AND L. R. SCOTT, *The Mathematical Theory of Finite Element Methods*. Springer, New York, third ed., (2008).

-
- [21] H. BUCHNER, G. KNOLL, M. FUCHS, A. RIENÄCKER, R. BECKMANN, M. WAGNER, J. SILNY AND J. PESCH, *Inverse localization of electric dipole current sources in finite element models of the human head*. *Electroenc. Clin. Neurophysiol.*, vol. 102, pp. 267-278, (1997).
- [22] A. BUFFA, M. COSTABEL AND D. SHEEN, *On traces for $\mathbf{H}(\mathbf{curl}, \Omega)$ in Lipschitz domains*. *Journal of Mathematical Analysis and Applications*, vol. 276, 2, pp. 845-867, (2002).
- [23] P. G. CIARLET, *The Finite Element Method for Elliptic Problems*, in: *Classics in Applied Mathematics*, vol. 40, Society for Industrial and Applied Mathematics (SIAM), Philadelphia, PA, (2002).
- [24] P. G. CIARLET, *Basic error estimates for elliptic problems*, in *Handbook of Numerical Analysis*, Vol. II, P. G. Ciarlet and J.-L. Lions, eds., North-Holland, Amsterdam, pp. 17351, (1991).
- [25] M. COSTABEL, *Symmetric methods for the coupling of finite elements and boundary elements*. *Boundary Elements IX*, Vol. 1 (Stuttgart, 1987), pp. 411-420, (1987).
- [26] M. COSTABEL, *A symmetric method for the coupling of finite elements and boundary elements*. *The Mathematics of Finite Elements and Applications*, VI (Uxbridge, 1987), pp. 281-288, (1988).
- [27] G. DASSIOS AND A. S. FOKAS, *Electro-magneto-encephalography for a three-shell model: dipoles and beyond for the spherical geometry*. *Inverse Problems*, vol. 25, 3, pp. 035001, 20, (2009).
- [28] G. DASSIOS, A. S. FOKAS AND F. KARIOTOU, *On the non-uniqueness of the inverse MEG problem*. *Inverse Problems*, vol. 21, 2, pp. L1-L5, (2005).
- [29] G. DASSIOS AND D. HADJILOIZI, *On the non-uniqueness of the inverse problem associated with electroencephalography*. *Inverse Problems*, vol. 25, 11, pp. 115012, 18, (2009).
- [30] M. DAUGE, *Problèmes de Neumann et de Dirichlet sur un polyèdre dans \mathbf{R}^3 : régularité dans des espaces de Sobolev L_p* , *C. R. Acad. Sci. Paris Sér. I Math.*, vol. 307, pp. 2732, (1988).
- [31] M. DAUGE, *Neumann and mixed problems on curvilinear polyhedra*, *Integral Equations Operator Theory*, vol. 15, pp. 227-261, (1992).
- [32] R. DAUTRAY AND J.-L. LIONS, *Analyse Mathématique et Calcul Numérique pour les Sciences et les Techniques*, Vol. 5, in : *Collection Enseignement*, vol. 5, INSTN, Masson, Paris, (1988).

-
- [33] A. EL BADIA AND T. HA DOUNG, *Some remarks on the problem of source identification from boundary measurements*. Inverse Problems, vol. 14, 4, pp. 883-891, (1998).
- [34] A. EL BADIA AND T. NARA, *An inverse source problem for quasi-static Maxwell's equations*. Journal of Inverse and Ill-Posed Problems, vol. 18, 7, pp. 741-764, (2010).
- [35] LAWRENCE C. EVANS, *Partial Differential Equations*, second ed., in: Graduate Studies in Mathematics, vol. 19, American Mathematical Society, Providence, RI, (2010).
- [36] A. S. FOKAS, Y. KURYLEV AND V. MARINAKIS, *The unique determination of neuronal currents in the brain via magnetoencephalography*. Inverse Problems, vol. 20, 4, pp. 1067-1082, (2004).
- [37] D. GILBARG AND N.S. TRUDINGER, *Elliptic Partial Differential Equations of Second Order*, second ed. Springer-Verlag, Berlin, (1983).
- [38] P. GRISVARD, *Elliptic Problems in Nonsmooth Domains*, in: Monographs and Studies in Mathematics, vol. 24, Pitman, Boston, MA, (1985).
- [39] M. HÄMÄLÄINEN, R. HARI, R. J. ILMONIEMI, J. KNUUTILA AND O. V. LOUNASMAA, *Magnetoencephalography – theory, instrumentation, and applications to noninvasive studies of the working human brain*, vol. 65, pp. 413-497, (1993).
- [40] S. HE AND V. G. ROMANOV, *Identification of dipole sources in a bounded domain for Maxwell's equations*. Wave Motion, vol 28, 1, pp. 25-40, (1998).
- [41] V. ISAKOV, *Inverse Source Problems*. Mathematical Surveys and Monographs, American Mathematical Society, Providence, RI, pp. xiv+193, (1990).
- [42] T. KANG AND K. I. KIM, *Fully discrete potential-based finite element methods for a transient eddy current problem*. Computational Geosciences, vol. 11, 3, pp. 207-218, (2007).
- [43] T.KANG, K.I.KIM AND Z.WU, *An E-based splitting finite element method for time-dependent eddy current equations*. Journal of Computational and Applied Mathematics, vol. 196, 2, pp.358-367, (2006).
- [44] R. KRESS, L. KÜHN AND R. POTTHAST, *Reconstruction of a current distribution from its magnetic field*. Inverse Problems, vol. 18, 4, pp. 1127-1146, (2002).
- [45] V. D. KUPRADZE, *Dynamical problems in elasticity*. Progress in solid mechanics, North-Holland, vol. III, (1963).

- [46] S. LEW, C. H. WOLTERS, T. DIERKES, C. RÖER AND R. S. MACLEOD, *Accuracy and run-time comparison for differential potential approaches and iterative solvers in finite element method based EEG source analysis*, Applied Numerical Mathematics. An IMACS Journal, vol. 59, 8, pp. 1970-1988, (2009).
- [47] C. MA, *The finite element analysis of a decoupled T - ψ scheme for solving eddy-current problems*. Applied Mathematics and Computation, vol. 205, 1, pp.352-361, (2008).
- [48] W. MACLEAN, *Strongly Elliptic Systems and Boundary Integral Equations*, Cambridge University Press, Cambridge, (2000).
- [49] S. MEDDAHI AND V. SELGAS, *A mixed-FEM and BEM coupling for a three-dimensional eddy current problem*. M2AN. Mathematical Modelling and Numerical Analysis, vol. 37, 2, pp. 291-318, (2003).
- [50] S. MEDDAHI, J. VALDÉS, O. MENÉNDEZ AND P. PÉREZ, *On the coupling of boundary integral and mixed finite element methods*. Journal of Computational and Applied Mathematics, vol. 69, 1, pp. 113-124, (1996).
- [51] J. C. MOSHER, R. M. LEAHY AND P. S. LEWIS, *EEG and MEG: forward solutions for inverse methods*, vol. 46, pp. 245-259, (1999).
- [52] J.-C. NÉDÉLEC, *Acoustic and Electromagnetic Equations*, in: Applied Mathematical Sciences, vol. 144, Springer-Verlag, New York, (2001).
- [53] H. W. NICHOLSON, *What does the voltmeter read?*. Am. J. Phys., vol. 73, 12, pp. 1194-1196, (2005).
- [54] R. NOCHETTO, *Pointwise a posteriori error estimates for elliptic problems on highly graded meshes*, Mathematics of Computation, vol. 64, 209, pp. 1-22, (1995).
- [55] P. S. NOVIKOV, *Sur le problème inverse du potentiel*. Doklady Akad. Nauk SSSR (N.S.), vol. 18, pp. 165-168, (1983).
- [56] T. ŌKAJI, *Strong unique continuation property for time harmonic Maxwell equations*. Journal of the Mathematical Society of Japan, vol. 54, 1, pp. 89-122, (2002).
- [57] R. PLONSEY AND D. B. HEPPNER, *onsiderations of quasi-stationarity in electrophysiological systems..* Bull. Math. Biophys. 29, pp. 657664 (1967).
- [58] S. PURSIAINEN, *Raviart-Thomas-type sources adapted to applied EEG and MEG: implementation and results*. Inverse Problems, vol. 28, 6, (2012).

-
- [59] S. PURSIAINEN, A. SORRENTINO, C. CAMPI AND M. PIANA, *Forward simulation and inverse dipole localization with the lowest order Raviart–Thomas elements for electroencephalography*. Inverse Problems, vol. 27, 4, (2011).
- [60] A. QUARTERONI AND A. VALLI, Numerical Approximation of Partial Differential Equations, in: Springer Series in Computational Mathematics, vol. 23, Springer-Verlag, (1994).
- [61] J. SARVAS, *Basic mathematical and electromagnetic concepts of the biomagnetic inverse problem*. Physics in Medicine and Biology, vol. 32, 1, pp. 11-22, (1987).
- [62] P.H. SCHIMPF, C.R. RAMON AND J. HAUEISEN, H, *Dipole models for the EEG and MEG*, IEEE Trans. Biomed. Eng., vol. 49, 5, pp.409-418, (2002).
- [63] V. SELGAS, *Análisis Matemático y Numérico de las Ecuaciones de Maxwell Cuasiestáticas*, Ph.D. Thesis, Universidad de Oviedo, Spain, (2005).
- [64] J. R. SHEWCHUK, *Delaunay refinement algorithms for triangular mesh generation*, Computational Geometry. Theory and Applications, vol. 22, 1-3, pp.21-74, (2002).
- [65] A. VALLI, *Solving an electrostatics-like problem with a current dipole source by means of the duality method*. Appl. Math. Lett. 25(10), 1410-1414 (2012).
- [66] WEINSTEIN, D AND ZHUKOV, L AND JOHNSON, C., *Lead-field Bases for Electroencephalography Source Imaging*, Annals of Biomedical Engineering, vol. 28, 9, pp. 1059-1066, (2000).
- [67] C. H. WOLTERS, H. KÖSTLER, C. MÖLLER, J. HÄRDTLEIN, L. GRASEDYCK AND W. HACKBUSCH, *Numerical mathematics of the subtraction method for the modeling of a current dipole in EEG source reconstruction using finite element head models*. SIAM J. Sci. Comput., vol. 30, 1, pp. 24-45, (2007).
- [68] Y. YAN AND P.L. NUNEZ AND R.T. HART, *Finite-element model of the human head: Scalp potentials due to dipole sources*, Med. Biol. Eng. Comput., vol. 29, pp. 475-481, (1991).
- [69] W. ZHENG, Z. CHEN AND L. WANG, *An adaptive finite element method for the H - ψ formulation of time-dependent eddy current problems*. Numer. Math, vol. 103, pp. 667-689, (2006).
- [70] J. E. ZIMMERMAN, P. THIENE AND J. T. HARDING, *Design and operation of stable rf-biased superconducting point-contact quantum devices, and a note on the properties of perfectly clean metal contacts*. J. Appl. Phys., 41, pp.1572-1580 (1970).